



**Double Degree Doctorate between
UNIVERSITA' DEGLI STUDI DI MILANO**

FACOLTA' DI SCIENZE DEL FARMACO

Department of Pharmaceutical Sciences

PhD Course in Pharmaceutical Sciences (XXXI Cycle)

and

THE UNIVERSITY OF ABERDEEN

Development of allosteric PFKFB3 phosphatase modulators

Doctorate Coordinator at Università Degli Studi di Milano: Prof. Giancarlo Aldini

Supervisors:

Prof. Maria Luisa Gelmi

Honorary Prof. Matteo Zanda

Dr. Sergio Dall'Angelo

Helena Macut

PhD candidate

R11493

Academic years 2016-2019





This PhD programme was founded in the frame of

**HORIZON 2020 - Marie Skłodowska-Curie
ITN-European Joint Doctorate
MOGLYNET-programme**

“MOGLYNet: “*Modulation of glycolytic flux as a new approach for treatment of atherosclerosis and plaque stabilization: a multidisciplinary study*”

The project leading to this application has received funding from the European Union's Horizon 2020 research and innovation programme under the Marie Skłodowska-Curie grant agreement No 67552.

Declaration

I hereby declare that this thesis has been composed by myself and it has not been accepted in any previous application for a degree at these, or any other University. The work described herein has been performed by myself, except where expressly indicated otherwise. All sources of information have been specifically acknowledged by means of reference, and verbatim extracts have been distinguished by quotation marks.

Helena Macut, May 2019

A handwritten signature in black ink that reads "Helena Macut". The signature is written in a cursive style with a large initial 'H' and 'M'.

I would like to express my sincere gratitude to my advisor Prof. Maria Luisa Gelmi for her continuous support of my PhD study and related research. Her guidance helped me in all the time of research and writing of this thesis. I would also like to thank my second advisor, Prof. Matteo Zanda for his support and immense knowledge.

Besides my advisors, I would like to thank the other members of Moglynet network, especially Dr. Sara Pellegrino, Dr. Luca Regazzoni and Ettore Gilardoni and Dr. Sergio Dall'Angelo for their solid support, motivation and patience.

A special thanks from the heart goes to Dr. Delia Tarantino for tremendous help during the most challenging parts of this research work. This results would not be possible without her immense experience and patience. My honest thanks goes also to my Moglynet colleagues, Xiao Hu, Virginia Cristofori and Carlo De Dominicis for excellent teamwork and friendship. It was a truly great experience to meet you and work with you on this project.

Last but not the least, I would like to thank my family and closest friends for supporting me throughout the PhD experience and in my life in general.

I shall be telling this with a sigh
Somewhere ages and ages hence:
Two roads diverged in a wood, and I,
I took the one less travelled by,
And that has made all the difference.

(R. Frost)

TABLE OF CONTENTS

Declaration.....	3
Abbreviations and Symbols	4
I. ABSTRACT.....	7
II. INTRODUCTION	8
a) ATHEROSCLEROSIS	8
b) PHOSPHOFRUCTOKINASE/FRUCTOSE-2,6-BISPHOSPHATASE	9
c) PFKFB3 AND PATHOLOGICAL ANGIOGENESIS	11
d) PFKFB3 TARGET POTENTIAL.....	12
e) PHOSPHATASE ACTIVATION ADVANTAGES	13
III. PROJECT AIM.....	14
IV. CHAPTER 1: PFKFB3 PHOSPHATASE ACTIVITY ALLOSTERIC MODULATORS.....	16
a) INTRODUCTION	16
Solid Phase Peptide Synthesis. Overview.....	16
Protein expression and purification. Overview.....	20
Microscale thermophoresis (MST). Overview	21
b) DESIGN	26
c) RESULTS	29
i) Synthesis- SPPS	29
ii) Binding assay- microscale thermophoresis	36
AD and its synthetic analogues.....	36
iii) Conformational analysis with circular dichroism (CD) and dynamic light scattering (DLS)	42
iv) Kinase activity assay	46
v) Thermofluor.....	46
vi) Phosphatase activity assay.....	47
vii) Cell tests	48
viii) Protein expression and purification.....	51
d) DISCUSSION	53
V. CHAPTER 2: PFKFB3 CRYSTALLIZATION	58
a) INTRODUCTION	58
Protein crystallization. An overview.	58
b) RESULTS.....	63

c)	DISCUSSION	64
VI.	CHAPTER 3: ATP COMPETITIVE PFKFB3 KINASE INHIBITORS	66
a)	INTRODUCTION	66
b)	DESIGN	66
i)	AZI-based computational strategy	66
ii)	AZPP-based computational strategy	67
c)	RESULTS	67
i)	Kinase activity results	67
ii)	Binding affinity results	72
	Surface plasmon resonance.....	75
	Overview.....	75
	Results. SPR kinetics	76
d)	DISCUSSION	77
VII.	CHAPTER 4: F-6-P BINDING SITE KINASE INHIBITORS	79
a)	DESIGN.....	79
b)	RESULTS.....	80
c)	DISCUSSION	81
VIII.	CONCLUSION	82
IX.	MATERIALS AND METHODS.....	83
a)	COMPUTATIONAL PART	83
	PFKFB3 Protein Structure for Virtual Screening	83
	Virtual screening.....	83
	MD simulations.....	85
	AZI-based computational strategy	86
b)	PEPTIDE SYNTHESIS	87
	Protocol for the manual peptide synthesis	87
	Resin handling	87
	Attachment of the first residue.....	88
	Wang resin.	88
	Rink amide resin.	88
c)	CIRCULAR DICHROISM.....	90
d)	DYNAMIC LIGHT SCATTERING.....	90
e)	PFKFB3 EXPRESSION	90
f)	KINASE ASSAY	92

g) THERMOFLUOR.....	94
h) MST BINDING ASSAY.....	95
i) PHOSPHATASE ASSAY	96
PFKFB3 phosphatase activity measurements.....	96
Instrumental analysis.	96
j) ENDOTHELIAL MIGRATION ASSAY.....	97
k) ENDOTHELIAL CELL PROLIFERATION AND SURVIVAL EXPERIMENT- MTT ASSAY	98
l) SURFACE PLASMON RESONANCE	98
m) PFKFB3 CRYSTALLIZATION.....	99
Optimization attempt 1 and 2.....	100
Optimization attempt 3	102
Optimization attempt 4	104
Optimization attempt 5	104
Optimization attempt 6	105
Optimization attempt 7	106
Screening attempt 1	107
Screening attempt 2	109
Screening attempt 3	112
Screening attempt 4	114
Screening attempt 5	116
Screening attempt 6	118
Screening attempt 7	120
X. APPENDIX.....	123
1st STRATEGY SCREENING- ZINC LIBRARY	123
2nd STRATEGY SCREENING- ZINC LIBRARY	124
2nd STRATEGY SCREENING- ZINC ADME LIBRARY	126
EXPERIMENTAL DATA.....	127
XI. REFERENCES	161

Abbreviations and Symbols

AD autoregulatory domain

ADP adenosine diphosphate

ATP adenosine triphosphate

AZI Astra Zeneca Indole compounds

AZPP Astra Zeneca pyrrolepyrimidinone compounds

CAPS *N*-cyclohexyl-3-aminopropanesulfonic acid

CD circular dichroism

CTC resin 2-Chlorotriyl chloride resin

DCM dichloromethane

2-DG 2-Deoxyglucose

DIC *N,N'*-Diisopropylcarbodiimide

DIPEA *N, N'*-diisopropylethyl amine

DLS dynamic light scattering

DMAP dimethylallyl pyrophosphate

DMF *N,N'*-dimethylformamide

DMSO dimethyl sulphoxide

EC endothelial cell

EDTA ethylene diaminetetraacetic acid

ESI MS Electrospray ionization mass spectrometry

F-6-P fructose-6-phosphate

F-2,6-P₂ fructose-2,6-bisphosphate

Fmoc 9-fluorenylmethoxycarbonyl

FPLC fast protein liquid chromatography

h hours

HBTU 2-(1H-Benzotriazole-1-yl)-1,1,3,3-tetramethylammonium hexafluorophosphate

HDL high density lipoprotein

HEPES 4-(2-hydroxyethyl)-1-piperazineethanesulfonic acid

HOBt Hydroxybenzotriazole

HPLC high performance liquid chromatography

IC₅₀ half maximal inhibitory concentration

LC-MS liquid chromatography-mass spectroscopy

LDL-C low density lipoprotein cholesterol

MALDI TOF MS matrix-assisted laser desorption/ionization time of flight mass spectroscopy

MeOH methanol

MD molecular dynamics

MES 2-(N-morpholino)ethanesulfonic acid

min minutes

K_M Michaelis constant

MRM multiple reaction monitoring

MS mass spectrometry

MST microscale thermophoresis

m/z mass to charge ratio

Ox LDL oxidized low density lipoprotein

PDB Protein Data Bank

PEG polyethylene glycol

PFKFB3 6-phosphofructo-2-kinase/fructose-2,6-biphosphatase 3

PFK1 Phosphofructokinase-1

PLANTS Protein-Ligand ANT System

RA residual activity

RMSD root mean square distance

RP-HPLC reversed phase high performance liquid chromatography

s seconds

SEC size exclusion chromatography

SPPS solid-phase peptide synthesis

SPR surface plasmon resonance

*t*Bu tert-butyl

TFA trifluoroacetic acid

TFE trifluoroethanol

TIS triisopropylsilane

Thz thiazole

Tris tris(hydroxymethyl)aminomethane

UV ultraviolet

VS- virtual screening

Amino acids letter code

A alanine (Ala)

C cysteine (Cys)

D aspartic acid (Asp)

E glutamic acid (Glu)

F phenylalanine (Phe)

G glycine (Gly)

H histidine (His)

I isoleucine (Ile)

K lysine (Lys)

L leucine (Leu)

M methionine (Met)

N asparagine (Asp)

P proline (Pro)

Q glutamine (Gln)

R arginine (Arg)

S serine (Ser)

T threonine (Thr)

V valine (Val)

W tryptophan (Trp)

Y tyrosine (Tyr)

I. ABSTRACT

Cardiovascular disease is a severe health problem, especially in the Western world. Its primary cause is atherosclerosis, which is characterized by the arterial wall thickening. Modern therapeutic strategies have restricted efficacy and the mortality still remains high. Current research has supported the idea of targeting dysregulated endothelial cell (EC) metabolism as a novel therapeutic strategy. In the scope of this PhD research work, we aim to further explore the possibilities for an improved treatment of this life threatening disease.

EC glycolytic flux is up-regulated during angiogenesis and it is controlled by 6-phosphofructo-2-kinase/fructose-2,6-bisphosphatase (PFKFB3), which is hence an innovative target for atherosclerosis therapy. PFKFB3 is a homodimeric bifunctional enzyme that has a very high kinase to phosphatase activity ratio. Its activity is controlled by the N-terminus autoregulatory domain in the kinase region.

The main task of this research work was to explore the alternatives for PFKFB3 modulation apart from potentially problematic ATP kinase inhibition. Virtual screening was performed on the targeted allosteric binding site and here we present the synthesis and biological evaluation of the selected libraries of PFKFB3 allosteric phosphatase modulators deriving from two design strategies. *In vitro* activity measurement and binding assays were performed on the isolated recombinant enzyme. A phosphatase activity measurement method was developed in-house using LC-MS and the binding assay was performed using microscale thermophoresis. Three peptides (**HM-20-22**) were found to be able to bind PFKFB3 with a micromolar affinity. **HM-21** and **22** were able to modulate the PFKFB3 phosphatase activity and interestingly showed the same overall effect on the enzyme kinetics as in the case of a very potent ATP competitive inhibitor. The outcome of the research work presented here suggests that it is possible to use an alternative approach in blocking PFKFB3 activity without inhibiting the kinase. This intriguing discovery could have a significant impact on further research about this important metabolic target and the possibility of its use in atherosclerosis therapy.

II. INTRODUCTION

a) ATHEROSCLEROSIS

Atherosclerosis is a chronic inflammatory process in the blood vessel wall leading to luminal narrowing and subsequent cardiovascular events [1]. It has been a major cause of death in developed countries for decades. Atherosclerosis is a disease of vascular intima, characterized by intimal plaques, in which all the vascular system from aorta to coronary arteries can be involved. The progress of the disease is slow and it has several stages: fatty streaks formation, atheroma formation and atherosclerotic plaques formation (Figure 1).

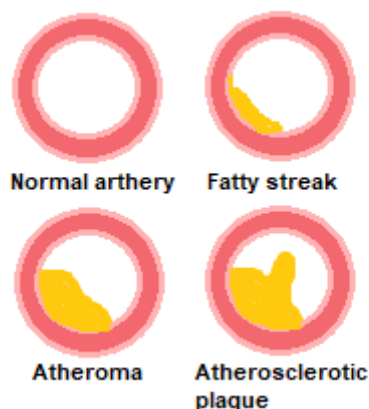


Figure 1: Stages of atherosclerotic plaque formation process.

In the first stage, fatty material is located in the central core of the plaque and it is covered by a fibrous cap. Formation of these plaques starts with the deposition of small low density lipoprotein cholesterol (LDL-C) crystals in the intima and its underlying smooth muscle. The increased concentration of LDL in the intima and increased duration of their stay in the lesion lead to spontaneous oxidation of the trapped particles [2]. Cytokines and oxidized lipids play an important role in the activation of endothelial cells. During early stage of atherosclerosis, leukocytes, monocytes and T lymphocytes infiltrate into vascular intima [3]. Oxidized LDL (Ox-LDL) causes the activation of T cells as it is an antigen for them and consequently, macrophages are activated. Macrophages then perform the uptake and accumulation of Ox-LDL by their scavenger receptors, present on the surface of macrophages, endothelial cells, fibroblast and smooth muscle cells, which will be then converted to foam cells [4]. The expression of these receptors increases during differentiation of monocytes to macrophages by cytokines and oxidized lipids.

The plaques grow with the proliferation of fibrous tissues and the surrounding smooth muscle, swell inside the arteries and consequently reduce the blood flow. An excess of connective tissue produced by fibroblasts and deposition of calcium in the lesion cause arterial hardening or sclerosis. In the late stage there is a clot formation and thrombosis due to the uneven surface of arteries, which leads to sudden obstruction of blood flow [5] and, in the absence of immediate medical intervention, can also lead to death.

Although the exact causes and risk factors of atherosclerosis are still unclear, certain conditions and habits may increase the chance of developing this disease. The known risk factors include high cholesterol and LDL, low high density lipoprotein (HDL), hypertension, smoking, diabetes, obesity and age [6, 7]. Although the disease can be prevented or delayed with a healthy lifestyle, atherosclerosis-related cardiovascular disease still has a high incidence and imposes an enormous burden on healthcare systems. Currently available treatments are largely restricted to regulating hypertension and hyperlipidemia or controlling homeostasis to prevent thrombotic complications. However, these strategies do not directly address the inflammatory mechanisms driving the progression of the disease [6].

The vessel function is controlled by the endothelium, a single layer of endothelial cells (ECs) that lines the blood vessel lumen. The inability of ECs to perform their physiological function contributes to cardiovascular disease and diabetes [8], while new vessels are formed in diseases such as cancer and age-related macular degeneration [9]. Therefore, targeting ECs to prevent dysfunction or inhibit pathological angiogenesis is potentially beneficial for a wide variety of diseases. It has been clearly shown that pathological blood vessel responses are associated with metabolic alterations in ECs and these metabolic alterations mediate important aspect of the disease. Furthermore, it has been demonstrated that increased EC glucose metabolism is a key feature of angiogenic and hyper-proliferative ECs. Hence, targeting the EC metabolism could be a novel and viable therapeutic strategy to affect pathological angiogenesis [10]. Recently, there has been a successful proof of concept in targeting EC metabolism by pharmacological inhibition of the glycolytic enzyme phosphofructokinase/fructose-2,6-bisphosphatase 3 (PFKFB3) [10-12].

b) PHOSPHOFRUCTOKINASE/FRUCTOSE-2,6-BISPHOSPHATASE

PFKFBs are a family of homodimeric bifunctional enzymes which includes the PFKFB3 isoform (Figure 2). The N-terminal half of the enzyme subunit (kinase domain) catalyzes the synthesis of fructose-2,6-bisphosphate (F-2,6-P₂) using fructose-6-phosphate (F-6-P) and

adenosine 5'phosphate (ATP) as substrates. Conversely, the C-terminal half of PFKFB (biphosphatase domain) is responsible for the hydrolysis of F-2,6-P₂ into F-6-P and inorganic phosphate (P_i). Different mechanisms control these two mutually opposing catalytic activities so that either activity prevails in a given physiological condition.

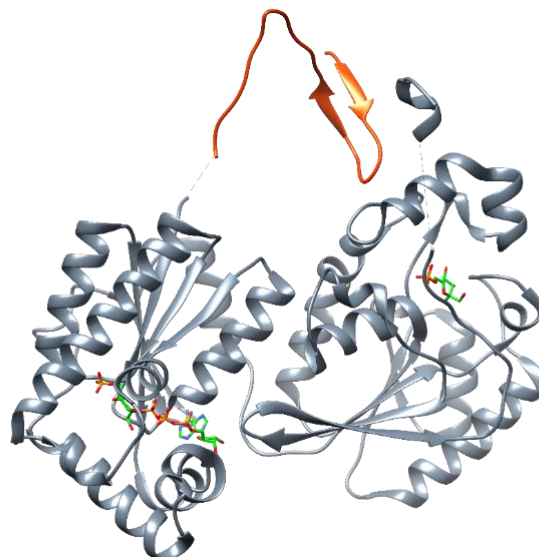


Figure 2: Crystal structure of homodimeric PFKFB3 with substrate in the binding site and autoregulatory domain shown in orange.

The glycolytic cycle is presented in Figure 3. The product of PFKFB kinase is F-2,6-P₂, the most potent allosteric activator of 6-phosphofructo-1-kinase (PFK-1) that converts fructose-6-phosphate (F-6-P) to fructose-1,6-bisphosphate (F-1,6-P₂) in the rate-limiting step of glycolysis [13]. On the other hand, F-2,6-P₂ is also an inhibitor of gluconeogenic enzyme fructose-1,6-bisphosphatase (F-1,6-P₂ase). As such, this small molecule switches between the two pathways of glucose metabolism within the liver, playing thus a crucial role in maintaining glucose homeostasis and controlling the glycolysis rates in other tissues [14, 15]. Ultimately, PFKFB controls the rate of glucose metabolism by controlling the F-2,6-P₂ production/degradation [14, 16].

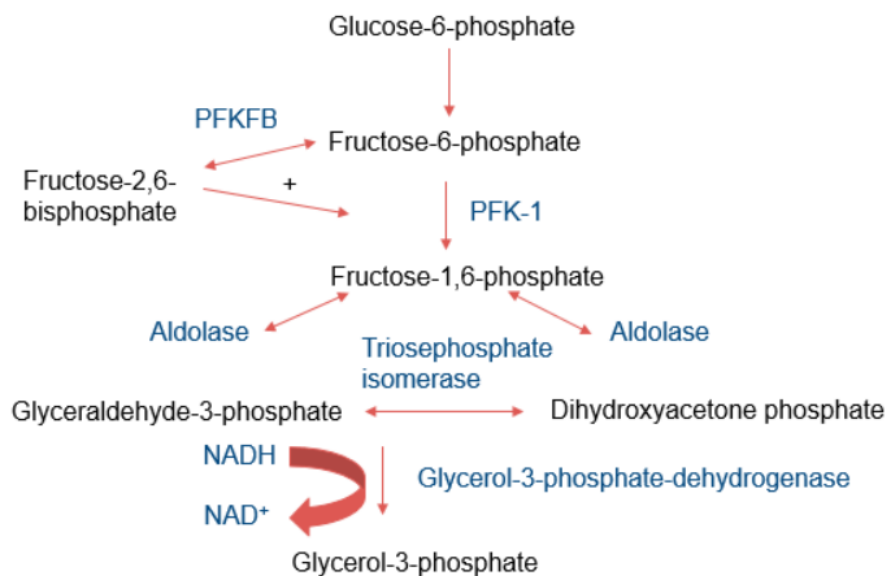


Figure 3: Schematic presentation of glycolysis.

Since the regulation of F-2,6-P₂ is optimized on a tissue-specific manner, there are four PFKFB isoforms, encoded by separate genes *pfkfb 1-4*. The four isoforms are: liver (PFKFB1), heart (PFKFB2), testis (PFKFB4) and inducible forms (PFKFB3) [17-20]. According to the available crystal structures of PFKFB1, PFKFB3 and PFKFB4 [21-23] these isoforms are highly homologous (85 %). However, due to very divergent N- and C-terminal regulatory domains they differ in their kinetic properties and responses to regulatory signals.

Unlike the other constitutive isoforms, PFKFB3 is hypoxia-inducible [24] and has a uniquely high, 700 fold, 6-phosphofructo-2-kinase to fructose-2,6-bisphosphatase ratio compared to other isoforms and it is the most significantly upregulated in ECs. Different studies suggested PFKFB3 is a causative molecule of the so called Warburg effect [25, 26], a phenomenon when glycolysis levels are highly elevated in tumour cells. Therefore, it has been suggested that PFKFB3 may be a promising target for the treatment of pathological angiogenesis and its associated diseases [12, 27].

c) PFKFB3 AND PATHOLOGICAL ANGIOGENESIS

Angiogenesis is the growth of new blood vessels and when dysregulated, it can lead to the development of various malignant, ischaemic, inflammatory and immune diseases [28, 29]. In the process of angiogenesis, ECs are critical and their PFKFB3 driven glycolytic activity is very high. In fact, ECs produce up to 85% of their ATP from glycolysis, which is much higher than any other healthy cells and it is similar to that of tumour cells. Recent studies showed that

PFKFB3 plays a significant role in physiological as well as pathological ECs glycolysis. The fundamental principles for the role of PFKFB3 derives from the effect of this enzyme on endothelial migration and proliferation. PFKFB3 knockdown ECs exhibit defects in the formation of filopodia and lamellipodia. Furthermore, silencing PFKFB3 significantly impaired T-lymphocyte proliferation. Therefore, inhibition of this enzyme can lead to a meaningful suppression of pathological angiogenesis. In addition to cancers, also other diseases such as retina angiogenesis and angiogenesis in atherosclerotic lesion that contributes to the formation and progression of atherosclerosis, are associated with pathological angiogenesis. Hence, based on the reported implications of PFKFB3 in glycolysis and consequently, in pathological angiogenesis, this enzyme may serve as a very effective therapeutic target in the regulation of glycolytic pathway and finally in the control of neovessel formation in the atherogenic process. [10-12].

d) PFKFB3 TARGET POTENTIAL

In the past, antiglycolytic therapies had several side-effects such as cross-inhibition of other glycolytic targets, off-target effects and poor pharmacokinetic properties. In addition, compounds such as 2-deoxyglucose (2-DG) have to compete with high concentrations of glucose in blood and therefore have to be delivered in high, already toxic amounts. The origin of these problems can be traced to specificity issues, as these therapies did not act exclusively on glycolysis, but also on other glucose metabolism pathways and they inhibited glycolysis nearly completely and permanently, causing ATP depletion and toxicity [30, 31]. Using PFKFB3 as a target of interest differs from previous strategies in various aspects. Firstly, since it is an intracellular enzyme, lower concentrations (μM - nM) of compounds can compete with glucose plasma levels (mM). Secondly, unlike 2-DG and related compounds that stop glucose metabolism upstream in the pathway, PFKFB3 is a defined downstream target and acts on glycolytic flux specifically without abolishing glycolytic side pathways. Finally, there is a solid evidence that PFKFB3 inhibition decreases pathological angiogenesis in murine disease models [10].

e) PHOSPHATASE ACTIVATION ADVANTAGES

The activation of phosphatase activity would increase the production of kinase substrate F-6-P and by the negative feedback loop principle, the kinase activity would thus decrease and the final outcome of this process would be reduced glycolysis.

This approach would have several advantages in comparison to an ATP competitive kinase inhibition approach. Firstly, human kinome consists of 518 kinases (nearly 2% of human genome) and the kinase ATP pocket is highly conserved, which is the cause for the poor selectivity of most ATP competitive inhibitors [32, 33]. Secondly, promiscuous binding contributes to additional toxicity and limits the clinical use of these compounds. Furthermore, such inhibitors have to compete with high intracellular ATP levels (mM), while the ATP Michaelis constant (K_M) values for most kinases are in low micromolar range. Consequently, it is common that there is a poor agreement between biochemical and cellular potency for ATP-competitive compounds. In order to see a significant inhibition effect *in vivo*, the compound should have an excellent affinity, usually low nanomolar or even picomolar range [34, 35]. Lastly, also resistance towards ATP competitive inhibitors may occur over time due to common and rapid ATP pocket mutations [36, 37].

III. PROJECT AIM

This research study was done as a part of Horizon 2020 MSCA European Joint Doctorate Moglynet (Modulation of glycolytic flux as a new approach for treatment of atherosclerosis and plaque stabilization: a multidisciplinary study). This project was carried out in continuous strong collaboration with the other early stage researchers and research fellows from the network. In particular, Xiao Hu was in charge of *in silico* part of this work. Dr. Delia Tarantino (Department of Bioscience, University of Milan) provided support for *in vitro* biological tests and supervision concerning the protein crystallization. In addition, Dr. Luca Regazzoni (Department of Pharmaceutical Sciences, University of Milan) supervised the setup of LC-MS method for phosphatase activity evaluation. Anahita Abdali, Laura Parma and Sarath Babu Nukala performed migration and proliferation assays for selected peptides. Finally, Dr. Sergio Dall'Angelo (Institute of Medical Sciences, University of Aberdeen) supervised the development of surface plasmon resonance (SPR) method for kinase binding profile evaluation.

The principal aim of this PhD work was to synthesize and biologically evaluate selected allosteric PFKFB3 phosphatase modulators. The research work was arranged in different stages that led to the final objective of this task, which was to evaluate if PFKFB3 phosphatase could be allosterically modulated and whether the final outcome of this modulation would be the desired kinase inhibition.

Experimental activities were organized as follows (some tasks were performed in parallel):

1. *In silico* experiments investigating the function of PFKFB3 β -hairpin shaped N-terminal domain followed by chemical synthesis of its synthetic analogues and α -helices in its close proximity
2. Development of design strategies for a possible PFKFB3 phosphatase allosteric modulation. A back-up strategy was needed due to the substantial complexity of this research project. A library of best scoring peptides was synthesized using Solid Phase Peptide Synthesis (SPPS) and adequately purified and characterized.
3. Human recombinant PFKFB3 was expressed in the appropriate host system and adequately purified in order to be used for further *in vitro* experiments.
4. The selected peptides were tested for their kinase activity using an appropriate kinase activity kit.

5. The selected peptides were tested for their binding affinity towards the target using microscale thermophoresis (MST).
6. Further *in silico* experiments were performed to improve the binding and additional series of peptides were synthesized using SPPS.
7. Crystallization of PFKFB3 protein followed by a crystallization trial (soaking and co-crystallization method) for the compound with the highest affinity for PFKFB3.
8. Set-up of a new phosphatase activity assay addressed to allosteric modulators in order to confirm their activity, explore the enzyme kinetics and the modulators' effect on it.

Although the principal aim of this research work was to evaluate the possibility of allosteric modulation of the target of interest, there were also side projects apart from the leading project. A collaboration with the other Moglynet PhD students, Virginia Cristofori and Carlo De Dominicis, working in the work package concerning the design and synthesis of ATP competitive PFKFB3 kinase inhibitors was done in parallel with the main project. Activities regarding this work package were as follows:

1. Potential kinase inhibitors were tested for their kinase activity and IC₅₀ values were determined where applicable.
2. The MST binding assay was carried out for compounds that exhibited significant kinase inhibitory activity.
3. A surface plasmon resonance (SPR) method was set up for a kinetics study of the most potent PFKFB3 kinase inhibitors.
4. Exploration of the possibility of inhibiting the kinase through competitive inhibition with the other PFKFB3 substrate, F-6-P.

IV. CHAPTER 1: PFKFB3 PHOSPHATASE ACTIVITY ALLOSTERIC MODULATORS

a) INTRODUCTION

The leading aim of the research work presented herein was to evaluate the possibility of an allosteric modulation of the target of interest. The starting point of this challenging task was a preliminary computational study addressing the function of PFKFB3 N-terminal AD and subsequent chemical synthesis and conformational evaluation of its synthetic analogues. These research activities were followed by the development of two design strategies for a possible PFKFB3 allosteric modulation and subsequently by synthesis of a library of short peptides using **SPPS** techniques. The biological evaluation of peptides with the kinase activity assay and **MST** binding assay required a substantial amount of the enzyme. Hence, the recombinant human PFKFB3 had to be prepared continuously making therefore **protein expression** an important task of this research work. In addition, as a confirmation of the phosphatase activity enhancement, a completely new **LC-MS phosphatase activity assay** was set up and used to evaluate the most promising peptides. Finally, the selected peptides were evaluated in several **cell tests**, where their effect on cell migration and proliferation was assessed.

Solid Phase Peptide Synthesis. Overview

The solid phase strategy for peptide synthesis was developed by Robert Bruce Merrifield in 1960s [38] and it is the most conventional procedure for peptide chemists ever since. The concept of this approach is a repetitive amidation reaction between the amino group of one amino acid and the carboxylic group of the other one. The original technique for the synthesis has drastically improved over years in terms of design of orthogonal protecting groups, new functionalized solid supports (resins) and efficient amide coupling reagents. Furthermore, new procedures and automated systems have made possible the synthesis of longer peptide sequences [39-41].

The basis of SPPS is carboxyl group oriented building of the C-terminal peptide chain on an insoluble and stable solid support. Side chain functional groups have to be covered with protecting groups and therefore unable to react and form side products. Moreover, the protecting group of the α -amino group of the first amino acid is removed prior to the reaction

with the second amino acid. An excess of the second amino acid is added and its carboxyl group activated for amide bond formation through activated ester generation or by coupling reagent. After coupling reaction excess reagents are washed, the N-terminus of the newly synthesized dipeptide is deprotected and the third amino acid is added. This procedure is repeated until the completion of the desired sequence. In the last step, the peptide is cleaved from the solid support and the side chain protection groups are removed. SPPS general procedure is schematically presented in Figure 4.

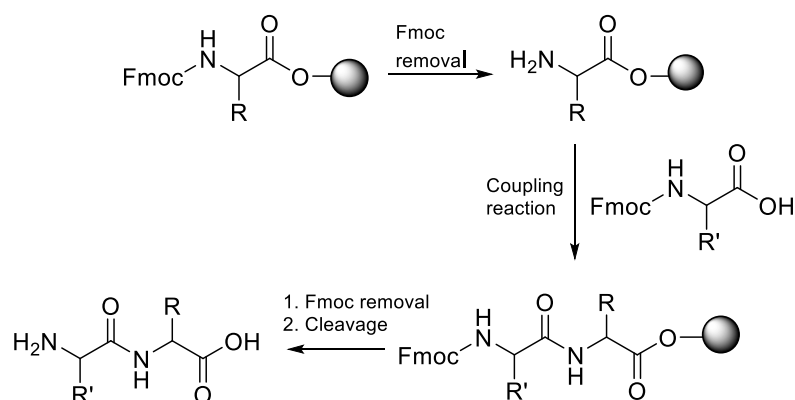


Figure 4: Schematic representation of a dipeptide synthesis on solid phase using Fmoc protecting groups.

The most commonly used temporary protecting groups for the *N*-terminal amino group are *tert*-butoxycarbonyl (Boc) group, which is sensitive to acids, eg. TFA, and the fluoren-9-ylmethylcarbonyl (Fmoc) group, sensitive to organic bases, eg. piperidine. The Fmoc group is nowadays preferred over Boc because it is removed under milder conditions and cleavage can be monitored by measuring the fluorescence of the resulting fluorenyl by-product shown in Figure 5. In addition, since many side chain protecting groups are removed under acidic conditions [39], piperidine reaction is specific only for α -amino group deprotection.

The main advantage of SPSS is that the excess of amino acids and reagents (base, coupling reagents) is simply washed with solvents dimethylformamide (DMF) and dichloromethane (DCM). However, despite washing with solvents, unwanted products from incomplete or side reactions can accumulate on the support and contaminate the final product. Therefore, there is always a need for additional purification of the final product.

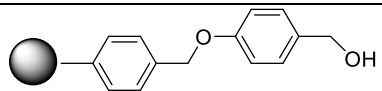
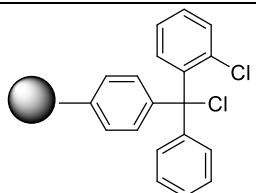
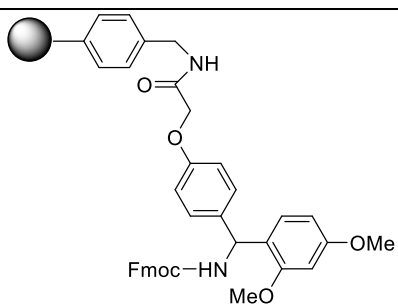
Side chain protecting groups.

Side chain functional groups have to be protected during synthesis in order to achieve better efficiency of reactions. In general, acid sensitive protective groups are more desirable because they can be removed with TFA during the cleavage step.

First amino acid attachment.

The procedure for the attachment of the first residue depends on the choice of resin and it is the most important step in the peptide synthesis. Resins typically used in SPPS have a matrix of polystyrene cross-linked with 1% divinylbenzene. They have a spherical shape and display a broad particle size distribution in the range of 75-150 μm and 37-75 μm . 1 % degree of cross-linking offers the best compromise between mechanical stability and swelling properties. A narrow particle size distribution is very important since the homogeneous size of the employed polymer particles is crucial for achieving uniform reaction conditions throughout each individual resin bead [42]. The examples of the most commonly used resins in Fmoc strategy SPPS include Wang resin, Rink amide/acid resin, Chlorotrityl chloride (CTC) resin (Table 1).

Table 1: Common Fmoc chemistry resin linkers.

Resin	Linker	Cleaved peptide	Reagents for cleavage
Wang resin		Peptide acid	TFA (scavengers)
2-Chlorotrityl resin		Protected peptide acid	DCM/Acetic acid: 9/1
Rink amide resin		Peptide carboxamide	TFA (scavengers)

The Fmoc group from the N-terminus of the resin-bound peptide chain is removed prior to the coupling of the next residue. This reaction is usually done with piperidine solution in DMF. The key step of the reaction is the fluorene ring deprotonation and the generation of aromatic pentadiene intermediate. This step is followed by fast elimination and dibenzofulvene formation, which is then scavenged by piperidine forming the adduct and thus preventing alkylation of the released amino group (Figure 5) [43].

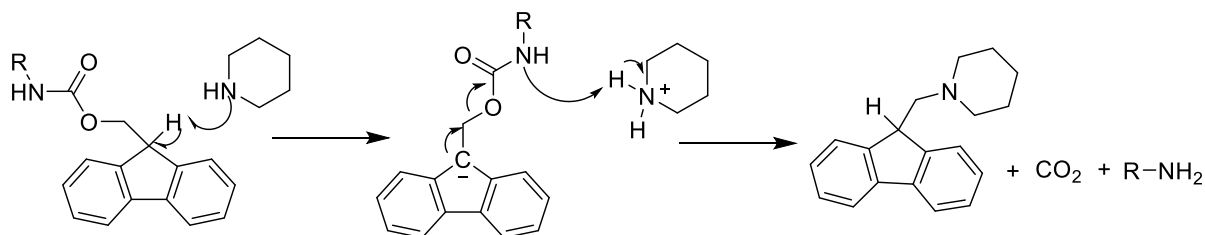


Figure 5: Mechanism of Fmoc deprotection reaction.

Coupling reaction.

This reaction is the introduction of N^{α} -protected amino acid. There are several commercially available coupling reagents, presented in Figure 6, that activate the carboxyl group of the incoming amino acid *in situ*. In order to increase the likelihood for a complete acylation, the incoming amino acid is used in excess, usually 2-10 fold over the resin functionality. The main advantage of this type of coupling reaction is that it is fast and done *in situ* using a small amount of organic solvent, usually DMF or DCM and a base, e.g. *N,N*-Diisopropylethylamine (DIPEA) [44, 45].

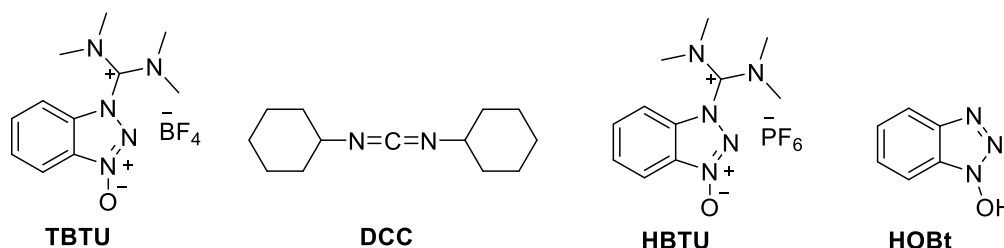


Figure 6: Common coupling reagents.

In this study, we used HOBt and HBTU coupling reagents since they are efficient and causing little racemization. The mechanism of N -acylation using HBTU is presented below (Figure 7). In the first step, base deprotonates the carboxylic acid and the resulting carboxylate attacks the electron deficient carbon atom of HBTU. Then the resulting anion reacts with the newly formed activated carboxylic acid derived intermediate to form an activated ester. In the last step, the amine reacts with the activated ester to form an amide bond.

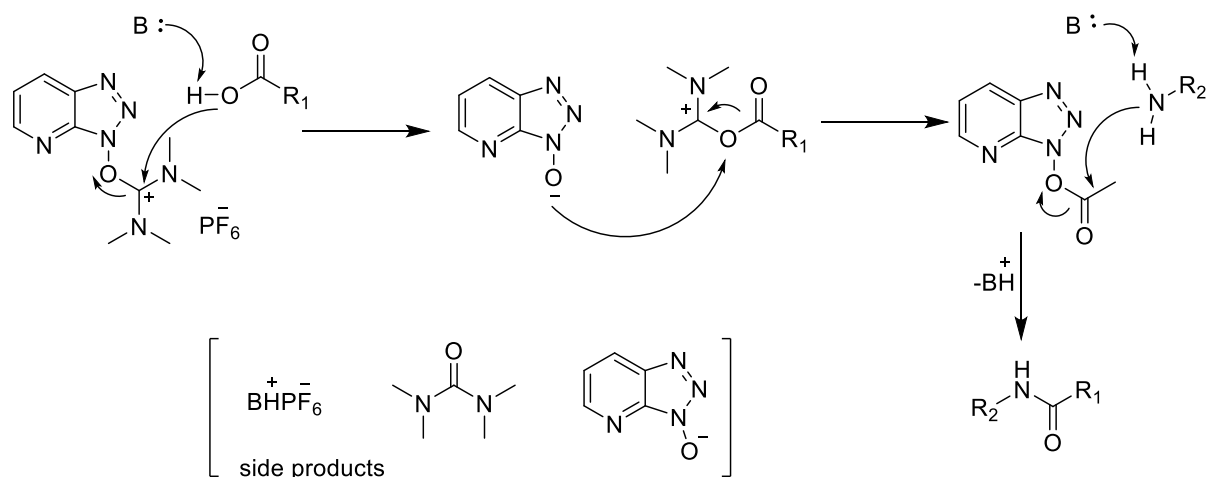


Figure 7: Mechanism of N-acylation using HBTU

Protein expression and purification. Overview

The production of recombinant proteins in microbial systems represented a key milestone in modern biochemistry. Large amounts of animal and plant tissues are no longer needed for protein production and the ability to express recombinant proteins in large quantity allows its full biochemical characterization. In addition, the production of recombinant proteins is widespread nowadays and it brought an enormous improvement in research and enabled their industrial and commercial use [46].

The host cell selection is essential when initiating the expression process and it will determine the molecular tools, equipment and reagents need for the procedure. Microbial host systems are: bacteria, yeast, filamentous fungi and unicellular algae. However, if eukaryotic post-translational modifications are present, a prokaryotic expression system may not be suitable [47] and eukaryotic cells such as epithelial cell lines CHO (Chinese hamster ovary cells) have to be used instead. Nevertheless, *Escherichia coli* (*E. coli*) is usually the preferred microbial cell factory and it is suitable for expressing stably folded, globular proteins from prokaryotes and eukaryotes up to 95 kDa [48]. A further advantage is represented by its fast growth kinetics and its doubling time is around 20 min in optimal growth conditions [49]. Furthermore, high cell density cultures are easily achieved and rich complex media can be made from commercially available and inexpensive components [46].

In the modern recombinant expression system, the expression is usually induced from a plasmid that had a system compatible genetic background. An expression plasmid has the following genetic elements: origin of replication, antibiotic resistance marker, transcriptional

promoters, translation initiation regions and transcriptional and translational terminators [50]. Nowadays, due to numerous commercially available systems and protocols, the protein production step is made much more convenient; however, protein purification still remains one of the challenges. The majority of purification steps can be integrated by high-performance liquid chromatography and the final purity of the protein can be optimized by using the most suitable column. Furthermore, characterization of the purified protein with e.g. SDS-PAGE analysis, UV absorption spectroscopy, inspection of gel filtration chromatogram, mass spectrometry, static or dynamic light scattering or measuring protein thermal stability is crucial in order to ensure that different batches of the same protein have comparable properties [51]. Finally, considering there is an immense variety of different proteins, there are many possible routes to obtain a high-quality protein and the whole process requires a fair amount of expertise.

Microscale thermophoresis (MST). Overview

MST is a rather new method that allows quantitative analysis of protein interactions in free solution. It is based on the physical principle of thermophoresis, which is induced by binding-caused changes of diverse molecular properties. The main advantages of MST in comparison to other biophysical techniques are the low sample consumption and short measurement times. MST is a useful technique for investigating various biochemical interactions such as: protein-protein interaction, protein-peptide interaction, membrane protein interactions and small molecule-enzyme binding. [52].

Sample preparation.

Fluorescence of one of the binding partners is essential for the detection of thermophoretic movement. The fluorescence source can originate from fluorescent label, attached on one binder, fluorescent fusion protein or protein intrinsic UV- range fluorescence (only in label-free instrument). In MST instruments that require labelling, visible light with three different types of LED filters (red, blue, green) is used for the fluorescence excitation, while in label free instruments, the wavelength for excitation is 280 nm and for emission 260 nm so that the intrinsic UV-fluorescence of proteins can be excited and detected.

In most cases, one of the binding partners has to be labelled prior to measurement. Most commonly used are crosslinker reactive groups, where the fluorescent dye is attached to the

crosslinker, which covalently binds the protein. It is possible to label the protein through lysine using *N*-hydroxysuccinimide (NHS) that binds the primary Lys amines on the *N*-terminus or through cysteine using maleimide dye that reacts with sulfhydryl groups of reduced Cys residues. Biomolecules usually contain more than one potential dye-binding site, however, it has been shown that the position of the fluorescent label doesn't affect the thermophoretic assay. Although fluorescent labels provide very high sensitivity of the measurement and sub-nM concentrations can be used, certain MST instruments allow also less sensitive, but label-free measurement. This type of measurement can be very useful in rare cases when the fluorescent label interferes with the binding as in the case of some membrane proteins, which are very sensitive to modifications. Label-free MST utilizes intrinsic protein fluorophores that originate from aromatic amino acids, tyrosine, phenylalanine and most importantly, tryptophan. The amount of protein required to obtain a measurable UV-fluorescence signal in a label-free MST is at least one degree of amplitude higher than when using labelled proteins. The affinity can be quantified up to $K_d \geq 50$ nM without label and as low as pM range when using a labelled protein [53].

In an MST experiment, the non-fluorescent binding partner is titrated over a constant concentration of the fluorescent partner. The samples are usually prepared as 1:1 mixtures of both partners and put into MST capillaries made from ultra-pure glass, which can have no coating, hydrophobic or hydrophilic polymer coating. Capillaries are placed on a temperature-controlled tray as shown in Figure 8. The lowest concentration of the titrated partner has to be sufficiently low to be able to measure the thermophoretic movement of the unbound state. On the other hand, the maximum concentration has to be higher than the expected binding affinity in order to be able to reach the saturation of the fully bound complex. It is usually recommended that the highest concentration of the titrated partner is 20-fold higher than the dissociation constant. [54]

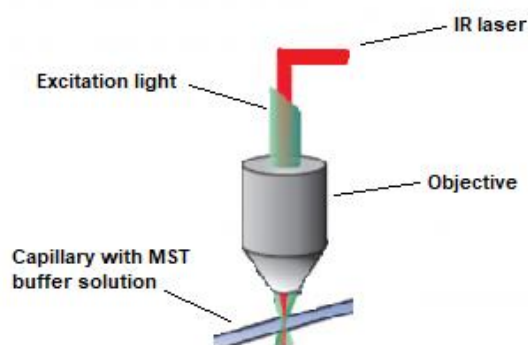


Figure 8: MST setup. The sample solution inside a capillary is placed on a sample tray and locally heated with an IR laser [52].

The principle of MST.

Thermophoresis (or thermodiffusion) is the directed movement of molecules along temperature gradients and it has been known for over 150 years [55]. It can be described as a molecular flow, which is directly proportional to the temperature gradient with the thermal diffusion coefficient.

$$j = -cD_T \text{ grad } T$$

J: molecular flow, c: molecule concentration, D_T : thermal diffusion coefficient, T: temperature.

In steady state, the thermophoretic flow is compensated by mass diffusion:

$$j = -D \text{ grad } T$$

D: diffusion coefficient.

The magnitude of thermodiffusion is determined by Soret coefficient, S_T , which is defined as the ratio of D and D_T .

$$S_T = \frac{D}{D_T}$$

Therefore, for a given spatial temperature difference the steady state concentration change is:

$$\frac{c_{hot}}{c_{cold}} = \exp(-S_T \Delta T)$$

c_{hot} : molecule concentration in the hot area, c_{cold} : molecule concentration in the cold area.

Given that the buffer conditions, size of thermophoresis probes charge, solvation entropy and molecules conformation are constant, thermophoretic depletion is dependent on the interface between molecule and solvent. Since at least one of these parameters is usually affected by biomolecular binding events, thermophoresis can be used as a powerful all-optical tool for the quantification of biomolecular affinity. [52, 56]

MST instruments excite the molecules with an infrared (IR) laser with a wavelength of 1480 nm. The water from the sample absorbs the heat from the laser and a localized temperature gradient is formed. IR radiation is focused precisely on the spot where the fluorescence is measured before, during and after the laser is turned on. Before heating with the laser, the initial fluorescence (Figure 9, region I) is measured and it should be constant for all samples. Once the IR laser is turned on, there is a sudden change in fluorescence intensity, called temperature (T) jump (Figure 9, region II). This temperature-dependent change of fluorescence is sensitive to the fluorophore's local environment and therefore can be influenced by conformational changes or binding close to that area. The fast heating by the IR laser and the T-jump occur at a very short timescale of several 100 ms. Hence, it can be easily distinguished from the

following slower, diffusion-limited thermophoresis (Figure 9, region III), which lasts several seconds. The thermophoretic motion generates a concentration gradient of fluorophores until the plateau is reached. In this fluorescence intensity steady state, thermodiffusion is counterbalanced by mass diffusion. In the next step of the measurement, the IR laser is turned off and the sample is cooled off due to the immediate fluorescence recovery. This phase is called inverse T-jump (Figure 9, region IV) and it occurs due to the fluorophore's temperature dependence. Lastly, mass diffusion driven back diffusion (Figure 9, region V) leads to the compensation of the concentration gradient and the measurement is concluded. [57]

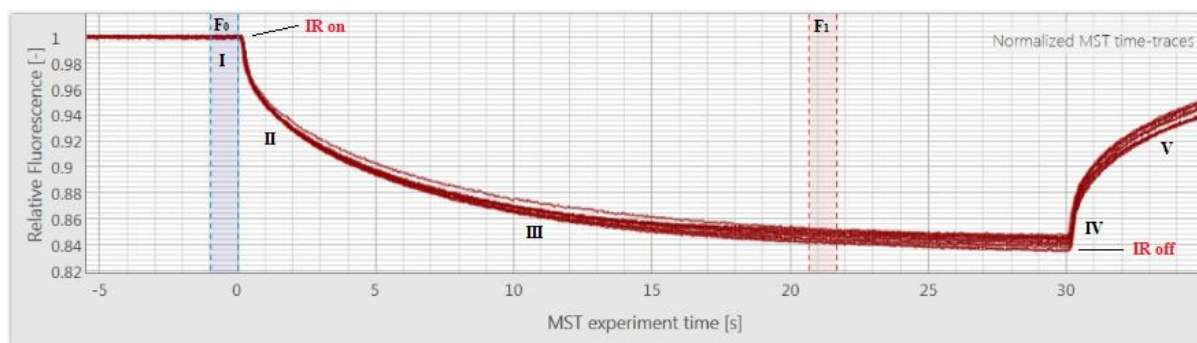


Figure 9: Graphic presentation of the fluorescence time trace measurement recorded by MST instrument.

In MST measurement, the binding is quantified using relative fluorescence, where F_1 is the fluorescence measured several second after turning on the heating laser and the traces of unbound and bound state can be discriminated. F_0 corresponds to the initial fluorescence or the fluorescence after the T-jump.

$$F_{norm} = \frac{F_1}{F_0}$$

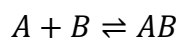
F_{norm} : normalized fluorescence; F_1 : fluorescence after thermodiffusion; F_0 : initial fluorescence or fluorescence after T-jump.

Binding affinity is quantified by analysing the change in F_{norm} as a function of the concentration of the titrated binding partner, usually ligand. Given that the thermophoretic movement of bound and unbound state superpose linearly, the bound fraction (FB) is described by:

$$F_{norm} = (1 - FB)F_{norm,unbound} + (FB)F_{norm,bound}$$

FB: fraction bound, $F_{norm, unbound}$: normalized fluorescence of the unbound state, $F_{norm, bound}$: normalized fluorescence of the bound state.

In most cases, a simple model according to the law of mass action can be applied to describe the binding event. The binding process of a partner A and a partner B leading to the formation of the complex AB is described by:



A: binding partner A; B: binding partner B; AB: bound complex of binding partners A and B.

The binding affinity is quantified by the equilibrium dissociation constant, K_D , defined as:

$$K_D = \frac{[A]_{free}[B]_{free}}{[AB]}$$

K_D : equilibrium const.; $[A]_{free}$: concentration of free partner A; $[B]_{free}$: concentration of free partner B; $[AB]$: concentration of bound complex of A and B.

Since the free concentrations are not known, total concentrations are used. Total concentrations of A and B are defined as follows:

$$[A] = [A]_{free} + [AB]$$

$$[B] = [B]_{free} + [AB]$$

Therefore,

$$K_D = \frac{[A]_{free}[B]_{free}}{[AB]} = \frac{([A] - [AB])([B] - [AB])}{[AB]}$$

If A is the titrated partner and B is the partner with fluorophore and const. concentration, the following equation has to be solved in order to obtain the K_D :

$$FB = \frac{[AB]}{[B]} = \frac{[A] + [B] + K_D - \sqrt{([A] + [B] + K_D)^2 - 4[AB]}}{2[B]}$$

In the graphic representation of the MST measurement, F_{norm} is plotted on y-axis (per mil scale) and the concentration of the titrated partner x-axis (log10 scale). In this semi-log plot the binding curve should have a characteristic s-shape or mirrored s-shape.

b) DESIGN

Evidence from crystallographic Protein Data Bank (PDB) data revealed a possible auto-regulatory 10-residue-long domain at the *N*-terminus, forming a secondary β -hairpin structure. Multiple crystal structures have indicated the interaction of this domain with the part of the phosphatase domain in the close proximity to the phosphatase catalytic site. Further experimental studies confirmed the potential auto-regulatory activity of this region by sequence splicing; an approximate 10-fold increase in phosphatase/kinase activity ratio was observed for the *N*-terminus-truncated wild type liver PFKFB isoform [58].

The leading design idea was therefore to focus on perturbing the interaction between the PFKFB3 auto-regulatory domain (AD) and the phosphatase domain to indirectly achieve diminished kinase activity.

In order to test this idea, a preliminary study was introduced based on the hypothesis that there might be an equilibrium between the AD bound to the phosphatase and the other with the AD unbound. In the unbound condition, a synthetic β -hairpin mutated peptide would act as a competitor of the AD. An alanine-scan was performed prior to the mutation in order to determine important amino acid residues in the β -hairpin region (Figure 10). *In silico* simulations suggested that mutations of AD Ile12 to a positively charged (Arg or Lys) or aromatic ring-containing (Trp or Tyr) amino acid could significantly increase the binding affinity on the truncated protein (protein without the AD) and conversely, a mutation of Trp13 to Asp would have the opposite effect. Moreover, two alpha helices in close proximity to the AD were proposed for binding experiments with the AD. A library of peptides, **AD and its synthetic analogues**, suggested for synthesis and binding evaluation is presented in Table 2 in the following section. However, at this point it should be stressed that this study was preliminary and the idea of using a truncated variant of the protein was suitable merely as a benchmark for the computational screening. Any eventually identified compound would have been useful only as a probe to verify the mechanism and not as a real phosphatase activator since the truncated PFKFB3 is not the protein's physiological state.

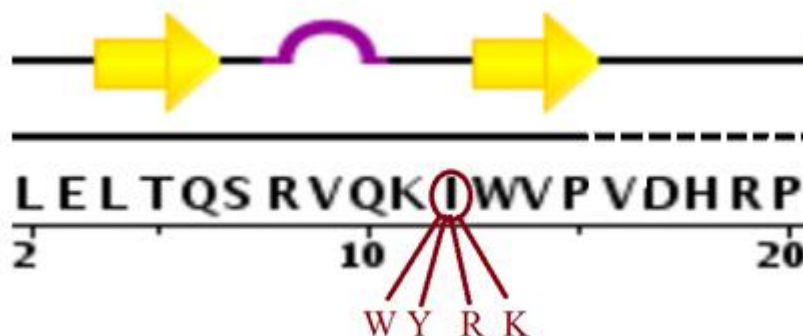


Figure 10: Sequence of the wild type AD with the target point of modification.

Furthermore, two strategies have been devised for the design of potential **phosphatase modulators** that would target the proposed interference with the β -hairpin-shaped PFKFB3 AD:

i) the initial strategy was to target the AD binding site for direct blockage of the interaction between the AD and phosphatase domain (Figure 11A). This process would necessarily involve the initial insertion of the designed molecule in between the auto-regulatory domain and the phosphatase domain, followed by the disturbance of interactions. However, from the first strategy, virtual screening, we observed that all ligands targeting the exposed binding site have a very high solvent exposure due to a relatively shallow cavity of the binding site of interest. This property resembles a typical protein-protein interaction surface, which could be problematic when the ligand is a small molecule because high solvent exposure can lead to a high entropic penalty from ligands and solvent upon binding. Furthermore, during initial virtual screening using a large docking sphere, we noticed that most of the high scored ligands moved into a secondary pocket near to the intended β -hairpin binding site, which is right at the interface of the two monomers. Additional visual inspection and analysis proposed that this secondary binding site could have the potential to stabilize the ligand binding in close proximity to the β -hairpin region and hence, an alternative strategy was suggested.

ii) the leading idea of the second strategy is to target a channel like space adjacent to the binding site and located in between the two monomers (Figure 11B). This channel is highly negatively charged and has multiple polar amino acid residues such as Lys318, Glu360, Gln367 and Glu370. Furthermore, the insertion of a ligand in this space might lead to binding destabilization of the β -hairpin domain.

Two libraries of compounds, one for each strategy, were generated from ZINC database (a free database of commercially available compounds for virtual screening) in order to select molecules that would potentially interfere with auto-regulatory activity of the targeted domain. Any compounds targeting kinase were manually removed in order to prevent the PFKFB3 kinase site interference. The selection of top ranked ligands from the libraries of preselected compounds was achieved according to docking scores by adding molecules that have good molecular interactions, which means that there is a high number of interaction pairs and low interaction energy using force field based evaluation. Some of the highly ranked molecules appeared on searches for both strategies. 9 highly ranked peptides (see Table 3 in the Results section; detailed list in the Appendix, p. 123-126) were selected for synthesis and 4 compounds were purchased (see Table 6; detailed list in the Appendix, p. 123-126).

Since our capacity for synthesis was limited and ZINC database offers compounds from multiple vendors, where not all of them were available, we decided to screen also a library of easily accessible commercial compounds. Asinex commercial libraries were screened and 12 top-ranked molecules were chosen for *in vitro* experiments (see Table 7). Asinex library was chosen for screening because it is a commercial library and a small amount of each compound can be easily purchased from Asinex company for an *in vitro* test. By buying 12 top-ranked compounds from the virtual screening, we wanted to increase the probability of finding a compound that binds.

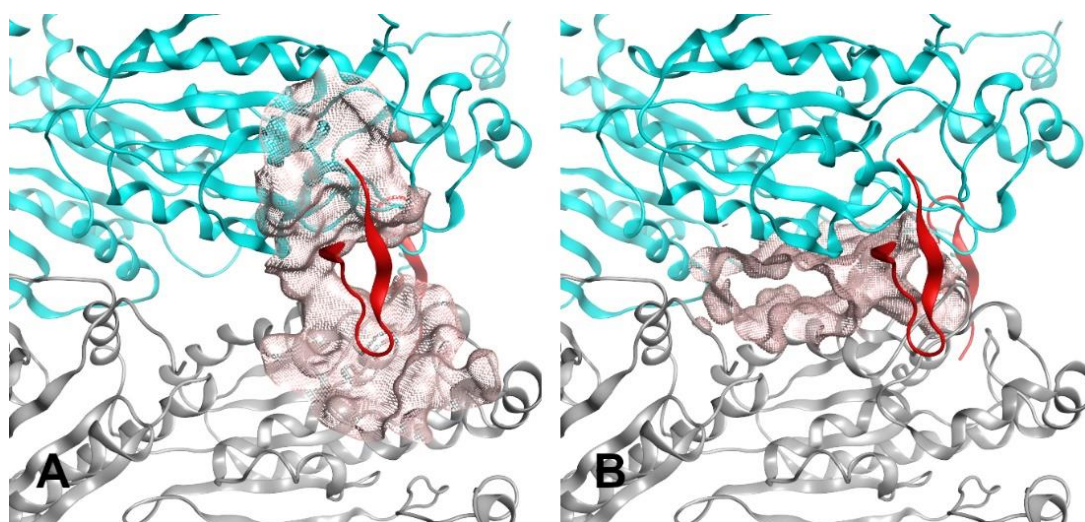


Figure 11: The molecular surfaces of the targeted binding sites (shown in pink). A: the binding surface of the auto-regulatory domain. B: the secondary binding site (negatively charged channel) close to the auto-regulatory domain.

Finally, an optimization attempt in terms of improving binding poses in the binding pocket by overlapping poses between the binding peptides was performed in order to see if any amino acid could be replaced. In the case two amino acids were roughly overlapping with each other, the smaller amino acid was changed to a larger one (e.g. Ile to Tyr or Trp) to obtain a new peptide. In addition, docking studies were performed on the new peptide list and the modified sequences were selected according to the scoring outcome and poses they adopted. Finally, 16 peptides, analogues of the best binding peptides from the ZINC library, were selected for synthesis and binding evaluation and are presented in Tables 4 and 5 in the following section.

c) RESULTS

i) Synthesis- SPPS

AD and its synthetic analogues.

Eight peptides, suggested from the preliminary screening strategy, described on p. 27 were synthesized on Wang resin using SPPS (Table 2). After purification and characterization they were used for the secondary structure determination and binding affinity assay.

Table 2: AD and its synthetic analogues.

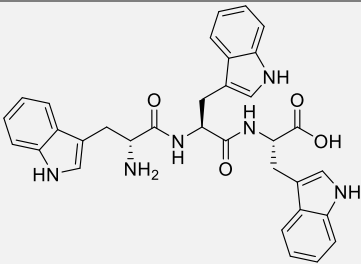
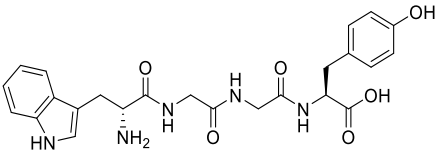
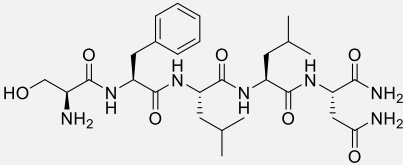
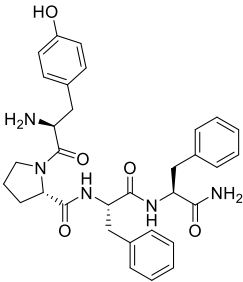
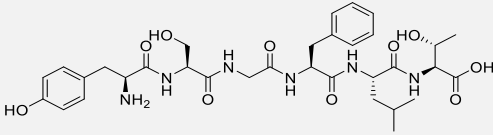
NAME (SEQUENCE)	STRUCTURE	MW
HM-4 (WILD TYPE)	LTQSRVQKIWVPV	1553.85
HM-5 (A12 HELIX)	LKSTIQTAEALRLPYEQW	2147.44
HM-6 (A16 HELIX)	PEEYALREQDKYYRYPTG	2441.62
HM-7 (I12W)	LTQSRVQKWWVPV	1626.92
HM-8 (I12Y)	LTQSRVQKYWVPV	1603.89
HM-9 (I12R)	LTQSRVQKRWVPV	1596.90
HM-10 (I12K)	LTQSRVQKKWVPV	1568.88
HM-11 (W13D)	LTQSRVQKIDVPV	1482.74

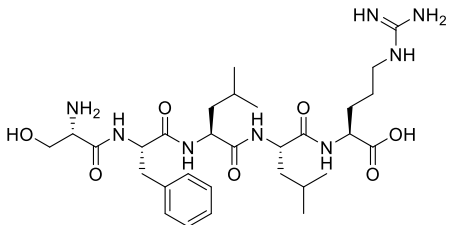
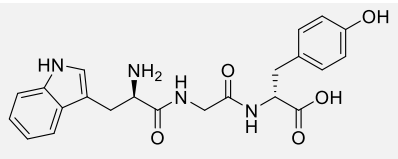
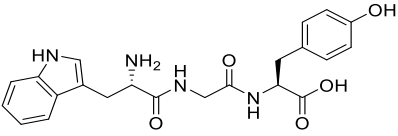
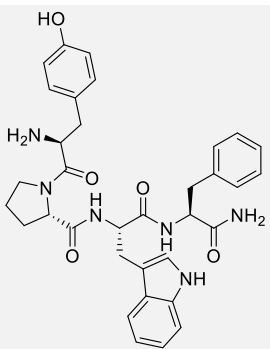
Phosphatase activity modulators.

Peptides were synthesized on Wang or Rink amide resin depending on the desired C-terminal part (free acid or carboxamide). Standard SPPS protocols were applied for the synthesis and peptides were purified with preparative HPLC and characterized.

According to the results of virtual screening of ZINC library using previously described strategies 1 and 2 (p. 27-28), a series of 9 small peptides was prepared (Table 3).

Table 3: Small peptides selected from design strategies 1 and 2.

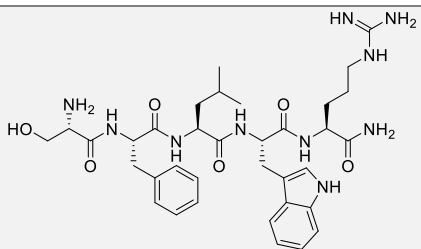
PEPTIDE	SEQUENCE	STRUCTURE	MW	STRATEGY
HM-15	wWW		576.64	1/2
HM-16	wGGY		481.50	1/2
HM-18	SFLLRN- CONH ₂		747.89	1/2
HM-19	YPFF- CONH ₂		571.67	1/2
HM-20	YSGFLT		686.75	1/2

HM-21	SFLLR- CONH ₂		633.80	2
HM-22	wGy		424.45	1/2
HM-27	WGY		424.45	1/2
HM-28	YPWF- CONH ₂		610.70	2

A further optimisation of the best binding compounds according to MST experiments (MST results are presented in the section Binding assay on p. 38) was performed and the following peptides, presented in Tables 4 and 5, were synthesized using SPPS. The synthesized peptides were divided into 2 groups:

a) *HM-21 analogues*

Table 4: HM-21 analogues.

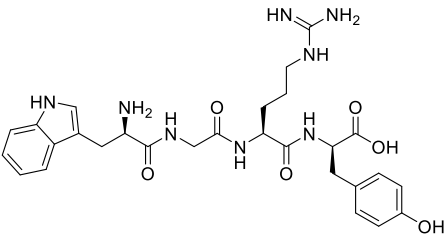
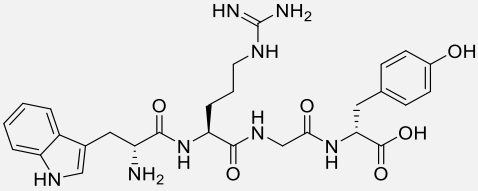
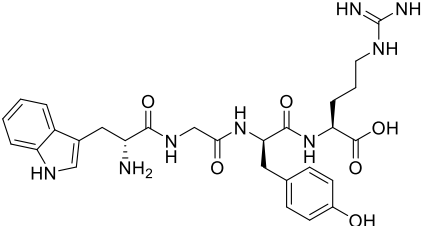
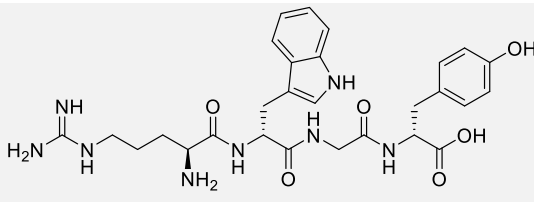
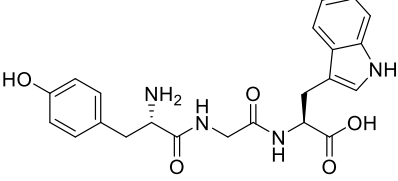
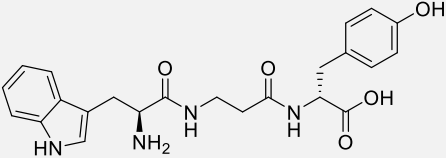
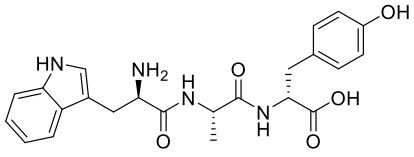
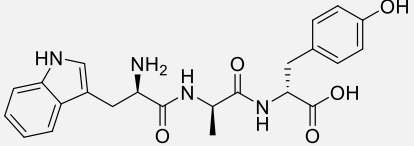
PEPTIDE	SEQUENCE	STRUCTURE	MW
HM-38	SFLWR-CONH ₂		706.82

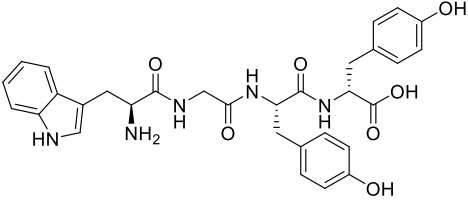
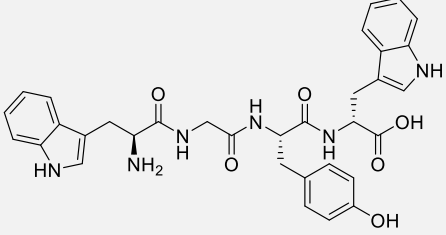
HM-39	SFLYR-CONH ₂		683.80
HM-41	SYLLR-CONH ₂		649.78
HM-42	SWLLR-CONH ₂		672.81
HM-63	SFWL-CONH ₂		550.63

b) *HM-22 analogues*

Table 5: HM-22 analogues.

PEPTIDE	SEQUENCE	STRUCTURE	MW
HM-32	wRy		523.58

HM-34	wGRy		580.63
HM-35	wRGy		580.63
HM-50	wGyR		580.63
HM-51	RwGy		580.63
HM-53	YGW		424.45
HM-54	Wβ-Ay		438.48
HM-55	wAy		438.48
HM-56	way		438.48

HM-64	WGYy		587.62
HM-65	WGYw		610.66

Commercial compounds from ZINC and Asinex.

4 small molecule compounds selected from the ZINC library (Table 6) and 12 small molecules selected from the Asinex library (Table 7) were purchased.

Table 6: Commercially available compounds from ZINC library selected from design strategies 1 and 2.

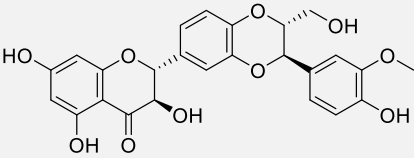
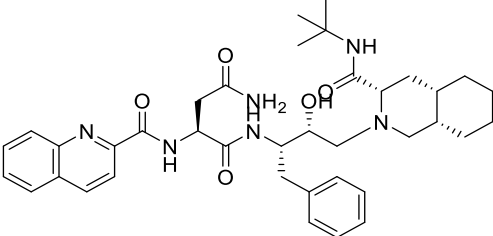
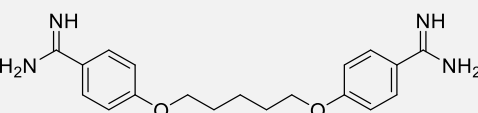
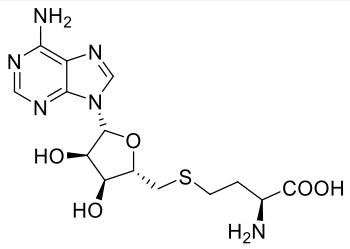
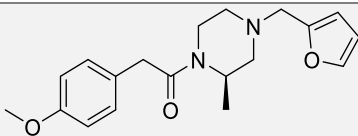
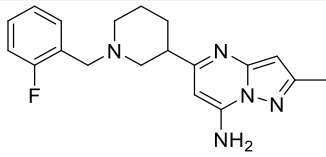
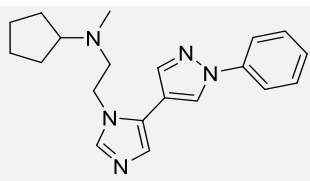
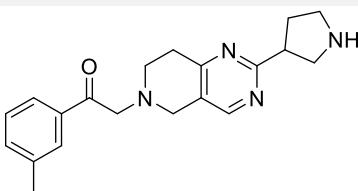
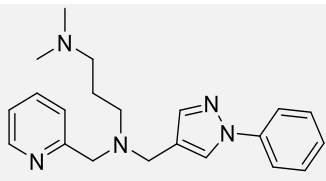
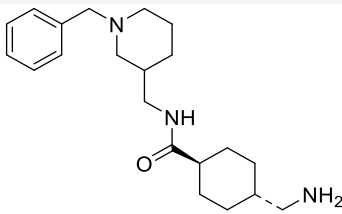
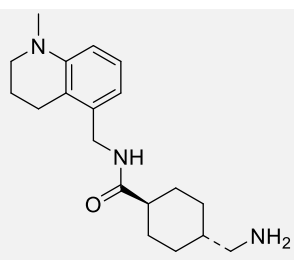
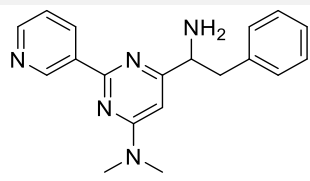
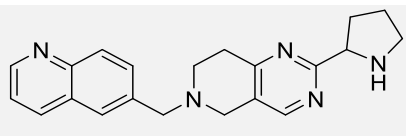
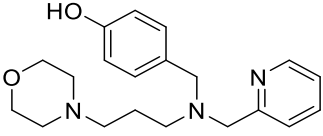
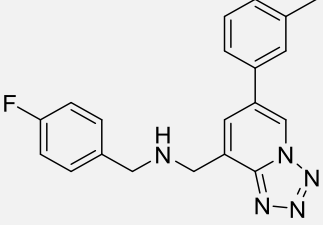
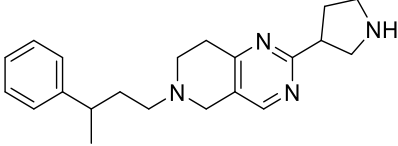
COMPOUND	STRUCTURE	MW	STRATEGY
SILIBININ		482.44	1/2
SAQUINAVIR		670.86	1
PENTAMIDINE		340.43	1/2
S-ADENOSYL-L-HOMOCYSTEINE		384.41	1

Table 7: Commercially available compounds from Asinex library.

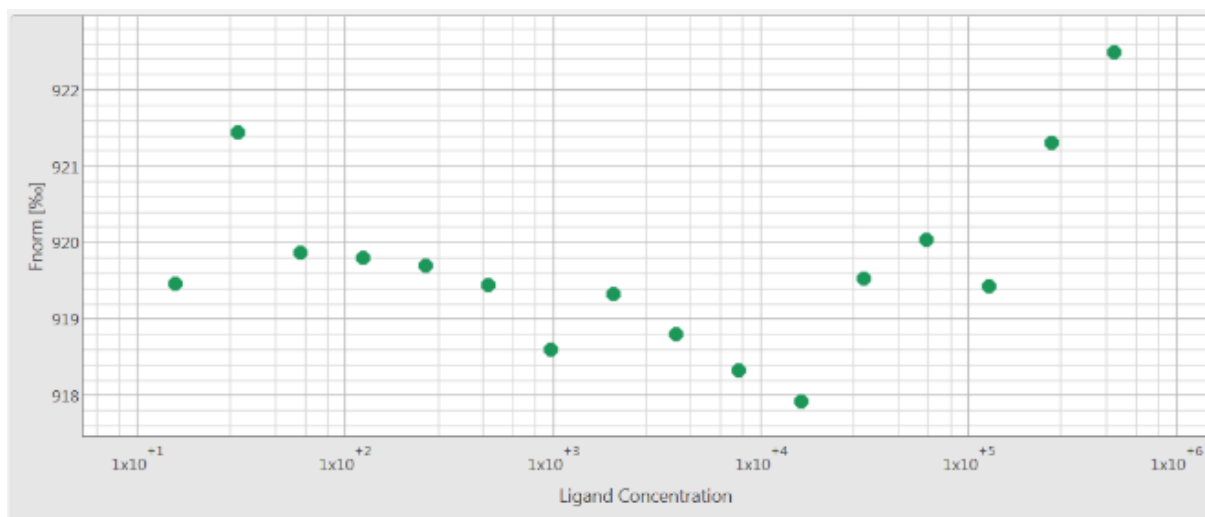
COMPOUND	STRUCTURE	MW	STRATEGY
AAM 12251247		328.41	1/2
SYN 14225500		339.42	1/2
SYN 23714454		335.46	1/2
SFA 21712810		336.44	1/2
LEG 15398864		394.48	1/2
SYN 18382510		343.52	1/2
SYN 18382508		315.46	1/2
AOP 22837785		319.41	1/2
SFA 21712893		345.45	1/2

SYN 15028165		341.46	1/2
LMG 14809313		347.40	1/2
SFA 21721813		336.48	1/2

ii) Binding assay- microscale thermophoresis

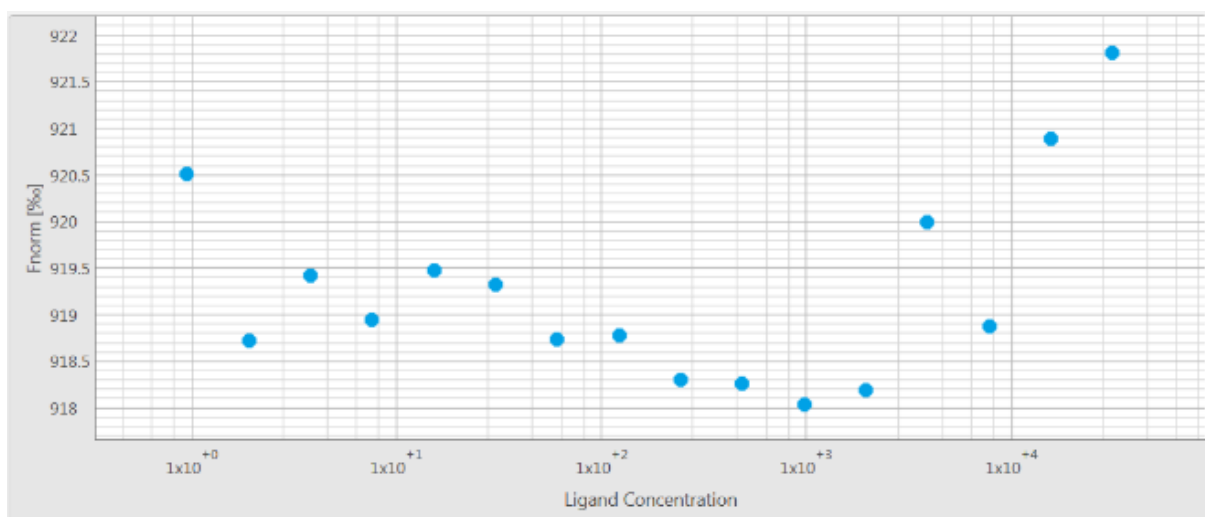
AD and its synthetic analogues.

Virtual experiments on the truncated protein showed that Ile12 mutation to a positively charged/aromatic amino acid residue should affect the binding affinity. However, this variant of the protein was not available for experimental studies and the binding affinity assay was performed on the intact protein. Unfortunately, the mutated synthetic peptides were unable to bind the intact protein and we were not able to confirm our preliminary hypothesis. Below are shown the results for the wild type AD and one of the mutated synthetic analogues (Figures 12 and 13, respectively). Clearly, there is no evidence of binding for the tested concentration range. The signal to noise ratio and response amplitude of the measurement are too low to detect any evidence of binding.



PARAMETER	RESULT
KD	failed
RESPONSE AMPLITUDE	failed
STANDARD ERROR	failed

Figure 12. MST result for the wild type AD.



PARAMETER	RESULT
KD	failed
RESPONSE AMPLITUDE	failed
STANDARD ERROR	failed

Figure 13. MST result for I12R mutated AD.

Phosphatase modulators.

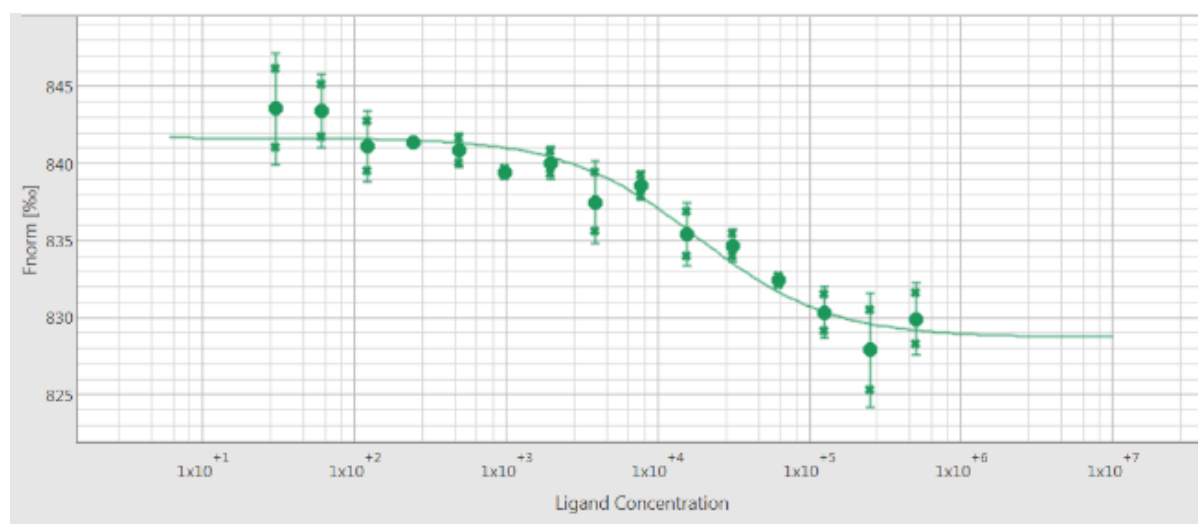
All compounds from Tables 3-7 (25 peptides and 16 commercial compounds) were tested for the binding affinity for PFKFB3 and 3 peptides were found to bind the protein in micromolar range (Table 8, orange region). The binding affinity was determined for at least 2 independent measurements carried out on different days but under the same experimental conditions. **HM-22** (Figure 14) showed the best affinity towards the target (3 μM), **HM-20** (Figure 15) had the affinity of 18 μM and **HM-21** (Figure 16) 44 μM . Interestingly, **HM-18**, a **HM-21** analogue with an additional Asn and **HM-27**, a stereoisomer of **HM-22** had no affinity towards the target. This information encouraged us to prepare **HM-21** (Table 8, blue region) and **HM-22** analogues (Table 8, yellow region) and evaluate their binding affinity. Unfortunately, the analogues were unable to bind, which could be explained with the fact that their side chains do not form additional interactions in the binding site or they are unable to adopt a proper binding pose. In addition, all commercial compounds selected from ZINC and Asinex library (Table 9) showed no binding affinity towards the target. Therefore, we decided to focus on binding peptides **HM-20-22** and their additional biological evaluation.

Table 8: PFKFB3 binding results for selected peptides.

NAME	SEQUENCE	K _D (μM)
HM-15	wWW	No binding
HM-16	wGGY	No binding
HM-18	SFLLRN	No binding
HM-19	YPPF	No binding
HM-20	YSGFLT	18 ± 1
HM-21	SFLLR-CONH ₂	44 ± 3
HM-22	wGy	3 ± 1
HM-28	YPWF- CONH ₂	No binding
HM-38	SFLWR-CONH ₂	No binding
HM-39	SFLYR-CONH ₂	No binding
HM-41	SYLLR-CONH ₂	No binding
HM-42	SWLLR-CONH ₂	No binding
HM-63	SFWL-CONH ₂	No binding
HM-27	WGY	No binding
HM-32	wRy	No binding
HM-34	wGRy	No binding
HM-35	wRGy	No binding
HM-50	wGyR	No binding
HM-51	RwGy	No binding
HM-53	YGW	No binding
HM-54	Wβ-Ay	No binding
HM-55	wAy	No binding
HM-56	way	No binding
HM-64	WGYy	No binding
HM-65	WGYw	No binding

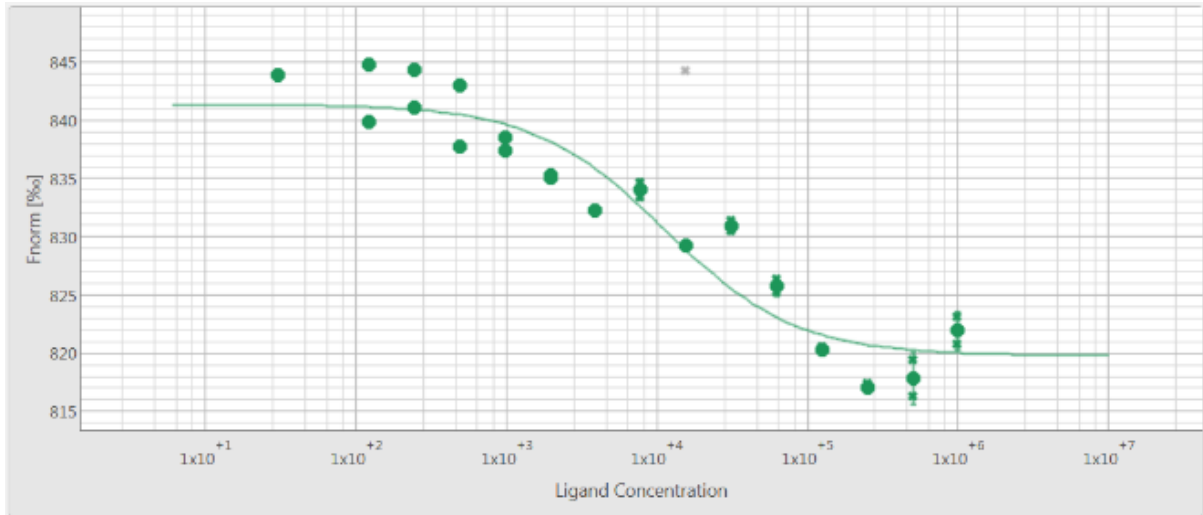
Table 9: PFKFB3 binding results for selected commercial compounds.

COMPOUND	K_D (μ M)
SILIBININ	No binding
SAQUINAVIR	No binding
PENTAMIDINE	No binding
S-ADENOSYL-L-HOMOCYSTEINE	No binding
AAM 12251247	No binding
SYN 14225500	No binding
SYN 23714454	No binding
SFA 21712810	No binding
LEG 15398864	No binding
SYN 18382510	No binding
SYN 18382508	No binding
AOP 22837785	No binding
SFA 21712893	No binding
SYN 15028165	No binding
LMG 14809313	No binding
SFA 21721813	No binding



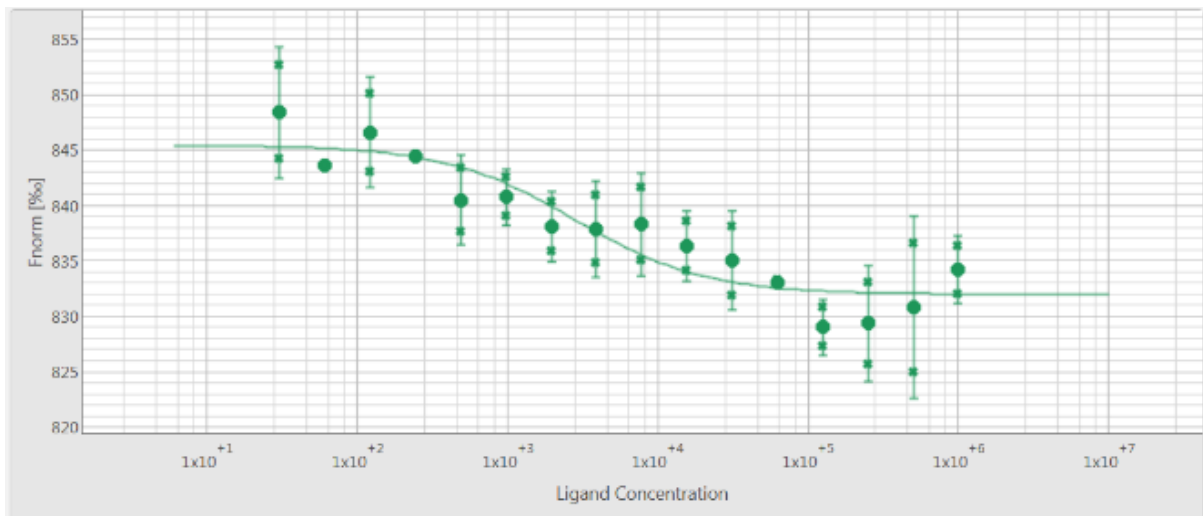
PARAMETER	RESULT
KD	18.299 nM
RESPONSE AMPLITUDE	12.9514
STANDARD ERROR	1.2809

Figure 14: Binding affinity profile for peptide HM-20.



PARAMETER	RESULT
KD	44.366 nM
RESPONSE AMPLITUDE	21.7952
STANDARD ERROR	2.6667

Figure 15: Binding affinity profile for peptide HM-21.



PARAMETER	RESULT
KD	2.7892 nM
RESPONSE AMPLITUDE	13.4474
STANDARD ERROR	1.4594

Figure 16: Binding affinity profile for peptide HM-22.

iii) Conformational analysis with circular dichroism (CD) and dynamic light scattering (DLS)

AD and its synthetic analogues.

CD conformational experiments were carried out for the wild type AD (Figure 17) and synthetic analogues of AD including the mutated sequences with a positively charged/aromatic amino acid residue (Figures 18 and 19).

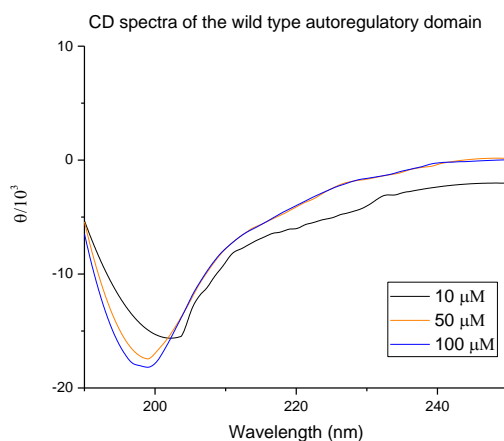


Figure 17: CD spectrum in the 190–250 nm region of different concentration of the wild type AD. The ellipticity is expressed as mean residue molar ellipticity.

As described previously, virtual experiments showed that Ile12 is an important amino acid residue and we aimed to see the effect of its replacement with another residue on the secondary structure of the peptide. The CD experiments were carried out for three different concentrations of each peptide.

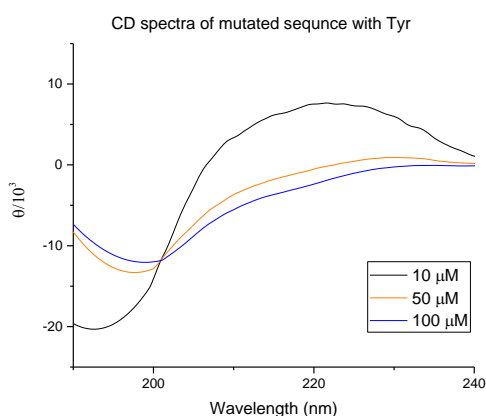


Figure 18: CD spectrum in the 190–240 nm region of the I12Y mutated AD. The ellipticity is expressed as mean residue molar ellipticity.

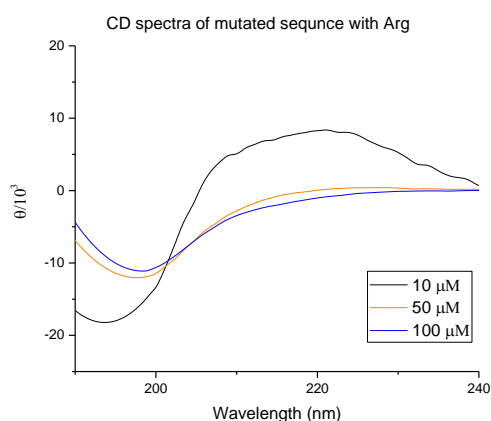


Figure 19: CD spectrum of the I12R mutated AD.

From Figures 17-19 it is evident that: *i*) the wild type sequence forms an unordered structure, while modified peptides form a more ordered β -hairpin; *ii*) there are differences in the CD spectra with increasing concentration, that can be an evidence for aggregation.

Furthermore, in order to calculate the ordered and unordered secondary structure content of peptides of interest, Dichroweb [59, 60] was used. Dichroweb is a web server, accessible upon free registration that enables on-line analyses of CD spectroscopic data and calculates protein/peptide secondary structure content as well as provides graphical analysis comparing experimental data and calculated structures.

The results (Table 10) show that the differences in CD spectra of different concentrations of the wild type sequence are not due to the change of the folding. Conversely, a change in the folding occurs for modified sequences when the concentration is raised by the factor of 10.

Table 10: Dichroweb presentation of results.

NAME	CONCENTRATION	HELIX	STRAND	TURN	UNORDERED
HM-4	10 μ M	3.0 %	8.8 %	12.1 %	66.5 %
	100 μ M	3.1 %	7.5 %	12.0 %	69.1 %
HM-8	10 μ M	10.0 %	11.0 %	15.3 %	42.5 %
	100 μ M	2.88 %	10.1 %	19.3 %	39.1 %
HM-9	10 μ M	4.5 %	20.7 %	19,9 %	38.0 %
	100 μ M	2.1 %	19.5 %	39.0%	40.0%

Since CD data suggested there might be aggregation at higher peptide concentrations (50-100 μ M), DLS experiments were done for the wild type and modified sequences. As shown below, the wild type sequence (Figure 20A) is a poly-dispersed sample in the DLS range analysis, while the modified sequences are less poly-dispersed. The modified sequence with Tyr (Figure 20B) is less stable (no reproducible results), whereas the modified sequence with Arg forms less poly-dispersed unstable nanoaggregates with dimensions in the 250-300 nm range.

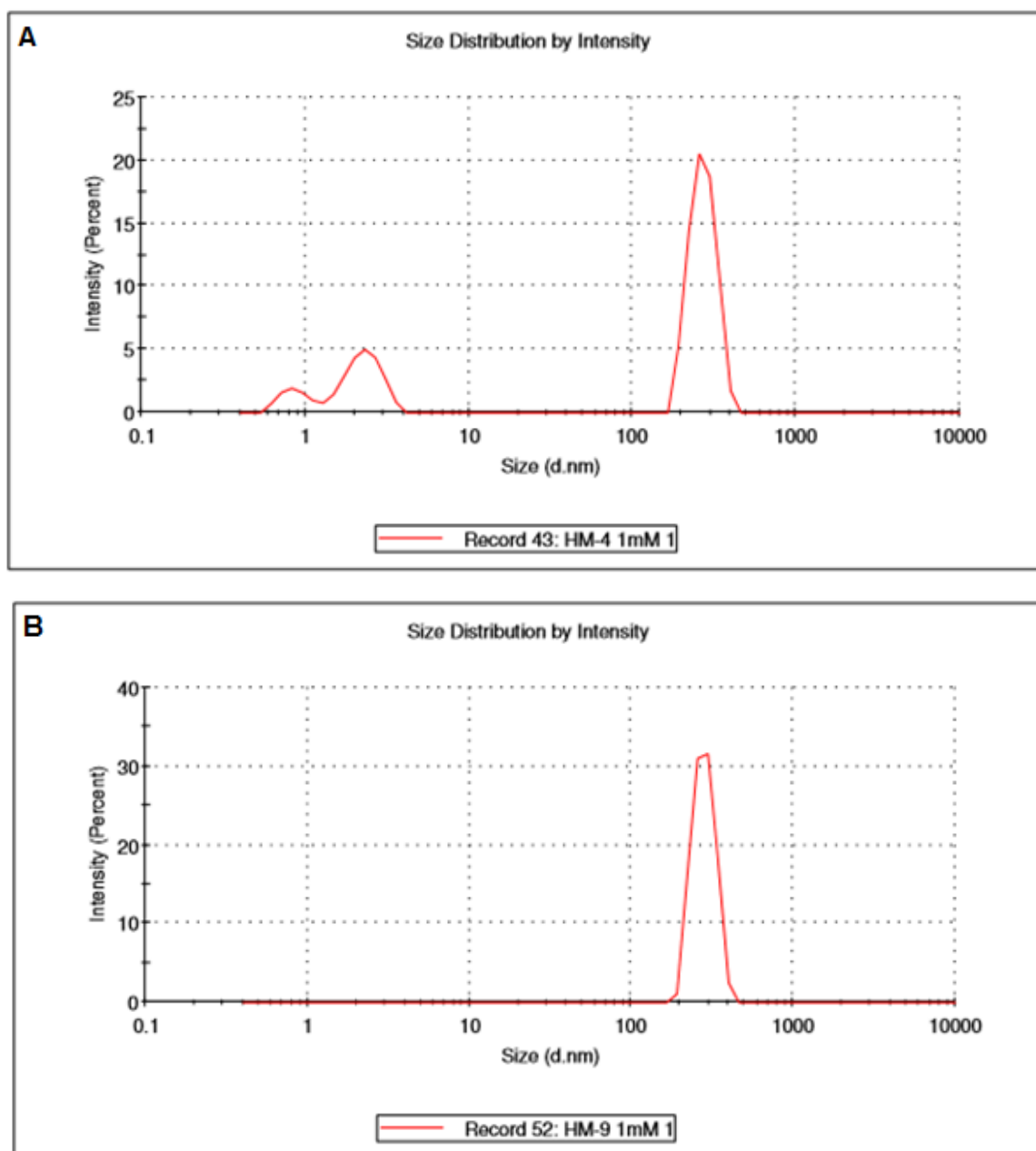


Figure 20: DLS analysis of the wild type domain (part A) and the I12R modified AD sequence (part B).

From the CD and DLS experiments we were able to get substantial information regarding the secondary structure of the synthetic wild type β -hairpin shaped AD and its mutated analogues. Both techniques confirmed aggregation, which was concentration dependent for all tested samples. In addition, the analysis of CD results with Dichroweb showed that the modification of amino acid Ile to Arg and Tyr switches the system from an unordered to a more ordered one.

Phosphatase modulators.

Conformational analysis experiments were carried out for the best binding compounds according to MST results (presented in the previous section). The CD experiments were carried out for 50 μM peptide concentration in 50 mM phosphate buffer (PBS) or with addition of 50% trifluoroethanol (TFE).

CD spectrum of peptide **HM-20** (Figure 21) shows a random coil when the peptide is in PBS and a tendency to assume β -sheet conformation, when 50% TFE was added.

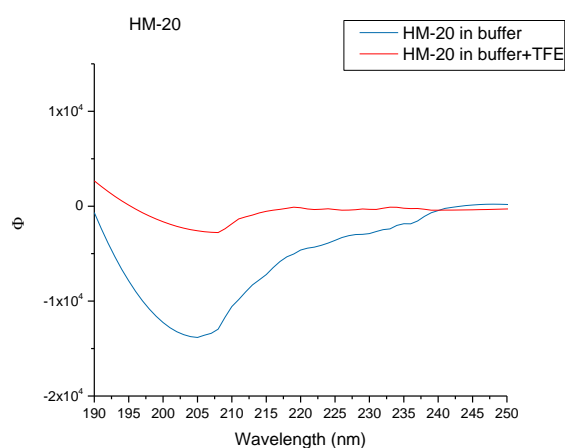


Figure 21: CD spectrum in the 190–250 nm region 50 μM peptide HM-20 in PBS or PBS and 50 % TFE. The ellipticity is expressed as mean residue molar ellipticity.

CD spectrum of peptide **HM-21** (Figure 22) shows a random coil when the peptide is in PBS and a slight β -sheet conformation, when 50% TFE was added.

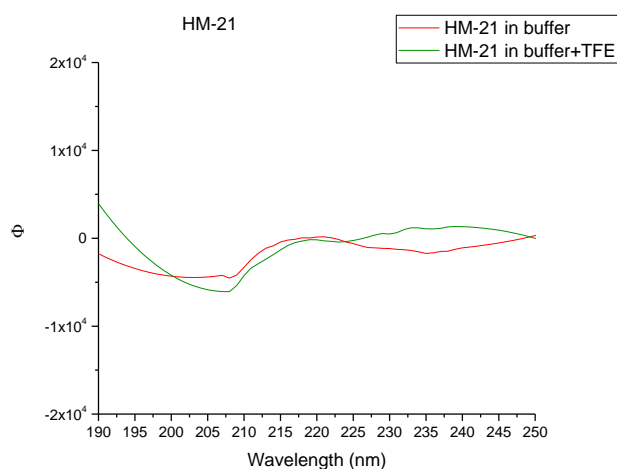


Figure 22: CD spectrum in the 190–250 nm region of 50 μM peptide HM-21 in PBS or PBS and 50 % TFE. The ellipticity is expressed as mean residue molar ellipticity.

Peptide **HM-22** (Figure 23) is a random coil in PBS, even when 50% TFE was added. Due to the aromatic moieties, CD is not a suitable technique for the conformational analysis of peptide **HM-22**.

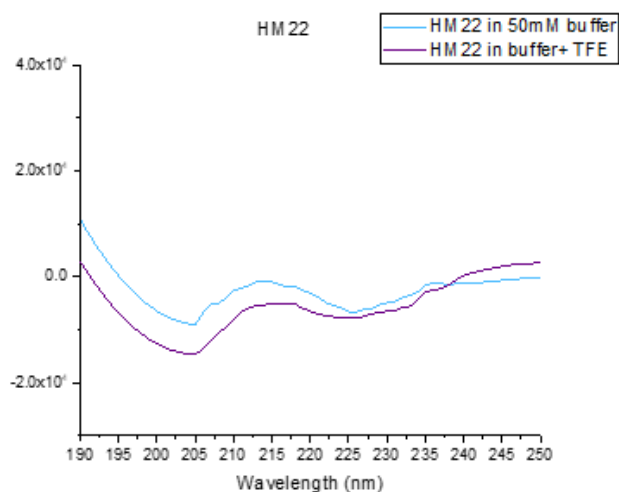


Figure 23: CD spectrum in the 190–250 nm region of 50 μ M peptide HM-22 in PBS or PBS and 50 % TFE. The ellipticity is expressed as mean residue molar ellipticity.

iv) Kinase activity assay

All compounds were tested in order to experimentally confirm that they do not have any effect on the PFKFB3 kinase activity and that the effect observed *in vitro* assays is only due to the phosphatase modulation. Rewardingly, none of the tested compounds showed any kinase activity in the assay concentration range (< 100 μ M).

v) ThermoFluor

ThermoFluor assay was used to determine the effect of the selected phosphatase modulators (**HM-20-22**) on PFKFB3 stability. SYPRO Orange dye was used in the reaction because it binds to the hydrophobic patches or denatured protein and fluoresces. With the increased temperature and protein unfolding, we were able to monitor (using qPCR) the increase in fluorescence and determine the melting point. From the elaborated results (presented below, Figure 24) it can be concluded that the presence of the selected peptides does not significantly affect the protein stability.

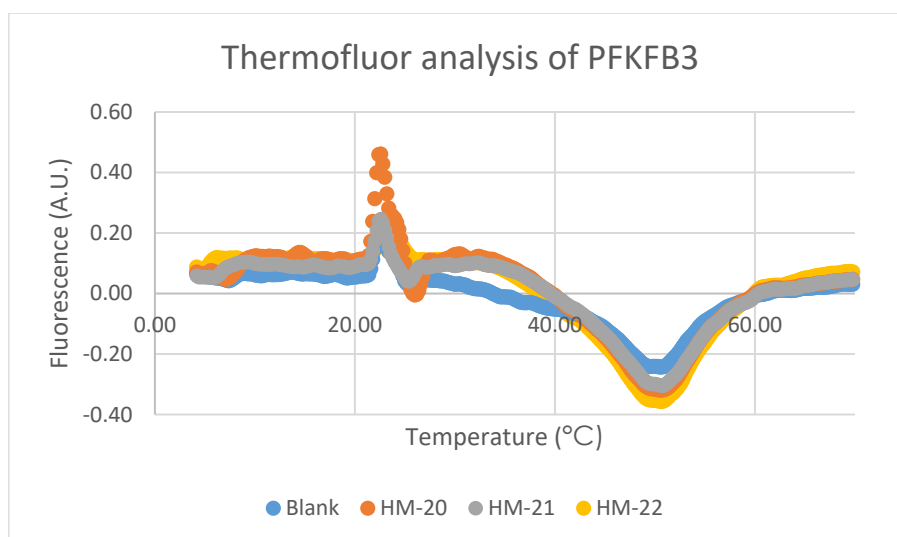


Figure 24: ThermoFluor for PFKFB3 protein with or without presence of HM-20-22.

vi) Phosphatase activity assay

LC-MS method was developed to evaluate the ability of binding peptides to affect the PFKFB3 phosphatase activity. Using this method we were able to monitor the amount of F-6-P generated via phosphatase driven hydrolysis of F-2,6-P₂ with or without the presence of the selected compounds and calculate the maximum velocity (V_{max}) of the enzyme.

Firstly, an enzyme phosphatase kinetics experiment was performed to assess the enzymatic activity and to find the best model for describing it. The phosphatase substrate was equilibrated with the enzyme at different concentrations, while the amount of enzyme was kept constant. PFKFB3 phosphatase velocity is presented as a function of the substrate concentration, as shown in Figure 25.

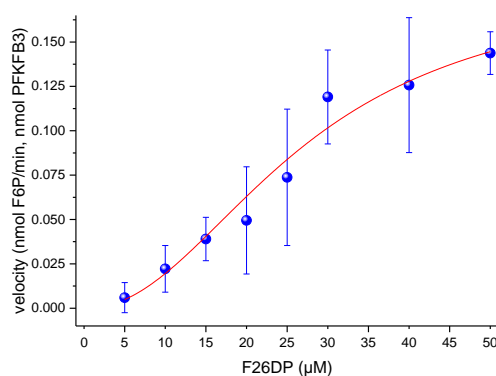


Figure 25. Phosphatase velocity (nmol/min of F-6-P per nmol of enzyme) as a function of the substrate concentration (F-2,6-P₂) for recombinant PFKFB3.

A sigmoidal trend was observed and to describe this, a Hill equation was applied rather than Michaelis-Menten equation for determining the best parameters:

$$V = \frac{V_{max} \times [S]^h}{K_{half}^h + [S]^h}$$

Where V is the kinetic velocity, V_{max} the maximum velocity at enzyme saturation, [S] the substrate concentration, K_{half} the substrate concentration giving a half of maximum velocity and h the Hill coefficient.

The experimental parameters of the best fitting Hill equation are summarized in Table 11, where the values for the kinetics of the enzyme alone or in presence of compounds **HM-18**, **20**, **21**, **22**, **17** and control compound **AZ-33** [61].

Table 11: Summary of the Hill equation parameters for PFKFB3 alone or in presence of the tested compounds

compound	V_{max}	±	S.E.	K_{half}	±	S.E.	h	±	S.E.
blank	0.16	±	0.03	21.51	±	5.57	2.03	±	0.66
HM-20	0.18	±	0.04	26.54	±	5.71	2.39	±	0.68
HM-21	0.81	±	0.29	58.42	±	25.88	1.50	±	0.21
HM-22	0.91	±	0.43	71.72	±	44.97	1.30	±	0.20
HM-18	0.19	±	0.06	28.12	±	10.95	1.95	±	0.69
HM-27	0.21	±	0.09	32.83	±	15.32	2.24	±	0.96
AZ-33	0.71	±	0.11	50.31	±	9.86	1.44	±	0.10

Maximum velocity (V_{max}) of the enzyme increased when positive control **AZ-33** and peptides **HM-21** and **HM-22** were added (see Table 11, V_{max} shown in blue). Phosphatase assay results proved that the phosphatase activity of PFKFB3 can in fact be modulated via allosteric modulation and that the chosen kinase inhibitor was also able to modulate the phosphatase.

vii) Cell tests

Endothelial migration assay.

This assay was used to test the antiangiogenic activity of four peptides, **HM-20**, **21**, **22** and **27**, by testing the effects on endothelial cell migration. One way ANOVA statistical test was used to determine whether the effect of the peptide on the cell migration is significant or not. ECs VEGF-induced migration was not reduced by **HM-20**, **22** and **27** at 10 μ M and 100 μ M peptide concentration. Migration of ECs induced by 10 ng/mL VEGF was however significantly

inhibited by compound **HM-21** (Figure 26) at both concentration tested (10 μ M and 100 μ M; significant effect is marked with an asterisk) after 18 and 24 h. This result is very interesting since PFKFB3 plays an important role in EC migration. With this assay we got an experimental proof that our peptide **HM-21** is able to enter into the cell and reduce the cell migration, most probably by indirect PFKFB3 inhibition.

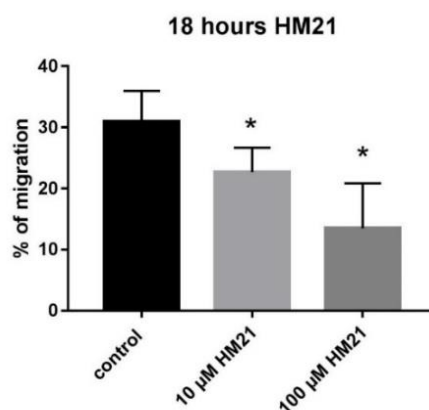


Figure 26: Endothelial migration assay for peptide HM-21; the significant effect of HM-21 on cell migration is marked by an asterisk. (* $p < 0.05$).

Endothelial cell proliferation and survival experiment using the MTT assay.

MTT assay was used to determine whether the selected peptides have anti-proliferative effect on ECs. The statistical significance of the results was calculated with one way ANOVA. ECs proliferation was very weakly inhibited at concentration of 30 μ M, 100 μ M and 300 μ M of **HM-22** and 30 μ M, 100 μ M and 300 μ M of **HM-20**, while there was absolutely no change in proliferation using compound **HM-21**. **HM-27** slightly reduced the proliferation rate of ECs at 30 μ M and quite significantly at 100 μ M, but was excluded from further experiments since it is a compound that doesn't bind the PFKFB3 enzyme. In conclusion, MTT assay (Figure 27) showed that **HM-20-22** do not have a meaningful effect on the EC metabolic activity and are not cytotoxic in the tested concentration range.

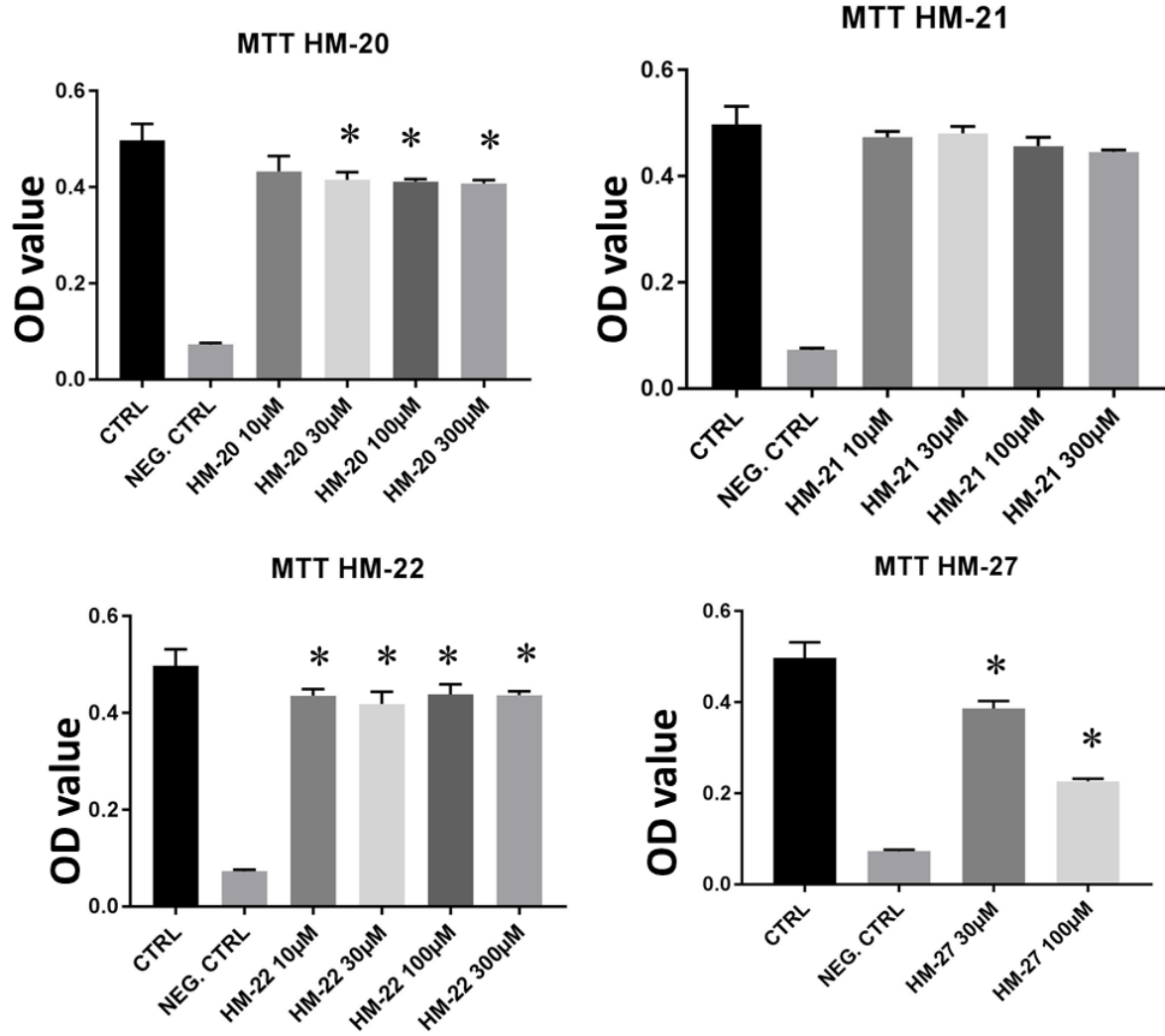


Figure 27: Endothelial proliferation assay for peptides **HM-20-22** and **HM-27**; OD value= optical density value. The significant effect of peptides HM-20-22 and 27 on cell proliferation is marked by an asterisk (* $p < 0.05$).

viii) Protein expression and purification

PFKFB3 protein was expressed and purified as described in the Materials and methods section. Figure 28 presents the chromatogram of the first purification step with His Tag affinity Ni column chromatography.

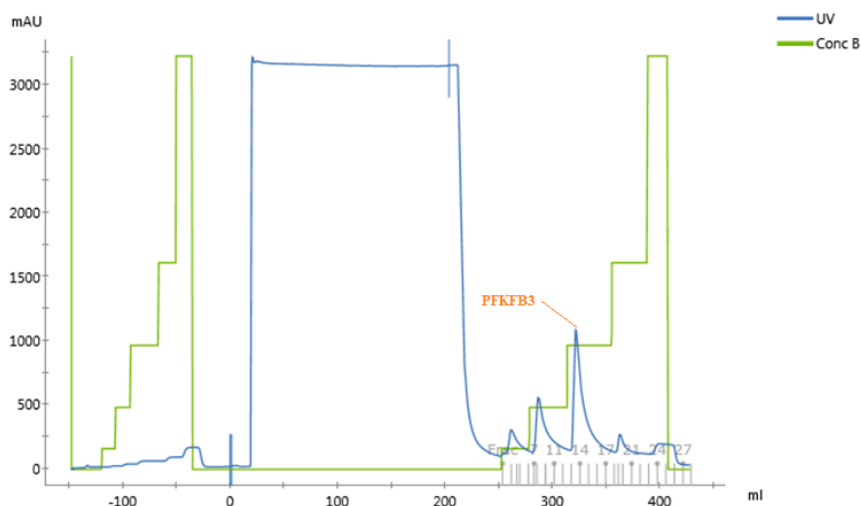


Figure 28: Affinity chromatogram for PFKFB 3 with a PFKFB3 peak marked with orange line.

The second purification step was done with Mono Q ion exchange chromatography on strong anion exchange column (Figure 29).

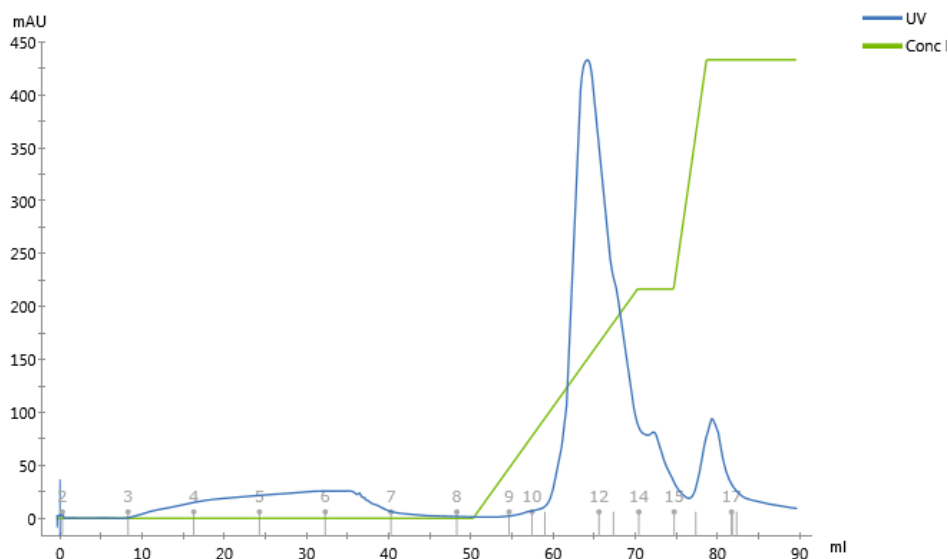


Figure 29: Mono Q anion exchange chromatogram for PFKFB3.

The purification process was monitored with a SDS Page gel shown in Figure 30 and the desired protein had a band at approx. 60 kDa (MW of a monomer is 59609 Da).

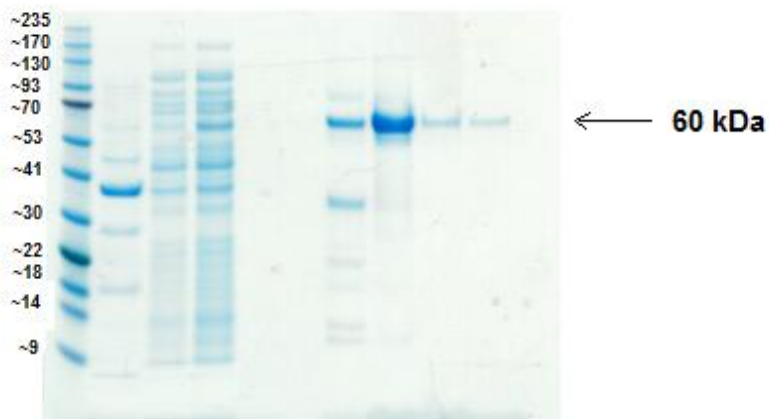


Figure 30: SDS-Page gel of freshly expressed PFKFB3 protein.

Size exclusion chromatography (SEC) was done in order to show the purity of the protein and to confirm that its oligomerization state is dimer (Figure 31).

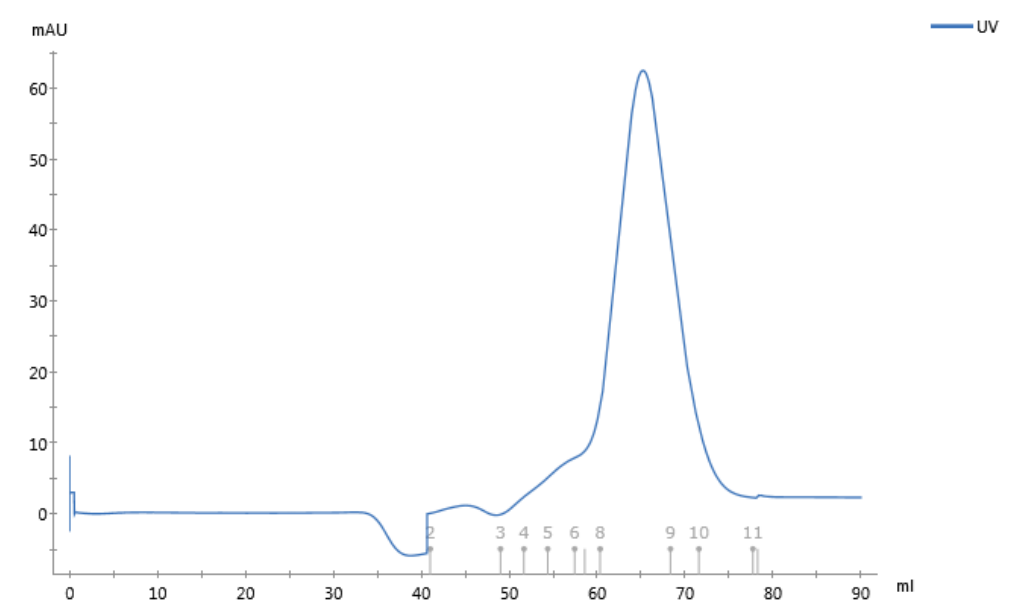


Figure 31: SEC chromatogram for purified PFKFB3 dimer.

Finally, a DLS experiment was performed in order to show that the sample is not aggregated and it is homogeneous.

d) DISCUSSION

Among 33 peptides synthesized in-house and 16 commercial compounds, 3 peptides showed a low micromolar binding affinity towards PFKFB3 and were therefore chosen for further optimization and *in vitro* evaluation. Unfortunately, the attempt to optimize the binding affinity of PFKFB3 binders **HM-20-22** was unsuccessful as there was no improvement in the binding affinity. The possible reason for this is that the chosen allosteric binding pocket is very tight as it is situated between the two monomers and it is also very specific. Both **HM-21** and **HM-22** have backbone-to-backbone hydrogen bonds that are dominant interactions in stabilising peptide-to-PFKFB3 binding, as shown in the 2-D interaction graph (Figure 32). Hence it is likely that the peptide sidechains play an indirect role in the binding by fitting into hollows of PFKFB3, as all larger sidechains were determined with decent receptor exposure. The fitting of sidechains locks the peptide in place and ensures the accessibility to the hydrogen bonding points on PFKFB3. Thus, changes in the sidechains by replacement with another amino acid likely alter the size of sidechains and disrupt the hydrogen bond interactions. Hence, the modified peptides could not adopt the proper binding pose in the binding pocket, which resulted in the inability to bind the native enzyme.

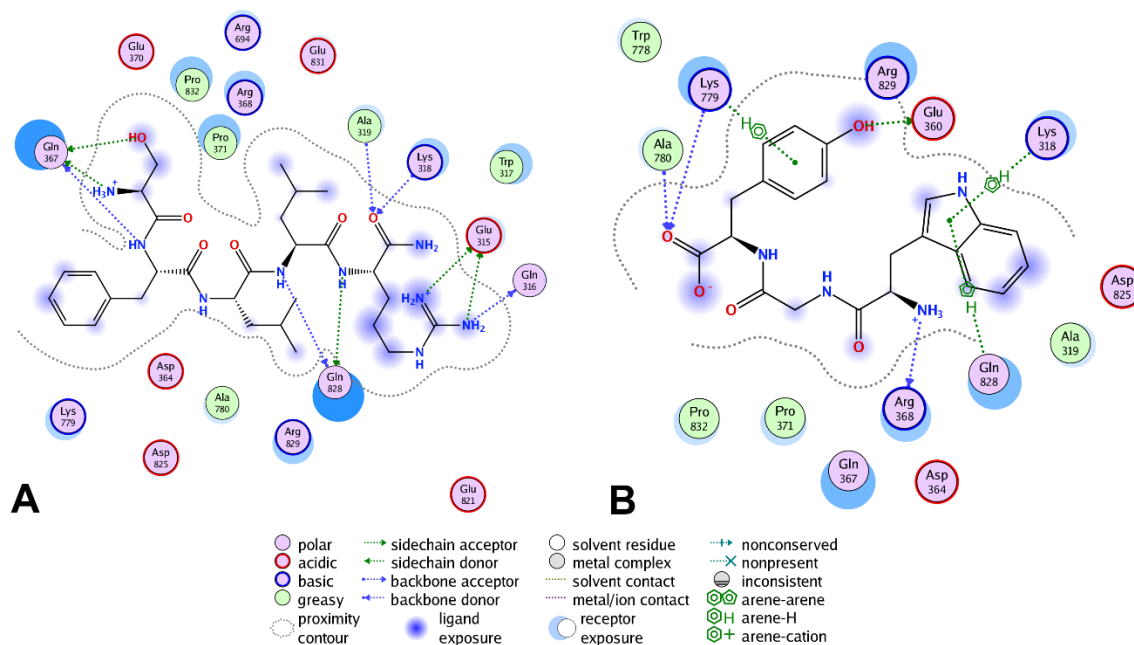


Figure 32: 2D ligand interaction figures of HM-21 (32a) and HM-22 (32b).

Furthermore, an LC-MS/MS phosphatase assay was developed for determination of phosphatase activity of the best binding modulators **HM-20-22**. A sigmoidal trend was observed for the PFKFB3 kinetics, which suggests that the PFKFB3 phosphatase site has

allosteric modulation sites. Specifically, a Hill coefficient value higher than one indicates a positive cooperativity between different sites or subunits [62, 63]. The assay gave no false positives since no significant variations on Hill equation parameters were observed after incubation with negative control compounds **HM-18** and **HM-27**, which were already tested by MST and resulted unable to bind the enzyme. Moreover, the enzyme binding is not sufficient for the modification of its phosphatase activity, since no significant variations on Hill equation parameters was observed upon incubation with the compound **HM-20**, which was previously identified as PFKFB3 binder by MST. In fact, the Hill equation fitting parameters obtained after incubation of PFKFB3 with **HM-20** were similar to those obtained by the enzyme alone. Interestingly, a modulation of phosphatase activity was induced by **AZ-33**, which is a very potent PFKFB3 ATP competitive kinase inhibitor [61]. Specifically, an almost tenfold increase of the enzyme maximum velocity and a loss of the sigmoidal shape were observed as suggested by the decrease of Hill coefficient down to almost one, which is the value expected for a Michaelis-Menten kinetics with no cooperativity. This implies that the phosphatase activity of PFKFB3 is self-inhibited and can be allosterically activated upon ATP binding site occupation. The phosphatase activity of the enzyme seems self-inhibited in an uncompetitive way since its maximum velocity is increased upon binding of an ATP competitive inhibitor, **AZ-33**.

It is rather intriguing that compounds **HM-21** and **HM-22** gave kinetics modifications comparable to **AZ-33**, although they were designed to bind an allosteric site far from ATP binding pocket. This demonstrates that PFKFB3 phosphatase activity can be conveniently stimulated without kinase deactivation, which was unmodified in the presence of compounds **HM-21** and **HM-22** as well as other compounds from our library. Surprisingly, compound **HM-20** did not cause any kinetics modifications although it binds to the target.

In order to get an *in silico* explanation for this interesting results, atomic correlation analysis was performed for all the amino acid residues for the last 100 ns of each MD simulation. Apart from the local dynamic correlation within kinase or phosphatase regions, we noticed a weak correlating zone that connects the ATP binding site to the phosphatase active site for all the simulated trajectories analysed (Figure 33 A). This occurs through the chained interactions between three α -helices – $\alpha 1$, $\alpha 17$, and $\alpha 18$. Moreover, $\alpha 17$ is the essential element to perturb activity of the phosphatase; part of it lies parallel to the Glu322-Ala325 loop flooring the phosphatase site (Figure 33 B). More interestingly, this loop region is also indirectly connected to the AD that modulates the phosphatase activity (Figure 33 C). The similar fold-changes of phosphatase activity between using **AZ-33** and splicing auto-regulatory domain also centers the mechanism onto the correlation overlapping region – $\alpha 17$. On the other hand, compounds

HM-21 and **HM-22** took a more direct approach by directly affecting the conformation of $\alpha 17$ (Figure 33 D). Both **HM-21** and **HM-22** adapted more kinked binding poses after docking (Figure 34 B and 34 C, respectively), suggesting that much more volume of the binding space are occupied. These lead to the similar activation outcome as accomplished by ATP and the β -hairpin region. Compound **HM-20**, however, adopted a more extended and relaxed binding pose (Figure 34 A), likely resulted in the un-perturbed phosphatase activity while still capable of binding to PFKFB3. Of course, it might also be possible that compound **HM-20** binds PFKFB3 on a different and non-functional binding site.

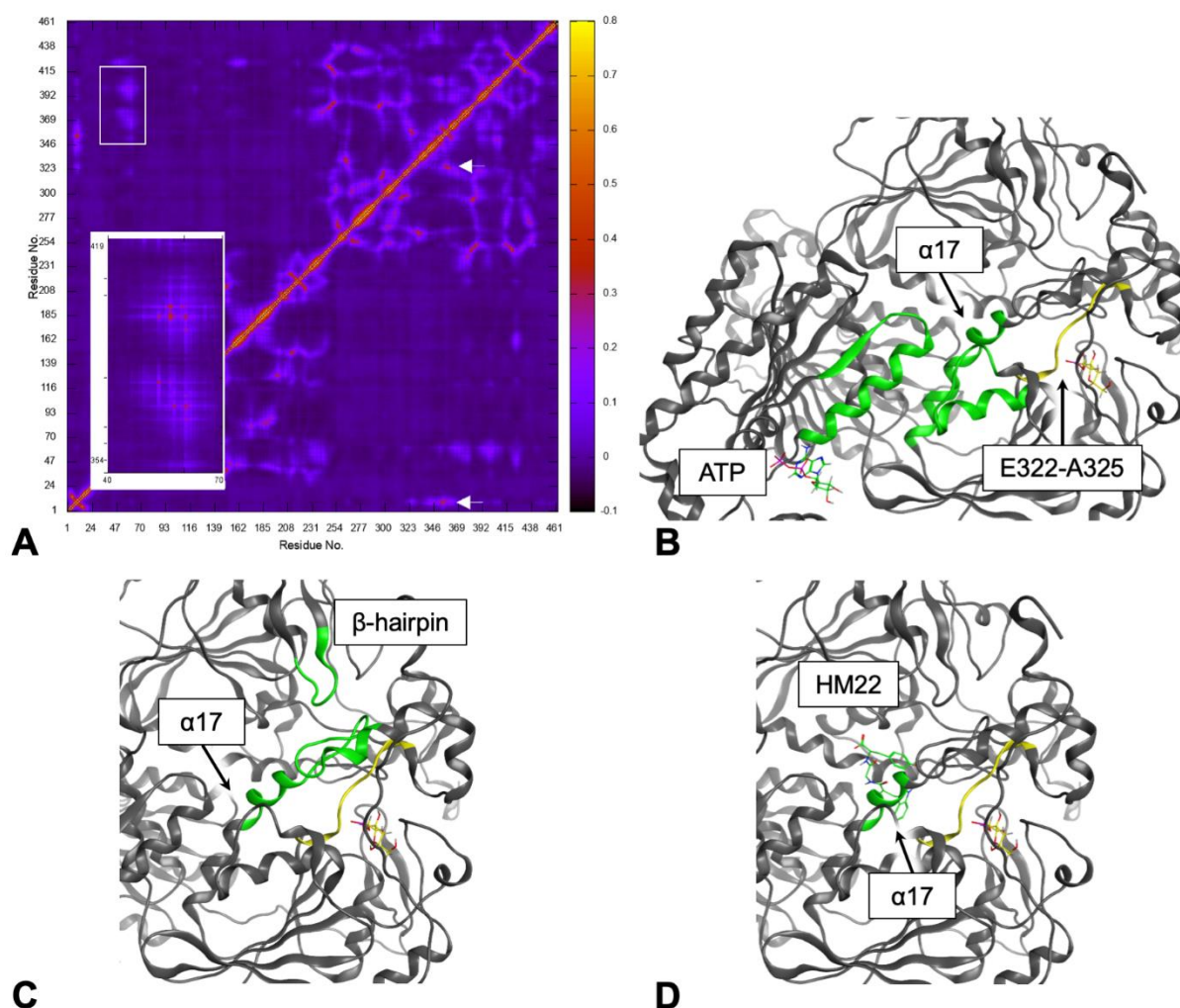


Figure 33: The atomic correlation heat map (A) by amino acid residues of MD simulation using apo PFKFB3, and the dynamically correlated regions under different scenario (B-D). In A, the box and the zoomed-in sub-plot show the three weakly correlated α -helices as is highlighted in B. The two arrows in A show the stronger correlations of the auto-regulatory domain (β -hairpin) to the E322-A325 loop (shown in yellow) through part of the $\alpha 17$ -helix (Y362-E370). The β -hairpin-to-phosphatase correlated regions are illustrated in C. In D, the docked pose of **HM-22** indicates that the peptide is interfering with E322-A325 loop directly through $\alpha 17$ -helix.

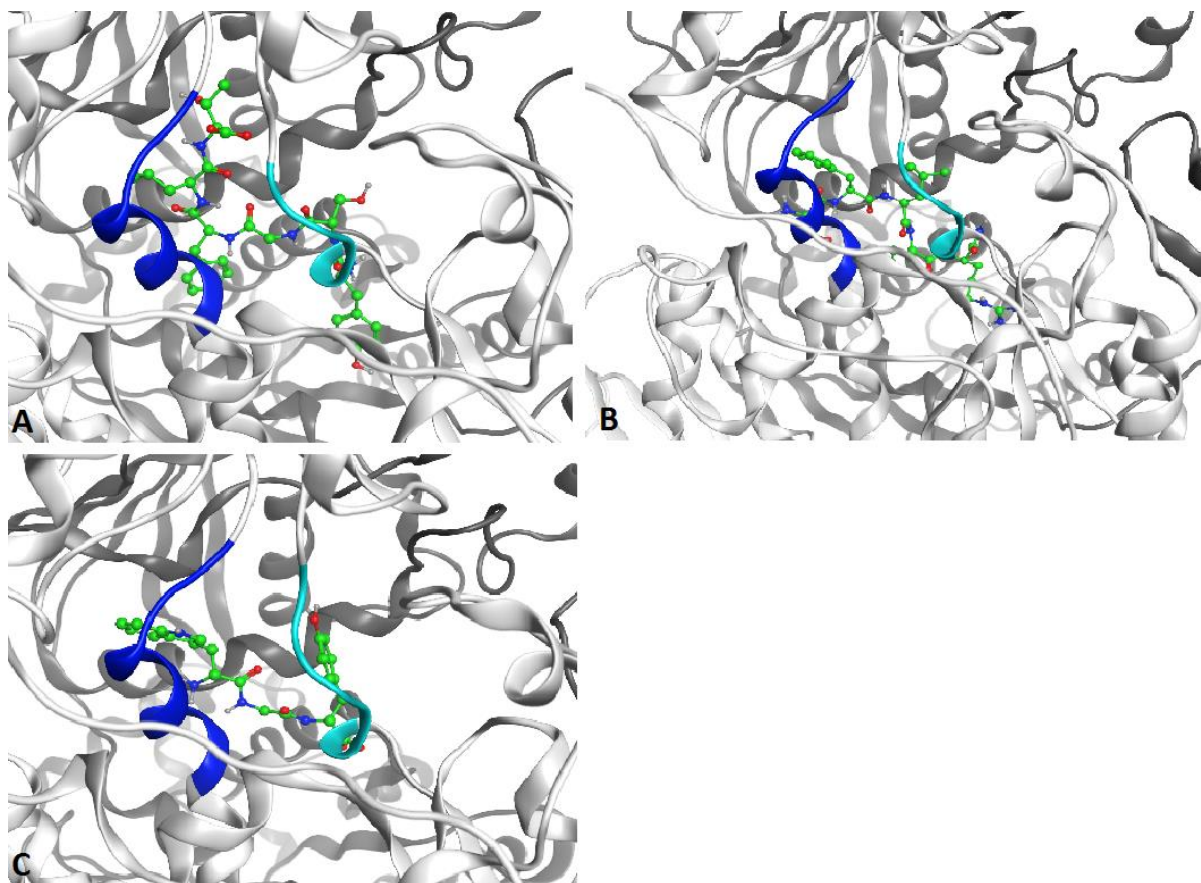


Figure 34: 3-D docking poses in the PFKFB3 allosteric binding site. Binding pose of **HM-20** is shown in A, binding pose of **HM-21** in B and binding pose of **HM-22** in C.

Furthermore, the three most promising peptides, **HM-20-22**, were evaluated in a MTT assay and migration assay. The tested peptides were found to have no significant effect on cell proliferation, which is important since any cytotoxic effect is undesired in our case. Although our peptides may serve merely as useful probes to investigate the possibility of allosteric modulation, it is important that they do not exhibit any toxic effect that could have an impact on further *in vitro* tests. In addition, the migration ability of the most promising peptides was evaluated in a scratch assay and peptide **HM-21** was found to be able to reduce the cell migration, which was a rewarding result for an early stage enzyme binder. With the migration assay we proved that our peptide reduces EC migration most likely through an indirect PFKFB3 inhibition, because it is a peptide designed to bind to the allosteric phosphatase site. Despite its good binding affinity and activating effect on the enzyme kinetics, **HM-22** did not show any effect on the EC migration, which could be due its inability to enter into the cell. In order to test this, a fluorescein-labelled derivative should have been prepared and tested in a migration assay.

The findings of this research work are very interesting not only for the scope of evaluating the possibility of allosteric modulation, but also in terms of better understanding its unique mechanisms of action. PFKFB3 has an ATP-dependent kinase activity, while its phosphatase activity is independent of ADP. Notably, both ATP and F-2,6-P₂ are allosteric activators of PFK1, which is the regulatory enzyme controlling glycolysis. Since the purpose of glycolysis is ATP production, PFK1 is feedback-inhibited by a high ATP/ADP ratio. Therefore, it is reasonable that a high ATP/ADP ratio also induces PFKFB3 ATP binding, thus stimulating the enzyme phosphatase activity which undergoes PFK1 inhibition by decreasing F-2,6-P₂ concentration. On the contrary, when ATP concentration is low, PFKFB3 phosphatase activity is inhibited to stimulate the production of F-2,6-P₂, which allosterically activates PFK1.

The identification of the molecular mechanism responsible for PFKFB3 auto-modulation is beyond the scope of the research work herein reported. However, the cooperation leading to the uncompetitive inhibition of PFKFB3 phosphatase site can be hypothesized to be linked to the enzyme auto-phosphorylation occurring during F-2,6-P₂ hydrolysis. In fact, the phosphatase activity of PFKFB3 is ADP independent, the enzyme being itself the acceptor of the phosphate group. Compelling evidence of this mechanism has been given by monitoring the radioactivity incorporation of PFKFB3 in a solution containing ³²P-radiolabelled substrate [64]. However, it has also been demonstrated that when enzyme phosphorylation reaches a steady state the limiting step of the reaction can be the breakdown of the phosphorylated enzyme, as observed for the slow radioactivity release of ³²P-radiolabelled PFKFB3 in a solution containing non-radiolabelled substrate [64]. The change of the kinetic shape such as the one we observed can occur if the ATP binding produces a conformational change, which undergoes a reduced affinity for the substrate and causes a faster breakdown of the phosphorylated enzyme. However, we have no experimental data to support this hypothesis.

V. CHAPTER 2: PFKFB3 CRYSTALLIZATION

a) INTRODUCTION

Since PFKFB3 has never been allosterically modulated and our design strategy is completely new, there are no crystal structures available in PDB with a ligand in the binding site of interest. Therefore, the aim of this part of research work was to obtain a crystal of PFKFB3 with our best binder (**HM-22**) in the binding site, either by soaking method or co-crystallization. Considering that the protocol for PFKFB3 crystallization was known in literature [21], our starting point was to obtain a crystal of the protein first and soak it with the compound.

Protein crystallization. An overview.

The first crystals of haemoglobin were observed from worms and fish in the latter half of the 19th century. Plant seed proteins were the first crystallized proteins in 1880s [65]. However, a major success was made decades later in 1920s with the crystallization of insulin and the demonstration that the enzymes can be obtained in crystalline forms [66]. In 1970s and 1980s the demand for protein crystals rapidly increased and new approaches were introduced in this field. However, the biggest step forward was made a decade later with a huge improvement in genetic engineering and molecular biological research which lead to the development of recombinant DNA technology and X-ray crystallography [67].

Although there has been a huge improvement of crystallization techniques in terms of rational approaches to protein crystallization, there is still a need for a so called trial-and-error approach. The crystallization process is usually time consuming and it is a matter of systematic searching of the best parameters for the crystal formation. Even though only few crystals might be needed, the amount of the protein required for the trial could be quite huge. Once there is an evidence of some kind of crystals, the previously found parameters have to be optimized in order to yield the best possible material for the X-ray diffraction analysis.

The composition of macromolecular crystals is from 25% to 90% of solvent, depending on the particular macromolecule, but the average solvent percentage is about 50%. The remaining volume is thus occupied by the protein or nucleic acid making the entire crystal a sort of ordered gel filled by substantial interstitial spaces through which there is a free diffusion of solvent and other small molecules. Macromolecular crystals differ from low-molecular weight crystals in

many ways despite morphology and appearance similarities. They are soft and fragile, limited in size, cannot be dehydrated, have weak optical properties, temperature sensitive and poorly diffract X-ray properties. The higher the degree of internal order of a crystal the more extensive is its diffraction pattern. Furthermore, the degree of crystalline order is closely related to how detailed could be the crystal structure analysis. Usually, it is not sufficient to determine the protein structure with only one crystal, but several crystals have to be analysed. The major reason for poor diffraction properties of macromolecular crystals is the presence of huge solvent regions. On the other hand, even though the high solvent content means poor diffraction, it allows the protein structure to remain unchanged from that found in solution. This means that important biochemical features such as ligand binding, enzymatic and spectroscopic characteristics remain the same as for a fully solvated molecule giving the biochemists crucial information about the macromolecule behaviour in physiological conditions. [68, 69].

Methods for screening and optimization

As mentioned above, there are two phases in a long and time consuming process of protein crystallization. The first stage is the identification of chemical, biochemical and physical parameters that yield some crystalline material, and the second is optimization of these conditions to acquire optimal material for diffraction analysis. There are two approaches for screening the crystallization conditions, the first being the systematic variation of the most important variables (precipitant type and concentration, pH and temperature) and the second one, which is so called “shotgun” approach. The major disadvantage of the first method is that it requires a significantly higher quantity of the protein, which could be problematic in some cases. The second method is more convenient as it requires significantly less precious material and nowadays, a huge variety of commercial screening kits are available.

Once some crystals or even microcrystals of protein origin are obtained, the second stage of work - which is the optimization of the acquired conditions - can start. Components (buffer, salt, ions) as well as pH and temperature of the solution yielding crystals have to be considered and additional plates with slightly modified conditions have to be prepared.

Crystallization process

There are two inseparable steps in the crystallization of every molecule, nucleation and growth. Nucleation is a first-order phase transition where molecules pass from a fully disordered state to an ordered one, making this step most difficult to address theoretically as well as experimentally. This step occurs through the formation of a transition state, in which molecules are partially ordered. Macromolecules grow by the classical mechanisms of dislocation growth and growth by two-dimensional nucleation, along with two other less common mechanisms, which are normal growth and three-dimensional nucleation [70]. Both, nucleation and growth are dependent on the supersaturation of mother liquor and hence, crystallization of a macromolecule requires the presence of a supersaturated state as shown in the phase diagram in Figure 35.

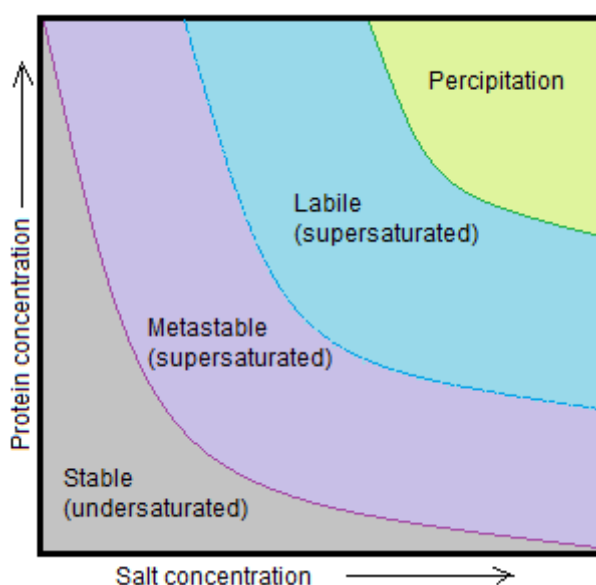


Figure 35: The phase diagram for the crystallization of macromolecules.

Supersaturation

The solubility of the protein in mother liquor has to be significantly reduced in order to reach the supersaturation. This can be done *i*) by altering the protein itself (e.g. a pH induced change in the ionization state of the protein), *ii*) by altering the chemical activity of the water (e.g. salt addition), *iii*) by altering the degree of attraction of one protein molecule for another (e.g. change of pH or bridging ions addition) and/or *iv*) by altering the nature of the interactions between the protein and the solvent (e.g. the addition of polymers or ions). There are several

techniques for achieving supersaturation; the most commonly used are microtechniques because they require a small amount of sample. The most popular procedures for vapour diffusion (presented in Figure 36) are sitting-drop and hanging-drop, while microbatch method is the most popular batch method using micro drops under oil. There is a wide variety of commercially available crystallization plates.

i) Sitting drop vapour diffusion crystallization

The principle of vapour diffusion method is straightforward. A drop composed of a mixture of protein sample and reagents is placed in vapour equilibration with a liquid reservoir of reagent. Usually the concentration of the reagent in the drop is lower than in the reservoir. To achieve equilibrium, water leaves the drop and eventually finish up in the reservoir and the sample undergoes an increase in relative supersaturation. As water leaves the drop, the sample and reagents concentration is increased. Equilibration is achieved when the reagent concentration in the drop is the same as the concentration in the reservoir.

ii) Hanging drop vapour diffusion crystallization

The principle of hanging drop diffusion method is the same as in the sitting drop methods, the only difference is the drop orientation.

iii) Microbatch

Microbatch crystallization is a method where the protein sample and reagents are combined and sealed in a plate under a layer of paraffin oil [71]. A small drop of sample is combined with the crystallization reagent and pipetted under a small layer of paraffin oil, which allows no diffusion of water. In a microbatch experiment there is no significant change of the concentration of protein sample and reagents during the trial.

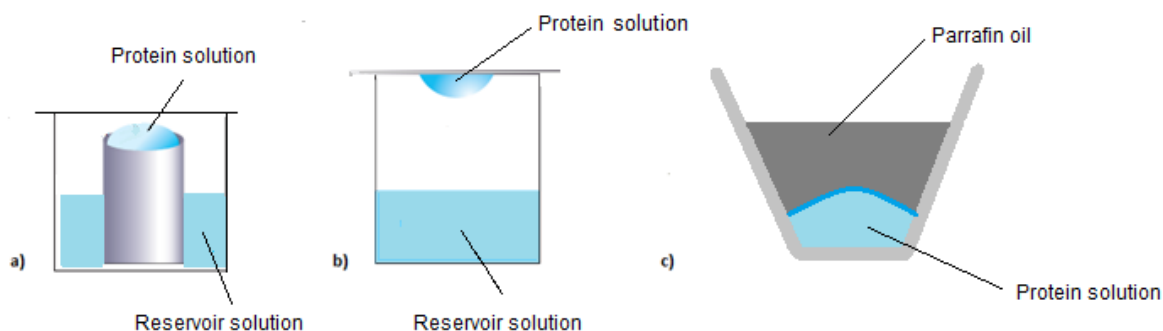


Figure 36: a) sitting drop method, b) hanging drop method, c) microbatch method

However, it is important to be aware that the best method for optimization of screening conditions may not be the same as used for screening. The screening and optimization plates can be prepared either manually, which is time consuming and more sample is needed, or with the help of robotic devices. The latter are most commonly used in high-throughput laboratories, especially in large pharmaceutical industries, although they are quite common also in structural biology specialized academic research laboratories. Robotic systems can be used to screen numerous matrices of conditions and they use submicrolitre amounts of protein and mother liquor. Furthermore, they can also be used to examine and evaluate the results of crystallization trials [72], however, in most academic research laboratories this is still done manually as experience is still a huge factor for this important step.

Precipitants

In general, a very wide range of crystallization agents and precipitants are used. The precipitants can be grouped into five different classes according to their mechanisms for promoting crystallization: salts, organic solvents, long-chain polymers, low molecular weight polymers and non-volatile compounds. The typical agents for the first two classes are ammonium sulphate and ethanol, respectively, while a model representative of the third class would be polyethylene glycol 4000. In the fourth class we usually place polyethylene glycols with molar weight lower than 1000.

Salts are essential for the formation of ordered crystals because salt ions are competing for water molecules and thus dehydrating proteins. Since their efficiency is dependent on ionic strength, multivalent ions (anions) such as sulphates, phosphates and citrates are the most commonly used. Apart from ionic strength, pH is a very important factor that influences the solubility of the protein. Organic solvents are added to the mother liquor because they reduce the dielectric of the medium and hence increase the attraction between macromolecules. They have to be used at low temperatures and added slowly with good mixing. Polymers are an important part of the crystallization mixture because they cause volume-exclusion effects and induce the separation of macromolecules from the solution. Since they have no consistent conformation, they spread randomly in solution and occupy a lot of space, which results in a decrease of available space for macromolecules, which then segregate, aggregate and finally form a solid state, preferably crystals.

Other factors influencing the crystallization process

Apart from precipitants, there are many other factors that can affect the crystallization of macromolecules [73]. Undoubtedly, the concentration of the protein is of great importance and it can be from 2 mg/mL up to as high as 100 mg/mL. Furthermore, although they have lesser importance than the precipitants, also gravity, temperature, electric and magnetic fields and viscosity cannot be neglected.

It has been shown that also certain chemical compounds or small molecules may have huge influence on the crystallization trial success [73, 74]. This so called additives include *i)* physiologically or biochemically relevant molecules such as coenzymes, substrate analogues, inhibitors, metal ions and prosthetic groups; *ii)* chemical protectants such as reducing agents BME, DTT and heavy metal ion scavengers such as EDTA and EGTA; *iii)* solubilizing agents and detergents; *iv)* poisons such as ethanol, DMSO, acetone, dioxane; *v)* osmolytes, co-solvents and cosmotropes; *vi)* compounds that can stabilize proteins through noncovalent bonds; *vii)* compounds or materials that enhance nucleation such as PEG or Jeffamine.

b) RESULTS

A total number of 20 crystallization plates (13 optimization and 7 screening plates) was prepared and small crystals grew after 4 weeks in the following conditions. Crystallization trials which resulted in growth of small crystals were as follows:

1. Optimization attempt 3 plate (PFKFB3 8 mg/mL, 20 °C) at conditions: Tris HCl pH = 7.4, 20 % w/v PEG 4000.
2. Screening attempt 3 Morpheus plate (PFKFB3 8 mg/mL, 4 °C) at conditions: 0.03 M sodium nitrate, 0.03 M sodium phosphate dibasic, 0.03 M ammonium sulphate, 0.05 M Tris pH = 8.5, 0.05 M Bicine.
3. Screening attempt 4 JCSG plate (PFKFB3 8 mg/mL, 4 °C) at conditions:
 - 0.2 M magnesium chloride hexahydrate, 0.1 M HEPES pH = 7.5, 30 % v/v PEG 200.
 - 0.2 M magnesium chloride hexahydrate, 0.1 Tris pH = 8.5, 20 % w/v PEG 8000.
 - 0.1 M CAPS pH = 10.5, 40 % v/v 2-Methyl-2,4-pentanediol.
 - 1 M ammonium phosphate dibasic, 0.1 M sodium acetate pH = 4.5.
4. Screening attempt 5 Natrix plate (PFKFB3 8 mg/mL, 4 °C) at conditions:

- 0.1 M magnesium acetate tetrahydrate, 0.05 M MES monohydrate pH = 5.9, 20 % v/v 2-Methyl-2,4-pentanediol.
- 0.2 M ammonium chloride, 0.1 M magnesium chloride hexahydrate, 0.05 M HEPES pH = 6.7, 2.5 M hexanediol.
- 0.2 M ammonium chloride, 0.15 M magnesium acetate tetrahydrate, 0.05 M HEPES pH = 6.9, 5 % w/v PEG 4000.
- 0.005 M magnesium sulphate monohydrate, Tris HCl pH = 8.4, 2.9 M hexanediol, 30 % v/v PEG 400.
- 0.1 M potassium chloride, 0.01 M magnesium chloride hexahydrate, Tris HCl pH = 8.4, 30 % v/v PEG 400.

Crystal material was collected and prepared for X-ray analysis as described in Materials and methods section o. Unfortunately, X-ray analysis showed that there is no diffraction for the selected material and the crystal structure could not be determined.

c) DISCUSSION

The crystallization trial was set up in order to get a PFKFB3 crystal that would be soaked with our most promising phosphatase modulator, **HM-22**. A crystal structure of **HM-22** bound to the allosteric site would give us the ultimate confirmation of our design strategy.

Since the protocol for PFKFB3 crystallization is published by Kim et. al. [21], and we received the plasmid from the same group, it was surprising and unexpected that we were unable to repeat the crystallization procedure. Published crystals were obtained in 2-3 weeks by sitting drop vapour diffusion method with 1:1 mixture of the protein sample (8 mg/mL) with a mother liquor of 50 mM Tris-HCl pH =7.5, 20–25% ethylene glycol, 12% dioxane, 5% glycerol, and 12% polyethylene glycol 4000. In our first crystallization trial we prepared the same conditions, but we did not obtain any crystal material. Therefore, an optimization of the published conditions was prepared and 100 mM Tris buffer was prepared in a wider pH range (7.1-8.1). In addition, also the amount of PEG was slightly modified and conditions 5-16 % of PEG were tested. Moreover, Tris buffer was replaced with 100 mM HEPES in pH range 7-7.5 or 50 mM MES in pH range 6-7. Finally, also conditions with sodium malonate were prepared in a wider pH range (5-10) and the concentration of PEG 4000 was increased up to 22 %. Apart from pH modifications, buffer change and precipitant concentration modifications, also temperature was a variable. Plates were prepared in duplicates, one plate was placed in controlled room temperature conditions (20 °C), while the other one was kept in a refrigerator at 4 °C. The only

obtained crystal material from our optimization was at Tris HCl pH = 7.4, 20 % w/v PEG 4000 at 20 °C, however, the crystal lattice was unordered and there was no X-ray diffraction.

After unsuccessful optimization trials, screening strategy was pursued. Seven commercially available crystal screens (Crystal screen HT, Index, Morpheus, JCSG, Natrix, Proplex and PACT) were used and plates were prepared with 8 mg/mL protein concentration in duplicates and placed at 20 or 4 °C. Some crystal material was obtained from Morpheus, JCSG and Natrix plates and nine samples were collected and analysed with X-ray. Unfortunately, once again the analysed material was not crystallized protein, but precipitated salts instead and we were unable to get any useful information.

As considerable effort has been made in order to crystallize the protein without success and this is a process that requires substantial amount of protein to be expressed (the commercial protein was considered too expensive to be purchased in such quantities), we decided to concentrate on other aspects of our project.

VI. CHAPTER 3: ATP COMPETITIVE PFKFB3 KINASE INHIBITORS

a) INTRODUCTION

The research work presented herein is merely a short overview of the research activity Design and Synthesis of novel ATP competitive PFKFB3 kinase inhibitors. The computational part and the synthesis were done by Virginia Cristofori, while the synthesis of control compounds was performed by Carlo De Dominicis. My contribution to this part of the project was the biological evaluation of compounds; kinase activity determination, MST binding affinity and SPR binding kinetics.

The aim of this research work was to find a novel class of potent PFKFB3 ATP competitive inhibitors using *in silico* methods. Furthermore, the best scoring compounds were synthesized using modern organic synthesis techniques and evaluated for their activity and affinity towards the target. In addition, an optimization computational study was done to further improve the potency of already published PFKFB3 inhibitors and selected compounds were synthesized and evaluated for their kinase activity.

b) DESIGN

The design of new candidate PFKFB3 kinase domain inhibitors was carried out with the aid of computational tools, based on the 3D structural information of both protein and active ligands. Two classes of ATP competitive inhibitors developed by AstraZeneca were used as reference compounds in two distinct virtual screening workflows: a) the phenoxy-indole and indazole (herein referred as AZI) ligands [61], and b) the dihydropyrrolopyrimidinone (herein referred as AZPP) ligands [75]. Methods used in the selection of compounds are described in the materials and methods section.

i) AZI-based computational strategy

Data of the predicted ligands' binding affinity were merged and through a consensus scoring criterion of selection, six compounds were selected for an *in vitro* assay. Two commercially available compounds were purchased (**VS-3** and **VS-4**) and four molecules were synthesised (**VS-1**, **VS-2**, **VS-8** and **VS-9**).

ii) AZPP-based computational strategy

A library of about 500 derivatives based on the dihydropyrrolopyrimidinone PFKFB3 ligands recently reported by St-Gallay et al. [75] was built for a new search in a more restricted chemical space [76]. Molecules from the new library were designed from the original active dihydropyrrolopyrimidinone scaffold, focusing on compounds amenable to *i)* being functionalised with a variety of diverse substituents on the active scaffold and *ii)* be produced through a divergent synthetic strategy, namely by introducing structural modifications on a common key precursor. With the purpose of synthesising and exploring a broad spectrum of derivatives, developing a structure-activity relationship (SAR) study, the most promising compounds from the new structure-based virtual screening were synthesized and tested. Three of the reported active compounds in St-Gallay et al. were also synthesised for being tested in kinase activity experimental assay as positive controls with activity concentration being in the low micromolar range.

c) RESULTS

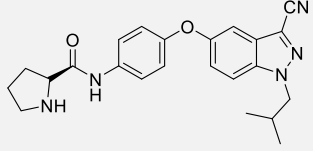
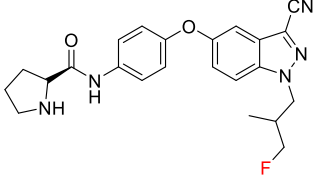
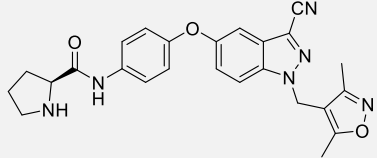
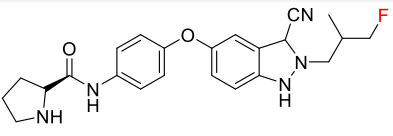
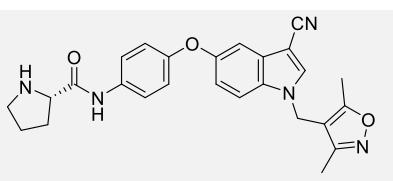
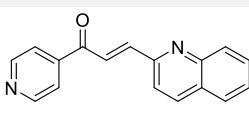
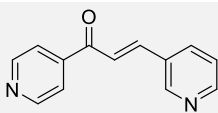
i) Kinase activity results

- AstraZeneca phenoxyindole and indazole compounds and their analogues

Reference compounds **AZ-33**, **67** and **68** as well as **3-PO** and **PFK-15** were tested using the same protocol and conditions as previously described [72]. Compounds **AZ-33** and **68** exhibited IC_{50} values that were in the same range as reported in literature. Also in our assay **3-PO** was completely inactive ($IC_{50} > 100 \mu M$), which raises further questions regarding the credibility of the **3-PO** data published in recent years. For compounds **AZ-67** and **PFK-15** there were some differences between the reported values and our values. **AZ-67** showed micromolar potency in our assay, while it has been reported as a low nanomolar inhibitor. Furthermore, **PFK-15** proved slightly less active in comparison to the literature value [84]. In addition, a fluorinated analogue of **AZ-68** was tested for the kinase activity and it was found to be significantly less active than its non-fluorinated version. **F-AZ-68** is a submicromolar PFKFB3 inhibitor, while **AZ-68** is a very potent low nanomolar inhibitor. Also **ZCDD-110**,

an **AZ-68** analogue where the other pyrazole nitrogen is alkylated, was tested and its IC_{50} value was 4.5 μ M, which is approx. three orders of magnitude less active than **AZ-68**.

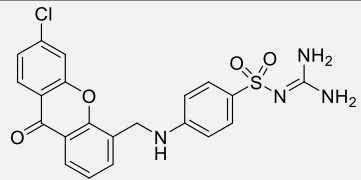
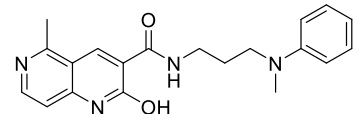
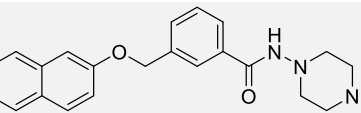
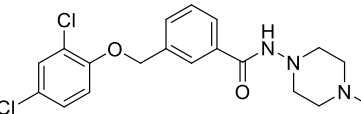
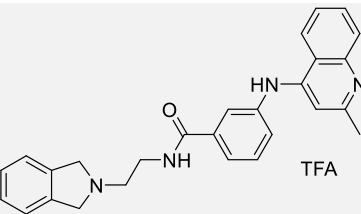
Table 11: Reference ATP competitive PFKFB3 inhibitors and their analogues.

COMPOUND	MW	STRUCTURE	IC_{50}	REPORTED IC_{50}
AZ-68	403.49		3.2 ± 1.5 nM	4 nM [72]
F-AZ-68	421.48		0.76 ± 0.07 μ M	-
AZ-33	456.51		21.2 ± 8 nM	3 nM [72]
ZCDD-110	423.21		4.53 ± 0.72 μ M	-
AZ-67	455.52		1.30 ± 0.09 μ M	11 nM [72]
PFK-15	260.30		22.6 ± 3.11 μ M	0.21 μ M [84]
3-PO	210.24		Not active	Not active [72] 22.9 μ M [84]

- *AZI ligands*

Compounds presented in Table 12 were chosen from virtual screening (described in the Design section of this chapter) and successfully synthesized and characterized at the University of Aberdeen. Unfortunately, they do not exhibit a significant kinase activity and therefore, only residual activity was calculated for these compounds. Compounds **VS-1** and **VS-2** have no effect on the target. **VS-3** and **4** slightly activate the enzyme at 100 μM , but have almost no effect at 10 μM concentration. Candidate compounds **VS-8** and **VS-9** reduce the residual activity of PFKFB3 by two thirds, but this effect seems to be concentration independent since values are similar for both tested concentrations. The most interesting compound from this series is **VS-9** that has a residual activity of 31 % at 100 μM concentration and 60 % at 10 μM concentration.

Table 12: AZI ligands; RA= residual activity.

COMPOUND	MW	STRUCTURE	RA % (AT 100 μM)	RA % (AT 10 μM)
VS-1	456.90		110 \pm 1.56	104 \pm 1.52
VS-2	350.42		100 \pm 3.34	81.1 \pm 3.53
VS-3	375.47		197 \pm 2.88	212 \pm 3.93
VS-4	394.30		286 \pm 5.45	111 \pm 1.74
VS-8	536.56		36.0 \pm 1.03	32.5 \pm 1.74

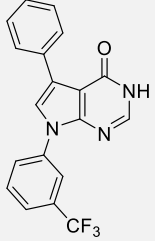
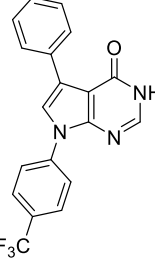
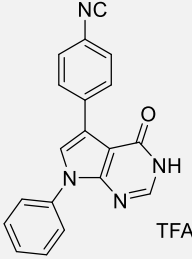
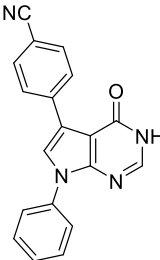
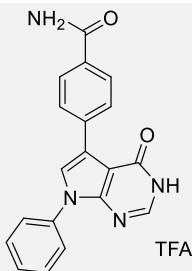
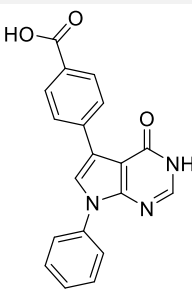
VS-9	483.47		31.3 ± 1.07	60.4 ± 2.84
-------------	--------	--	-----------------	-----------------

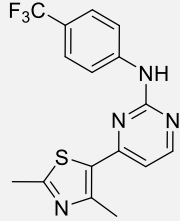
- *AZPP ligands*

Compounds **AZ-c-h** and **TM-5** presented in Table 13 were selected via *in silico* optimization of previously published compound **AZ-a** [75] (described in detail in the Design section of this chapter). **AZ-a** is a low micromolar PFKFB3 inhibitor ($IC_{50}= 5 \mu M$) and its residual activity is 9.3 % at 100 μM , while **AZ-b** is a submicromolar inhibitor ($IC_{50}= 0.25 \mu M$) from the same series of previously published compounds and its RA at 100 μM is 4.2 %. New compounds **AZ-c, f** and **g** inhibit approx. 60 % of enzymatic activity at 100 μM . **AZ-h** inhibits about 50 % of PFKFB3 kinase activity at 100 μM , while **AZ-d** and **TM-5** have only a very weak effect on the enzyme (for **TM-5** RA= 73 % at 100 μM). **AZ-e** has RA of 40 % at 100 μM , however, this effect is not concentration dependant since the same effect is achieved also at 10 μM concentration.

Table 13: AZPP ATP competitive kinase inhibitors.

COMPOUND	STRUCTURE	MW	RA % (at 100 μM)	RA % (at 10 μM)
AZ-a		317.35	9.31 ± 0.015	23.1 ± 0.748
AZ-b		347.37	4.24 ± 0.126	8.18 ± 0.497

AZ-c		355.32	30.2 ± 0.056	30.3 ± 0.729
AZ-d		355.32	65.1 ± 1.21	37.5 ± 1.54
AZ-e		426.36	40.2 ± 1.29	40.4 ± 0.257
AZ-f		312.33	25.8 ± 0.804	39.3 ± 1.32
AZ-g		444.37	27.3 ± 0.064	49.0 ± 0.967
AZ-h		428.37	55.7 ± 0.998	61.7 ± 1.37

TM-5		350.36	73.4 ± 0.163	67.7 ± 0.188
-------------	---	--------	------------------	------------------

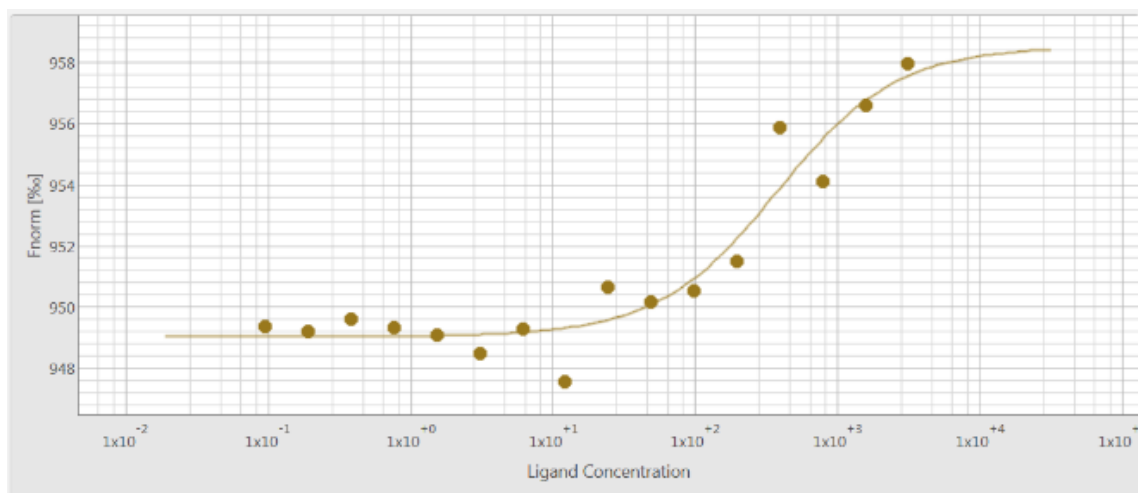
ii) Binding affinity results

Binding affinity was determined for all kinase inhibitors exhibiting a significant kinase activity towards the target (Table 14). However, some compounds (e.g. **AZ-33** and **AZ-67**) had solubility issues at higher concentrations that were needed for a good MST measurement and therefore, an alternative technique for kinetics study for this compounds was proposed.

A very potent inhibitor, **AZ-68** that has a reported IC_{50} value of 4 nM [61] binds to PFKFB3 with a low micromolar binding affinity of 0.35 μ M as shown in Figure 37. On the other hand, its fluorinated analogue, **F-AZ-68** is significantly less potent with a determined IC_{50} value of 0.76 μ M, binds with an affinity of 32 μ M (Figure 38). Interestingly, **3-PO**, the reference PFKFB3 inhibitor in numerous publications and studies that resulted inactive in our kinase assay also showed no evidence of binding in the tested concentration range (Figure 39). In addition, also a reference compound **PFK-15** with a reported IC_{50} [61] of 0.21 μ M does not shown any binding affinity in our assay (Figure 40).

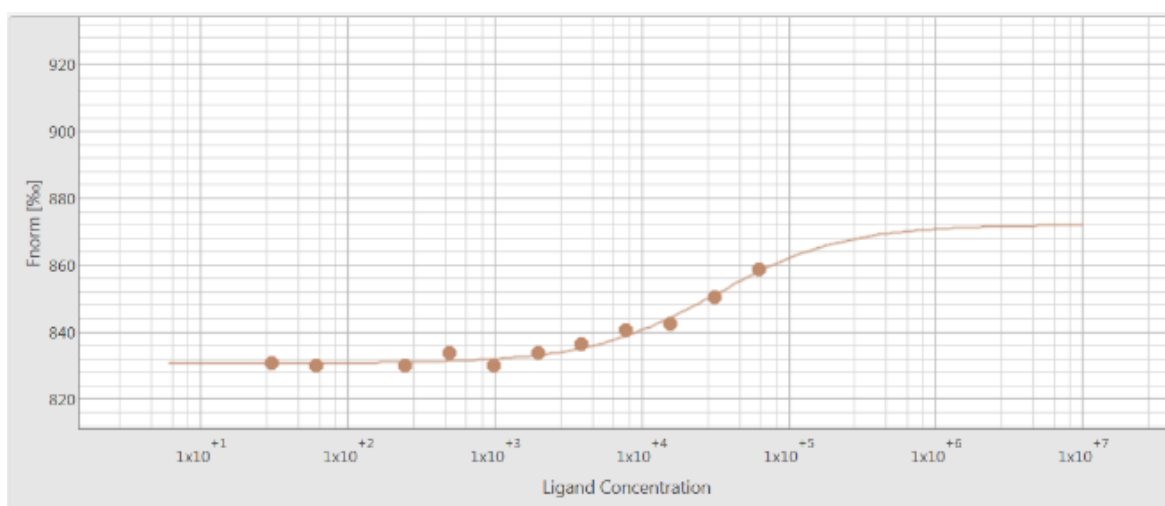
Table 14: Binding affinity for chosen kinase inhibitors.

COMPOUND	BINDING AFFINITY
AZ-68	$(0.350 \pm 0.96) \mu$ M
F-AZ-68	$(32.1 \pm 1.63) \mu$ M
3-PO	No binding
PFK-15	No binding



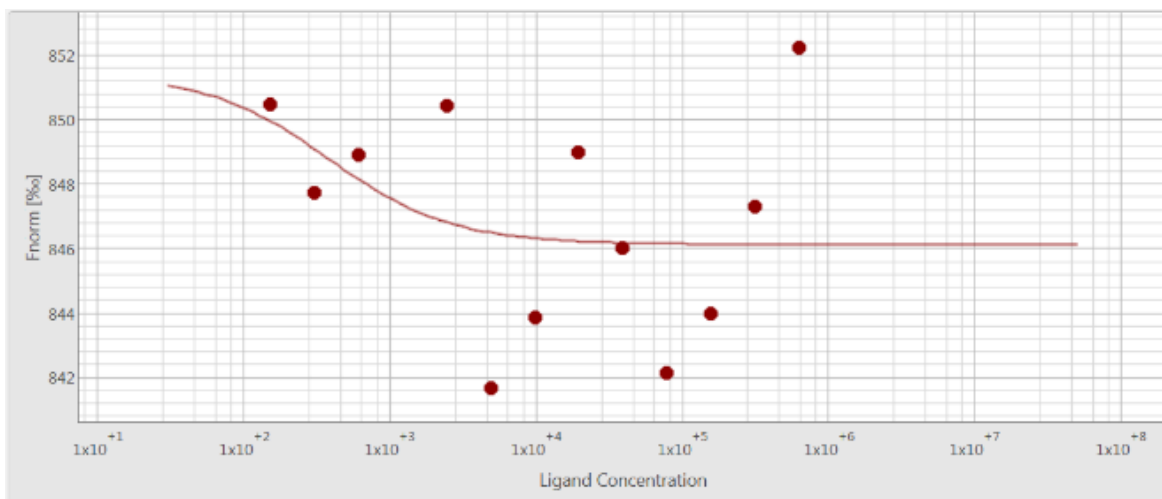
PARAMETER	RESULT
KD	350.3 nM
RESPONSE AMPLITUDE	9.4951
STANDARD ERROR	0.9589

Figure 37: MST Binding affinity profile for compound AZ-68.



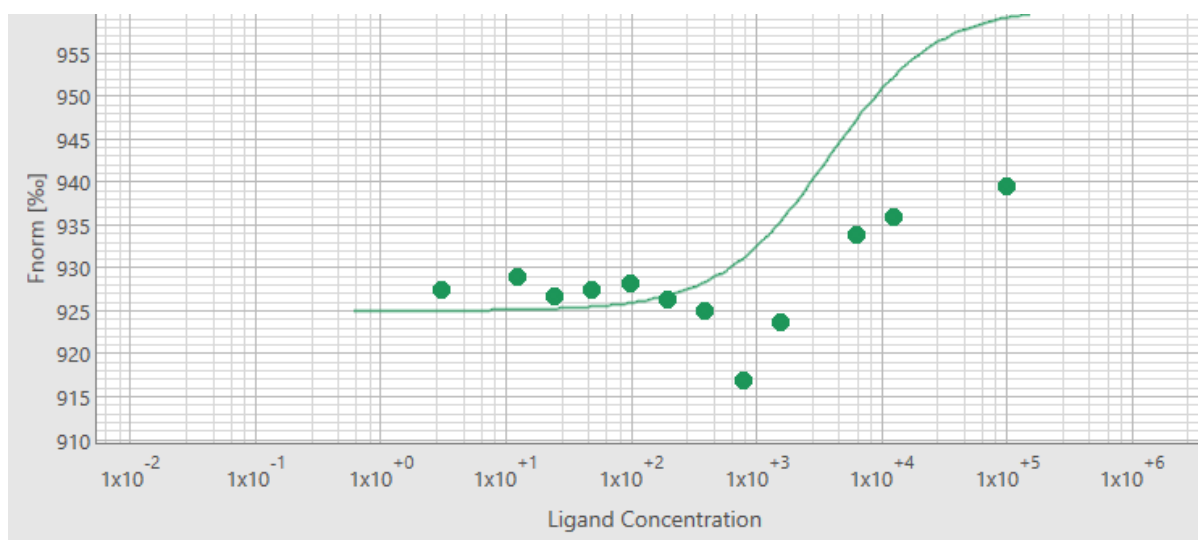
PARAMETER	RESULT
KD	32.142 μ M
RESPONSE AMPLITUDE	41.3747
STANDARD ERROR	1.6279

Figure 38: MST Binding affinity profile for compound F-AZ-68.



PARAMETER	RESULT
KD	failed
RESPONSE AMPLITUDE	failed
STANDARD ERROR	failed

Figure 39: MST Binding affinity profile for compound 3-PO.



PARAMETER	RESULT
KD	failed
RESPONSE AMPLITUDE	failed
STANDARD ERROR	failed

Figure 40: MST Binding affinity profile for compound PFK-15.

Surface plasmon resonance

Overview

SPR is a phenomenon that occurs when polarized light beam strikes a metal surface (normally gold and silver) and generates plasmons, electron charge density waves, that reduce the intensity of reflected light at a particular resonance angle, which is in proportion to the mass on a sensor surface. This method was introduced in the 1990s as a new approach that allows label-free detection of biomolecular interactions [77, 78]. Due to this technique's exquisite sensitivity to the refractive index of the medium next to the metal surface, it is possible to precisely measure the adsorption of molecules on the metal surface and their possible interactions with specific ligands. SPR is nowadays widely used in pharmaceutical industry for real-time measurement of ligand-receptor interaction kinetics, screening of lead compounds and also measurement of DNA-hybridization, enzyme-substrate interactions, protein conformation studies, label-free immunoassays, etc. [79]

In SPR assays, target molecules, normally proteins, are immobilized on a gold sensor surface and a sample of eventual interacting partner is injected over the surface through a series of flow cells. Polarized light is directed against the sensor surface during the interaction process and the angle of minimum intensity light is detected. As molecules bind and dissociate, this angle changes and the interaction profile in real time is thus recorded in a sensorgram (Figure 41). It provides quantitative data about binding, specificity, concentration, kinetics and affinity of an interaction.

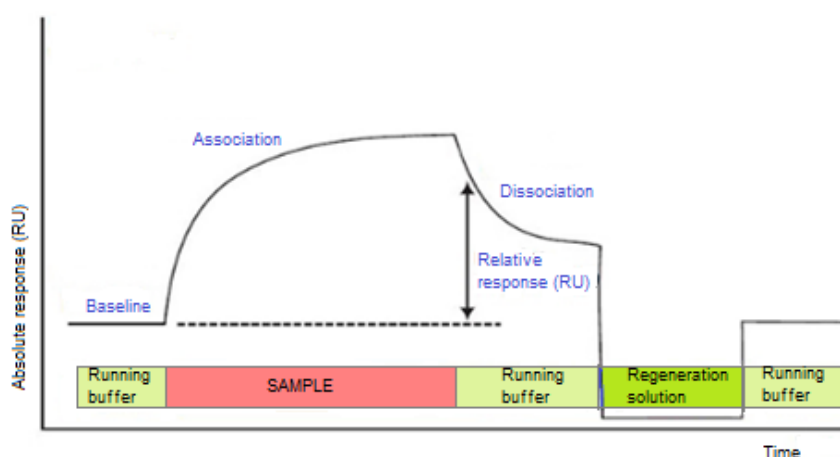


Figure 41: Sensorgram. During sample injection the analyte binds to the ligand and the positive response is shown. This response decreases during dissociation and regeneration buffer is passed over the chip after an analysis cycle is completed, removing bound analyte and regenerating the sensor chip [77].

Results. SPR kinetics

Biacore X100 kinetics experiments were run in multicycles (no chip regeneration between cycles) for control compounds **AZ-33** and **AZ-67** [61]. The most stable capture signal was detected when 50 nM PFKFB3 in running buffer was captured on NTA chip (Figure 42).

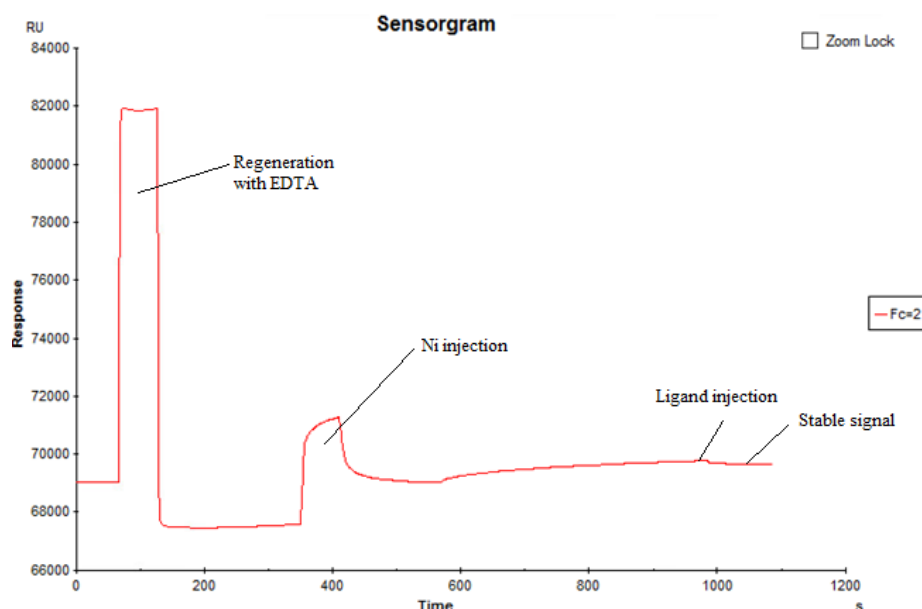
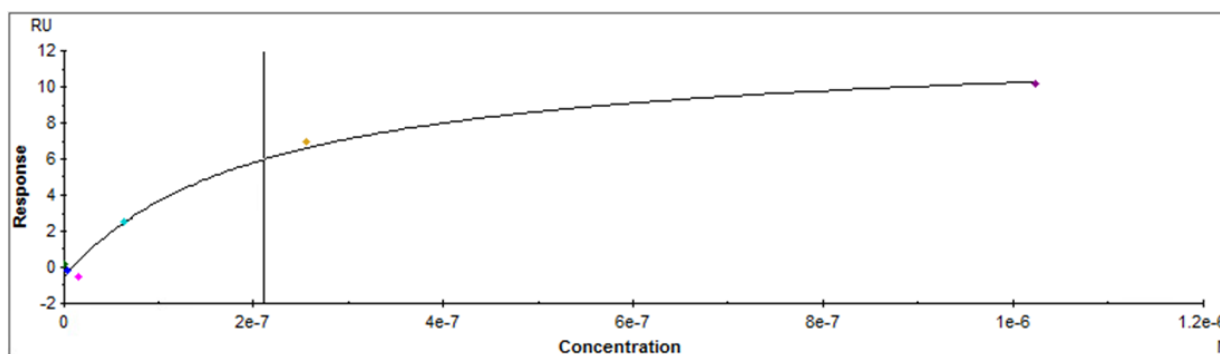


Figure 42: Capture of 50 nM PFKFB3 in running buffer. Regeneration with 0.35 M EDTA was done prior to the chip surface treatment with Ni and ligand capture.

A multicycle kinetics experiment was run for water soluble compound **AZ-33** and a submicromolar K_D value of 0.2 μM was calculated (Figure 43).



K_D (μM)	R_{MAX} (RU)	OFFSET (RU)	CHI^2 (RU ²)
0.211	13.12	-0.5801	0.445

Figure 43: SPR sensorgram for AZ-33.

The same method was applied for **AZ-67**, however, due to poor water solubility, 0.5 % DMSO had to be used in all samples. Therefore, a solvent correction step was introduced to the method and the resulting sensorgram did not meet the expectations and the experiment quality was too poor to conclude the binding.

d) DISCUSSION

By testing the kinase activity of the reference compounds **AZ-68** and **AZ-33** from AstraZeneca phenoxyindole and indazole series and obtaining the IC₅₀ values in the same range as reported in literature [61], we confirmed the quality of our kinase activity determination using our recombinant PFKFB3 and the kinase kit. However, significant differences in activity occurred in the case of compound **AZ-67**, which could be due to this compound's poor solubility in aqueous solutions. Furthermore, fluorinated **AZ-68** and an **AZ-68** analogue with a different *N*-alkylation on pyrazole ring resulted significantly less active. This means that the additional fluorine on *N*-isobutyl chain does not form additional interactions in the ATP binding site and that the position of the *N*-isobutyl substitution on indazole ring is crucial for good interactions with the binding site. This was confirmed also with the MST binding affinity study (p. 72-73) carried out for **AZ-68** and its fluorinated analogue where we observed a hundred-fold decrease of the binding affinity in the case of the latter. Moreover, **3-PO** inactivity and inability to bind PFKFB3 raised questions regarding the credibility of published data connected to this compound. Interestingly, the binding affinity of **AZ-68** (0.35 μM) is significantly different from its kinase activity (3.2 nM). Also for **AZ-33** where the binding affinity was determined with SPR, a similar trend is observed as the IC₅₀ value (21 nM) is significantly different from its binding affinity (0.21 μM). This difference could be explained with the fact that different kinase assay protocols can be used for the kinase activity experiment. In case where the assay was done according to manufacturer's protocol and the compound was not incubated with the enzyme prior to the substrate addition, we observed approximately 100-fold lower activities than in case when this incubation was done as described in the protocol reported by St.Gallay et al. [75]. It could be postulated that if the inhibitor is incubated with the enzyme first, there is no competitive inhibition with the substrate and therefore, the compound results more potent than it actually is. On the other hand, the binding affinity gives a more reliable information about the binding and cannot be manipulated since K_d is a thermodynamic constant and is calculated exclusively for the enzyme and ligand.

In addition, **AZI** compounds were inactive in our activity assay. This negative result could be due to the fact that *in silico* methods statistically require a larger number of compounds to be experimentally evaluated in order to show a positive result. The probability of success of computational calculations decreases in the case of more problematic targets, such as kinases.

Therefore, it would make sense to generate a larger library of compounds and screen them for kinase activity. By doing so, the probability of finding a hit compound would increase.

Finally, **AZPP** ligands library was generated in an attempt to optimize the inhibitory activity of a micromolar PFKFB3 inhibitor **AZ-a** [75]. The new compounds, however, did not exhibit increased potency towards the target. The possible explanation for this could be that the introduced modifications did not form additional interactions in the binding pocket and therefore only very modest potency (up to 5 fold RA decrease) was found. An alternative approach to address this task would be to choose a submicromolar inhibitor **AZ-b** as the starting compound for optimization because this compound was the most potent inhibitor from the study presented by St-Gallay et.al.

VII. CHAPTER 4: F-6-P BINDING SITE KINASE INHIBITORS

The research work presented under this chapter is a result of a short side project carried out by Xiao Hu and myself, where I was in charge of the experimental part. The leading idea of this project was to evaluate the possibility of inhibiting the PFKFB3 kinase with a F-6-P competitive inhibitor rather than ATP-competitive. The reasoning behind this idea was to avoid the well-known drawbacks of ATP-competitive kinase inhibition and take advantage of the fact that there are two different substrate binding sites on the PFKFB3 kinase domain. In order to tackle about the possibility of targeting the F-6-P binding site, a commercial Asinex library was screened and 12 compounds with the highest ranking were purchased and tested for their kinase activity.

a) DESIGN

As an alternative to the ATP competitive PFKFB3 kinase inhibition, the target potential of F-6-P pocket was explored. The leading idea of this side project was the fact that F-2,6-P₂ allosterically activates PFK-1 within the glycolysis cycle and the F-6-P binding site (Figure 44) seems a potential viable target and an efficient novel inhibition strategy with improved specificity. The pocket centre and size were defined by considering both the F-6-P and ATP binding sites. The VS- procedures for the kinase-inhibitor and the narrowed down lead-like libraries were run separately. 12 compounds targeting F-6-P binding site from Asinex commercial kinase inhibitors library were purchased and further evaluated *in vitro*.

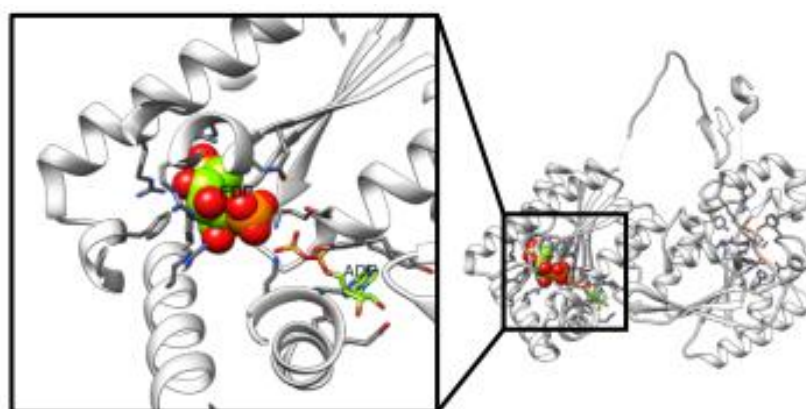
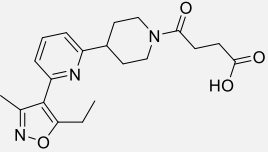
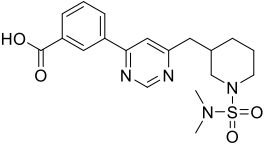
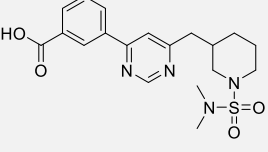
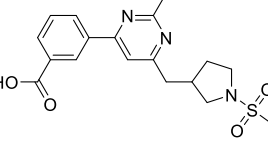
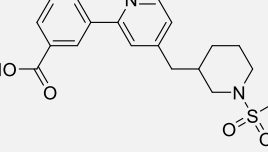
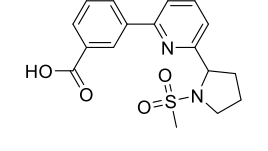
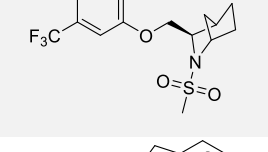
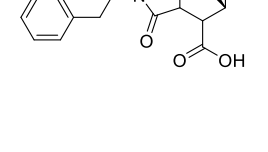


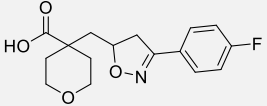
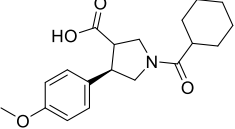
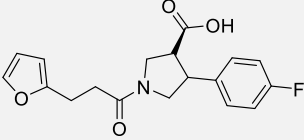
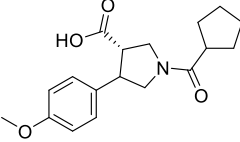
Figure 44: The relative position of binding site for F-6-P.

b) RESULTS

12 commercial compounds from Asinex were tested and residual activity was calculated for 10 and 100 μM concentration as presented in Table 15.

Table 15: F-6-P binding site potential inhibitors PFKFB3 inhibitors.

COMPOUND	STRUCTURE	MW	RA % (AT (100 μM))	RA % (AT 10 μM)
BDF34126821		371.44	16.5 ± 0.443	15.6 ± 0.163
BDE33512311		360.43	15.9 ± 0.473	16.7 ± 0.110
BDE33512289		404.49	15.0 ± 0.600	16.7 ± 0.114
BDE33512262		375.44	15.4 ± 0.400	14.8 ± 0.0710
BDE32496825		374.46	17.2 ± 0.347	30.3 ± 0.461
BDE324968822		346.40	14.4 ± 3.090	15.3 ± 0.134
AAM19379470		349.37	15.8 ± 1.15	15.0 ± 1.69
SYN17480249		301.34	14.9 ± 1.77	14.7 ± 0.666

ADM15446753		307.32	18.1 ± 0.487	17.2 ± 1.41
AEM11794304		331.41	15.0 ± 0.250	18.8 ± 0.152
AEM11723378		331.34	15.2 ± 9.86	19.5 ± 0.158
AEM11729168		317.39	19.6 ± 12.8	20.3 ± 0.792

c) DISCUSSION

All twelve tested compounds showed a modest effect on the PFKFB3 kinase activity- the residual activity decreased by 5-6 fold. However, the RA was concentration independent and we were unable to determine the IC₅₀ value for those compounds with the standard protocol. The obtained results seem rather odd because all tested compounds gave a similar response in the kinase assay. However, the interference of the compounds with the kit was excluded since extra blanks with the compound, enzyme but no substrate or compound, substrate but no enzyme were introduced. According to the manufacturer's protocol, in case where those additional blanks give no or very low response, compounds' interference with the reagents from the kinase kit can be ruled out. Furthermore, positive and negative controls were used to confirm the test's credibility. Another possible explanation for the odd response in the kinase test could be compounds' toxicity, however, we have no experimental data (e.g. MTT test) to prove or disprove this statement.

Several suggestions have been made for compounds optimization however, this work was beyond the scope of the herein presented PhD project and would require a considerable amount of time and resources.

VIII. CONCLUSION

The final outcome of the main research project of the PhD work presented herein was the identification of peptides **HM-21** and **HM-22** that can bind and modulate the PFKFB3 bifunctional enzyme phosphatase activity without affecting its kinase activity. Interestingly, the effect of the most promising peptides, **HM-21** and **HM-22**, on PFKFB3 phosphatase maximal velocity is comparable to the effect of a very potent ATP-competitive kinase inhibitor, **AZ-33**. This finding is very important since we proved that PFKFB3 phosphatase can be allosterically modulated and the result of this modulation is an inhibitory effect of the overall enzymatic activity. MD simulations that were conducted on PFKFB3 in the unbound state and in the bound state with natural ligands or products, showed a possible correlation between the ATP binding site and the phosphatase active site. The key reason for this correlation is the α -helix α 17 that spreads from the ATP binding site to the Glu322-Ala325 loop that floors the phosphatase site. To sum up, experimental findings together with computational data suggest that ATP or its mimic might act as a negative modulator of glycolysis. In addition, we showed that the peptides developed to target the secondary allosteric site in between the two monomers can selectively modulate the PFKFB3 phosphatase kinetics. Furthermore, cell tests showed that our most promising peptides display no significant cytotoxicity in MTT assay and that **HM-21** inhibits the EC migration, which is probably through an indirect PFKFB3 inhibition. Unfortunately, we were unable to obtain a co-crystal of **HM-21** or **HM-22** in the binding pocket and thus experimentally and undoubtedly describe the binding poses of our peptides. Although the final conclusion of this PhD is mostly computational, this result might be of great interest to the scientific community in general and especially to the research groups working on this class of enzymes. Our peptides may serve as lead compounds in the development of even more potent phosphatase allosteric modulators. Hopefully, the tools to study this class of enzymes will open new therapeutic opportunities in the near future.

Moreover, also the short side project about the F-6-P binding site inhibitors might be of great interest to the other research groups working on the same target. Although we were unable to find a hit compound for the discovery of F-6-P competitive inhibitors, an attempt has been made towards this novel design strategy. Further *in silico* studies followed by experimental *in vitro* studies of a higher number of compounds might lead to a success and discovery of a new and more specific approach for PFKFB3 kinase inhibition.

IX. MATERIALS AND METHODS

a) COMPUTATIONAL PART

The investigation of the AD region function, single-position and double-position mutations were performed by LowMod mutation calculation included in MOE. Additionally, two preselected libraries of small molecules from ZINC database were submitted for virtual screening using the two proposed strategies. A list of 96 commercially available small molecules/peptides were suggested for experimental assays.

PFKFB3 Protein Structure for Virtual Screening

The PFKFB3 structure of PDB ID 2ILV was chosen as the starting structure for further processing. It provided a reasonable resolution of 2.50 Å, and a good length of β -hairpin region has been resolved. The complexed crystal has the natural ligands bound at both binding sites and a PISA-constructed dimeric structure was also available. Each monomer contained 449 amino acid residues. The MOE 2015 software package was applied for the dimeric structure preparations. All crystal water and the phosphonic acid were deleted. The missing loops (P28-N32 and S445-N453) of the crystal structure were constructed through a standard loop building procedure included in the “Structure Preparation” functionalities of MOE. The C-terminus was not included in all the crystal structures, hence it was also not modelled in this study. Both *N*- and *C*-termini were capped to prevent terminal artefacts. All missing hydrogens were added using Protonate 3D method provided in MOE.

Virtual screening

In order to fully expose the binding site to allow protein-restrained docking, the β -hairpin was stripped and this structure was applied for virtual screening as *apo* PFKFB3 hereafter. The intact protein structure with the β -hairpin in place was applied for virtual screening as *holo* PFKFB3 hereafter. Two preselected screening libraries were derived from ZINC database with the sizes of 644 and 4819 compounds, respectively. Each library was screened using both the *apo* and *holo* structures of PFKFB3. The size of the docking site was defined by the biggest molecule presented within the screened library by increasing the value more than 2Å and round

up to the closest integer (15 Å for both apo and holo structures). Different ring conformations were generated and evaluated by SPORES included in the PLANTS (Protein-Ligand ANT System) docking software [80]. SDWASH was applied to determine reasonable tautomerism states of the ligand and stereoisomers were evaluated using SDSTEREO. The structures were minimised briefly using the db_Minimize function within the MOE package. Docking of the generated conformers was performed using PLANTS with search speed set to 1. Ligands were ranked according to the score using PLANTS_{chemplp} scoring method.

A score cut-off was used to select the better ranked ligands for further interaction analysis. Due to differences in physical and chemical properties of the two targeted sites, the score cut-offs were set differently for the two strategies adapted; the PLANTS_{chemplp} score cut-off of -110 for the screening using the holo receptor and -100 for the apo receptor. The selected compounds from each library per structure applied underwent a further selection according to their interactions to the receptor. This interaction analyses were performed and visualised using ligand interactions function included within the MOE package. Separate lists of testing compounds were generated for each library per receptor structure, and further experimental tests were performed as aforesaid.

Asinex libraries were also adopted to find potential lead-like compounds. For the phosphatase allosteric site, the Asinex lead-like library was applied. The library contained 103175 compounds, which was not manageable. Thus, the library was processed using several criteria in chemical properties to shrink the size of library to be screened. The selected compounds had a molecular weight in the range from 250 to 350 Da, fewer than 5 hydrogen bond acceptors and a logP in the range from -0.4 to 3. The library was processed with MOE suite to generate correct 3D structures and briefly minimised. These initial treatments resulted in a shrunken lead-like library with a size of 6354 compounds. The library of compounds was firstly screened in triplicates using PLANTS docking package with empirical chemplp scoring method. The 1000 top ranked molecules were then passed onto MM-PBSA rescoring process. The 50 top re-scored complexes were analysed further by pose reproducibility among three repeats and visual inspection. 12 compounds were suggested to be purchased for further experimental validation.

For the kinase F-6-P binding site inhibitors, the generated candidate compounds from Asinex commercial library were further virtually screened and rescored as described above and 12 compound were selected for *in vitro* kinase activity test.

MD simulations

3 states of PFKFB3 underwent MD simulations: the unbound, the substrate-bound, and the product-bound states. The initial crystal structure (PDB ID: 2i1v²⁵) has already included the natural enzymatic products within the binding site. The *apo* structure was generated by deleting the bound ligands of 2i1v.²⁵ As for the substrate-bound state, the bound products were modified by adding or deleting an additional phosphate group at the correct position and minimized briefly *in situ* using MOE package.²⁶

Moreover, the foreign ligands (ATP, ADP, F2,6BP, and F6P) were re-parameterized for compatibility with AMBER simulation package.²⁹ The ATP and ADP parameters were published elsewhere³⁰ and were downloaded from Ref.³¹. The re-parameterizations of F2,6BP and F6P were performed with the RESP ESP charge Derive program (R.E.D.)³² and antechamber.^{33,34} The R.E.D. program was applied to assign partial charges to atoms presented within F2,6BP and F6P. The structures of F2,6BP and F6P were first submitted to conformational search in MOE²⁶ using the default settings. The two conformations with the lowest calculated conformational energies were saved for partial charge assignment. For each conformer, two orientations were also adopted during the charging process by rotating the molecule 180°. The terminal oxygens within the phosphate groups in both F2,6BP and F6P were forced to be equivalently charged within each functional group. The atom types of *gaff* were assigned using antechamber.^{33,34}

The *ff14SB*³⁵ and the *gaff*³³ force field were applied for PFKFB3 protein and the ligands, respectively. The topology and coordinate files required for MD simulation were generated using *tleap*.²⁹ The protein / complexes were firstly neutralized with sodium or chloride ions; 6 Cl⁻ were added for *apo* PFKFB3 and 10 Na⁺ were added for the product- and substrate-bound structures. The protein / complexes were then solvated with TIP3P explicit water molecules in a cubic box 12 Å from protein surface to the barrier. The neutralized and solvated structures were used as the starting structures for MD simulations.

MD simulations were run for *apo*, product-bound, and substrate-bound PFKFB3 structures, 3 replicates for each state. The *pmemd.MPI* module was applied for all the simulations.²⁹ The energy minimization, heating, and equilibration procedures prior to MD simulations were all performed in multi-step manners, same procedures for every run. Non-bonded cut-off of 8 Å was applied throughout. Energy minimization started with relaxing hydrogen positions with

other atoms restrained with 1000 steepest-descent (SD) followed by the conjugate gradient (CG) method to a maximum cycle of 5000. This step is followed by a 5000-max-cycle minimization (2000 SD+ CG) of water and ions. The minimization was then extended onto side chains of amino acid for another 5000 maximum cycles (2500 SD + CG).

The system then underwent 6 steps of heating to a final temperature of 300 K under the NVT condition (constant volume and temperature with total number of atoms unchanged). From this step on, SHAKE algorithm is applied to bond constraint involving hydrogen atoms and Langevin dynamics was applied for temperature scaling. Each heating step was performed with a controlled heating of 50 K gap over 5 ps with a 0.0005 ps time step, while protein backbone was weakly restrained ($10 \text{ kcal}\cdot\text{mol}^{-1}\cdot\text{\AA}^{-2}$). After each 50 K heating process, the system was equilibrated for an additional 5 ps at the targeted temperature.

After the temperature of the simulated system reached 300 K, a 200 ps equilibration was firstly performed under NVT condition with the backbone weakly restrained ($5 \text{ kcal}\cdot\text{mol}^{-1}\cdot\text{\AA}^{-2}$). The simulation condition is then switched to NPT (constant pressure and temperature with total number of atoms unchanged) and equilibrated for another 200 ps with the $5 \text{ kcal}\cdot\text{mol}^{-1}\cdot\text{\AA}^{-2}$ constraint still applied for protein backbones. Following this, 5 steps of 500-ps equilibration runs were performed to reduce the constraint weight on protein backbones gradually. Each step reduces the constraint by $1 \text{ kcal}\cdot\text{mol}^{-1}\cdot\text{\AA}^{-2}$ until the constraint was completely removed.

Lastly, MD simulations were performed under NPT condition at 300 K for 200 ns for each PFKFB3 state and repeat. The hydrogen-involved bond SHAKE constraint and Langevin temperature scaling were applied. Non-bonded cutoff was continued as 8 \AA and the simulation time step was set to 0.002 ps. Frames were recorded at a 1-ps frequency and the trajectories were written in the binary NetCDF format. The trajectories were processed and analyzed using *cpptraj*.²⁹

AZI-based computational strategy

A tiered virtual screening (VS-) was performed on a 3D conformational library [81] derived from the ZINC database containing about a million drug-like chemically diverse molecules. The hierarchical strategy started from the elucidation of a 3D pharmacophoric query bearing the steric and electronic features essential for kinase inhibition. The pharmacophore was used for preliminary filtering of the molecular library, retrieving thus only compounds matching the

query. The resulting subset of about 400 compounds fitting the pharmacophore map was submitted to molecular docking using PLANTS (Protein-Ligand ANT System) [80]. The system is based on stochastic optimization algorithm-to iteratively find the preferred binding mode of each ligand inside the PFKFB3 kinase binding site. All tautomers, stereoisomers and ring conformations were pre-generated with a fully automated tool, and after docking process, the lowest energy docked geometry of each ligand was considered for a visual inspection. Then, the docking poses were refined by performing short molecular dynamic (MD) simulations (1 ns) of the solvated complexes with Amber14 package [82]. The obtained MD trajectories were analysed to assess the system stability, considering a RMDS tolerance of 3 Å. Free binding energy of the ligand-protein interaction was calculated post-processing snapshots of MD simulations to a modified version of the Molecular Mechanics Generalized Born Surface Area calculation (MMGBSA), referred as Nwat-MMGBSA [76, 83] The latter allows to predict the free binding energy more efficiently by including a specific number of explicit water molecules (N_{wat}) around the ligand in addition to the implicit continuum solvation medium of the MMGBSA method. This calculation was repeated three times setting up 0, 30, and 60 water molecules as explicit hydration shell ($N_{\text{wat}} = 0, 30, 60$).

b) PEPTIDE SYNTHESIS

Amino acids, coupling reagents and other chemicals for SPPS were purchased from Sigma Aldrich and Fluorochem. Manual peptide synthesis vessels were purchased from Sepachrom. For automated microwave assisted solid phase synthesis a CEM Liberty instrument was used.

Protocol for the manual peptide synthesis

Resin handling

Swelling of the resin. The dry resin was placed in a peptide synthesis reactor and sufficient amount of DMF was added to cover the resin with two-three times bed volume. The reaction vessel was allowed to shake gently for 30 minutes. The solvent excess was removed by applying vacuum.

Washing: Three bed volumes of DMF/DCM were added to cover the resin and agitated for 10 s. The solvent was removed by applying vacuum. The whole process was repeated six times with DMF and three times with DCM.

Drying: After washing with DMF/DCM as described above, three beds of diethylether were added to cover the resin, agitated for 10 s and removed by vacuum. This process was repeated 3 times and then the resin was dried under the air for 30 min.

Attachment of the first residue

Wang resin. 250 mg of Wang resin (loading capacity 0.6 mmol/g) was placed in a reaction vessel and swelled as described above. Appropriate amino acid (5 eq.) and HOBt (5 eq.) were weighted in a 25 mL round bottom flask and dissolved in DCM. The mixture was stirred on ice bath and *N,N'*-Diisopropylcarbodiimide (DIC; 5 eq.) was added. After 20 min, the solvent was evaporated and dry residue re-suspended in DMF. DMAP (0.01 eq) was added to the mixture and the solution was added to the resin dropwise. After 1h of gentle shaking, the resin was washed as described above.

Rink amide resin. 250 mg of Rink amide PEG MBHA resin (loading capacity 0.6 mmol/g) was placed in a reaction vessel and the resin was swelled as described above. Three times bed volume of 20% piperidine solution in DMF was added to the resin and agitated for 5 min. The solution was removed by vacuum and additional three times bed volume of 20% piperidine solution in DMF was added to the resin, agitated for 15 min and washed as described above.

CTC resin. 250 mg of CTC resin (loading capacity 0.6 mmol/g) was placed in a reaction vessel and the resin was swelled as described above. Appropriate amino acid (5 eq.) was dissolved in DMF and mixed with DIPEA prior to the addition to the resin. The vessel with the resin was agitated for 1 h and then the solvent was removed by vacuum and 0.5 mL of MeOH was added to the resin and agitated for another 30 min.

Measurement of the Wang resin loading. After the first amino acid residue coupling, a small quantity of the resin was removed from reaction vessel and treated with 20% piperidine in DMF using the standard procedure and the deprotection solution was then collected. UV spectrometer was zeroed with a clean solution of 20% piperidine in DMF and the absorbance value was measured at 301 nm. The amount of released Fmoc during the deprotection was calculated using Beer's Law. The extinction coefficient of the Fmoc-piperidine adduct is 6000 $M^{-1}cm^{-1}$. The amount of Fmoc released into the deprotection solution is directly proportional to the amount of amino acid loaded onto the Wang resin.

Fmoc removal. Removal of the Fmoc group from the *N*-terminus of the resin-bound peptide is normally achieved by treating the resin with 20% piperidine in DMF. Three bed volumes of 20% piperidine in DMF was added to the resin and agitated for 5 min. The solution was

removed by vacuum and additional three times bed volume of 20% piperidine in DMF was added to the resin, agitated for 15 min and washed as described above.

Coupling reaction. Appropriate amino acid (5 eq.) was weighted and dissolved in DMF. HOBt/HOBT (5 eq.) solution and DIPEA (10 eq.) were added to the amino acid and the mixture was added to the swollen resin and agitated for 1h. After the coupling reaction was completed, the resin was washed according to previously mentioned protocol.

Cleavage from the resin. The cleavage cocktail that was used for peptides synthesized on Wang or Rink amide resin was TFA (88 %), water (5 %) and phenol (5 %) and TIS (2 %) as scavengers since most of the peptides had *t*-butyl based or trityl protecting groups on their side chains.

Cleavage cocktail TFA/water/phenol/thioanisole: 88/5/5/2 (10 mL) was added to the reaction vessel containing dry resin. The vessel was closed with a lid and gently agitated for 5h at room temperature. Then, the liquid was filtered to a centrifuge tube using vacuum and cold diethyl ether (20 mL) was added in order to precipitate the peptide from the cocktail. The mixture was then centrifuged 3 times at 3000 xg and the supernatant was removed from the solid residue. The peptide was gently dried over air and stored at -20°C.

The cleavage conditions for peptides synthesized on CTC resin are much milder, however, in case the side chain protection groups had to be removed, TFA cleavage cocktail had to be used afterwards.

Cleavage cocktail DCM/acetic acid: 9/1 (2.5 mL) was added to the reaction vessel containing dry resin. The vessel was closed with a lid and gently agitated for 1 h at room temperature. Then, the liquid was filtered to a centrifuge tube using vacuum and cold diethyl ether (20 mL) was added in order to precipitate the peptide from the cocktail. The mixture was then centrifuged 3 times at 3000 xg and the supernatant was removed from the solid residue. The peptide was gently dried over air and stored at -20 °C.

Purification with RP-HPLC. Peptides were purified with the following RP-HPLC method: gradient elution of 5–70% solvent B (solvent A: water/acetonitrile/TFA95/5/0.1; solvent B: water/acetonitrile/TFA 5/95/0.1) over 20 min at a flowrate of 20 mL/min using Jasco BS-997-01 equipment and a DENALI C-18 column from GRACE VYDAC (10 lm, 250 9 22 mm). Fractions containing the desired peptide (after confirmation with MS) were collected together, lyophilized and stored at -20 °C.

Analytical HPLC. Peptides were analysed with the following method: gradient elution over 20 min with two mobile phases: A = 95 % water, 5 % ACN, 0.1 % TFA; B = 95 % ACN, 5 %

Water, 0.1 % TFA. at a flowrate of 0.8 ml/min. For the analysis, a Jasco BS-997-01 equipment and detector series Star 800 from VARIAN were used.

Mass spectrometry. The mass spectra were recorded on a LCQ Advantage spectrometer from Thermo Finnigan for ESI-MS analysis and on Autoflex 3 from Bruker Daltonics for MALDI-TOF analysis.

c) CIRCULAR DICHROISM

CD spectra were collected using a Jasco J-810 spectropolarimeter. All samples were prepared from 100 μ M peptide stock solutions in 50 mM phosphate buffer (pH=7.4) and the final concentration of the peptide was 100 - 10 μ M. Spectra were recorded in the far UV region (190 to 250 nm) with a 0.1 nm step and 1 s collection time per step, taking three averages. The spectrum of the buffer was subtracted to eliminate interference from cell, solvent, and optical equipment. The CD spectra were plotted as mean residue ellipticity (degree x cm² x dmol⁻¹) versus wave length (nm). Noise-reduction was obtained using a Fourier-transform filter program from Jasco. The results were processed with OriginPro 2016.

d) DYNAMIC LIGHT SCATTERING

Peptides were dissolved in water to 1 mM final concentrations. Each sample was filtered using 0.2 μ m syringe filter and placed in disposable sizing cuvette. Malvern DLS instrument for used for the measurement. The samples were recorded at 25 °C for 80 s and the results were analysed with Malvern software.

e) PFKFB3 EXPRESSION

E. coli competent cells were purchased from Invitrogen, affinity and ion exchange column were purchased from GE Healthcare. Thrombin was purchased from sigma and centrifugal concentrators from Millipore.

BL21(DE3) competent *E. coli* bacterial strain was used for the expression. Agar plates with kanamycin 50 μ g/mL were prepared from 10 g/L tryptone X, 5g/L yeast extract, 5g/L sodium chloride and 15 g/L agar and autoclaved. 1 μ L of plasmid was transferred to complementary *E.coli* cells and cells were incubated on ice for 30 min. After that, a 10s heat shock at 42^oC was

made to force cells to close the pores and keep the plasmid inside the cell. Then, the cells were left on ice for additional 5 min. 800 μ L of rich LB medium was added to cells and they were incubated for 30 min at 37°C. The suspension of cells was spread on 2 plates (100 μ L suspension on each) and the plates were left overnight at 37°C. A starter culture was prepared from a single colony and transferred to 200 mL of LB media with kanamycin and incubated with agitation at 37°C. OD was measured using UV-VIS (λ = 600 nm) reached 0.8. Then, the starter culture was expanded by adding it to a larger volume of LB medium with antibiotic kanamycin. 4 large flasks with 1000 mL LB growth medium (10g/L tryptone, 5g/L yeast extract, and 5g/L NaCl, kanamycin 50 μ g/mL) were prepared and left to incubate until OD reached 0.6. After that, the expression was induced overnight with 0.4 mM IPTG.

After that the suspension was centrifuged at 5000xg for 20 min. The pellets containing cells were collected and cells were lysed with lysis buffer containing 20 mM Tris pH 8, 0.3 M NaCl, 1 mM DTT, 20 mM imidazole and EDTA-free complete protease inhibitors, then French-pressed and centrifuged again. The supernatant was purified through a 5 ml bed volume HiTrap nickel immobilized metal ion affinity chromatography column connected to a FPLC system.

The following buffers were used:

Buffer A: 50 mM NaH₂PO₄ pH 8, 0.3 M NaCl, 1 mM DTT and 20 mM imidazole

Buffer B: 50 mM NaH₂PO₄ pH 8, 0.3 M NaCl, 1 mM DTT and 500 mM imidazole

In order to get a pure protein, the buffer was changed to 50 mM Tris HCl pH 8, 10% glycerol, 20 mM KCl, 5 mM KPi, 1 mM DTT and 0.1 mM EDTA and Mono Q anion exchange chromatography was performed after concentrating the protein to 1mg/mL.

Mono Q buffer A: 50 mM Tris HCl pH 8, 20 mM KCl, 5 mM KPi, 10% glycerol, 1 mM DTT and 0.1 mM EDTA.

Mono Q buffer B: 50 mM Tris HCl pH 8, 1 M KCl, 5 mM KPi, 10% glycerol, 1 mM DTT and 0.1 mM EDTA.

In the case the protein was needed for a crystallization trial, there was an additional step in which the His-tag was removed using 500 U thrombin and the buffer was exchanged with the overnight dialysis to the Mono Q buffer A.

Purifying processes were monitored with SDS Page gel and the protein was kept in 20 mM Tris-HCl pH 8, 10 mM NaPi, 0.05 mM EDTA, 5 mM β -mercaptoethanol and 5% glycerol. The protein was concentrated to 8 mg/mL or more with 50-kDa molecular mass cut-off centrifugal concentrator. In this buffer the protein was stable several months at -20°C up to concentration of 20 mg/mL.

The oligomeric state of the protein was analysed by size exclusion chromatography (SEC) on Superdex 200 SEC column using the same buffer of purification process.

Furthermore, a DLS experiment was performed to measure poly-dispersion and aggregation of the sample. The analyses were carried out through a DynaPro instrument (Protein Solutions, Charlottesville, USA). 200 µl of purified protein, at a concentration of 1 mg/ml, were filtered through 0.1 µm filter, centrifuged at 12.000xg for 10 minutes and added to a clean cuvette. The measurements were performed at 10°C using the software Dynamics V5 (Protein Solution INC) with acquisition time of 30 s, a mean value of 30 measurements and a NaCl 3% solution as solvent. The acquired data were analyzed using the software Dynamics V6 (Protein Solution INC).

f) KINASE ASSAY [61]

For the purpose of this study we used ADP Glo™ Kinase assay purchased from Promega. This is a luminescent ADP detection assay that measures the kinase activity by quantifying the amount of ADP produced during the kinase reaction. This assay is suitable for virtually any kinase and substrate combination and does not require radioactively labelled components or antibodies. The kinase substrate can be a peptide, protein, lipid or sugar.

ADP Glo™ Kinase assay was performed in two steps and measured on a 384-well white plate, purchased from Greiner. Kinase base buffer containing 100 mM HEPES (pH 7.0), 400 mM KCl, 10 mM potassium phosphate (pH 7.0), 10 mM MgCl₂, 1 mM dithiothreitol, 0.2 mM Triton X100 was prepared prior to the assay. PFKFB3 enzyme was added to the base buffer immediately prior to starting the assay. Each well received 8 µL of enzyme diluted in the base buffer (final concentration in the assay was 150 nM). The tested compound was added to each well starting from 0.75 µM to 100 µM (8 concentrations). After 30 min incubation, each well received 8 µL of a mixture containing 100 µM ATP and 200 µM fructose-6-phosphate. The reactions were left to incubate for 1 hour before the addition of 16 µL of ADP Glo reagent that terminates the kinase reaction and depletes ATP. After the second incubation of 50 minutes at room temperature, 32 µL Kinase Detection Reagent was added. This reagent converts ADP to ATP and allows the newly synthesized ATP to be measured using a luciferase/luciferin reaction. After an additional hour, reaction mixtures were transferred to a Greiner white 384 well plate in triplicates and Tecan Magellan spectrometer® with enhanced luminescence module was used to measure the luminescence signal generated in each well. The signal is proportional to the ADP concentration produced and is correlated with kinase activity. If

applicable, IC₅₀ estimates were calculated using a commercially available software package from GraFit5. In the case of less potent compounds, only residual activity was calculated.

Prior to compounds evaluation, a sensitivity and linearity test of the kinase assay were performed. Three ATP to ADP standard conversion curves were prepared at the indicated ATP+ADP in 25 μ L of reaction buffer (100 mM HEPES pH 7, 400 mM KCl, 10 mM KPi pH 7, 10 mM MgCl₂, 1 mM DTT, 0.2 mM Triton X).

Reactions for standard curves were prepared in 96-well plate, wells B1-12 and C1-12 received 90 μ L of kinase reaction buffer. Preparation of the 1 mM series of ATP+ADP standards (Figure 45) is presented in Table 16.

Table 16: Preparation of the 1 mM series of ATP+ADP standards.

Well number	A1	A2	A3	A4	A5	A6	A7	A8	A9	A10	A11	A12
1 mM ADP (μ L)	100	80	60	40	20	10	5	4	3	2	1	0
1 mM ATP (μ L)	0	20	40	60	80	90	95	96	97	98	99	100

100 μ M series (Figure 46) was prepared by transferring 10 μ L of the sample in well A1 to well B1, well A2 to B2. etc. 10 μ M series (Figure 47) was prepared by transferring 10 μ L of the sample in well B1 to well C1, well B2 to C2. etc.

25 μ L of the sample from each well was transferred into separate wells of the new assay plate and ADP GloTM reagent (25 μ L) was added to each well. After 40 min incubation at room temperature, Kinase Detection Reagent (50 μ L) was added to each well. Luminescence was measured after additional 1 h incubation at room temperature and standard curves were generated.

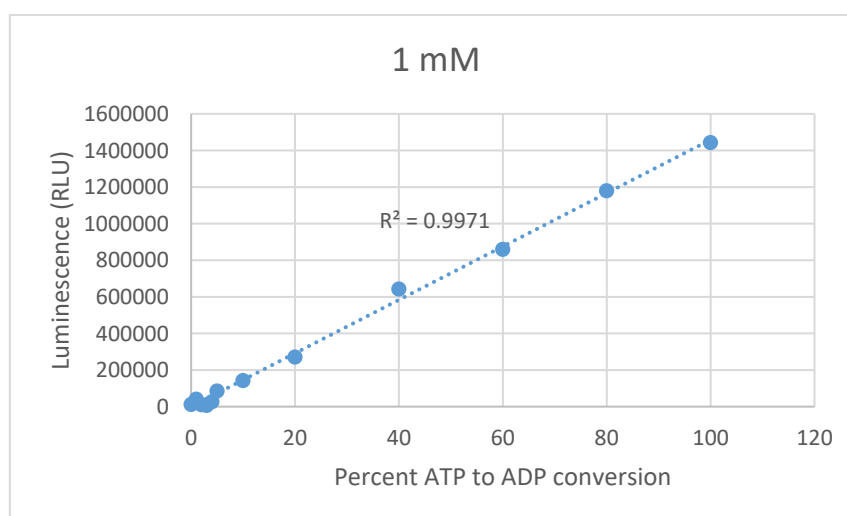


Figure 45: 1mM standard curve.

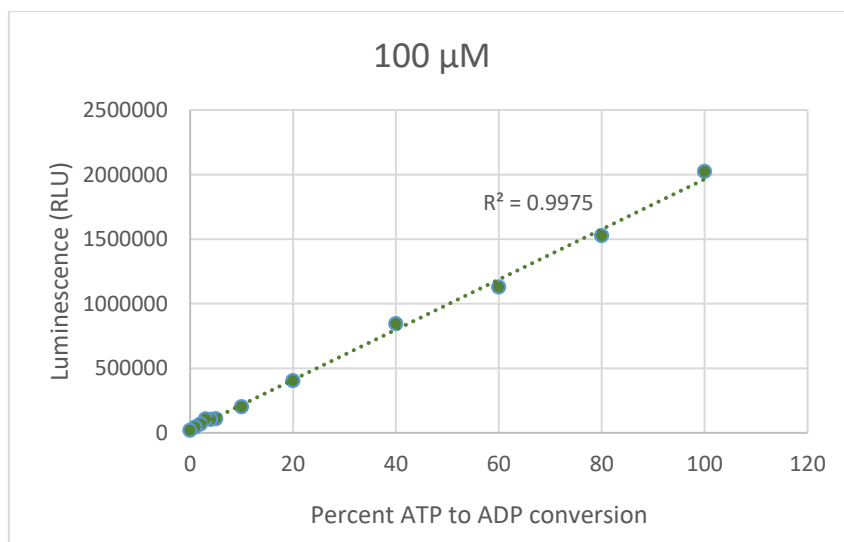


Figure 46: 100 μM standard curve.

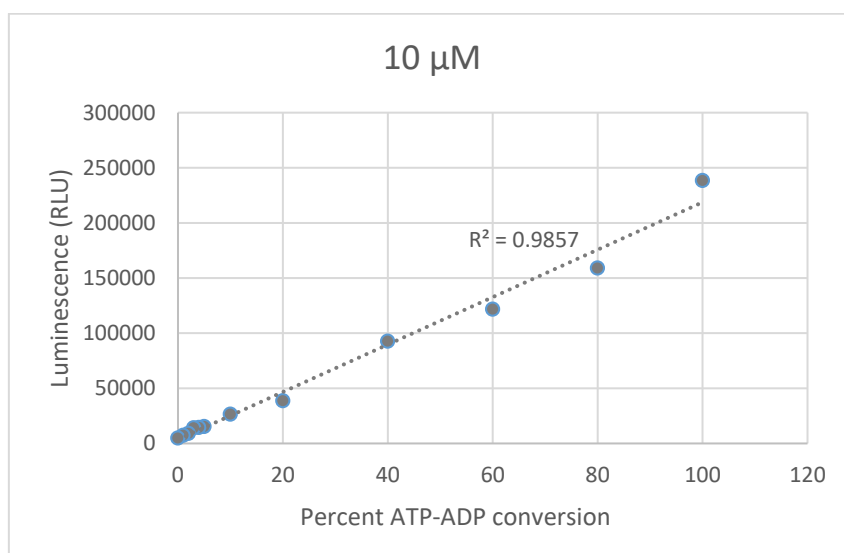


Figure 47: 10 μM standard curve.

A linear relationship was confirmed between the luminescent signal and the amount of ADP in the reaction buffer for all three ATP+ADP concentration series tested.

g) THERMOFLUOR

Thermofluorimetric (Thermal shift) assays for the evaluation of the PFKPF3 melting temperature (T_m) were conducted in a MiniOpticon Real Time PCR Detection System (Bio-Rad), using the fluorescent dye Sypro Orange. 4 μL aliquots of PFKPF3 solution (final protein concentration 35 μM) were diluted in 18 μL of its buffer, and mixed with 3.5 μL of Sypro orange (Sigma) diluted 60X. The sample plates were heated from 20 to 90 °C, with a heating rate of 0.2 °C/min. Fluorescence intensities were measured within excitation/emission ranges of 470–505 nm and 540–700 nm, respectively.

h) MST BINDING ASSAY

The dissociation constant was determined using Nanotemper Monolith NT.115 instrument. Premium capillaries, protein labelling kit and MST buffer were purchased from Nanotemper. Prior to the assay, the PFKFB3 protein was labelled with NHS-maleimide dye that reacts with Cys residues to form a covalent bond. In the first step, the protein buffer was exchanged to the labelling buffer using buffer exchange column A from the Nanotemper NHS-maleimide labelling kit. The buffer exchange column was placed in 1.5-2 mL microcentrifuge collection tube and centrifuged at 1500 x g for 1 minute to remove excess liquid. 300 μ L of labelling buffer was then added and the column was centrifuged again as described above. This step was repeated 3 times. After the column was equilibrated, 40-100 μ L of protein was placed in the centre of the resin, the column was put in a new microcentrifuge tube and centrifuged at 1500 x g for 2 minutes. After changing the buffer, the protein concentration was adjusted to 2-20 μ M using the labelling buffer. Maleimide dye solution was dissolved in labelling buffer and the dye concentration was 2-3 times higher than the protein concentration. Dye and the protein were mixed in 1:1 ratio (200 μ L final volume) and the mixture was left in the dark for 30 minutes. In the meantime, the purification column B from the labelling kit was prepared in order to remove the free dye. The column B was washed 3 times with 3 mL of MST buffer by flow through by gravity flow. A maximum labelling reaction volume of 500 μ L was placed to the center of column B and the sample was let to enter the bed completely. 600 μ L of MST buffer was added and the eluate was collected in 100-150 μ L fractions. The elution fractions fluorescence intensity was tested in the Monolith device. Labelled protein was split into 10 μ L aliquots and stored at -20°C.

In a typical MST binding experiment, a compound was dissolved in MST buffer and mixed with 100nM NHS-maleimide labelled recombinant PFKFB3 in 1:1 ratio. The mixture was incubated at room temperature for 20 minutes and full MST measurement was performed. If there was an evidence of binding, a full MST experiment was carried out for a large concentration range (16 conc.). Data was analyzed by Nanotemper software and K_d was calculated in the signal to noise ratio was >5 and response amplitude was at least 5.

i) PHOSPHATASE ASSAY

PFKFB3 phosphatase activity measurements

Phosphatase activity of PFKFB3 was measured by quantitation of the reaction product (i.e. fructose-6-phosphate, F-6-P) by means of liquid chromatography tandem mass spectrometry. Enzyme reaction rate was determined after 18 h of incubation at 37 °C in sterile (0.22 µm filtered) Tris buffer (20 mM Tris-HCl pH 8; 10 mM sodium phosphate; 5 mM 2-mercaptoethanol and 5 % of glycerol) at a final enzyme concentration of 100 nM. Both the enzyme and the substrate (i.e. fructose-2,6-diphosphate, F-2,6-P₂) were pre-warmed at 37 °C for five minutes before starting the kinetics by spiking the substrate into the enzyme solution. To plot the enzyme kinetic, the reaction rate was measured in independent experiments at different concentration of substrate (i.e. 5, 10, 15, 20, 25, 30, 40 and 50 µM).

Diafiltration on amicon-ultra filters (30 kDa MWCO) was used to stop the reactions. Both the residual substrate and the product were collected in the filtrate, while the enzyme was retained by the filter.

The same protocol was used to measure the effect of ligands on enzyme phosphatase activity. For such a purpose the reaction rate was measured at the same substrate concentrations, but the enzyme was incubated with the compound and pre-warmed before starting the kinetics. Compounds were incubated with the enzyme at a concentration 50 µM or equal to their K_d, if available.

Independent analyses were done without the enzyme (i.e. controls) to assess any degradation of the substrate in the same experimental condition used for the enzyme kinetics.

The concentration of the substrate produced by the kinetics was determined by interpolation with a calibration curve obtained by the analysis of F-6-P standards prepared in a concentration range between 0.5 µM and 50 µM. The velocity was calculated as nanomoles of F-6-P produced in one minute by a nanomole of PFKFB3, subtracting the nanomoles of F-6-P produced by self-degradation of the substrate from the nanomoles of F-6-P produced by the enzyme kinetic.

Instrumental analysis.

Quantitation of fructose 6 phosphate produced was provided by a Surveyor HPLC system connected to a TSQ Quantum Ultra triple quadrupole mass spectrometer by a Finnigan IonMax electrospray ionization (ESI) source assembled with a high flow stainless steel emitter (Thermo Scientific, Rodano, MI, Italy).

Filtrate containing the kinetics products were diluted 1:4 in water and placed into the autosampler rack which was cooled at 8°C to prevent sample degradation during analyses. Aliquots of 90 µL were injected and analyte separation was achieved at 40°C by using an Hypercarb column (100 x 2.1 mm; 5 µm particle size; 250 Å pore size, Thermo Scientific, Rodano, MI, Italy). Table 17 reports the mobile phases and gradient program used for the elution.

Table 17. Gradient program for the elution and quantitation of F-6-P by using Hypercarb column.

TIME (S)	%H ₂ O	% HCOO·NH ₄ ⁺ 0.1M
0.00	100	0
1.00	100	0
1.01	60	40
4.00	60	40
4.01	100	0
8.00	100	0

The flow from the column was directly sprayed into the mass spectrometer with no further splitting. Nebulization and ionization were achieved by 70 units of sheath gas, 25 units of auxiliary gas, a capillary temperature of 270 °C and a spray voltage of -4.5 kV.

The analyzer was scanning in multiple reaction monitoring (MRM) the negative ions reported in Table 18, with a scan time of 0.05 s and a resolution of 0.5 m/z for both the first and the third quadrupoles. The MRM transitions reported in Table 18 were previously optimized in a semi-automatic mode to achieve the best instrumental response and selectivity for fructose-6-phosphate, by flow injection of a standard solution.

Table 18. MRM transitions for selective determination of fructose6-phosphate.

PRECURSOR ION (M/Z)	FRAGMENT ION (M/Z)	COLLISION ENERGY (V)
258.92	79.1	45
258.92	97.1	20

j) ENDOTHELIAL MIGRATION ASSAY

Immortalized endothelial cells from mice and primary cells from humans were seeded in 12-well plates, allowed to reach confluence, and then starved overnight in DMEM plus 0.5% FBS or M199 plus 10% NBCSi. Each well was marked below the plate surface to create landmarks

to guide wounding and subsequent image analysis in the same location over various time points to monitor the migration of the cells into the wounded area. Each well was then scratched using a 200 μ L sterile pipette tip. Images of wounded areas were taken at time 0, 18 h and 24 h after incubation with 10 μ M and 100 μ M **HM-20, 21, 22, 27** and 10 ng/mL VEGF. Wounded areas were measured at time 0 (t_0), at time 18 (t_{18}) and time 24 (t_{24}) using ImageJ plugin “Wound healing”. Migration was expressed as the percentage of scratch closure after 18 h and 24 h compared with the corresponding time 0. % closure after 18hrs = $[(t_0 - t_{18})/t_0] \times 100$, % closure after 24 h = $[(t_0 - t_{24})/t_0] \times 100$. One-way ANOVA was used to elaborate the results.

k) ENDOTHELIAL CELL PROLIFERATION AND SURVIVAL EXPERIMENT- MTT ASSAY

This assay was used to test the antiangiogenic activity of four phosphatase modulators, **HM-20, 21, 22** and **27**, with respect to cell proliferation and cell survival.

Immortalized endothelial cells were seeded in 96-well plates, allowed to reach confluence, and then incubated with 10 μ M, 30 μ M, 100 μ M and 300 μ M **HM-20, 21, 22** and **27**. Results were calculated considering the absorbance of the positive control (cells with medium without stimuli) as 100 %, and using the following formula:

$$\% \text{ proliferation} = (\text{Absorbance Test} \times 100) / \text{Absorbance Positive Control}$$

l) SURFACE PLASMON RESONANCE

GE Healthcare Biacore X100 was used for the experiments. NTA sensor chip and NTA reagent kit were purchased from GE Healthcare and used with the selected running buffer HBS-P buffer (pH 7.4; 10 μ M HEPES, 0.15 M NaCl and 0.005 % Tween 20; filtered with 0.22 μ m filter). Sensor chip was equilibrated at room temperature for 30 min and Biacore instrument was prepared with the running buffer. The NTA chip was docked and the surface conditioned with a 1-minute pulse of 0.35 M EDTA regeneration solution. After an extra wash with the running buffer, one minute pulse of Nickel solution was injected to saturate the NTA chip with Nickel. The histidine-tagged ligand was diluted in the running concentration in different concentrations (200 nM, 100 nM, 50 nM, 25 nM, 12.5 nM) and injected with 10 μ L flow. 50 nM His-tagged PFKFB3 gave the best ligand capture response and this concentration was later used for all experiments. Compounds were diluted in running buffer with max 0.5 % DMSO and 6 concentrations (1024 nM, 254 nM, 64 nM, 16 nM, 4 nM, 1 nM) were tested for each

compound. Each kinetics experiment was performed in triplicates and experiment was run in multicycles. Ligand was captured on the chip prior to each new kinetics experiment and regenerated at the end of experiment, but not in between cycles. Contact time was 60 s, dissociation time 600 s and the flow rate 10 $\mu\text{L/s}$.

m) PFKFB3 CRYSTALLIZATION

Sitting drop crystallization experiments of PFKFB3 (8-22 mg/ mL) were prepared using Oryx-8 crystallization robot (Douglas Instruments, East Garston, UK), from a 1/1 or 1/2 or 2/1 mixture of the protein with the reservoir solution (final drop volume 0.3 mL. Before X-ray data collection, crystals were soaked in a cryoprotectant solution (1.4 M Na citrate, 100 mM Na cacodylate pH 6.2, and 25% glycerol) in the presence of 62.5 nM dsRNA and 100 mM GTP for 36 hours, then flash-cooled in liquid nitrogen. Analyzed crystals showed no diffraction at the ESRF Synchrotron (Grenoble, France) beam line ID29.

Microbatch crystallization experiments on PFKFB 3 were prepared using an Oryx-8 crystallization robot (Douglas Instruments, East Garston, UK), from a 1:1 or 1/2 or 2/1 mixture (drop volume 0.4 ml) of protein (8 mg/ml) and reservoir solution covered by Al's oil (a mixture of 50% Paraffin oil and 50% Silicon oil). No crystals were obtained using microbatch method. Numerous attempts were made in order to crystallize PFKFB3 protein and conditions are described in detail below.

Optimization attempt 1 and 2; 2 identical plates were prepared, one with the concentration of the protein 10 mg/mL and the other 8 mg/mL. 1:1, 1:2, 2:1 drops.

Well	Buffer	pH	Percipitant 1	Percipitant 2	Percipitant 3	Percipitant 4
A1	100 mM Tris	7	5 % w/v PEG 4000	12 % v/v dioxane	5 % w/v glycerol	20% v/v Ethylene glycol
A2						21% v/v Ethylene glycol
A3						23% v/v Ethylene glycol
A4						25% v/v Ethylene glycol
A5			7 % w/v PEG 4000			20% v/v Ethylene glycol
A6						21% v/v Ethylene glycol
A7						23% v/v Ethylene glycol
A8						25% v/v Ethylene glycol
A9			10 % w/v PEG 4000			20% v/v Ethylene glycol
A10						21% v/v Ethylene glycol
A11						23% v/v Ethylene glycol
A12						25% v/v Ethylene glycol
B1	100 mM Tris	7.5	12 % w/v PEG 4000	12 % v/v dioxane	5 % w/v glycerol	20% v/v Ethylene glycol
B2						21% v/v Ethylene glycol
B3						23% v/v Ethylene glycol
B4						25% v/v Ethylene glycol
B5			5 % w/v PEG 4000			20% v/v Ethylene glycol
B6						21% v/v Ethylene glycol
B7						23% v/v Ethylene glycol
B8						25% v/v Ethylene glycol
B9	7 % w/v PEG 4000	20% v/v Ethylene glycol				
B10		21% v/v Ethylene glycol				
B11		23% v/v Ethylene glycol				
B12		25% v/v Ethylene glycol				
C1	100 mM Tris	7.5	10 % w/v PEG 4000	12 % v/v dioxane	5 % w/v glycerol	20% v/v Ethylene glycol
C2						21% v/v Ethylene glycol
C3						23% v/v Ethylene glycol
C4						25% v/v Ethylene glycol
C5			12 % w/v PEG 4000			20% v/v Ethylene glycol
C6						21% v/v Ethylene glycol
C7						23% v/v Ethylene glycol
C8						25% v/v Ethylene glycol

Well	Buffer	pH	Percipitant 1	Percipitant 2	Percipitant 3	Percipitant 4
A1	100 mM HEPES	7	5 % w/v PEG 4000	12 % v/v dioxane	5 % w/v glycerol	20% v/v Ethylene glycol
A2						21% v/v Ethylene glycol
A3						23% v/v Ethylene glycol
A4						25% v/v Ethylene glycol
A5			7 % w/v PEG 4000			20% v/v Ethylene glycol
A6						21% v/v Ethylene glycol
A7						23% v/v Ethylene glycol
A8						25% v/v Ethylene glycol
A9			10 % w/v PEG 4000			20% v/v Ethylene glycol
A10						21% v/v Ethylene glycol
A11						23% v/v Ethylene glycol
A12						25% v/v Ethylene glycol
B1	100 mM HEPES	7.5	12 % w/v PEG 4000	12 % v/v dioxane	5 % w/v glycerol	20% v/v Ethylene glycol
B2						21% v/v Ethylene glycol
B3						23% v/v Ethylene glycol
B4						25% v/v Ethylene glycol
B5			5 % w/v PEG 4000			20% v/v Ethylene glycol
B6						21% v/v Ethylene glycol
B7						23% v/v Ethylene glycol
B8						25% v/v Ethylene glycol
B9			7 % w/v PEG 4000			20% v/v Ethylene glycol
B10						21% v/v Ethylene glycol
B11						23% v/v Ethylene glycol
B12						25% v/v Ethylene glycol
C1	10 % w/v PEG 4000	20% v/v Ethylene glycol				
C2		21% v/v Ethylene glycol				
C3		23% v/v Ethylene glycol				
C4		25% v/v Ethylene glycol				
C5	12 % w/v PEG 4000	20% v/v Ethylene glycol				
C6		21% v/v Ethylene glycol				
C7		23% v/v Ethylene glycol				
C8		25% v/v Ethylene glycol				

Optimization attempt 3; concentration of the protein: 8 mg/mL; 2 pairs of identical plates were prepared, but one was left at 20 °C, while the other at 4 °C.

Well	Buffer	pH	Percipitant 1
A1	50 mM MES	6	5 % w/v PEG 4000
A2			7 % w/v PEG 4000
A3			10 % w/v PEG 4000
A4			12 % w/v PEG 4000
A5			15 % w/v PEG 4000
A6			20 % w/v PEG 4000
A7		6.3	5 % w/v PEG 4000
A8			7 % w/v PEG 4000
A9			10 % w/v PEG 4000
A10			12 % w/v PEG 4000
A11			15 % w/v PEG 4000
A12			20 % w/v PEG 4000
B1		6.4	5 % w/v PEG 4000
B2			7 % w/v PEG 4000
B3			10 % w/v PEG 4000
B4			12 % w/v PEG 4000
B5			15 % w/v PEG 4000
B6			20 % w/v PEG 4000
B7		6.6	5 % w/v PEG 4000
B8			7 % w/v PEG 4000
B9			10 % w/v PEG 4000
B10			12 % w/v PEG 4000
B11			15 % w/v PEG 4000
B12			20 % w/v PEG 4000
C1	6.7	5 % w/v PEG 4000	
C2		7 % w/v PEG 4000	
C3		10 % w/v PEG 4000	
C4		12 % w/v PEG 4000	
C5		15 % w/v PEG 4000	
C6		20 % w/v PEG 4000	
C7	7	5 % w/v PEG 4000	
C8		7 % w/v PEG 4000	
C9		10 % w/v PEG 4000	
C10		12 % w/v PEG 4000	
C11		15 % w/v PEG 4000	
C12		20 % w/v PEG 4000	

Well	Buffer	pH	Percipitant 1
D1	100 mM Tris	7.1	5 % w/v PEG 4000
D2			7 % w/v PEG 4000
D3			10 % w/v PEG 4000
D4			12 % w/v PEG 4000
D5			15 % w/v PEG 4000
D6			20 % w/v PEG 4000
D7		7.3	5 % w/v PEG 4000
D8			7 % w/v PEG 4000
D9			10 % w/v PEG 4000
D10			12 % w/v PEG 4000
D11			15 % w/v PEG 4000
D12			20 % w/v PEG 4000
E1		7.4	5 % w/v PEG 4000
E2			7 % w/v PEG 4000
E3			10 % w/v PEG 4000
E4			12 % w/v PEG 4000
E5			15 % w/v PEG 4000
E6			20 % w/v PEG 4000
E7		7.5	5 % w/v PEG 4000
E8			7 % w/v PEG 4000
E9			10 % w/v PEG 4000
E10			12 % w/v PEG 4000
E11			15 % w/v PEG 4000
E12			20 % w/v PEG 4000
F1	7.7	5 % w/v PEG 4000	
F2		7 % w/v PEG 4000	
F3		10 % w/v PEG 4000	
F4		12 % w/v PEG 4000	
F5		15 % w/v PEG 4000	
F6		20 % w/v PEG 4000	
F7	7.9	5 % w/v PEG 4000	
F8		7 % w/v PEG 4000	
F9		10 % w/v PEG 4000	
F10		12 % w/v PEG 4000	
F11		15 % w/v PEG 4000	
F12		20 % w/v PEG 4000	

Optimization attempt 4; concentration of the protein: 8 mg/mL; 2 pairs of identical plates were prepared, but one was left at 20 °C, while the other at 4 °C

Well	Buffer	pH	Percipitant 1	Percipitant 2	Percipitant 3	Percipitant 4
A1	100 mM Tris	7.1	20 % v/v ethylene glycol	12 % v/v dioxane	5 % glycerol	8 % v/w PEG 4000
A2						10 % v/w PEG 4000
A3						12 % v/w PEG 4000
A4						14 % v/w PEG 4000
A5						16 % v/w PEG 4000
A6						7.3
A7		10 % v/w PEG 4000				
A8		12 % v/w PEG 4000				
A9		14 % v/w PEG 4000				
A10		16 % v/w PEG 4000				
A11		7.4				
A12						10 % v/w PEG 4000
B1						12 % v/w PEG 4000
B2						14 % v/w PEG 4000
B3						16 % v/w PEG 4000
B4						7.5
B5		10 % v/w PEG 4000				
B6		12 % v/w PEG 4000				
B7		14 % v/w PEG 4000				
B8		16 % v/w PEG 4000				
B9		7.7				
B10						10 % v/w PEG 4000
B11						12 % v/w PEG 4000
B12						14 % v/w PEG 4000
C1	16 % v/w PEG 4000					
C2	8.1		8 % v/w PEG 4000			
C3		10 % v/w PEG 4000				
C4		12 % v/w PEG 4000				
C5		14 % v/w PEG 4000				
C6		16 % v/w PEG 4000				

Optimization attempt 5; concentration of the protein: 22 mg/mL (buffer plus ADP, F-6-P, EDTA); 2 pairs of identical plates were prepared, but one was left at 20 °C, while the other at 4 °C. The crystallization conditions were the same as in attempt 3).

Optimization attempt 6; concentration of the protein: 8 mg/mL, manual preparation, 1:1 drop, incubation at 20 °C.

Well	Buffer	pH	Percipitant 1	Percipitant 2	Percipitant 3
A1	100 mM Tris	7.1	20 % v/v ethylene glycol	12 % v/v dioxane	10 % v/w PEG 4000
A2					12 % v/w PEG 4000
A3					14 % v/w PEG 4000
A4					16 % v/w PEG 4000
A5		7.3			10 % v/w PEG 4000
A6					12 % v/w PEG 4000
A7					14 % v/w PEG 4000
A8					16 % v/w PEG 4000
A9		7.4			10 % v/w PEG 4000
A10					12 % v/w PEG 4000
A11					14 % v/w PEG 4000
A12					16 % v/w PEG 4000
B1		7.5			10 % v/w PEG 4000
B2					12 % v/w PEG 4000
B3					14 % v/w PEG 4000
B4					16 % v/w PEG 4000
B5		7.7			10 % v/w PEG 4000
B6					12 % v/w PEG 4000
B7					14 % v/w PEG 4000
B8					16 % v/w PEG 4000
B9		8.1			10 % v/w PEG 4000
B10					12 % v/w PEG 4000
B11					14 % v/w PEG 4000
B12					16 % v/w PEG 4000

Optimization attempt 7; concentration of the protein: 8 mg/mL, the crystallization buffer was changed to 20 mM Tris, 10 mM NaPi, 5 % glycerol, 0.5 mM β -mercaptoethanol, 0.5 mM EDTA, 1% v/v PEG 400, 3 mM MgCl₂. Robot preparation, 1:1, 1:2 and 2:1 drop, 2 pairs of identical plates microbatch and 2 identical plates of sitting drop technique were prepared, one plates (one microbatch and one sitting drop) were incubated at at 20 °C and the remaining two pletes at 4 °C.

Well	Buffer	pH	Percipitant
A1	200 mM Sodium malonate	5	16 % v/w PEG 3350
A2			18 % v/w PEG 3350
A3			20 % v/w PEG 3350
A4			22 % v/w PEG 3350
A5		6	16 % v/w PEG 3350
A6			18 % v/w PEG 3350
A7			20 % v/w PEG 3350
A8			22 % v/w PEG 3350
A9		7	16 % v/w PEG 3350
A10			18 % v/w PEG 3350
A11			20 % v/w PEG 3350
A12			22 % v/w PEG 3350
B1		7.5	16 % v/w PEG 3350
B2			18 % v/w PEG 3350
B3			20 % v/w PEG 3350
B4			22 % v/w PEG 3350
B5	10	16 % v/w PEG 3350	
B6		18 % v/w PEG 3350	
B7		20 % v/w PEG 3350	
B8		22 % v/w PEG 3350	

Screening attempt 1; concentration of the protein: 8 mg/mL; screening plate Crystal screen HT, incubation at 20°C.

Well	Salt	Buffer	pH	Precipitant
1	0.02 M Calcium chloride dihydrate	0.1 M Sodium acetate trihydrate	4.6	30 % (+/-)-2-Methyl-2,4-pentanediol
2				0.4 M Potassium sodium tartrate tetrahydrate
3				0.4 M Ammonium phosphate monobasic
4		0.1 M TRIS hydrochloride	8.5	2.0 M Ammonium sulfate
5	0.02 M Sodium citrate tribasic dihydrate	0.1 M HEPES sodium	7.5	30 % v/v (+/-)-2-Methyl-2,4-pentanediol
6	0.02 M Magnesium chloride hexahydrate	0.1 M TRIS hydrochloride	8.5	30 % v/w Polyethylene glycol 4,000
7		0.1 M Sodium cacodylate trihydrate	6.5	1.4 M Sodium acetate trihydrate
8	0.02 M Sodium citrate tribasic dihydrate		6.5	30% v/v 2-Propanol
9	0.02 M Ammonium acetate	0.1 M Sodium citrate tribasic dihydrate	5.6	30 % v/w Polyethylene glycol 4,000
10		0.1 M Sodium acetate trihydrate	4.6	
11		0.1 M Sodium citrate tribasic dihydrate	5.6	1.0 M Ammonium phosphate monobasic
12	0.02 M Magnesium chloride hexahydrate	0.1 M HEPES sodium	7.5	30 % v/v 2-Propanol
13	0.02 M Sodium citrate tribasic dihydrate	0.1 M TRIS hydrochloride	8.5	30 % v/v Polyethylene glycol 400
14	0.02 M Calcium chloride dihydrate	0.1 M HEPES sodium	7.5	28 % v/v Polyethylene glycol 400
15	0.02 M Ammonium sulfate	0.1 M Sodium cacodylate trihydrate	6.5	30 % w/v Polyethylene glycol 8,000
16		0.1 M HEPES sodium	7.5	1.5 M Lithium sulfate monohydrate
17	0.02 M Lithium sulfate monohydrate	0.1 M TRIS hydrochloride	8.5	30 % w/v Polyethylene glycol 4,000
18	0.02 M Magnesium acetate tetrahydrate	0.1 M Sodium cacodylate trihydrate	6.5	20 % w/v Polyethylene glycol 8,000
19	0.02 M Ammonium acetate	0.1 M TRIS hydrochloride	8.5	30 % v/v 2-Propanol
20	0.02 M Ammonium sulfate	0.1 M Sodium acetate trihydrate	4.6	25 % w/v Polyethylene glycol 4,000
21	0.02 M Magnesium acetate tetrahydrate	0.1 M Sodium cacodylate trihydrate	6.5	30 % w/v (+/-)-2-Methyl-2,4-pentanediol
22	0.02 M Sodium acetate trihydrate	0.1 M TRIS hydrochloride	8.5	30 % w/v Polyethylene glycol 4,000
23	0.02 M Magnesium chloride hexahydrate	0.1 M HEPES sodium	7.5	30 % v/v Polyethylene glycol 400

24	0.02 M Calcium chloride dihydrate	0.1 M Sodium acetate trihydrate	4.6	20 % v/v 2-Propanol
25		0.1 M Imidazole	6.5	1.0 M Sodium acetate trihydrate
26	0.02 M Ammonium acetate	0.1 M Sodium citrate tribasic dihydrate	5.6	30 % v/v (+/-)-2-Methyl-2,4-pentanediol
27	0.02 M Sodium citrate tribasic dihydrate	0.1 M HEPES sodium	7.5	20 % v/v 2-Propanol
28	0.02 M Sodium acetate trihydrate	0.1 M Sodium cacodylate trihydrate	6.5	30 % w/v Polyethylene glycol 8,000
29		0.1 M HEPES sodium	7.5	0.8 M Potassium sodium tartrate tetrahydrate
30	0.02 M Ammonium sulfate			30 % w/v Polyethylene glycol 8,000
31				30 % w/v Polyethylene glycol 4,000
32				2.0 M Ammonium sulfate
33				4.0 M Sodium formate
34		0.1 M Sodium acetate trihydrate	4.6	2.0 M Sodium formate
35		0.1 M HEPES sodium	7.5	0.8 M Sodium phosphate monobasic monohydrate, 0.8 M Potassium phosphate monobasic
36		0.1 M TRIS hydrochloride	8.5	8 % w/v Polyethylene glycol 8,000
37		0.1 M Sodium acetate trihydrate	4.6	8 % w/v Polyethylene glycol 4,000
38		0.1 M HEPES sodium	7.5	1.4 M Sodium acetate trihydrate
39			7.5	2 % v/v Polyethylene glycol 400, 2.0 M Ammonium sulfate
40		0.1 M Sodium citrate tribasic dihydrate	5.6	20 % v/v 2-Propanol, 20% w/v Polyethylene glycol 4,000
41		0.1 M HEPES sodium	7.5	10 % v/v 2-Propanol, 20% w/v Polyethylene glycol 4,000
42	Potassium phosphate monobasic			20 % w/v Polyethylene glycol 8,000
43				30 % w/v Polyethylene glycol 1,500
44				0.2 M Magnesium formate dihydrate
45	Zinc acetate dihydrate	0.1 M Sodium cacodylate trihydrate	6.5	18 % w/v Polyethylene glycol 8,000
46	Calcium acetate hydrate		6.5	
47		0.1 M Sodium acetate trihydrate	4.6	2.0 M Ammonium sulfate
48		0.1 M TRIS hydrochloride	8.5	2.0 M Ammonium phosphate monobasic

49	Lithium sulfate monohydrate		2 %w/v Polyethylene glycol 8,000
50			15 % w/v Polyethylene glycol 8,000

Screening attempt 2; concentration of the protein: 8 mg/mL; screening plate Index, incubation at 4 °C.

Well	Salt	Buffer	pH	Precipitant	
1	0.3 M Magnesium chloride hexahydrate, 0.3 M Calcium chloride dihydrate	0.1 M Imidazole + MES monohydrate	6.5	2.0 M Ammonium sulfate	
2					
3					
4					
5		0.1 M Sodium HEPES + MOPS	7.5	3.0 M Sodium chloride	
6					
7					
8					
9					
10					
11					
12					
13	0.3 M Sodium fluoride, 0.3M Sodium bromide, 0.3 M Sodium iodide	0.1 M Imidazole + MES monohydrate	6.5	0.3 M Magnesium formate dihydrate	
14				0.5 M Magnesium formate dihydrate	
15				0.3 M Magnesium formate dihydrate	
16					
17		0.1 M Sodium HEPES + MOPS	7.5	1.26 M Sodium phosphate monobasic monohydrate	
18				0.49 M Sodium phosphate monobasic monohydrate	
19				0.056 M Sodium phosphate monobasic monohydrate	
20				1.4 M Sodium citrate tribasic dihydrate	
21		0.1 M Tris + BICINE	8.5	1.8 M Ammonium citrate tribasic pH 7.0	
22				0.8 M Succinic acid pH 7.0	
23				2.1 M DL-Malic acid pH 7.0	
24				2.8 M Sodium acetate trihydrate pH 7.0	
25					3.5 M Sodium formate pH 7.0
26					1.1 M Ammonium tartrate dibasic pH 7.0
27					2.4 M Sodium malonate pH 7.0
28					35% v/v Tacsimate pH 7.0
29				60% v/v Tacsimate pH 7.0	
30	0.1 M Sodium chloride	0.1 M BIS-TRIS	6.5	1.5 M Ammonium sulfate	

31	0.8 M Potassium sodium tartrate tetrahydrate	0.1 M Tris	8.5	0.5 % w/v Polyethylene glycol monomethyl ether 5,000
32	1.0 M Ammonium sulfate	0.1 M BIS-TRIS	5.5	1 % w/v Polyethylene glycol 3,350
33	1.1 M Sodium malonate pH 7.0	0.1 M HEPES	7.0	0.5 % v/v Jeffamine ED-2001 pH 7.0
34	1.0 M Succinic acid pH 7.0		7.0	1 % w/v Polyethylene glycol monomethyl ether 2,000
35	1.0 M Ammonium sulfate		7.0	0.5 % w/v Polyethylene glycol 8,000
36	15 % Tacsimate pH 7.0		7.0	2 % w/v Polyethylene glycol 3,350
37				25 % w/v Polyethylene glycol 1,500
38		0.1 M HEPES	7.0	30 % v/v Jeffamine M-600 pH 7.0
39			7.0	30 % v/v Jeffamine ED-2001 pH 7.0
40		0.1 M Citric acid	3.5	25 % w/v Polyethylene glycol 3,350
41		0.1 M Sodium acetate trihydrate	4.5	
42		0.1 M BIS-TRIS	5.5	
43			6.5	
44		0.1 M HEPES	7.5	
45		0.1 M Tris	8.5	
46		0.1 M BIS-TRIS	6.5	20 % w/v Polyethylene glycol monomethyl ether 5,000
47			6.5	28 % w/v Polyethylene glycol monomethyl ether 2,000
48	0.2 M Calcium chloride dihydrate		5.5	45 % v/v (+/-)-2-Methyl-2,4-pentanediol
49			6.5	
50	0.2 M Ammonium acetate		5.5	
51			6.5	
52			0.1 M HEPES	
53		0.1 M Tris	8.5	
54	0.05 M Calcium chloride dihydrate	0.1 M BIS-TRIS	6.5	30 % v/v Polyethylene glycol monomethyl ether 550
55	0.05 M Magnesium chloride hexahydrate	0.1 M HEPES	7.5	
56	0.2 M Potassium chloride	0.05 M HEPES	7.5	35 % v/v Pentaerythritol propoxylate (5/4 PO/OH)
57	0.05 M Ammonium sulfate	0.05 M BIS-TRIS	6.5	30 % v/v Pentaerythritol ethoxylate (15/4 EO/OH)
58		0.1 M BIS-TRIS	6.5	45 % v/v Polypropylene glycol P 400
59	0.02 M Magnesium chloride hexahydrate	0.1 M HEPES	7.5	22 % v/v Polyacrylic acid sodium salt 5,100
60	0.01 M Cobalt(II) chloride hexahydrate	0.1 M Tris	8.5	20 % v/v Polyvinylpyrrolidone K 15
61	0.2 M L-Proline	0.1 M HEPES	7.5	10 % w/v Polyethylene glycol 3,350
62	0.2 M Trimethylamine N-oxide dihydrate	0.1 M Tris	8.5	20 % w/v Polyethylene glycol monomethyl ether 2,000

63	5% Tacsimate pH 7.0	0.1 M HEPES	7.0	10 % w/v Polyethylene glycol monomethyl ether 5,000
64	0.005 M Cobalt(II) chloride hexahydrate, 0.005 M Nickel(II) chloride hexahydrate, 0.005 M Cadmium chloride hydrate, 0.005 M Magnesium chloride		7.5	12 % w/v Polyethylene glycol 3,350
65	0.1 M Ammonium acetate	0.1 M BIS-TRIS	5.5	17 % w/v Polyethylene glycol 10,000
66	0.2 M Ammonium sulfate	0.1 M BIS-TRIS	5.5	25 % w/v Polyethylene glycol 3,350
67		0.1 M BIS-TRIS	6.5	
68		0.1 M HEPES	7.5	
69		0.1 M Tris	8.5	
70	0.2 M Sodium chloride	0.1 M BIS-TRIS	5.5	
71		0.1 M BIS-TRIS	6.5	
72		0.1 M HEPES	7.5	
73		0.1 M Tris	8.5	
74	0.2 M Lithium sulfate monohydrate	0.1 M BIS-TRIS	5.5	
75		0.1 M BIS-TRIS	6.5	
76		0.1 M HEPES	7.5	
77		0.1 M Tris	8.5	
78	0.2 M Ammonium acetate	0.1 M BIS-TRIS	5.5	
79		0.1 M BIS-TRIS	6.5	
80		0.1 M HEPES	7.5	
81		0.1 M Tris	8.5	
82	0.2 M Magnesium chloride hexahydrate	0.1 M BIS-TRIS	5.5	
83		0.1 M BIS-TRIS	6.5	
84		0.1 M HEPES	7.5	
85		0.1 M Tris	8.5	
86	0.2 M Potassium sodium tartrate tetrahydrate			20 % w/v Polyethylene glycol 3,350
87	0.2 M Sodium malonate pH 7.0			
88	0.2 M Ammonium citrate tribasic pH 7.0			
89	0.1 M Succinic acid pH 7.0			15 % w/v Polyethylene glycol 3,350
90	0.2 M Sodium formate			20 % w/v Polyethylene glycol 3,350
91	0.15 M DL-Malic acid pH 7.0			
92	0.1 M Magnesium formate dihydrate			15 % w/v Polyethylene glycol 3,350
93	0.05 M Zinc acetate dihydrate			20 % w/v Polyethylene glycol 3,350
94	0.2 M Sodium citrate tribasic dihydrate			
95	0.1 M Potassium thiocyanate			30 % w/v Polyethylene glycol monomethyl ether 2,000
96	0.15 M Potassium bromide			

Screening attempt 3: concentration of the protein: 8 mg/mL; screening plate Morpheus, incubation at 4 °C.

Well	Salt	Buffer	pH	Precipitants
1	0.03 M Magnesium chloride hexahydrate, 0.03 M Calcium chloride dihydrate	0.05 M Imidazole, 0.05 M MES monohydrate	6.5	<i>Precipitant mix 1</i> (50% v/v of a mixture of 40% v/v PEG 500 and 20%
2				<i>Precipitant mix 2</i> (50% v/v of a mixture of 40% v/v ethylene glycol and 20% w/v PEG 8000)
3				<i>Precipitant mix 3</i> (50% v/v of a mixture of 40% v/v glycerol and 20% w/v PEG 4000)
4				<i>Precipitant mix 4</i> (50% v/v of a mixture of 25% v/v MPD, 25% w/v PEG 1000 and 25% w/v PEG 3350)
5	0.05 M Sodium HEPES, 0.05 MOPS	7.5	<i>Precipitant mix 1</i>	
6			<i>Precipitant mix 2</i>	
7			<i>Precipitant mix 3</i>	
8			<i>Precipitant mix 4</i>	
9	0.05 M Tris, 0.05 M BICINE	8.5	<i>Precipitant mix 1</i>	
10			<i>Precipitant mix 2</i>	
11			<i>Precipitant mix 3</i>	
12			<i>Precipitant mix 4</i>	
13	0.03 M Sodium fluoride, 0.03M Sodium bromide, 0.03 M Sodium iodide	0.05 M Imidazole, 0.05 M MES monohydrate	6.5	<i>Precipitant mix 1</i>
14				<i>Precipitant mix 2</i>
15				<i>Precipitant mix 3</i>
16				<i>Precipitant mix 4</i>
17	0.05 M Sodium HEPES, 0.05 MOPS	7.5	<i>Precipitant mix 1</i>	
18			<i>Precipitant mix 2</i>	
19			<i>Precipitant mix 3</i>	
20			<i>Precipitant mix 4</i>	
21	0.05 M Tris, 0.05 M BICINE	8.5	<i>Precipitant mix 1</i>	
22			<i>Precipitant mix 2</i>	
23			<i>Precipitant mix 3</i>	
24			<i>Precipitant mix 4</i>	
25	0.03 M Sodium nitrate, 0.03 M Sodium phosphate dibasic, 0.03 M Ammonium sulphate	0.05 M Imidazole, 0.05 M MES monohydrate	6.5	<i>Precipitant mix 1</i>
26				<i>Precipitant mix 2</i>
27				<i>Precipitant mix 3</i>
28				<i>Precipitant mix 4</i>
29	0.05 M Sodium HEPES, 0.05 MOPS	7.5	<i>Precipitant mix 1</i>	
30			<i>Precipitant mix 2</i>	
31			<i>Precipitant mix 3</i>	
32			<i>Precipitant mix 4</i>	
33	0.05 M Tris, 0.05 M BICINE	8.5	<i>Precipitant mix 1</i>	
34			<i>Precipitant mix 2</i>	
35			<i>Precipitant mix 3</i>	
36			<i>Precipitant mix 4</i>	

37	0.02 M 1,6-Hexanediol, 0.02 M 1-Butanol, 0.02 M 1,2-Propanediol, 0.02 M 2-Propanol, 0.02 M 1,4-Butanediol, 0.02 M 1,3-Propanediol	0.05 M Imidazole, 0.05 M MES monohydrate	6.5	Precipitant mix 1
38				Precipitant mix 2
39				Precipitant mix 3
40				Precipitant mix 4
41		0.05 M Sodium HEPES, 0.05 MOPS	7.5	Precipitant mix 1
42				Precipitant mix 2
43				Precipitant mix 3
44				Precipitant mix 4
45		0.05 M Tris, 0.05 M BICINE	8.5	Precipitant mix 1
46				Precipitant mix 2
47				Precipitant mix 3
48				Precipitant mix 4
49	0.03 M Diethylene glycol, 0.03 M Triethylene glycol, 0.03 M Tetraethylene glycol, 0.03 M Pentaethylene glycol	0.05 M Imidazole, 0.05 M MES monohydrate	6.5	Precipitant mix 1
50				Precipitant mix 2
51				Precipitant mix 3
52				Precipitant mix 4
53		0.05 M Sodium HEPES, 0.05 MOPS	7.5	Precipitant mix 1
54				Precipitant mix 2
55				Precipitant mix 3
56				Precipitant mix 4
57		0.05 M Tris, 0.05 M BICINE	8.5	Precipitant mix 1
58				Precipitant mix 2
59				Precipitant mix 3
60				Precipitant mix 4
61	0.02 M D-Glucose, 0.02 M D-Mannose, 0.02 M D-Galactose, 0.02 M L-Fucose, 0.02 M D-Xylose, 0.02 M N-Acetyl-D-glucosamine	0.05 M Imidazole, 0.05 M MES monohydrate	6.5	Precipitant mix 1
62				Precipitant mix 2
63				Precipitant mix 3
64				Precipitant mix 4
65		0.05 M Sodium HEPES, 0.05 MOPS	7.5	Precipitant mix 1
66				Precipitant mix 2
67				Precipitant mix 3
68				Precipitant mix 4
69		0.05 M Tris, 0.05 M BICINE	8.5	Precipitant mix 1
70				Precipitant mix 2
71				Precipitant mix 3
72				Precipitant mix 4
73	0.02 M Sodium formate, 0.02 M Ammonium acetate, 0.02 M Sodium citrate tribasic dihydrate, 0.02 M Sodium potassium tartrate tetrahydrate, 0.02 M Sodium oxamate	0.05 M Imidazole, 0.05 M MES monohydrate	6.5	Precipitant mix 1
74				Precipitant mix 2
75				Precipitant mix 3
76				Precipitant mix 4
77		0.05 M Sodium HEPES, 0.05 MOPS	7.5	Precipitant mix 1
78				Precipitant mix 2
79				Precipitant mix 3
80				Precipitant mix 4
81		0.05 M Tris, 0.05 M BICINE	8.5	Precipitant mix 1
82				Precipitant mix 2
83				Precipitant mix 3
84				Precipitant mix 4
85	0.02 M DL-Glutamic acid monohydrate, 0.02 M DL-Alanine, 0.02 M Glycine, 0.02 M DL-Lysine monochloride, 0.02 M DL-Serine	0.05 M Imidazole, 0.05 M MES monohydrate	6.5	Precipitant mix 1
86				Precipitant mix 2
87				Precipitant mix 3
88				Precipitant mix 4
89		0.05 M Sodium HEPES, 0.05 MOPS	7.5	Precipitant mix 1
90				Precipitant mix 2
91				Precipitant mix 3
92				Precipitant mix 4
93		0.05 M Tris, 0.05 M BICINE	8.5	Precipitant mix 1
94				Precipitant mix 2
95				Precipitant mix 3
96				Precipitant mix 4

Screening attempt 4: protein: 8 mg/mL; screening plate JCSG, incubation at 4 °C.

Well	Salt	Buffer	pH	Precipitant
1	0.2 M Lithium sulfate	0.1 M Sodium acetate	4.5	50 % w/v PEG 400
2		0.1 M Sodium citrate	5.5	20 % w/v PEG 3000
3	0.2 M Ammonium citrate dibasic			20 % w/v PEG 3350
4	0.02 M Calcium chloride dihydrate	0.1 M Sodium acetate	4.6	30 % v/v MPD
5	0.2 M Magnesium formate dihydrate			20 % w/v PEG 3350
6	0.2 M Lithium sulfate	0.1 M Phosphate/citrate	4.2	20 % w/v PEG 1000
7		0.1 M CHES	9.5	20 % w/v PEG 8000
8	0.2 M Ammonium formate			20 % w/v PEG 3350
9	0.2 M Ammonium chloride			
10	0.2 M Potassium formate			
11	0.2 M Ammonium phosphate monobasic	0.1 M Tris	8.5	50 % v/v MPD
12	0.2 M Potassium nitrate			20 % w/v PEG 3350
13	0.8 M Ammonium sulfate	0.1 M Citrate	4	
14	0.2 M Sodium thiocyanate			20 % w/v PEG 3350
15		0.1 M BICINE	9	20 % w/v PEG 6000
16		0.1 M HEPES	7.5	10 % w/v PEG 8000, 8 % Ethylene glycol
17		0.1 M Sodium cacodylate	6.5	40 % v/v MPD, 5 % PEG 8000
18		0.1 M Phosphate/citrate	4.2	40 % v/v Ethanol, 5 % PEG 1000
19		0.1 M Sodium acetate	4.6	8 % w/v PEG 4000
20	0.2 M Magnesium chloride hexahydrate	0.1 M Tris	7	10 % w/v PEG 8000
21		0.1 M Citrate	5	20 % w/v PEG 6000
22	0.2 M Magnesium chloride hexahydrate	0.1 M Sodium cacodylate	6.5	50 % w/v PEG 200
23	1.6 M Sodium citrate tribasic dihydrate		6.5	
24	0.2 M Potassium citrate tribasic monohydrate			20 % w/v PEG 3350
25	0.2 M Sodium chloride	0.1 M Phosphate/citrate	4.2	20 % w/v PEG 8000
26	1 M Lithium chloride	0.1 M Citrate	4	20 % w/v PEG 6000
27	0.2 M Ammonium nitrate			20 % w/v PEG 3350
28		0.1 M HEPES	7	10 % w/v PEG 6000
29	0.8 M Sodium phosphate monobasic monohydrate, 0.8 M Potassium phosphate monobasic	0.1 M Sodium HEPES	7.5	
30		0.1 M Phosphate/citrate	4.2	40 % w/v PEG 300
31	0.2 M Zinc acetate dihydrate	0.1 M Sodium acetate	4.5	10 % w/v PEG 3000
32		0.1 M Tris	8.5	20 % v/v Ethanol
33		0.1 M Sodium/potassium phosphate	6.2	25 % v/v 1,2-Propanediol, 10 % Glycerol
34		0.1 MBICINE	9	10 % w/v PEG 20,000, 2 % 1,4-Dioxane
35	2 M Ammonium sulfate	0.1 M Sodium acetate	4.6	
36				10 % w/v PEG 1000, 10 % PEG 8000
37				24 % w/v PEG 1500, 20 % Glycerol
38	0.2 M Magnesium chloride hexahydrate	0.1 M Sodium HEPES	7.5	30 % v/v PEG 400
39	0.2 M Sodium chloride	0.1 M Sodium/potassium phosphate	6.2	50 % v/v PEG 200
40	0.2 M Lithium sulfate	0.1 M Sodium acetate	4.5	30 % w/v PEG 8000

41		0.1 M HEPES	7.5	70 % v/v MPD
42	0.2 M Magnesium chloride hexahydrate	0.1 M Tris	8.5	20 % w/v PEG 8000
43	0.2 M Lithium sulfate		8.5	40 % v/v PEG 400
44			8	40 % v/v MPD
45	0.17 M Ammonium sulfate			25.5 % w/v PEG 4000, 15 % Glycerol
46	0.2 M Calcium acetate hydrate	0.1 M Sodium cacodylate	6.5	40 % v/v PEG 300
47	0.14 M Calcium chloride dihydrate	0.07 M Sodium acetate	4.6	14 % v/v 2-Propanol, 30 % Glycerol
48	0.04 M Potassium phosphate monobasic			16 % w/v PEG 8000, 20 % Glycerol
49	1 M Sodium citrate tribasic dihydrate	0.1 M Sodium cacodylate	6.5	
50	2 M Ammonium sulfate, 0.2 M Sodium chloride	0.1 M Sodium cacodylate	6.5	
51	0.2 M Sodium chloride	0.1 M HEPES	7.5	10 % v/v 2-Propanol
52	1.26 M Ammonium sulfate, 0.2 M Lithium sulfate	0.1 M Tris	8.5	
53		0.1 M CAPS	10.5	40 % v/v MPD
54	0.2 M Zinc acetate dihydrate	0.1 M Imidazole	8	20 % w/v PEG 3000
55	0.2 M Zinc acetate dihydrate	0.1 M Sodium cacodylate	6.5	10 % v/v 2-Propanol
56	1 M Ammonium phosphate dibasic	0.1 M Sodium acetate	4.5	
57	1.6 M Magnesium sulfate heptahydrate	0.1 M MES	6.5	
58		0.1 M BICINE	9	10 % w/v PEG 6000
59	0.16 M Calcium acetate hydrate	0.08 M Sodium cacodylate	6.5	14.4 % w/v PEG 8000, 20 % Glycerol
60		0.1 M Imidazole	8	10 % w/v PEG 8000
61	0.05 M Cesium chloride	0.1 M MES	6.5	30 % v/v Jeffamine® M-600
62	3.2 M Ammonium sulfate	0.1 M Citrate	5	
63		0.1 M Tris	8	20 % w/v MPD
64		0.1 M HEPES	7.5	20 % v/v Jeffamine® M-600
65	0.2 M Magnesium chloride hexahydrate	0.1 M Tris	8.5	50 % v/v Ethylene glycol
66		0.1 M BICINE	9	10 % v/v MPD
67	0.8 M Succinic acid		7	
68	2.1 M DL-Malic acid		7	
69	2.4 M Sodium malonate dibasic monohydrate		7	
70	1.1 M Sodium malonate dibasic monohydrate	0.1 M HEPES	7	0.5 % v/v Jeffamine® ED-2003
71	1 M Succinic acid		7	1 % w/v PEG 2000 MME
72			7	30 % v/v Jeffamine® M-600
73			7	30 % v/v Jeffamine® ED-2003
74	0.2 M Magnesium chloride hexahydrate		7.5	22 % w/v Poly(acrylic acid sodium salt) 5100
75	0.01 M Cobalt(II) chloride hexahydrate	0.1 M Tris	8.5	20 % w/v Polyvinylpyrrolidone
76	0.2 M TMAO		8.5	20 % w/v PEG 2000 MME
77	0.005 M Cobalt(II) chloride hexahydrate, 0.005 M Cadmium chloride hemi(pentahydrate), 0.005 M Magnesium chloride hexahydrate, 0.005 M Nickel(II) chloride hexahydrate	0.1 M HEPES	7.5	12 % w/v PEG 3350
78	0.2 M Sodium malonate dibasic monohydrate			20 % w/v PEG 3350
79	0.1 M Succinic acid			15 % w/v PEG 3350
80	0.15 M DL-Malic acid			20 % w/v PEG 3350

81	0.1 M Potassium thiocyanate			30 % w/v PEG 2000 MME	
82	0.15 M Potassium bromide			30 % w/v PEG 2000 MME	
83	2 M Ammonium sulfate	0.1 M Bis-Tris	5.5		
84	3 M Sodium chloride		5.5		
85	0.3 M Magnesium formate dihydrate		5.5		
86	1 M Ammonium sulfate		5.5	1 % w/v PEG 3350	
87			5.5	25 % w/v PEG 3350	
88	0.2 M Calcium chloride dihydrate		5.5	45 % v/v MPD	
89	0.2 M Ammonium acetate		5.5	45 % v/v MPD	
90	0.1 M Ammonium acetate		5.5	17 % w/v PEG 10,000	
91	0.2 M Ammonium sulfate		5.5	25 % w/v PEG 3350	
92	0.2 M Sodium chloride		5.5		
93	0.2 M Lithium sulfate		5.5		
94	0.2 M Ammonium acetate		5.5		
95	0.2 M Magnesium chloride hexahydrate		5.5		
96	0.2 M Ammonium acetate		0.1 M HEPES	7.5	45 % v/v MPD

Screening attempt 5: concentration of the protein: 8 mg/mL; screening plate Natrix, incubation at 4 °C

Well	Salt 1	Salt 2	Buffer	pH	Precipitant
1	0.01M Magnesium chloride hexahydrate		0.05 M MES monohydrate	5.7	1.8 M Lithium sulfate monohydrate
2	0.01M Magnesium acetate tetrahydrate			6.1	2.5 M Ammonium sulfate
3	0.1 M Magnesium acetate tetrahydrate			5.9	20 % v/v (+/-)-2-Methyl-2,4-pentanediol
4	0.2 M Potassium chloride	0.01 M Magnesium sulfate heptahydrate		5.5	10% v/v Polyethylene glycol 400
5		0.01 M Magnesium chloride hexahydrate		5.5	5 % w/v Polyethylene glycol 8,000
6	0.1 M Ammonium sulfate			5.4	20 % w/v Polyethylene glycol 8,000
7	0.02 M Magnesium chloride hexahydrate			5.9	15% v/v 2-Propanol
8	0.1 M Ammonium acetate	0.005 M Magnesium sulfate heptahydrate		6.0	0.6 M Sodium chloride
9	0.1 M Potassium chloride	0.01 M Magnesium chloride hexahydrate		5.9	10 % v/v Polyethylene glycol 400
10	0.005 M Magnesium sulfate heptahydrate			6.0	5% w/v Polyethylene glycol 4,000

11	0.01 M Magnesium chloride hexahydrate		0.05 M Sodium cacodylate trihydrate	5.7	1.0 M Lithium sulfate monohydrate
12	0.01 M Magnesium sulfate heptahydrate			5.5	1.8 M Lithium sulfate monohydrate
13	0.015 M Magnesium acetate tetrahydrate			6.0	1.7 M Ammonium sulfate
14	0.1 M Potassium chloride	0.025 M Magnesium chloride hexahydrate		6.1	15% v/v 2-Propanol
15	0.04 M Magnesium chloride hexahydrate			6.0	5% v/v (+/-)-2-Methyl-2,4-pentanediol
16	0.04 M Magnesium acetate tetrahydrate			6.4	30% v/v (+/-)-2-Methyl-2,4-pentanediol
17	0.2 M Potassium chloride	0.01 M Calcium chloride dihydrate		6.1	10% w/v Polyethylene glycol 4,000
18	0.01 M Magnesium acetate tetrahydrate			6.0	1.3 M Lithium sulfate monohydrate
19	0.01 M Magnesium sulfate heptahydrate			6.3	2.0 M Ammonium sulfate
20	0.1M Ammonium acetate	0.015 M Magnesium acetate tetrahydrate		6.5	10% v/v 2-Propanol
21	0.2 M Potassium chloride	0.005 M Magnesium chloride hexahydrate		6.5	0.9 M 1,6-Hexanediol
22	0.08 M Magnesium acetate tetrahydrate			6.6	15 % v/v Polyethylene glycol 400
23	0.2 M Potassium chloride	0.01 M Magnesium chloride hexahydrate		6.5	10% w/v Polyethylene glycol 4,000
24	0.2 M Ammonium acetate	0.01 M Calcium chloride dihydrate		6.6	10% w/v Polyethylene glycol 4,000
25	0.08 M Magnesium acetate tetrahydrate			6.8	30 % w/v Polyethylene glycol 4,000
26	0.2 M Potassium chloride	0.1 M Magnesium acetate tetrahydrate		6.5	10 % w/v Polyethylene glycol 8,000
27	0.2 M Ammonium acetate	0.01 M Magnesium acetate tetrahydrate		7.0	30 % w/v Polyethylene glycol 8,000
28	0.05 M Magnesium sulfate hydrate			7.0	1.6 M Lithium sulfate monohydrate
29	0.01 M Magnesium chloride hexahydrate			7.1	4.0 M Lithium chloride
30				7.0	1.6 M Ammonium sulfate
31	0.005 M Magnesium chloride hexahydrate			6.7	25 % v/v Polyethylene glycol monomethyl ether 550
32	0.2 M Potassium chloride	0.01 M Magnesium chloride hexahydrate		6.9	1.7 M 1,6-Hexanediol
33	0.2 M Ammonium chloride			6.7	2.5 M 1,6-Hexanediol
34	0.1 M Potassium chloride	0.005 M Magnesium sulfate hydrate		6.8	15 % v/v (+/-)-2-Methyl-2,4-pentanediol
35		0.01 M Magnesium chloride hexahydrate		6.8	5 % v/v Polyethylene glycol 400
36		0.01 M Calcium chloride dihydrate		6.8	10% v/v
37		0.025 M Magnesium sulfate hydrate		6.8	20 % v/v Polyethylene glycol 200
38	0.2 M Ammonium acetate	0.15 M Magnesium acetate tetrahydrate	6.9	5 % w/v Polyethylene glycol 4,000	
39	0.1 M Ammonium acetate	0.02 M Magnesium chloride hexahydrate	6.9	5% w/v Polyethylene glycol 8,000	
40	0.01 M Magnesium chloride hexahydrate		7.4	1.6 M Ammonium sulfate	
41	0.1 M Potassium chloride	0.015 M Magnesium chloride hexahydrate	7.5	10 % v/v Polyethylene glycol monomethyl ether 550	
42	0.01 M Magnesium chloride hexahydrate		7.5	5 % v/v 2-Propanol	
43	0.05 M Ammonium acetate	0.01 M Magnesium chloride hexahydrate	7.5	10 % v/v (+/-)-2-Methyl-2,4-pentanediol	
44	0.2 M Potassium chloride	0.05 M Magnesium chloride hexahydrate	7.6	10 % w/v Polyethylene glycol 4,000	
45	0.025 M Magnesium sulfate hydrate		7.9	1.8 M Ammonium sulfate	
46	0.005 M Magnesium sulfate hydrate		8.4	2.9 M 1,6-Hexanediol	
47	0.1 M Potassium chloride	0.01 M Magnesium chloride hexahydrate	8.5	30 % v/v Polyethylene glycol 400	
48	0.2 M Ammonium chloride	0.01 M Calcium chloride dihydrate	8.2	30 % w/v Polyethylene glycol 4,000	

Screening attempt 6: concentration of the protein: 8 mg/mL; screening plate Proplex, incubation at 20 °C.

Well	Salt	Buffer	pH	Precipitant
1		0.1 M Tris	8	25 % v/v PEG 350 MME
2	0.1 M Calcium acetate hydrate	0.1 M MES	6	15 % v/v PEG 400
3	0.1 M Lithium chloride	0.1 M Sodium HEPES	7.5	20 % v/v PEG 400
4		0.1 M Tris	8	25 % v/v PEG 400
5		0.1 M MES	6.5	15 % v/v PEG 500 MME
6	0.2 M Sodium chloride	0.1 M Sodium/potassium phosphate	6.5	25 % w/v PEG 1000
7	0.1 M Ammonium sulfate	0.1 M Tris	7.5	20 % w/v PEG 1500
8	0.2 M Ammonium sulfate	0.1 M Sodium acetate	5.5	10 % w/v PEG 2000 MME
9	0.2 M Sodium chloride	0.1 M MES	6	20 % w/v PEG 2000 MME
10	0.1 M Potassium chloride	0.1 M Tris	8	15 % w/v PEG 2000 MME
11		0.1 M Sodium HEPES	7.5	25 % w/v PEG 2000 MME
12	0.2 M Sodium acetate trihydrate	0.1 M Sodium citrate	5.5	5 % w/v PEG 4000
13	0.2 M Lithium sulfate	0.1 M Tris	7.5	
14	0.1 M Calcium acetate hydrate	0.1 M Sodium acetate	4.5	10 % w/v PEG 4000
15	0.2 M Sodium acetate trihydrate	0.1 M Sodium citrate	5.5	
16	0.2 M Sodium chloride	0.1 M MES	6.5	
17	0.1 M Magnesium chloride hexahydrate	0.1 M Sodium HEPES	7.5	
18			7	
19	0.2 M Ammonium acetate	0.1 M Sodium acetate	4	15 % w/v PEG 4000
20	0.1 M Magnesium chloride hexahydrate	0.1 M Sodium citrate	5	
21		0.1 M Sodium cacodylate	6	
22	0.15 M Ammonium sulfate	0.1 M MES	6	
23			7	
24	0.1 M Magnesium chloride hexahydrate	0.1 M Sodium HEPES	7	
25	0.15 M Ammonium sulfate	0.1 M Tris	8	
26		0.1 M Sodium citrate	4.5	20 % w/v PEG 4000
27	0.2 M Ammonium acetate	0.1 M Sodium acetate	5	
28	0.2 M Lithium sulfate	0.1 M MES	6	
29		0.1 M Tris	8	
30	0.15 M Ammonium sulfate	0.1 M Sodium HEPES	7	
31		0.1 M Sodium citrate	5.6	20 % w/v PEG 4000, 20 % v/v 2-Propanol
32	0.2 M Sodium chloride	0.1 M Tris	8	20 % w/v PEG 4000
33		0.1 M Sodium cacodylate	5.5	25 % w/v PEG 4000
34	0.15 M Ammonium sulfate	0.1 M MES	5.5	
35		0.1 M Sodium cacodylate	6.5	
36	0.2 M Potassium iodide	0.1 M MES	6.5	
37	0.2 M Sodium chloride	0.1 M Sodium HEPES	7.5	
38		0.1 M MES	6.5	10 % w/v PEG 5000 MME, 12 % v/v 1-Propanol
39	0.1 M Potassium chloride	0.1 M Sodium HEPES	7	15 % w/v PEG 5000 MME
40	0.2 M Ammonium sulfate	0.1 M Tris	7.5	20 % w/v PEG 5000 MME
41	0.1 M Magnesium chloride hexahydrate	0.1 M MES	6	8 % w/v PEG 6000
42	0.15 M Sodium chloride	0.1 M Tris	8	

43		0.1 M Sodium citrate	5.5	15 % w/v PEG 6000
44	0.1 M Magnesium acetate tetrahydrate	0.1 M Sodium cacodylate	6.5	
45		0.1 M MES	6.5	15 % w/v PEG 6000, 5 % v/v MPD
46	0.1 M Potassium chloride	0.1 M Sodium HEPES	7.5	15 % w/v PEG 6000
47		0.1 M Tris	8.5	
48			8.5	20 % w/v PEG 6000
49	0.1 M Magnesium acetate tetrahydrate	0.1 M Sodium acetate	4.5	8 % w/v PEG 8000
50		0.1 M Sodium citrate	5	
51	0.2 M Sodium chloride	0.1 M Sodium cacodylate	6	
52		0.1 M Sodium HEPES	7	
53		0.1 M Tris	8	
54	0.1 M Calcium acetate hydrate	0.1 M Sodium cacodylate	5.5	12 % w/v PEG 8000
55		0.1 M Sodium phosphate	6.5	
56	0.1 M Magnesium acetate tetrahydrate	0.1 M MOPS	7.5	
57	0.2 M Sodium chloride	0.1 M Sodium HEPES	7.5	20 % w/ v PEG 8000
58	0.2 M Ammonium sulfate	0.1 M Tris	8.5	
59		0.1 M Sodium citrate	5	
60	0.2 M Ammonium sulfate	0.1 M MES	6.5	
61		0.1 M Sodium HEPES	7	10 % w/v PEG 10,000
62	0.2 M Lithium chloride	0.1 M Tris	8	
63	0.1 M Magnesium acetate tetrahydrate	0.1 M MES	6.5	18 % w/v PEG 12,000
64		0.1 M Sodium HEPES	7	
65	0.1 M Sodium chloride	0.1 M Tris	8	8 % w/v PEG 20,000
66		0.1 M Sodium HEPES	7	15 % w/v PEG 20,000
67	0.5 M Ammonium sulfate	0.1 M MES	6.5	
68	1.0 M Ammonium sulfate	0.1 M Sodium acetate	5	
69		0.1 M MES	6.5	
70		0.1 M Tris	8	
71	1.5 M Ammonium sulfate	0.1 M Sodium acetate	5	
72		0.1 M Sodium HEPES	7	
73		0.1 M Tris	8	
74	2.0 M Ammonium sulfate	0.1 M Sodium acetate	5	
75		0.1 M Sodium HEPES	7	
76		0.1 M Tris	8	
77	1.0 M Ammonium sulfate, 1.0 M Potassium chloride	0.1 M Sodium HEPES	7	
78	2.0 M Sodium formate	0.1 M Sodium acetate	5	
79	3.0 M Sodium formate	0.1 M Tris	7.5	
80		0.8 M Sodium/potassium phosphate	7.5	
81		1.3 M Sodium/potassium phosphate	7	
82		1.6 M Sodium/potassium phosphate	6.5	
83	1.0 M Sodium acetate trihydrate	0.1 M Sodium HEPES	7.5	
84	1.0 M Sodium citrate tribasic dihydrate		7	
85	2.0 M Sodium chloride	0.1 M Sodium citrate	6	
86	1.0 M Lithium sulfate	0.1 M MES	6.5	
87	1.6 M Lithium sulfate	0.1 M Tris	8	
88		0.1 M Sodium malonate dibasic monohydrate	6	
89	1.2 M Potassium sodium tartrate tetrahydrate	0.1 M Tris	8	

90	1.6 M Magnesium sulfate heptahydrate	0.1 M MES	6.5	
91		0.1 M Sodium acetate	5	2 % w/v PEG 4000, 15 % v/v MPD
92	0.05 M Calcium acetate hydrate	0.1 M Sodium cacodylate	6	25 % v/v MPD
93		0.1 M Imidazole	7	50 % v/v MPD
94	0.05 M Magnesium chloride hexahydrate	0.1 M MES	6.5	5 % w/v PEG 4000, 10 % v/v 2-Propanol
95	0.2 M Ammonium acetate	0.1 M Sodium HEPES	7.5	25 % v/v 2-Propanol
96	0.1 M Sodium chloride	0.1 M Tris	8	15 % v/v Ethanol, 5 % v/v MPD

Screening attempt 7: concentration of the protein: 8 mg/mL; screening plate PACT, incubation at 20 °C.

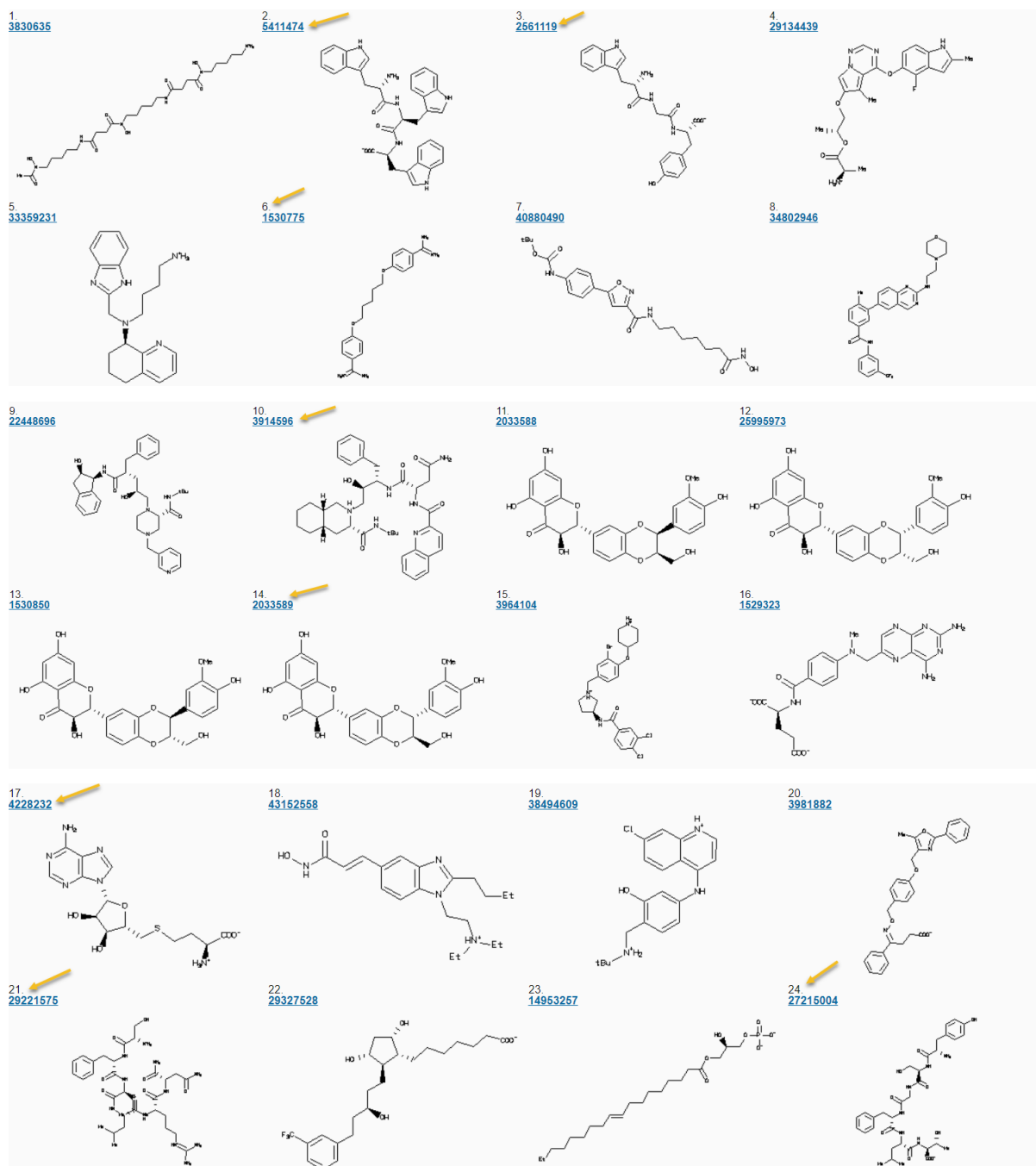
Well	Salt	Buffer	pH	Precipitant
1		0.1 M SPG	4	25 % w/v PEG 1500
2			5	
3			6	
4			7	
5			8	
6			9	
7	0.2 M Sodium chloride	0.1 M Sodium acetate	5	20 % w/v PEG 6000
8	0.2 M Ammonium chloride		5	
9	0.2 M Lithium chloride		5	
10	0.2 M Magnesium chloride hexahydrate		5	
11	0.2 M Calcium chloride dihydrate		5	
12	0.01 M Zinc chloride	5		
13		0.1 M MIB	4	25 % w/v PEG 1500
14			5	
15			6	
16			7	
17			8	
18			9	
19	0.2 M Sodium chloride	0.1 M MES	6	20 % w/v PEG 6000
20	0.2 M Ammonium chloride		6	
21	0.2 M Lithium chloride		6	
22	0.2 M Magnesium chloride hexahydrate		6	
23	0.2 M Calcium chloride dihydrate	6		
24	0.01 M Zinc chloride	6		
25		0.1 M PCTP	4	25 % w/v PEG 1500
26			5	
27			6	
28			7	
29			8	
30			9	
31	0.2 M Sodium chloride	0.1 M HEPES	7	20 % w/v PEG 6000
32	0.2 M Ammonium chloride		7	
33	0.2 M Lithium chloride		7	
34	0.2 M Magnesium chloride hexahydrate		7	
35	0.2 M Calcium chloride hexahydrate		7	
36	0.01 M Zinc chloride		7	

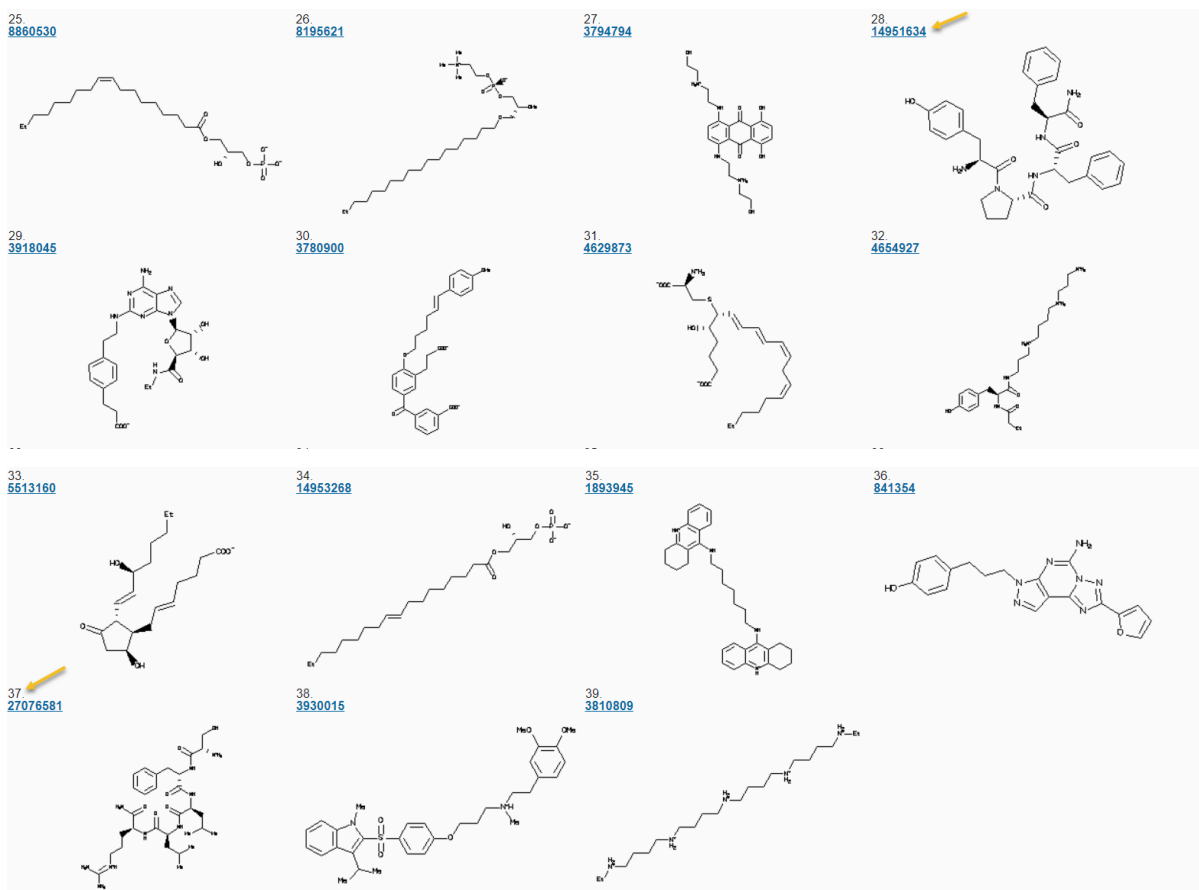
37			4	
38			5	
39			6	
40		0.1 M MMT	7	25 % w/v PEG 1500
41			8	
42			9	
43	0.2 M Sodium chloride		8	
44	0.2 M Ammonium chloride		8	
45	0.2 M Lithium chloride		8	
46	0.2 M Magnesium chloride hexahydrate	0.1 M Tris	8	20 % w/v PEG 6000
47	0.2 M Calcium chloride dihydrate		8	
48	0.002 M Zinc chloride		8	
49	0.2 M Sodium fluoride			
50	0.2 M Sodium bromide			
51	0.2 M Sodium iodide			
52	0.2 M Potassium thiocyanate			
53	0.2 M Sodium nitrate			
54	0.2 M Sodium formate			
55	0.2 M Sodium acetate trihydrate			
56	0.2 M Sodium sulfate			
57	0.2 M Potassium sodium tartrate tetrahydrate			
58	0.02 M Sodium/potassium phosphate			
59	0.2 M Sodium citrate tribasic dihydrate			
60	0.2 M Sodium malonate dibasic monohydrate			
61	0.2 M Sodium fluoride		6.5	
62	0.2 M Sodium bromide		6.5	
63	0.2 M Sodium iodide		6.5	
64	0.2 M Potassium thiocyanate		6.5	
65	0.2 M Sodium nitrate		6.5	
66	0.2 M Sodium formate		6.5	
67	0.2 M Sodium acetate trihydrate		6.5	
68	0.2 M Sodium sulfate	0.1 M Bis-Tris propane	6.5	PEG 3350
69	0.2 M Potassium sodium tartrate tetrahydrate		6.5	
70	0.02 M Sodium/potassium phosphate		6.5	
71	0.2 M Sodium citrate tribasic dihydrate		6.5	
72	0.2 M Sodium malonate dibasic monohydrate		6.5	
73	0.2 M Sodium fluoride		7.5	
74	0.2 M Sodium bromide		7.5	
75	0.2 M Sodium iodide		7.5	
76	0.2 M Potassium thiocyanate		7.5	
77	0.2 M Sodium nitrate		7.5	
78	0.2 M Sodium formate		7.5	
79	0.2 M Sodium acetate trihydrate		7.5	
80	0.2 M Sodium sulfate		7.5	
81	0.2 M Potassium sodium tartrate tetrahydrate		7.5	
82	0.02 M Sodium/potassium phosphate		7.5	
83	0.2 M Sodium citrate tribasic dihydrate		7.5	
84	0.2 M Sodium malonate dibasic monohydrate		7.5	
85	0.2 M Sodium fluoride		8.5	

86	0.2 M Sodium bromide	0.1 M Bis-Tris propane	8.5	PEG 3350
87	0.2 M Sodium iodide		8.5	
88	0.2 M Potassium thiocyanate		8.5	
89	0.2 M Sodium nitrate		8.5	
90	0.2 M Sodium formate		8.5	
91	0.2 M Sodium acetate trihydrate		8.5	
92	0.2 M Sodium sulfate		8.5	
93	0.2 M Potassium sodium tartrate tetrahydrate		8.5	
94	0.02 M Sodium/potassium phosphate		8.5	
95	0.2 M Sodium citrate tribasic dihydrate		8.5	
96	0.2 M Sodium malonate dibasic monohydrate		8.5	

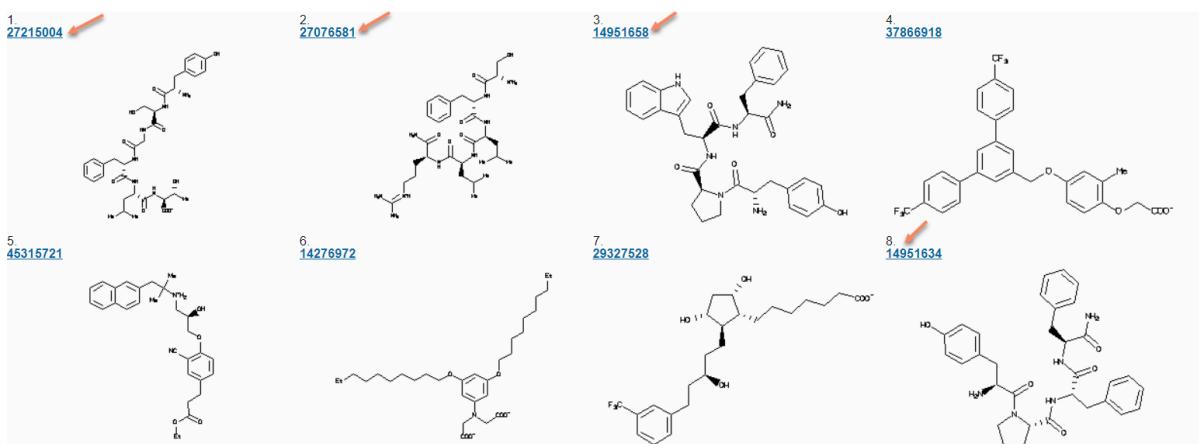
X. APPENDIX

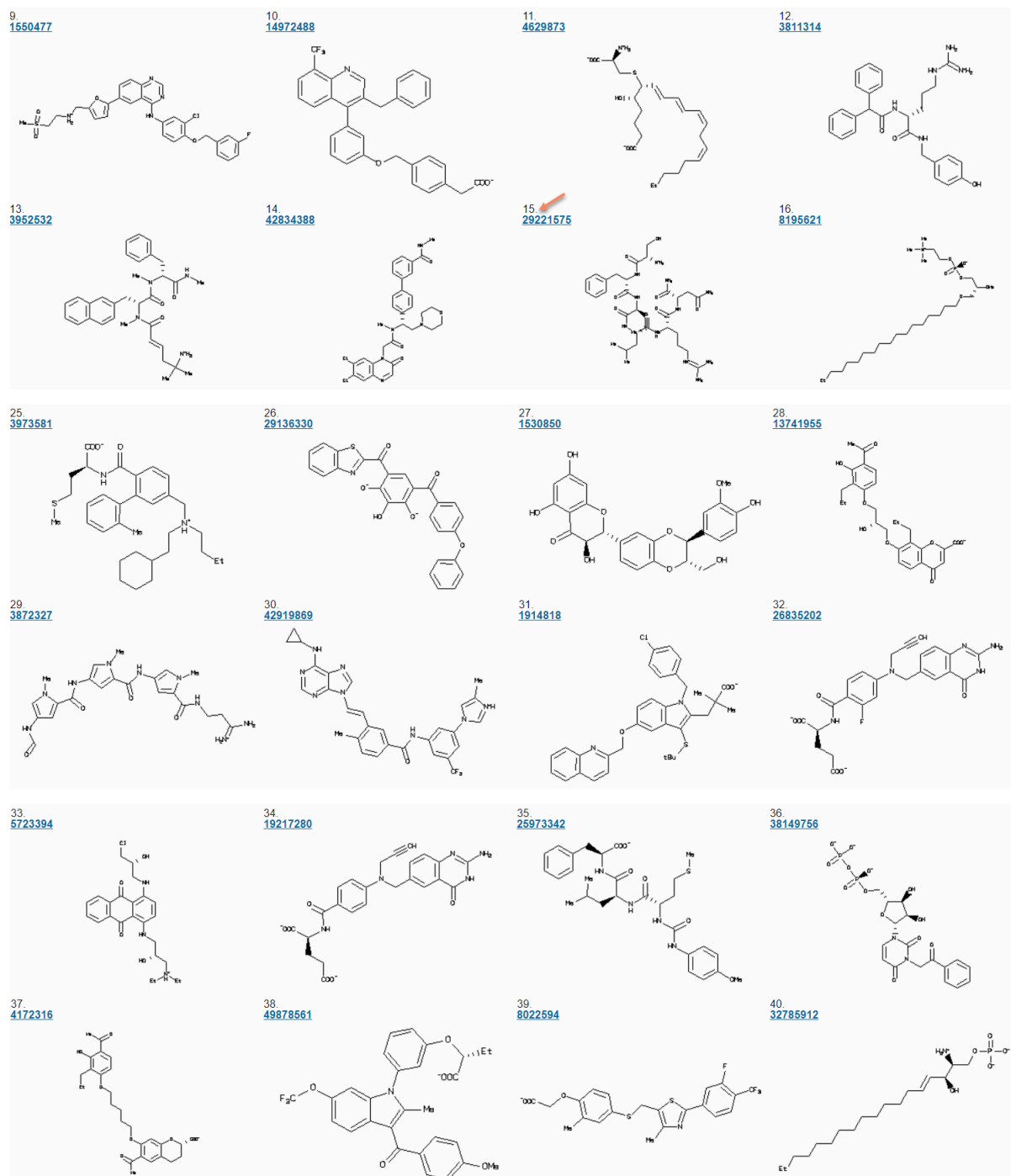
1st STRATEGY SCREENING- ZINC LIBRARY (selected ligands are marked with a yellow arrow)

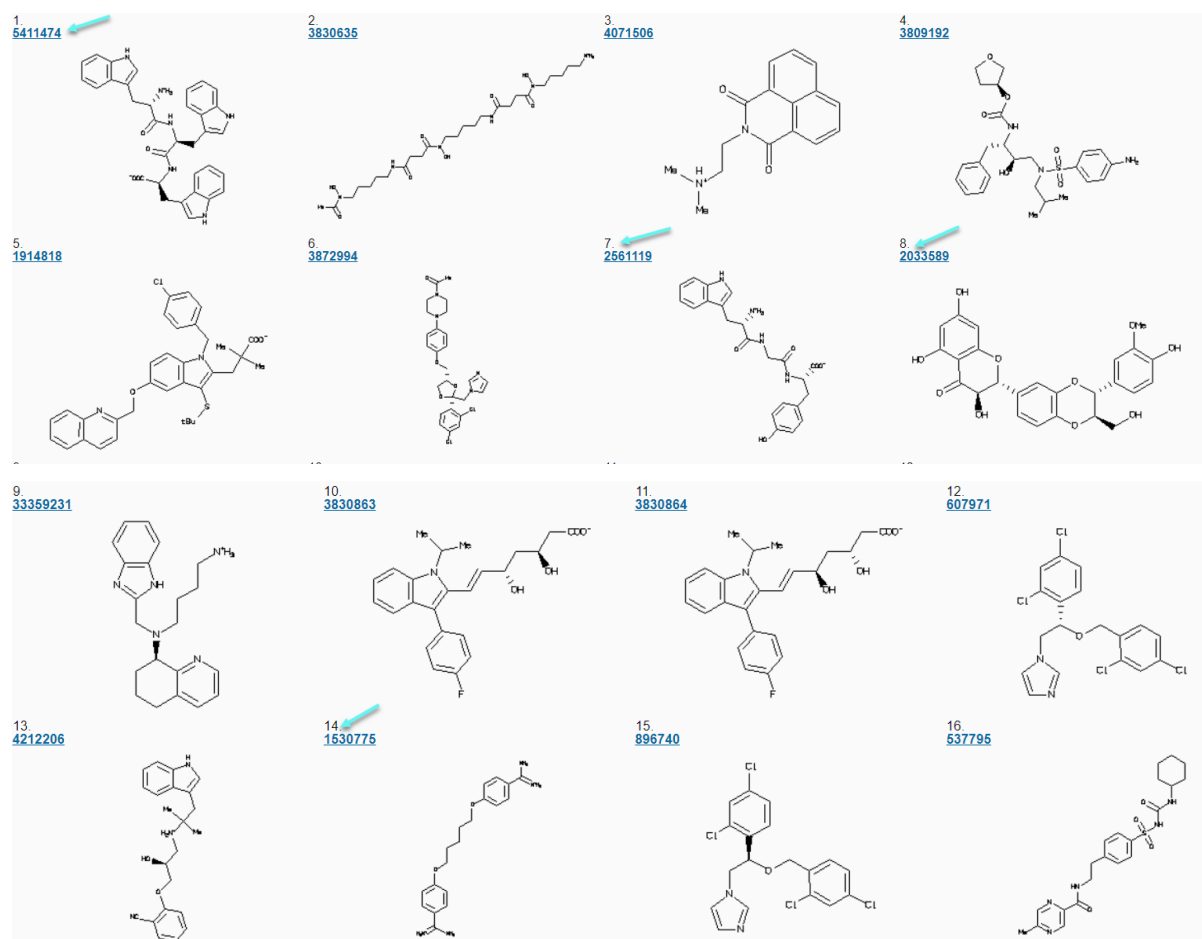




2nd STRATEGY SCREENING- ZINC LIBRARY (selected ligands are marked with an orange arrow)

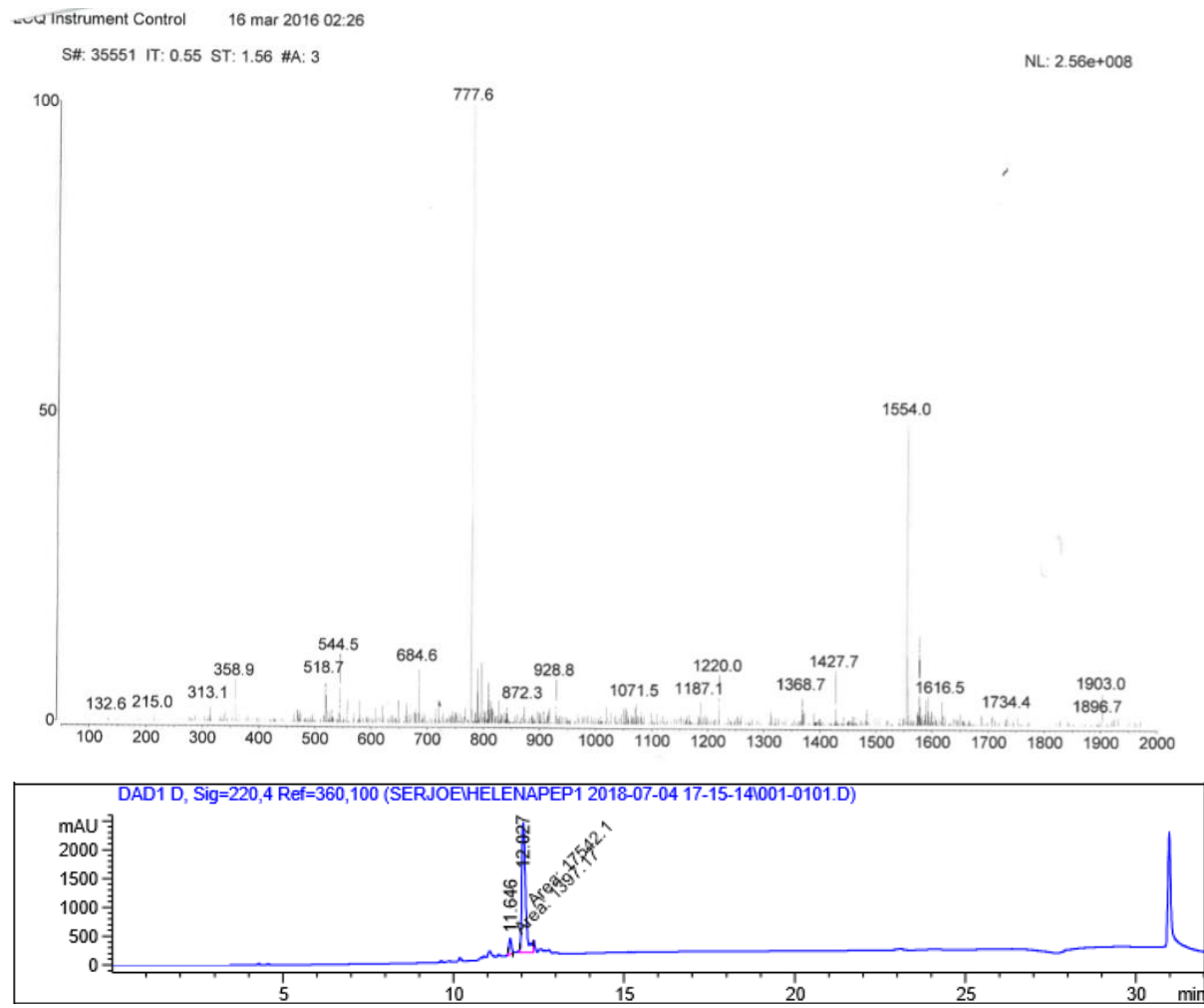




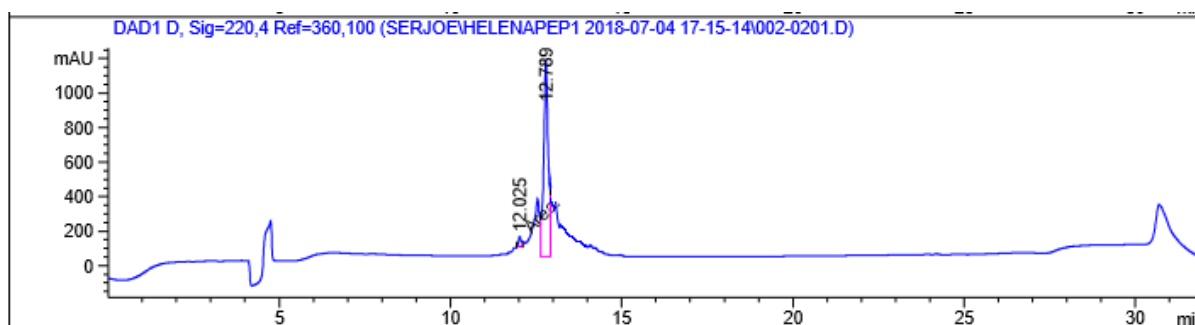
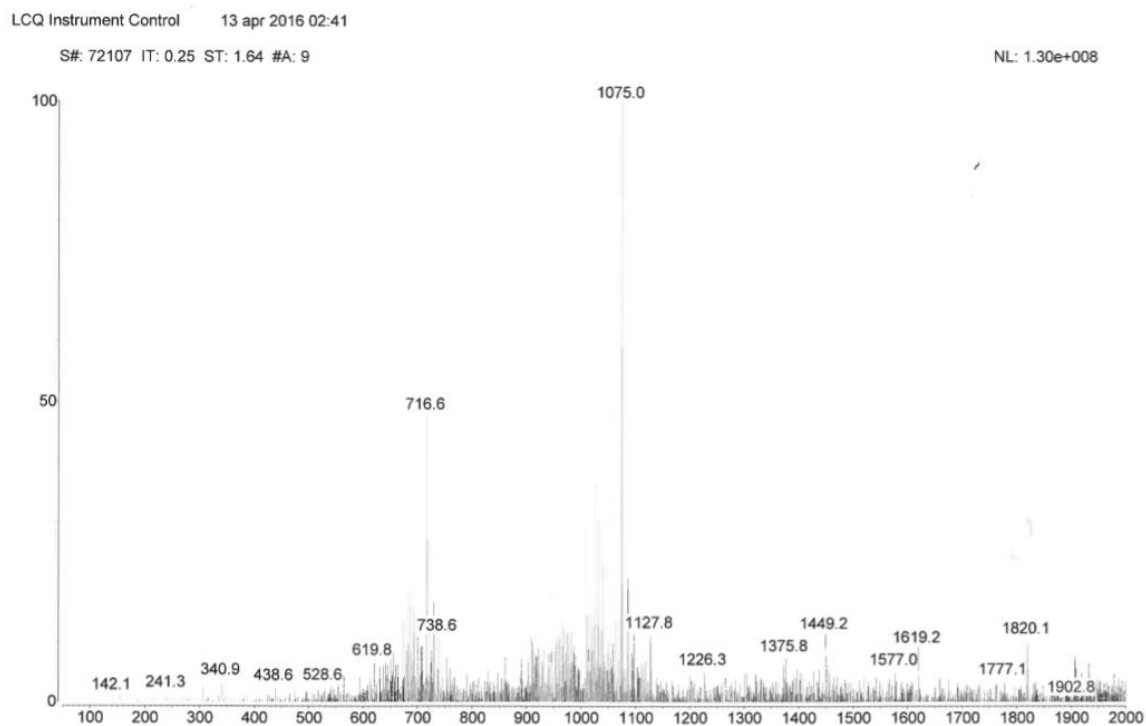
2nd STRATEGY SCREENING- ZINC ADME LIBRARY (selected ligands are marked with a blue arrow)

EXPERIMENTAL DATA

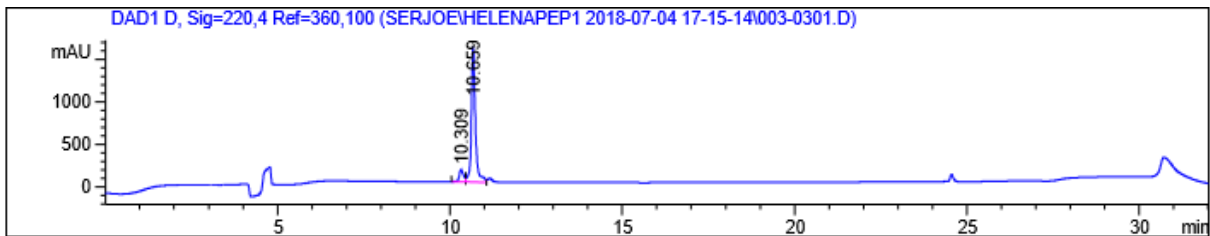
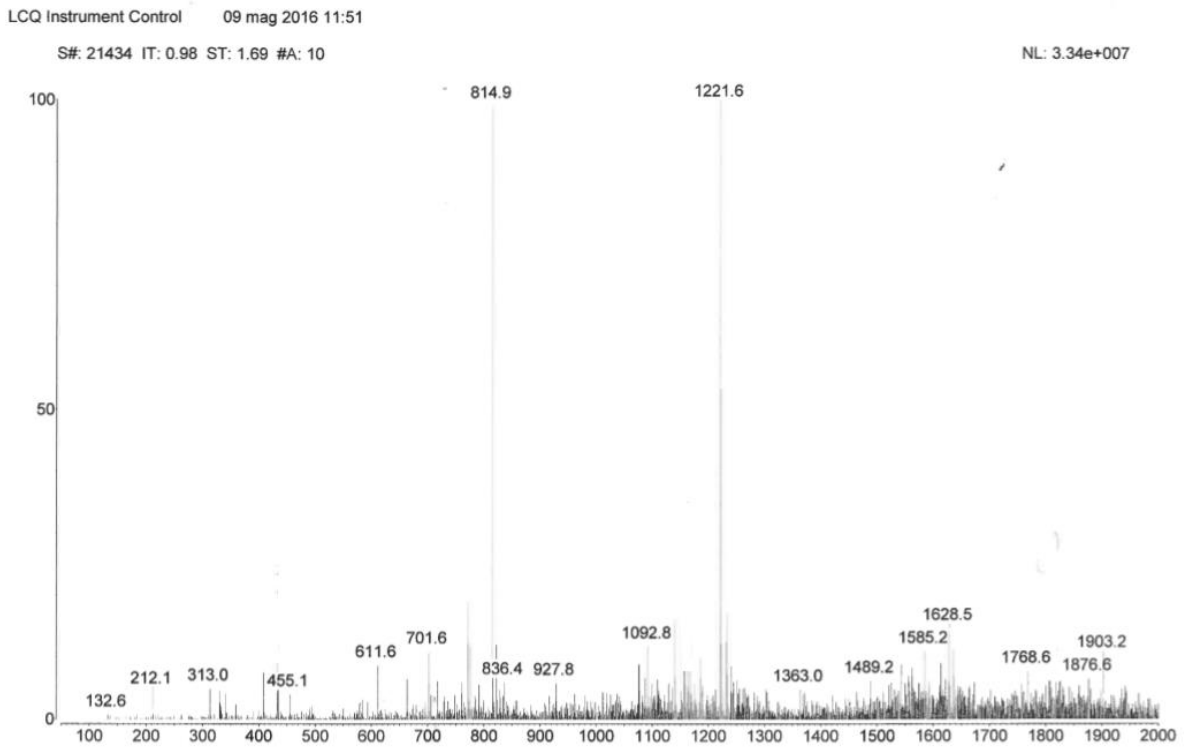
HM-4; calculated MW: 1553.85, found: MS (ESI) $m/z = 1554.0$ ($[M+H]^+$); HPLC: tr= 12.028 min, 92.6 % at 220 nm.



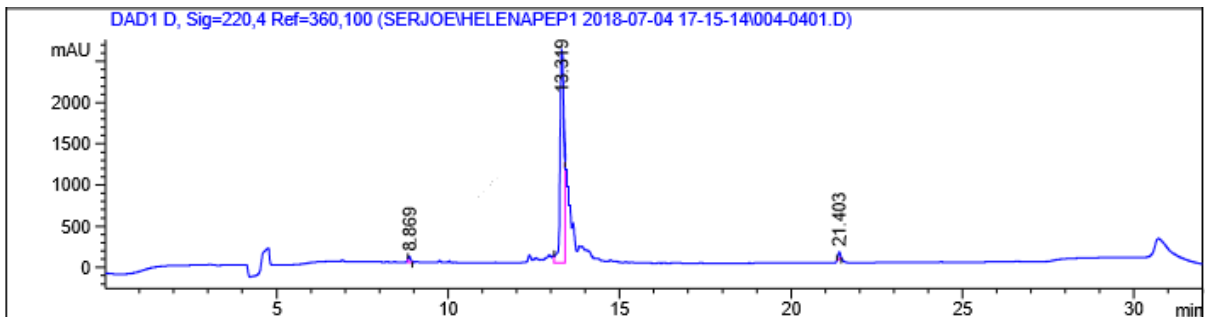
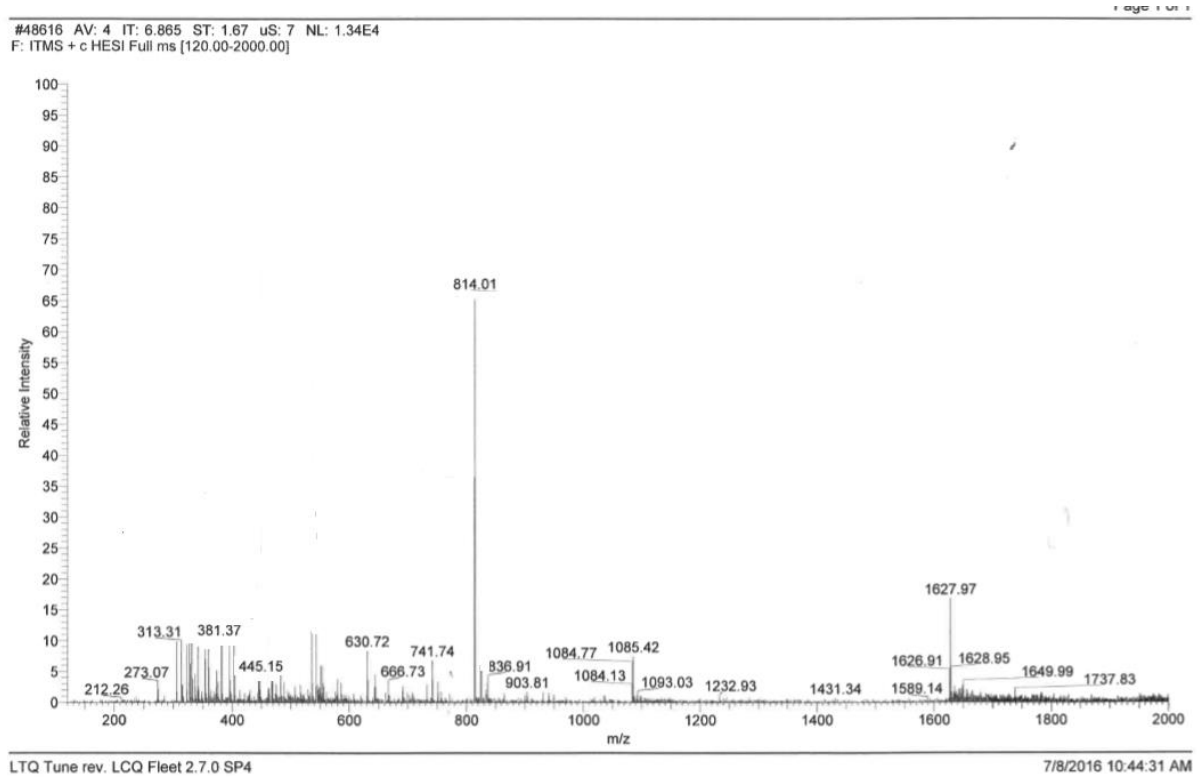
HM-5; calculated MW: 2147.44, found: MS (ESI) $m/z = 1550.0$ ($[M+2H]^{2+}$); HPLC: $t_r = 12.789$ min, 93.1% at 220 nm.



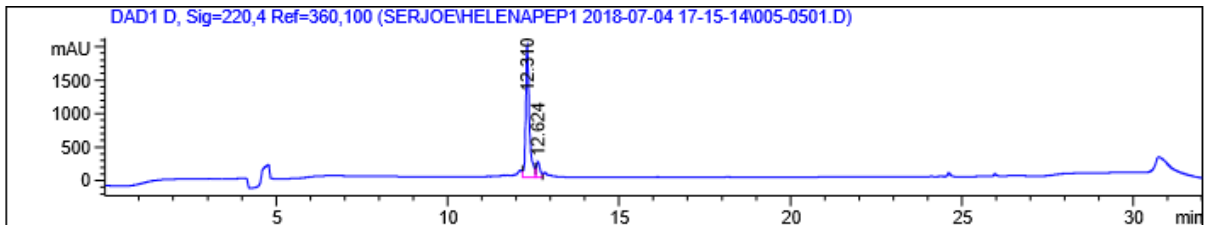
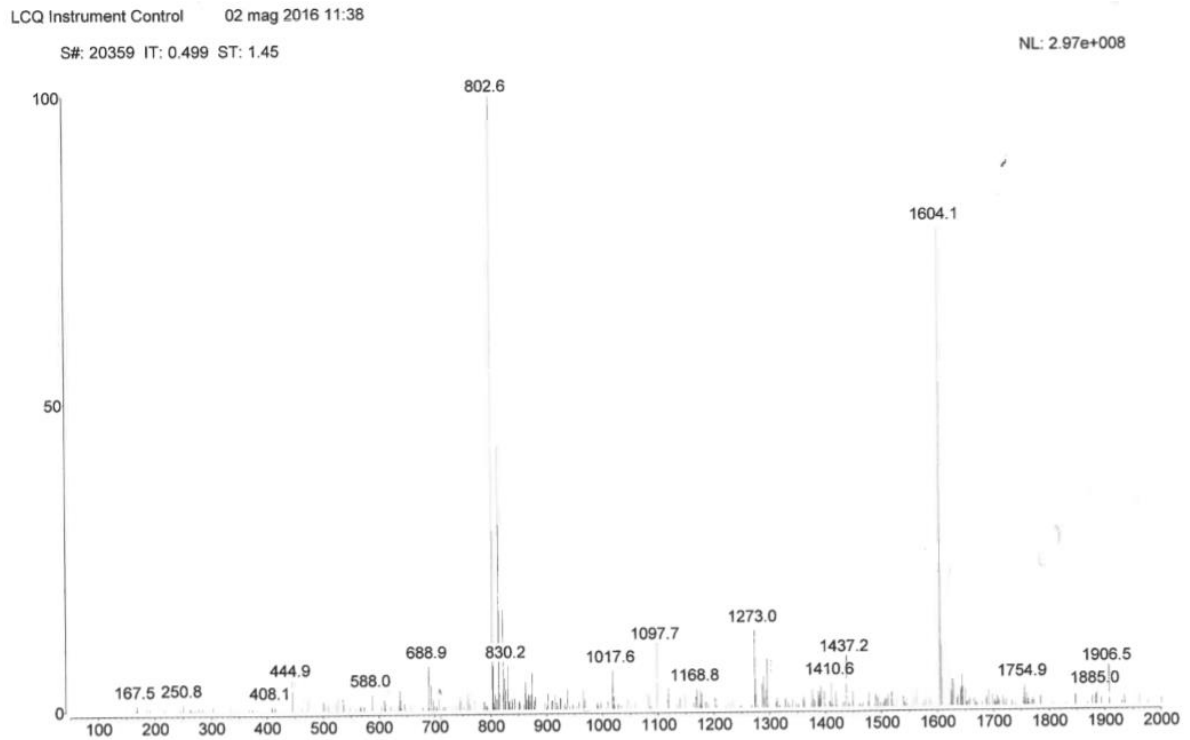
HM-6; calculated MW: 2441.62, found: MS (ESI) $m/z = 1221.6$ ($[M+2H]^{2+}$); HPLC: $t_r = 10.661$ min, 96.3 % at 220 nm.



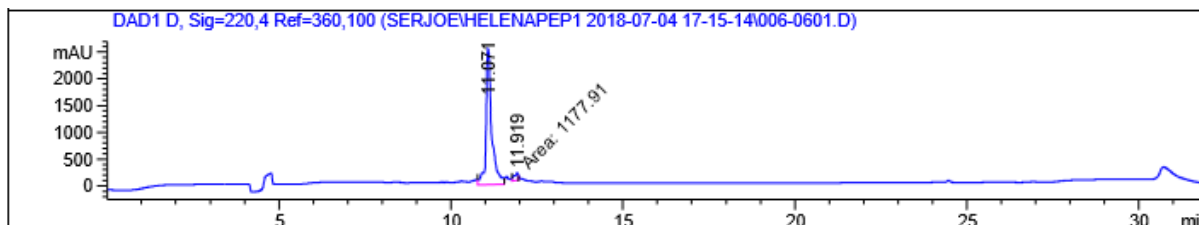
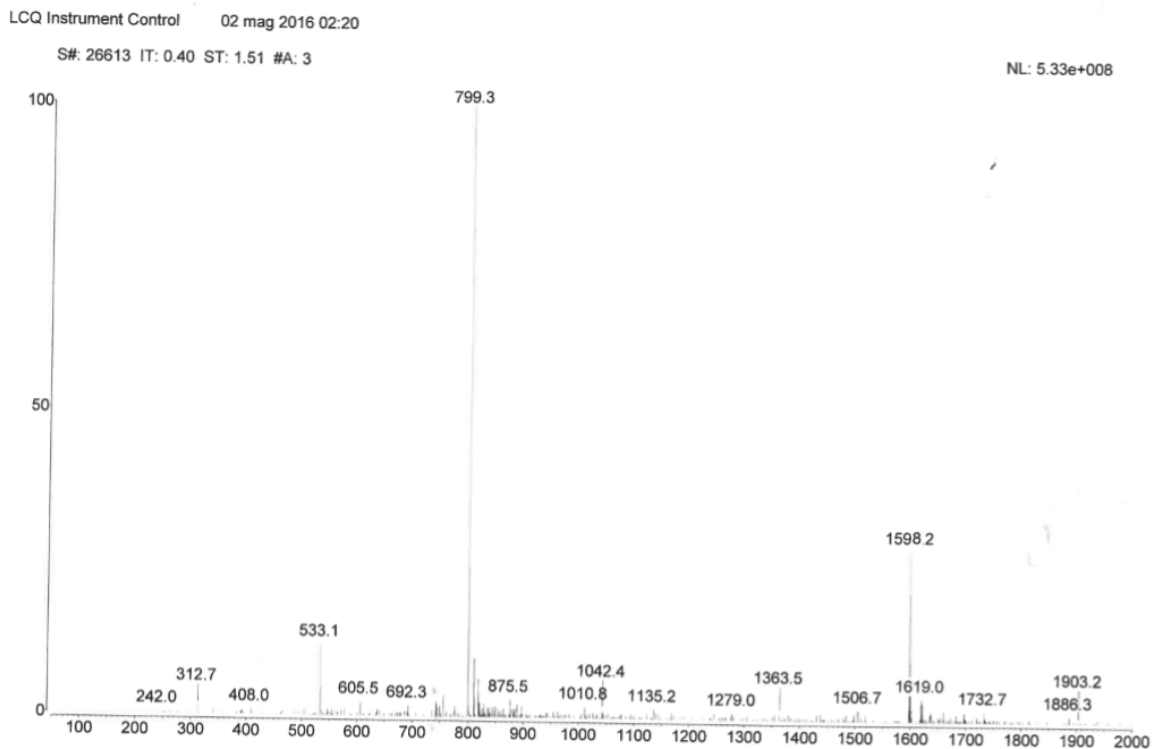
HM-7; calculated MW: 1626.94, found: MS (ESI) $m/z = 1627.97$ ($[M+H]^+$); HPLC: $t_r = 13.319$ min, 96.5 min at 220 nm.



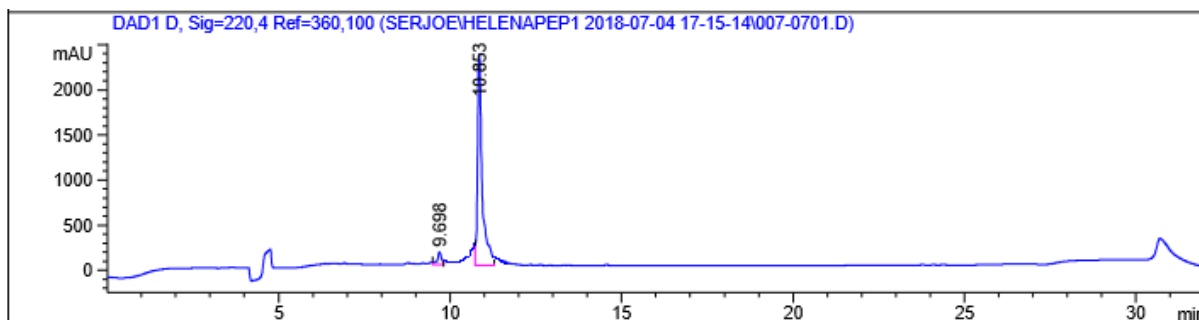
HM-8; calculated MW: 1603.89, found: MS (ESI) $m/z = 1604.1$ ($[M+H]^+$); HPLC: $t_r = 12.310$ min, 94.5 % at 220 nm.



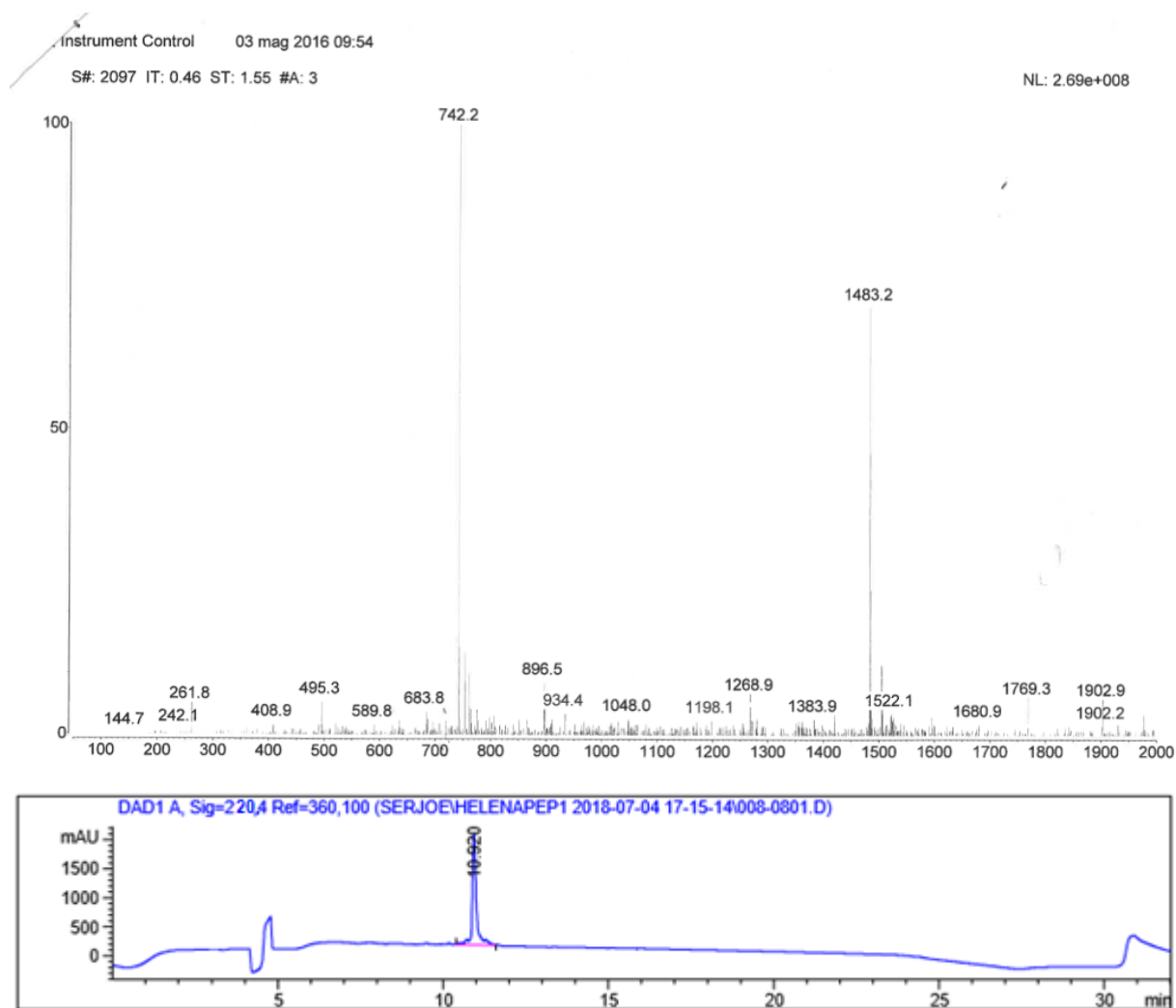
HM-9; calculated MW: 1596.90, found: MS (ESI) $m/z = 1598.2$ ($[M+H]^+$); HPLC: $t_r = 11.070$ min, 96.2 % at 220 nm.



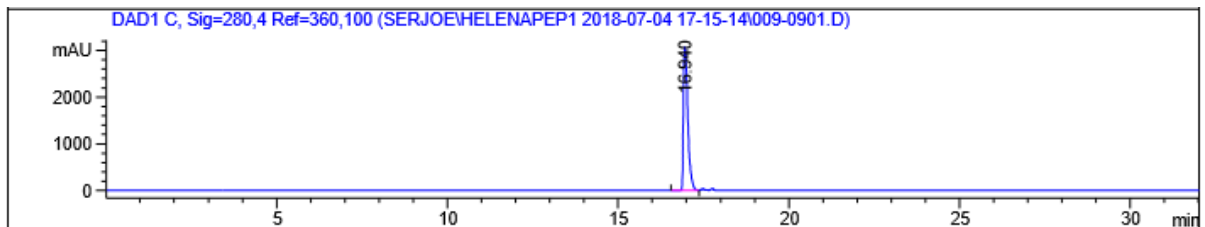
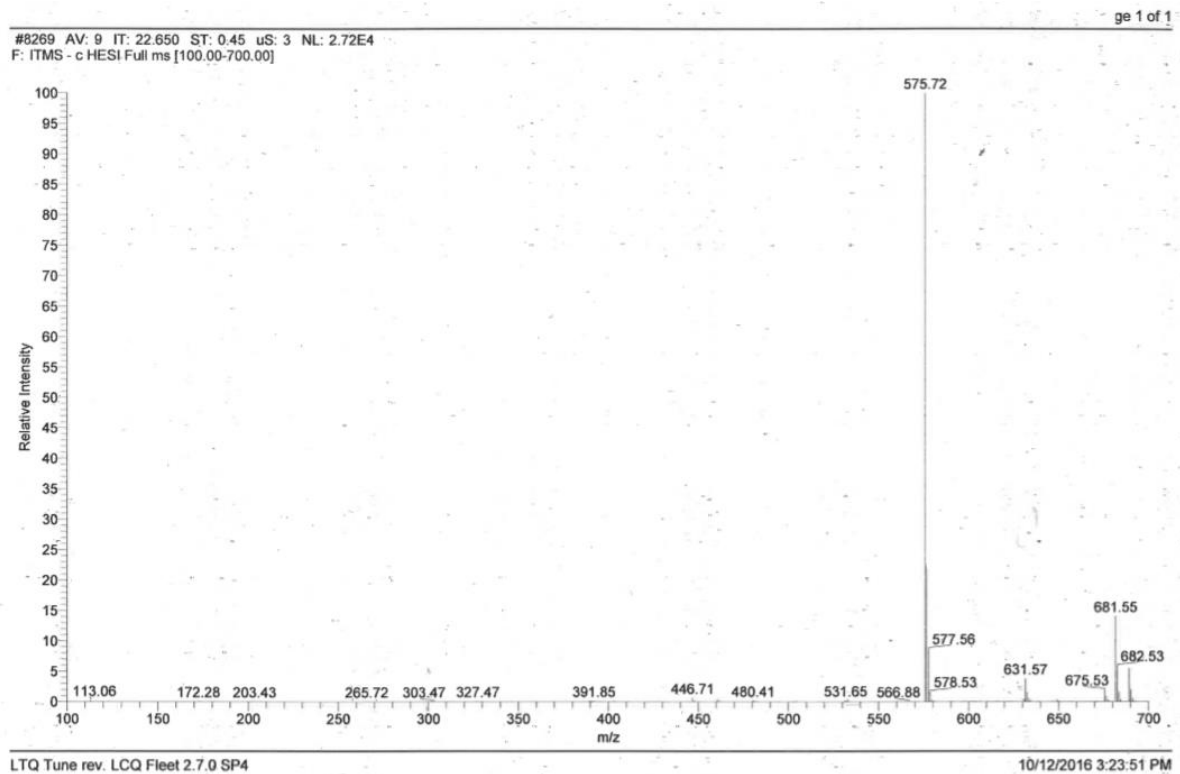
HM-10; calculated MW: 1568.88, found: MS (ESI) $m/z = ([M+H]^+)$; $t_r = 10.853$ min, 94.7 % at 220 nm.



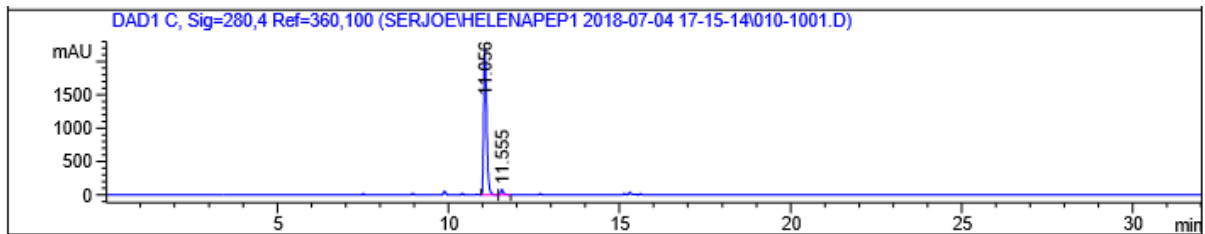
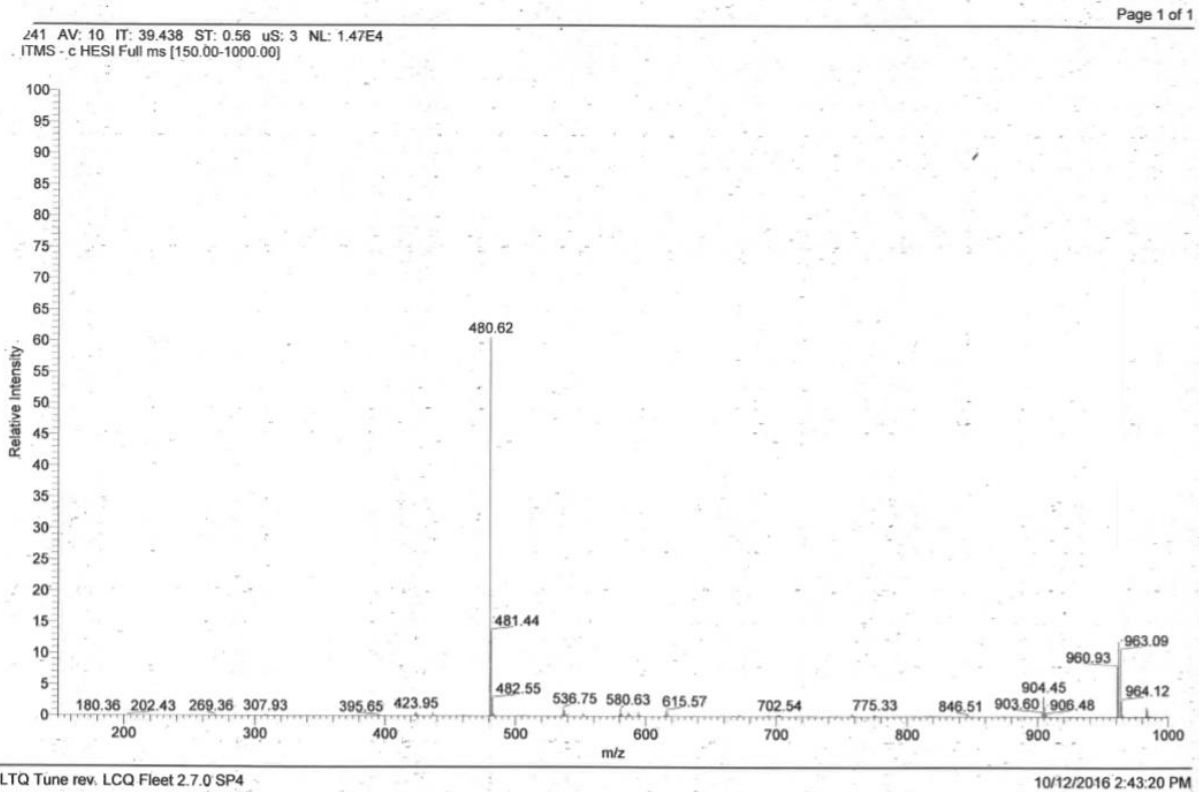
HM-11; calculated MW: 1482.74, found: MS (ESI) $m/z = 1483.2$ ($[M+H]^+$); HPLC: $t_r = 10.920$ min; 100 % at 220 nm.



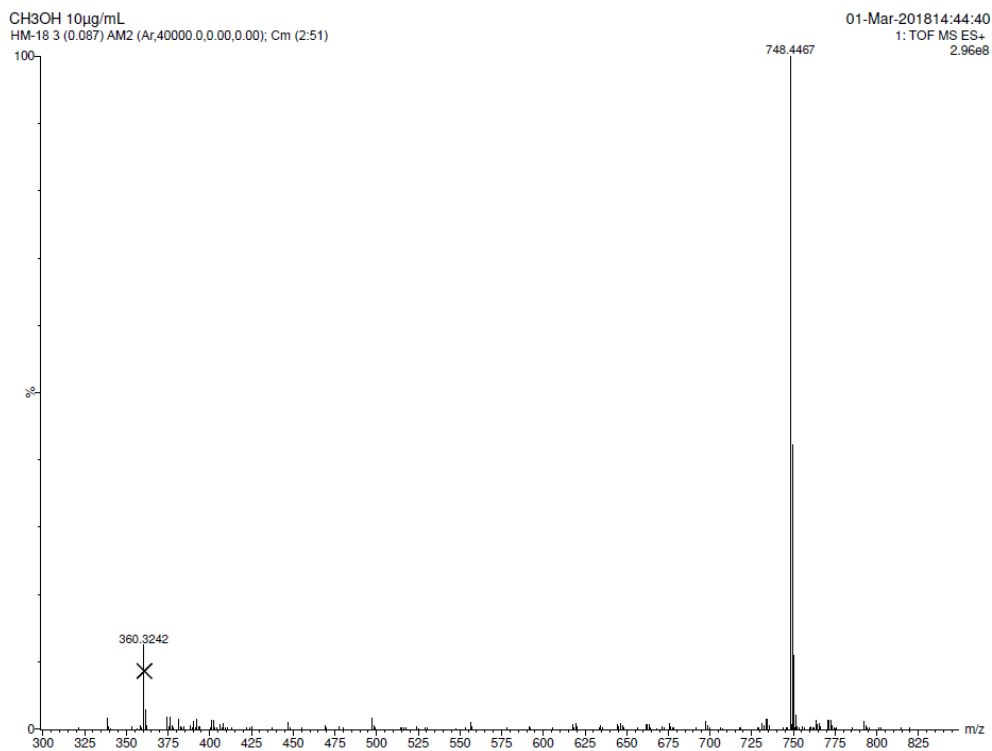
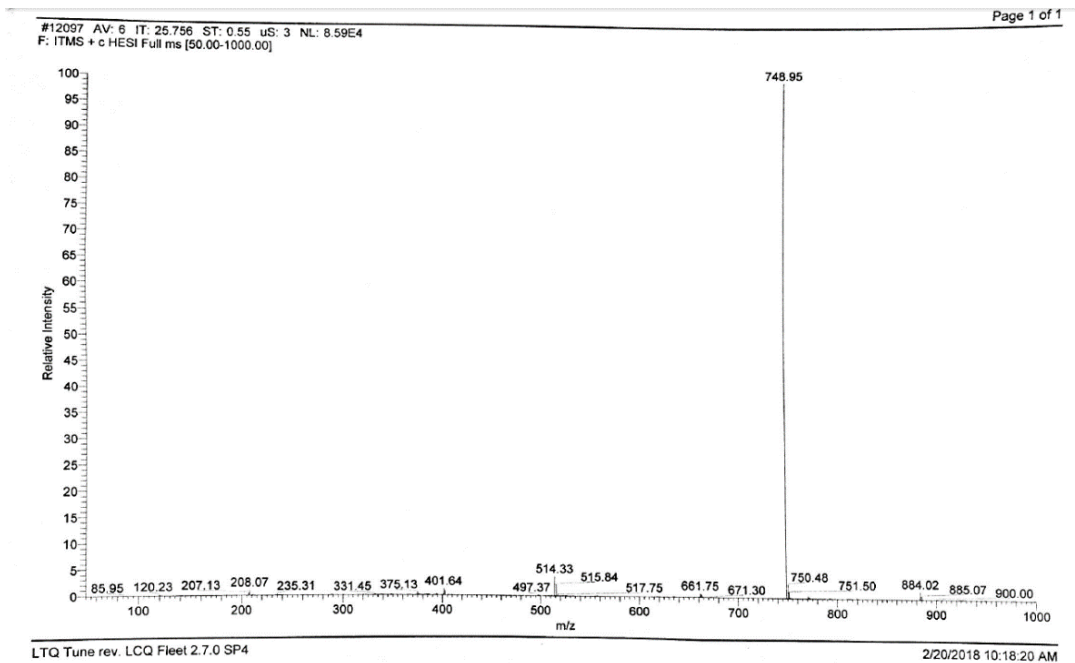
HM-15; calculated MW: 576.64, found MS (ESI) $m/z = 575.72$ ($[M-H]^-$); HPLC: $t_r = 16.940$ min, 100 % at 280 nm.

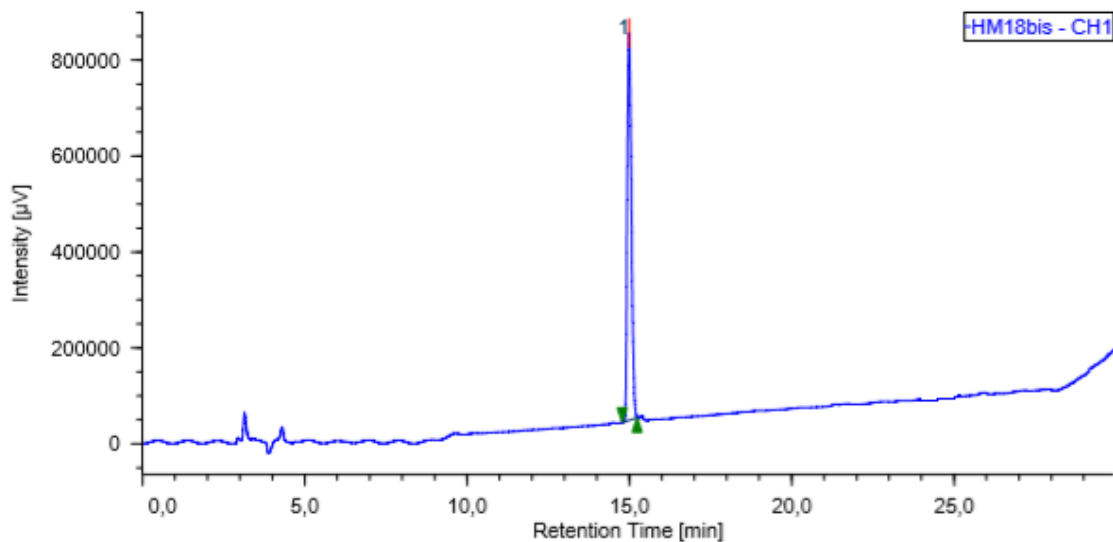


HM-16; calculated MW: 481.50, found: MS (ESI) $m/z = 480.6$ ($[M-H]^-$); HPLC: $t_r = 11.056$ min, 96.5 % at 280 nm.

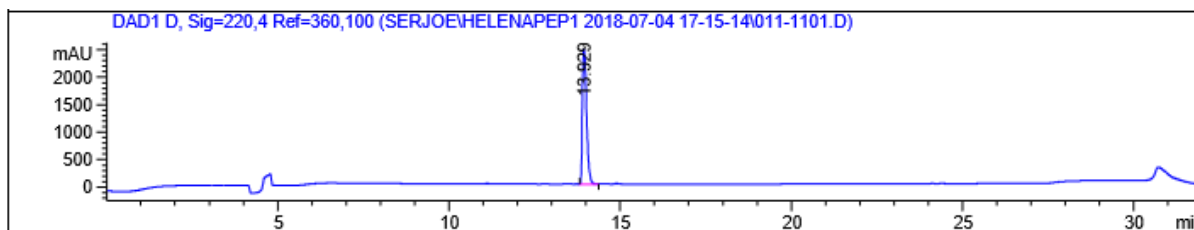
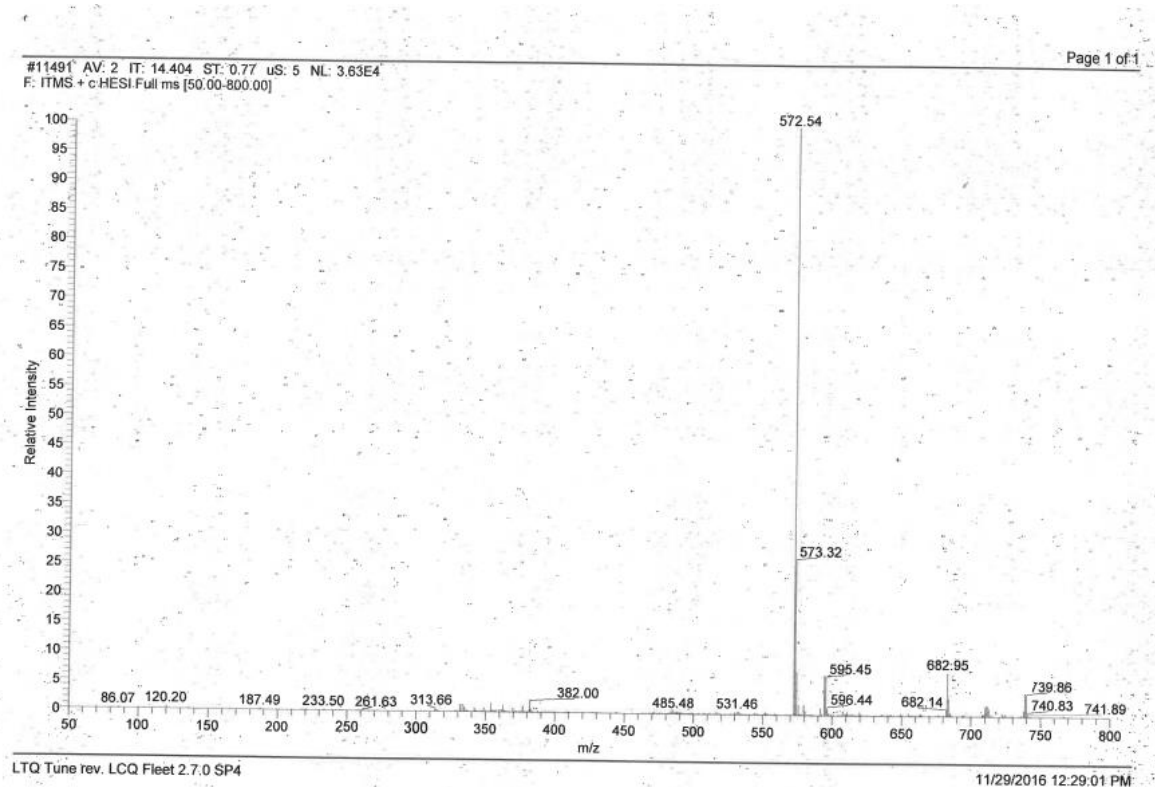


HM-18; calculated MW: 747.89, found: MS (ESI) $m/z = 748.9$ ($[M+H]^+$), HRMS ($([M+H]^+)$) for $C_{34}H_{59}N_{11}O_8$: calculated 748.4469, found 748.4467; HPLC: $t_r = 14.98$ min, 100 % at 220 nm.

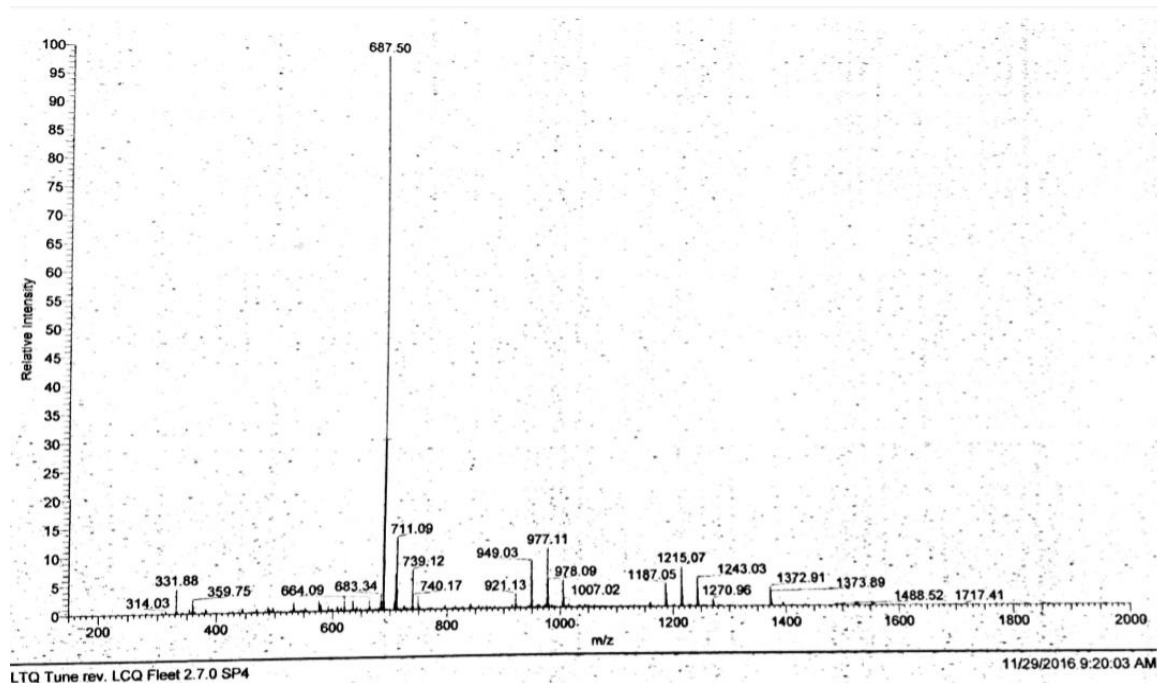




HM-19; calculated MW: 571.67, found: MS (ESI) $m/z = 572.5$ ($[M+H]^+$); HPLC: $tr=13.929$ min, 100 % at 220 nm.

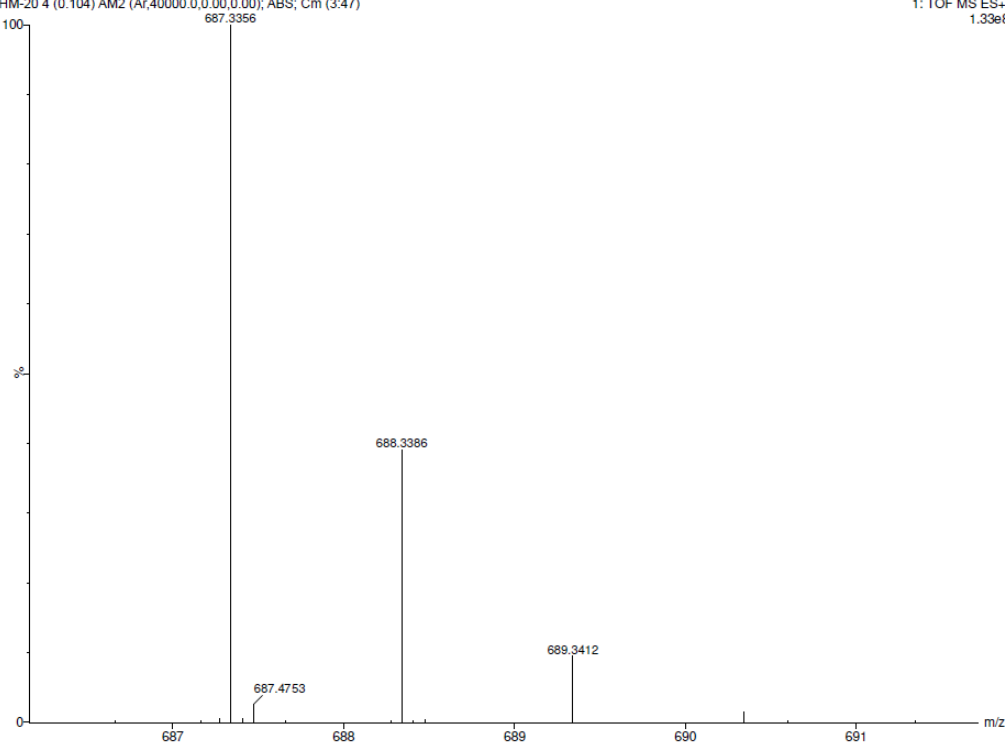


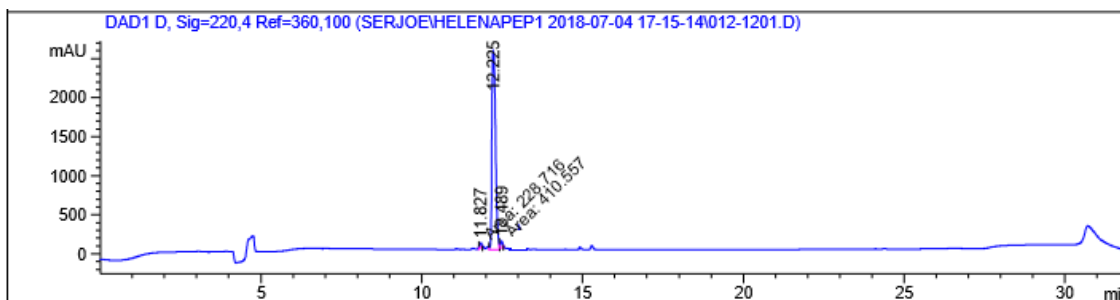
HM-20; calculated MW: 686.75, found: MS (ESI) $m/z = 687.5$ ($[M+H]^+$), HRMS ($[M+H]^+$) for $C_{33}H_{46}N_6O_{10}$: calculated 687.3356, found 687.3354; HPLC: $t_r = 16.00$ min; 96.9% at 220 nm.



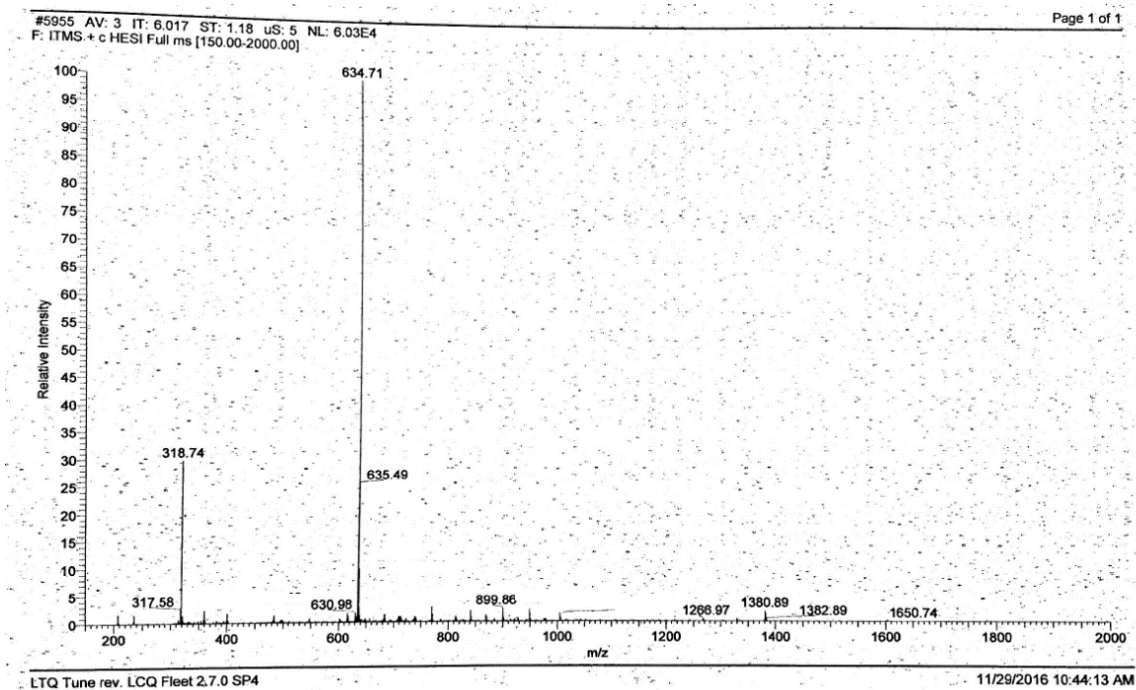
CH3OH 9µg/mL
 HM-20 4 (0.104) AM2 (Ar,40000.0,0.00,0.00); ABS; Cm (3:47)

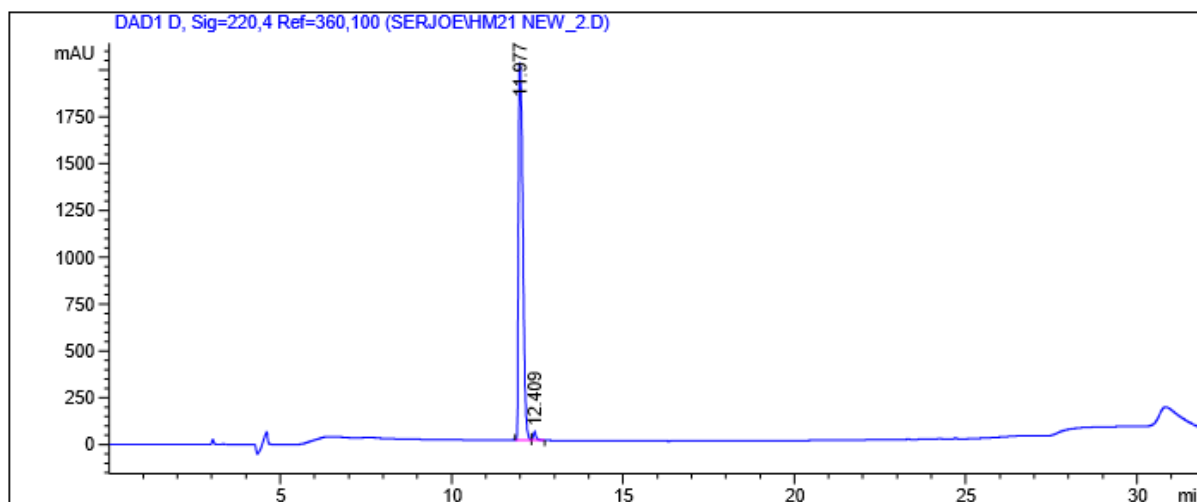
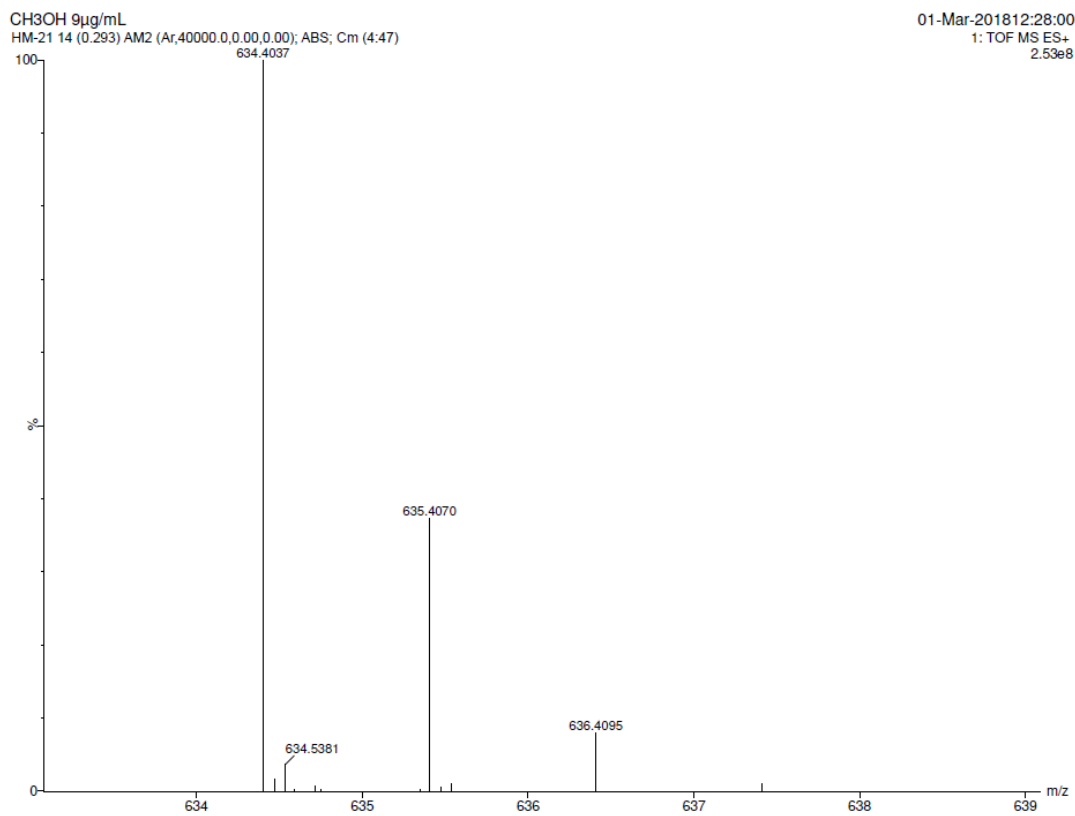
01-Mar-2018 11:43:05
 1: TOF MS ES+
 1.33e8



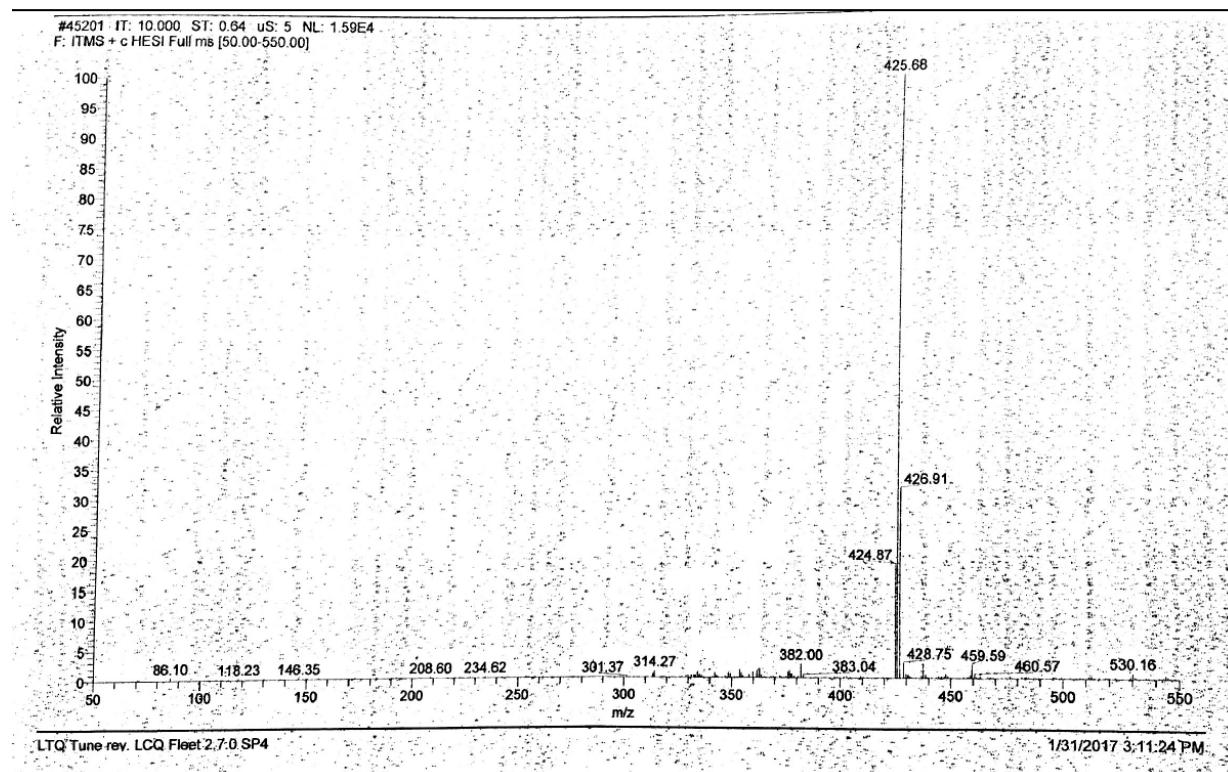


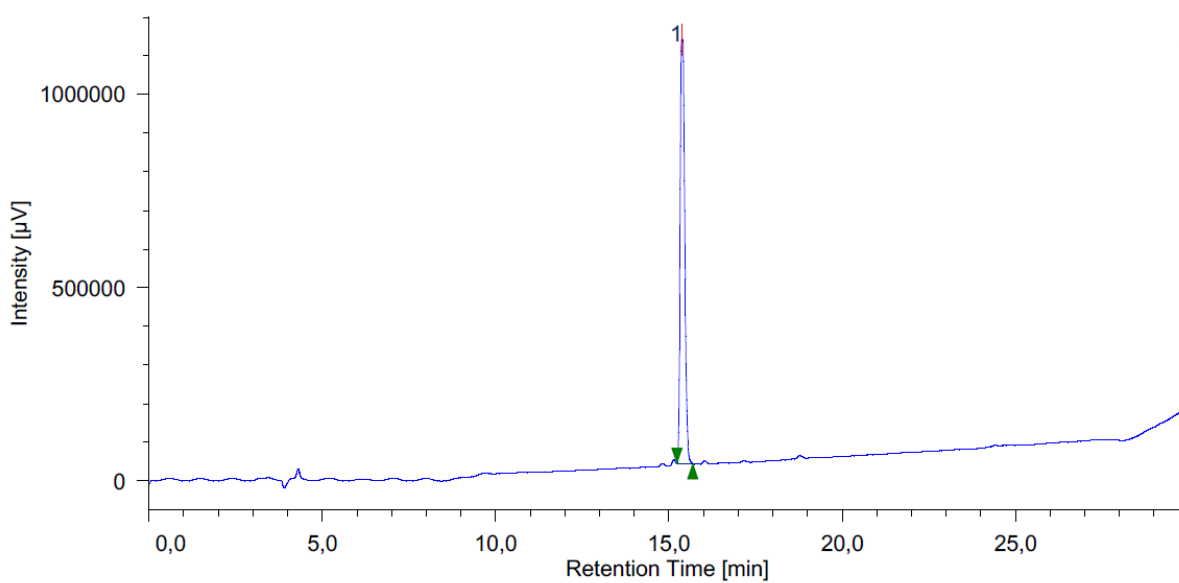
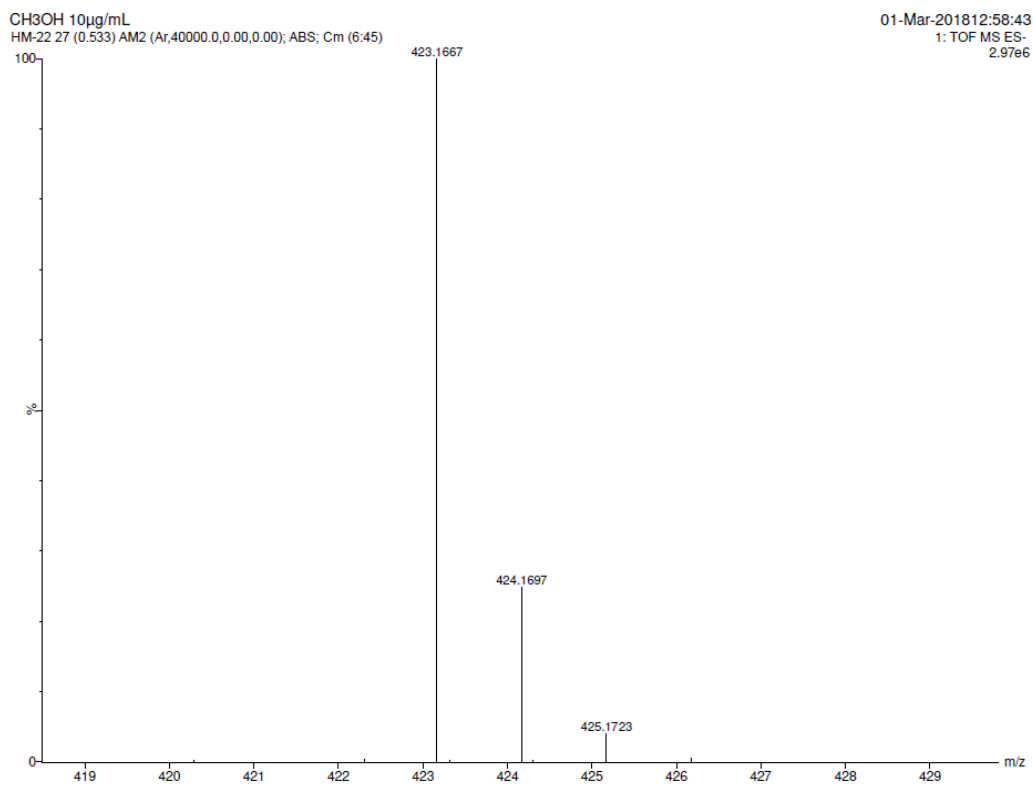
HM-21; calculated MW: 633.78, found: MS (ESI) $m/z = 634.7$ ($[M+H]^+$), HRMS ($[M+H]^+$) for $C_{30}H_{53}N_9O_6$: calculated 634.4037, found 634.4041; HPLC: $t_r = 11.977$ min; 98.41 % at 220 nm.



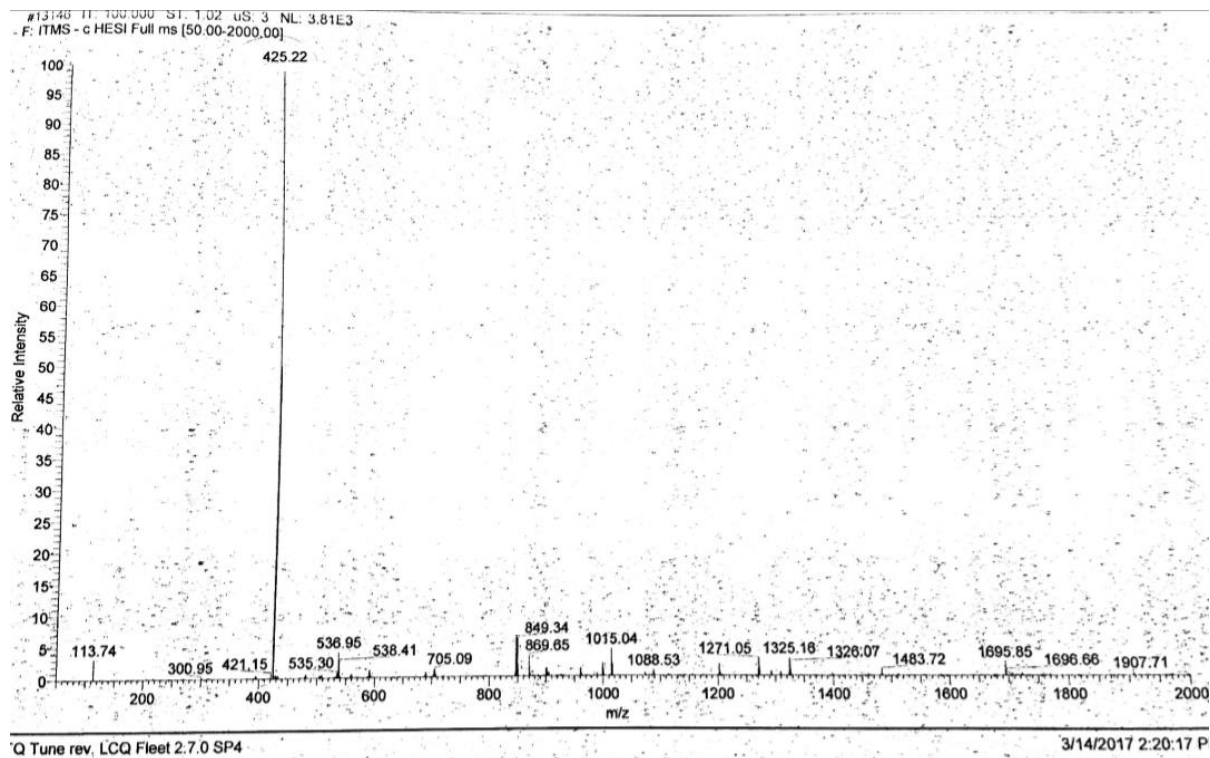


HM-22; calculated MW: 424.45, found: MS (ESI) $m/z = 425.68$ ($[M+H]^+$), HRMS ($[M-H]^-$) for $C_{22}H_{24}N_4O_5$: calculated 423.1667, found 423.1668; HPLC: $t_r = 15.38$ min, 100 % at 220 nm.



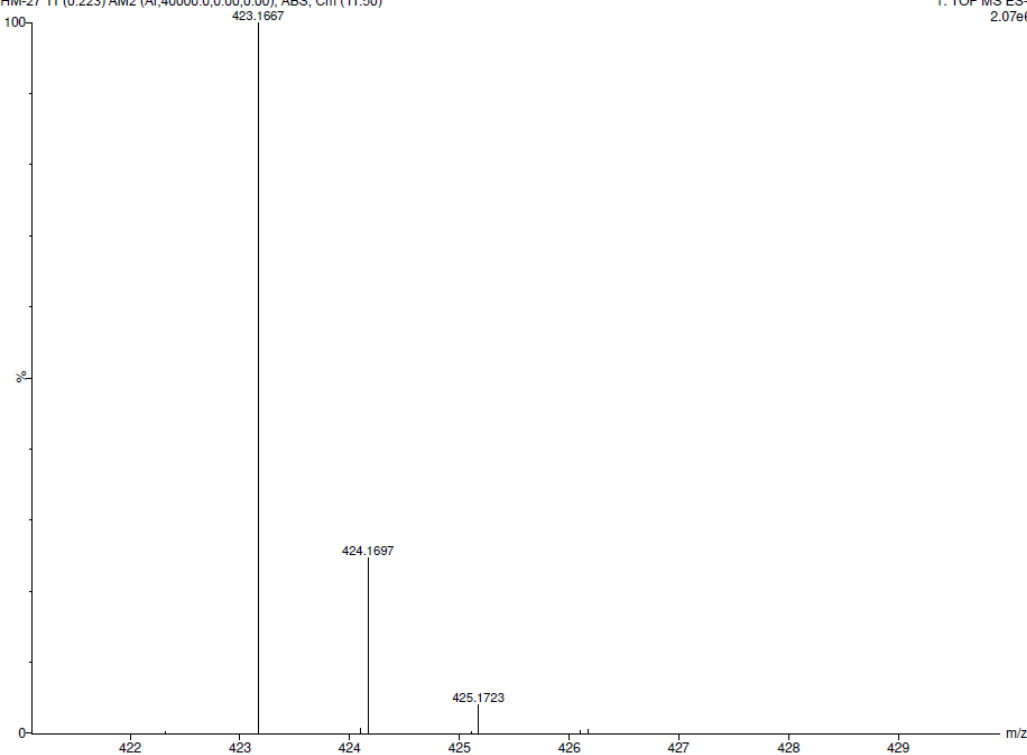


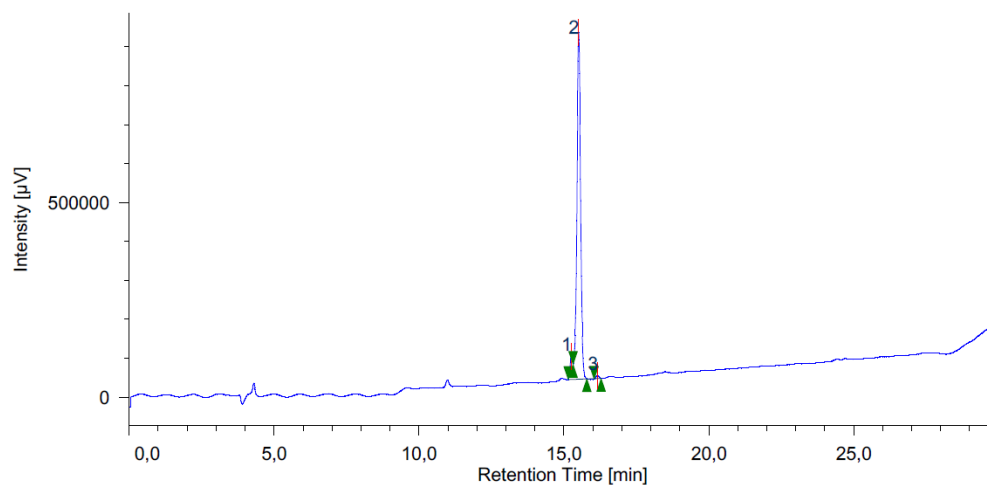
HM-27; calculated MW: 424.45, MS (ESI) $m/z = 425.22$ ($[M+H]^+$), HRMS ($[M-H]^-$) for $C_{22}H_{24}N_4O_5$: calculated 423.1667, found 423.1668; HPLC: $t_r = 15.51$ min, 94.82% at 220 nm.



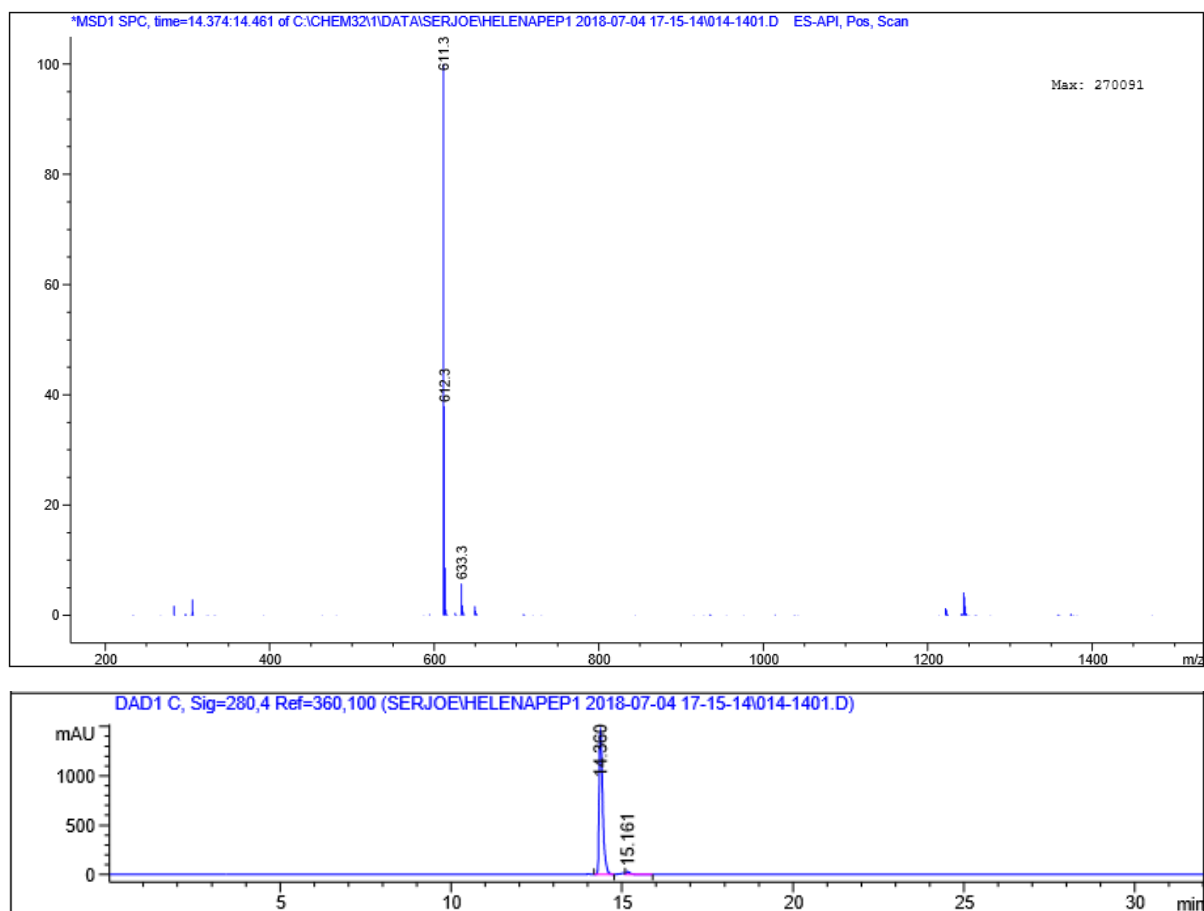
CH3OH 10µg/mL
HM-27 11 (0.223) AM2 (Ar.40000.0,0.00,0.00); ABS; Cm (11:50)

01-Mar-2018 15:02:28
1: TOF MS ES-
2.07e6

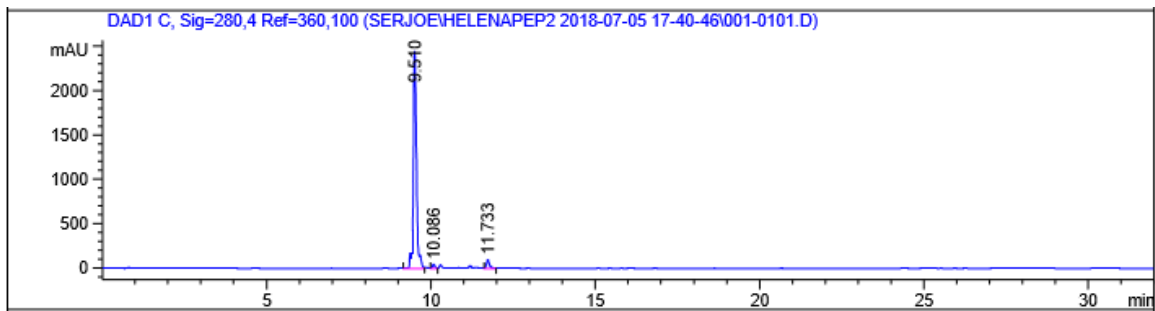
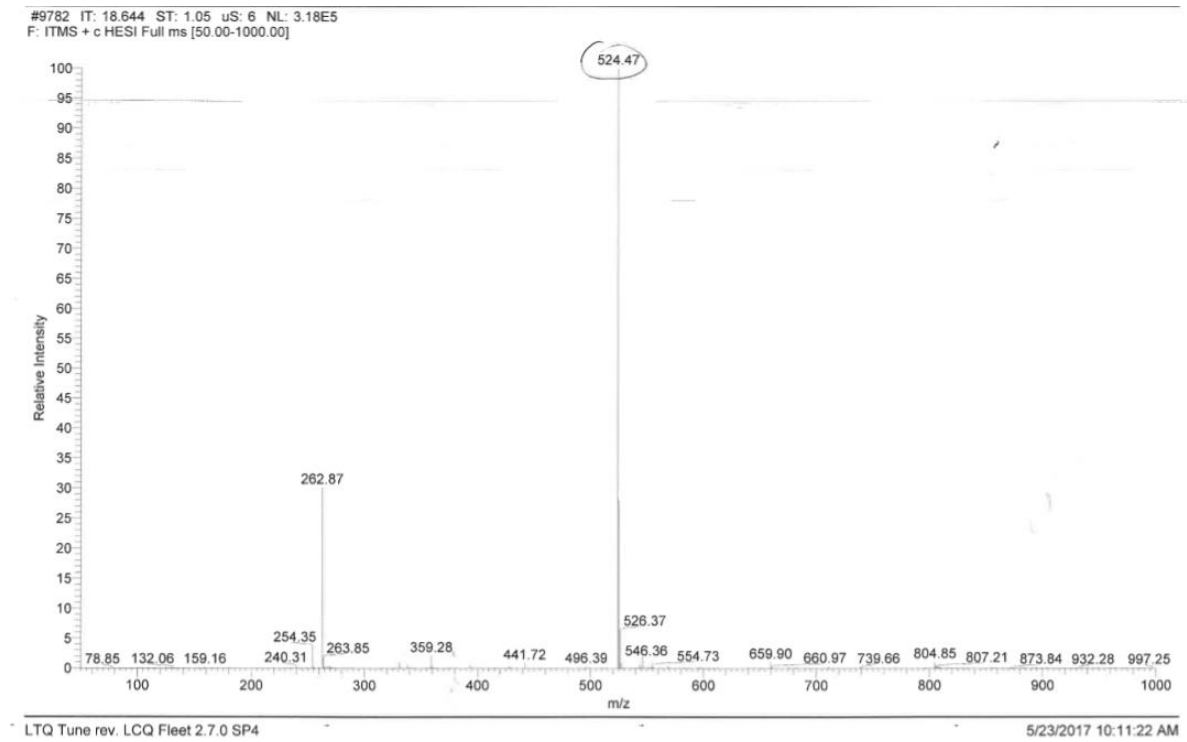




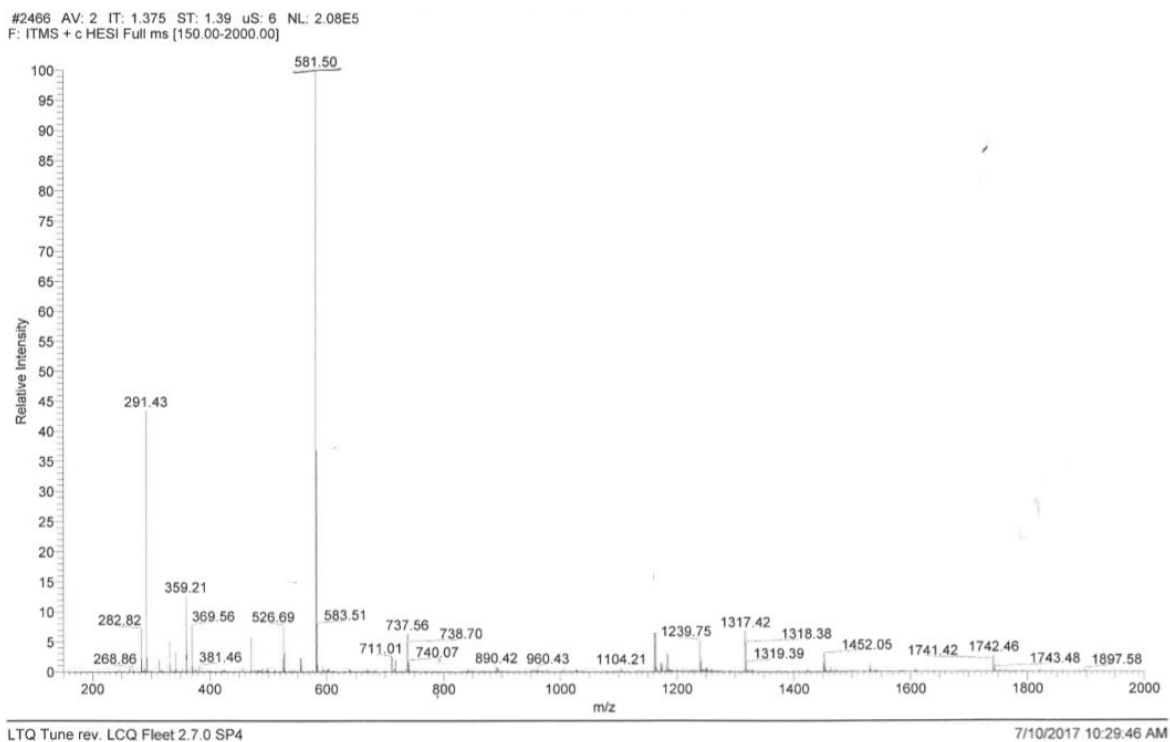
HM-28; calculated MW: 610.70, MS (ESI) $m/z = 611.3$ ($[M+H]^+$); HPLC: $t_r = 14.360$ min, 97.5 % at 280 nm.



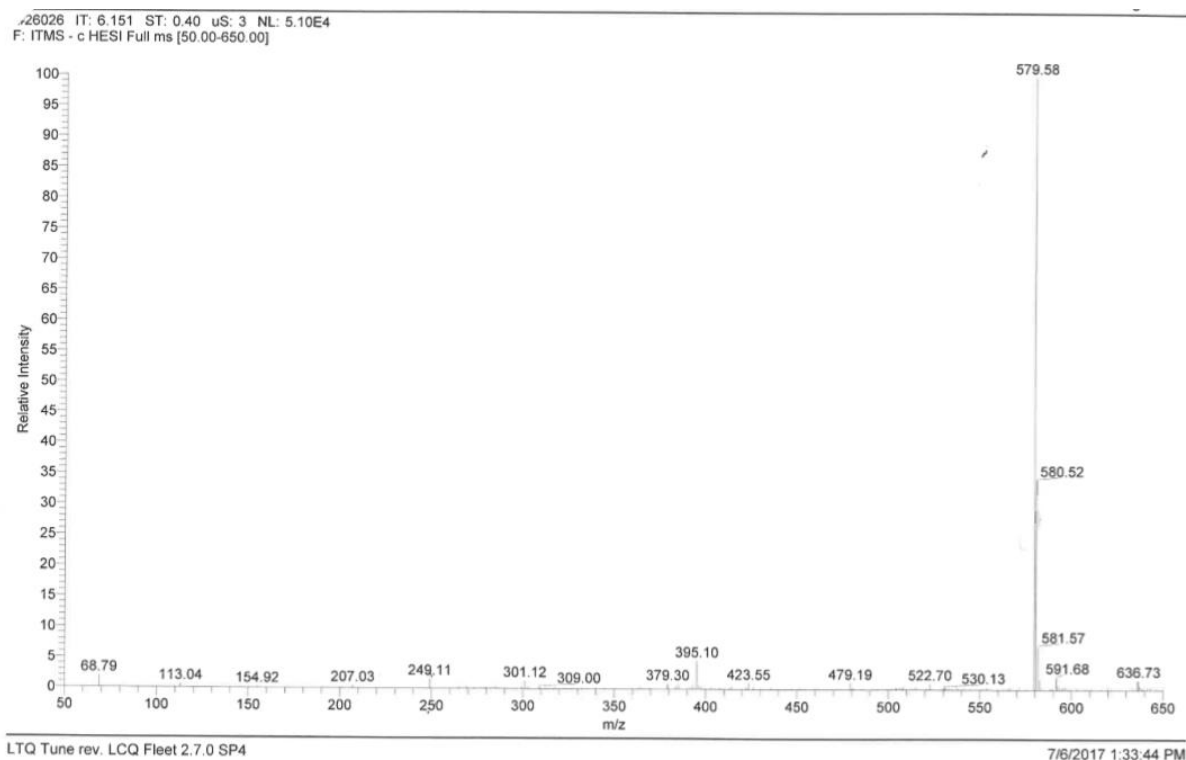
HM-32; calculated MW: 523.58, found: MS (ESI) $m/z = 524.47$ ($[M+H]^+$); HPLC: $t_r = 9.510$ min, 95.3 % at 280.4 nm.



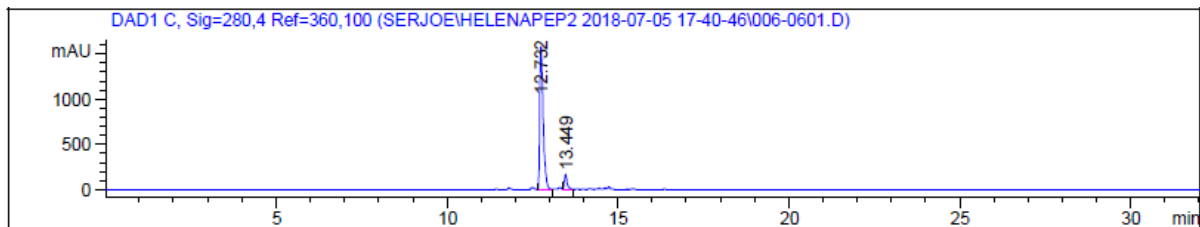
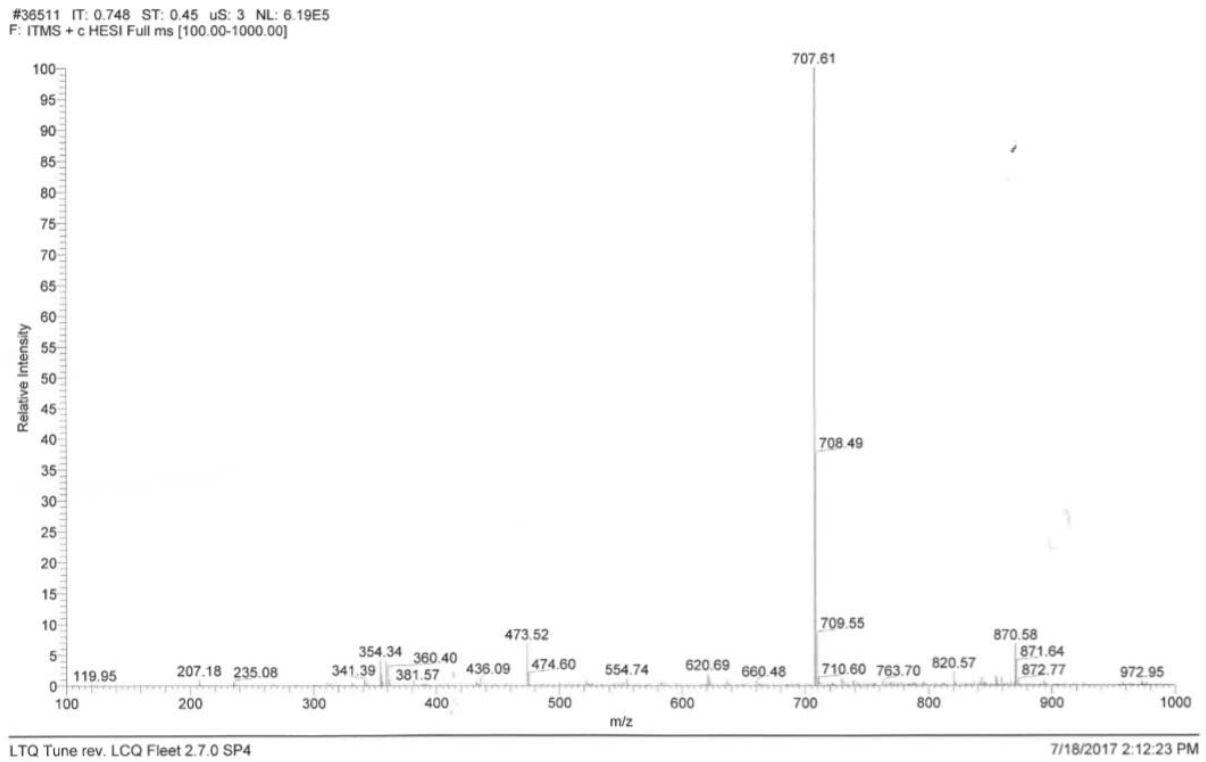
HM-34; calculated MW: 580.63, found: MS (ESI) $m/z = 581.50$ ($[M+H]^+$); unstable compound.



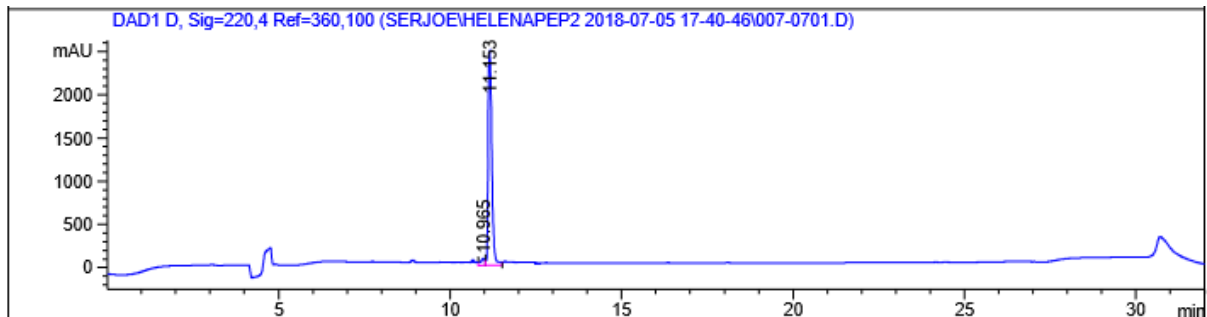
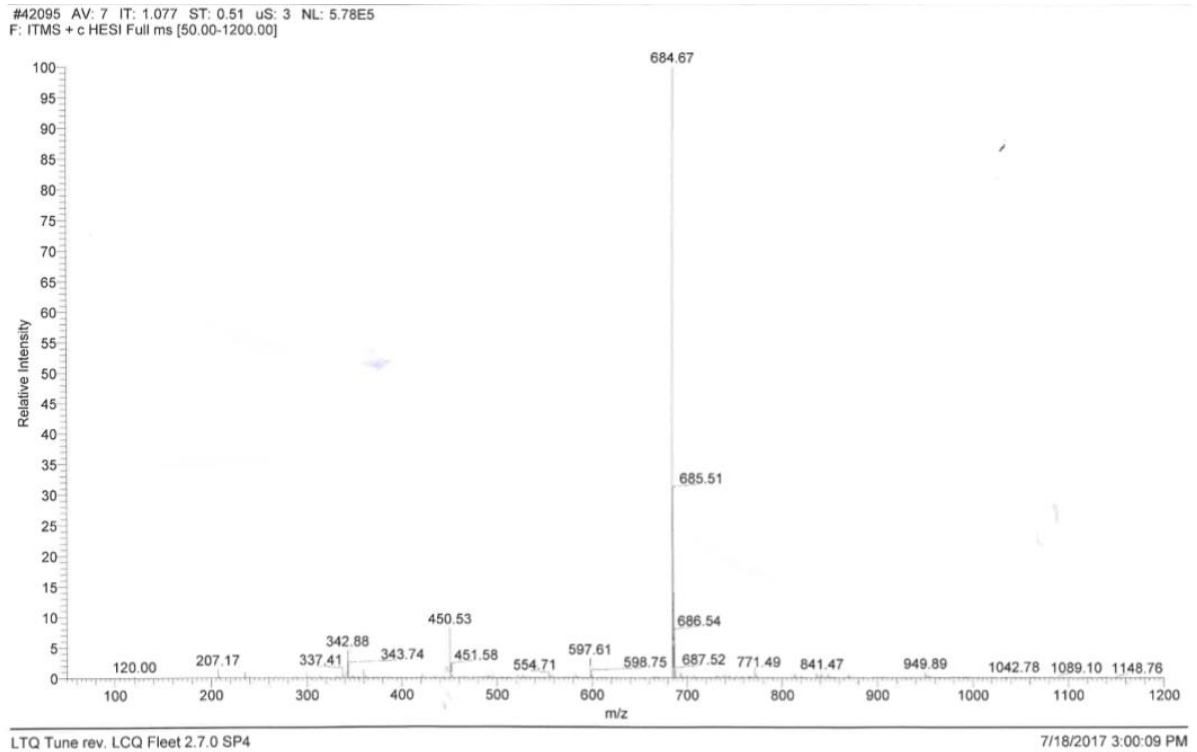
HM-35; calculated MW: 580.63, found: MS (ESI) $m/z = 579.58$ ($[M-H]^-$); unstable compound.



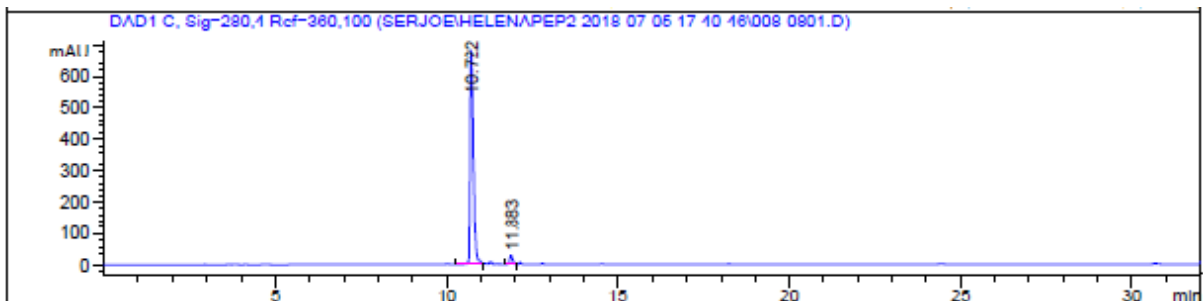
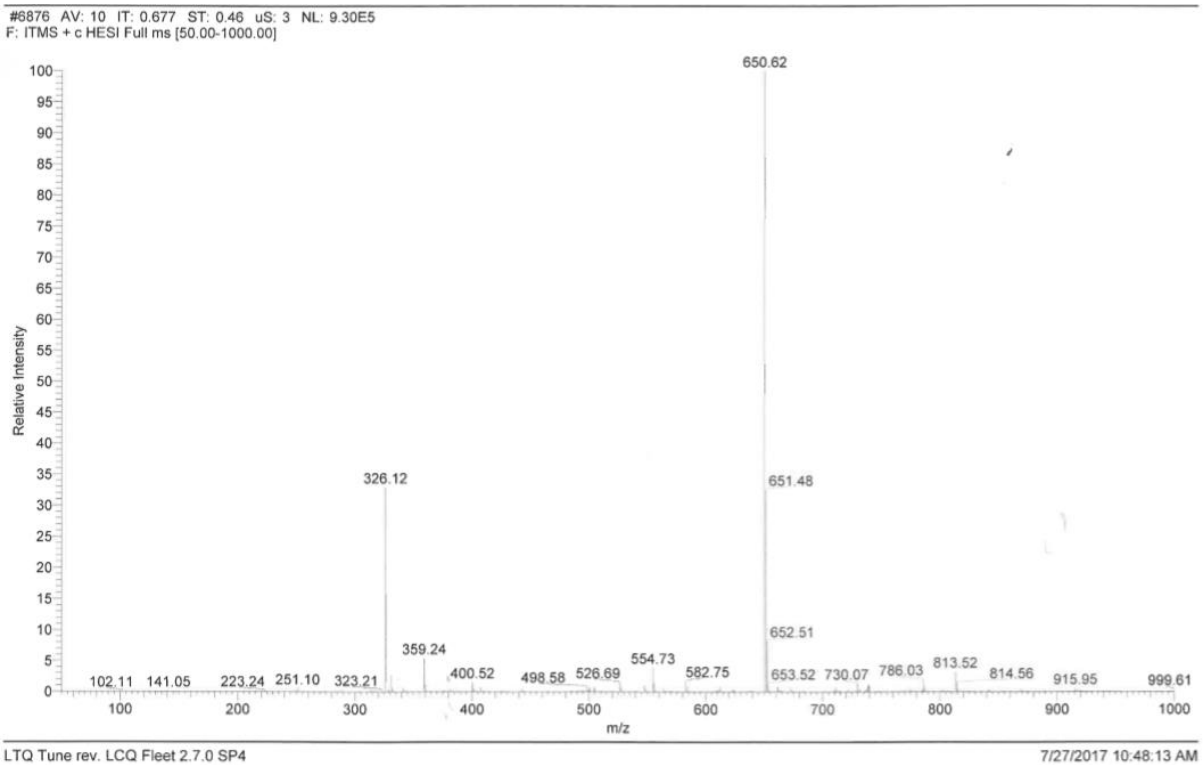
HM-38; calculated MW: 706.82, found: MS (ESI) $m/z = 707.61$ ($[M+H]^+$); HPLC: $t_r = 12.732$ min, 95.6 % at 280 nm.



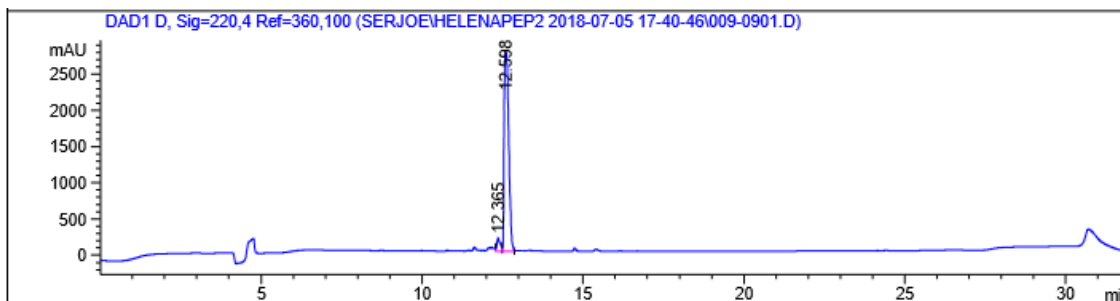
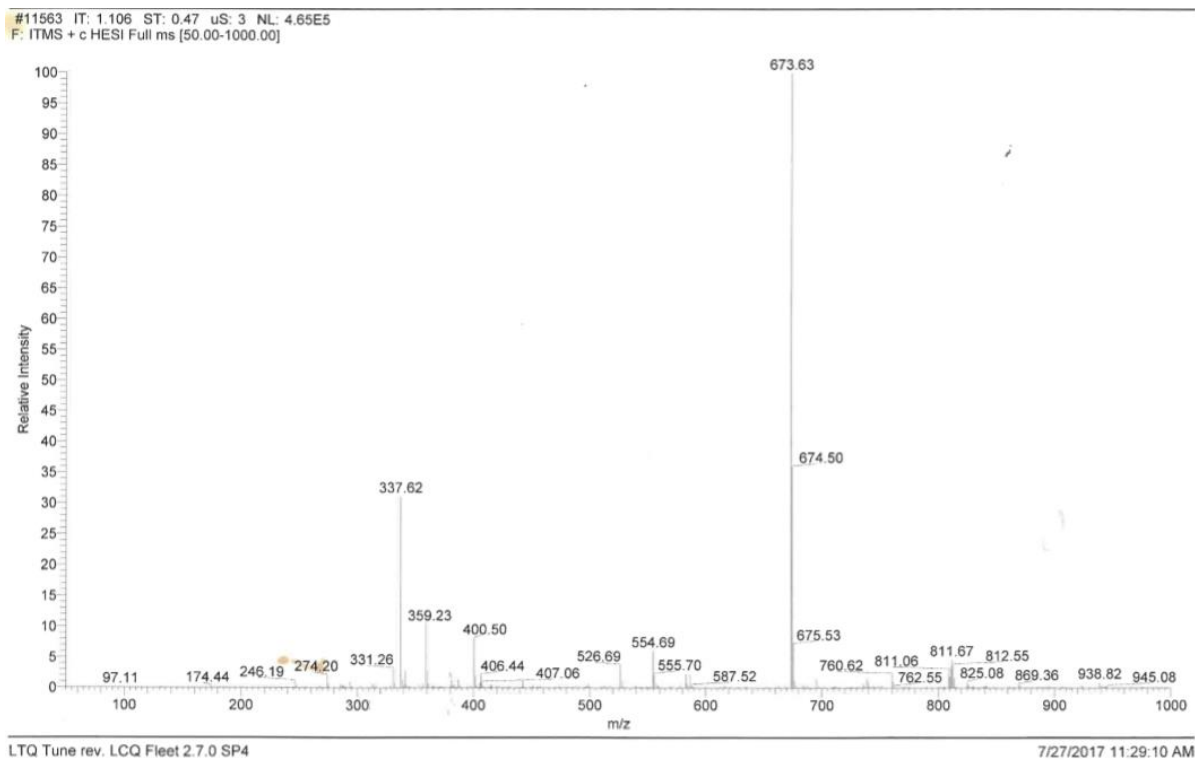
HM-39; calculated MW: 683.70, found: MS (ESI) $m/z = 684.67$ ($[M+H]^+$); HPLC: $t_r = 11.153$ min, 96.3 % at 220 nm.



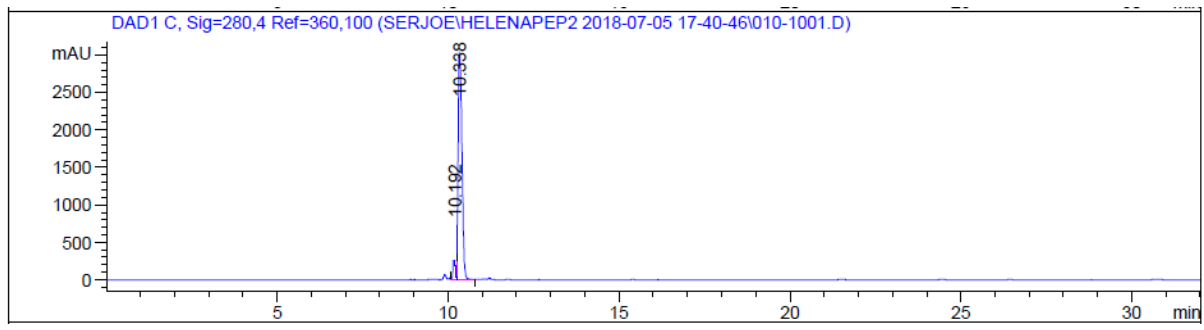
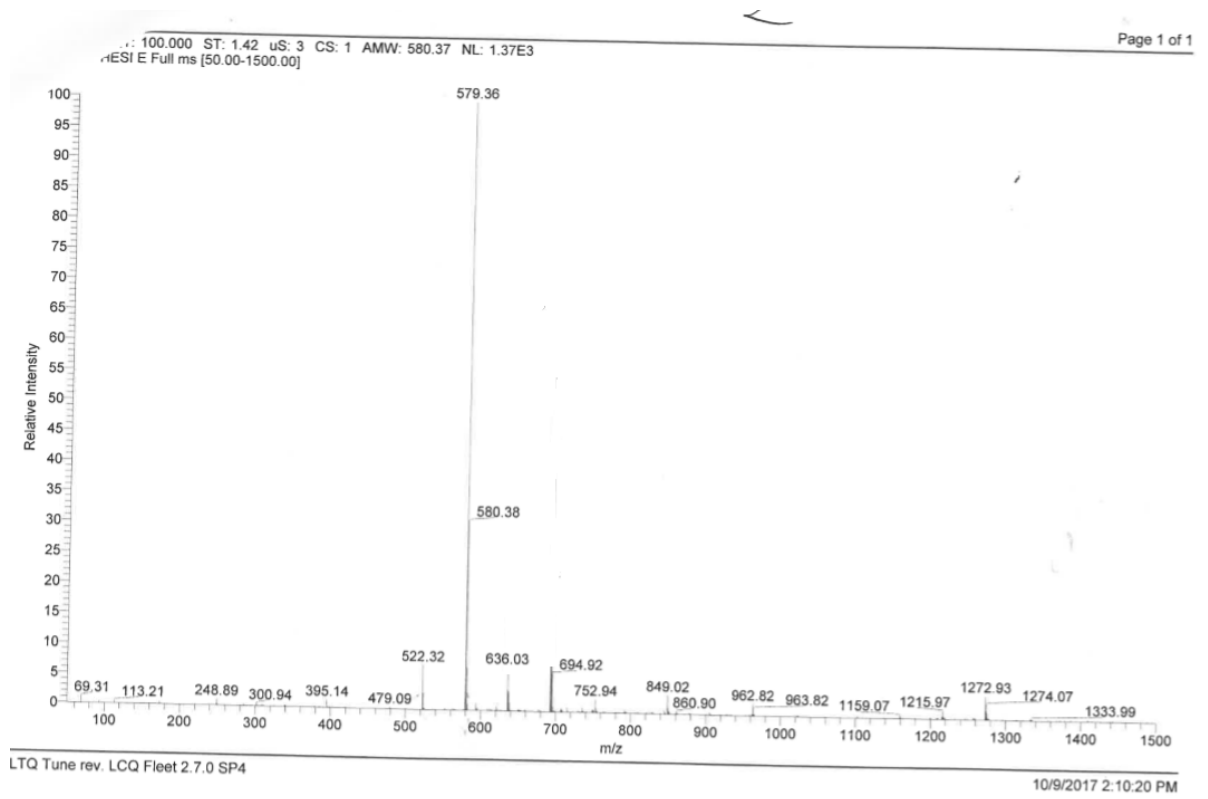
HM-41; calculated MW: 649.78, found: MS (ESI) $m/z = 650.62$ ($[M+H]^+$); HPLC: $tr = 10.722$ min, 94.1 % at 280 nm.



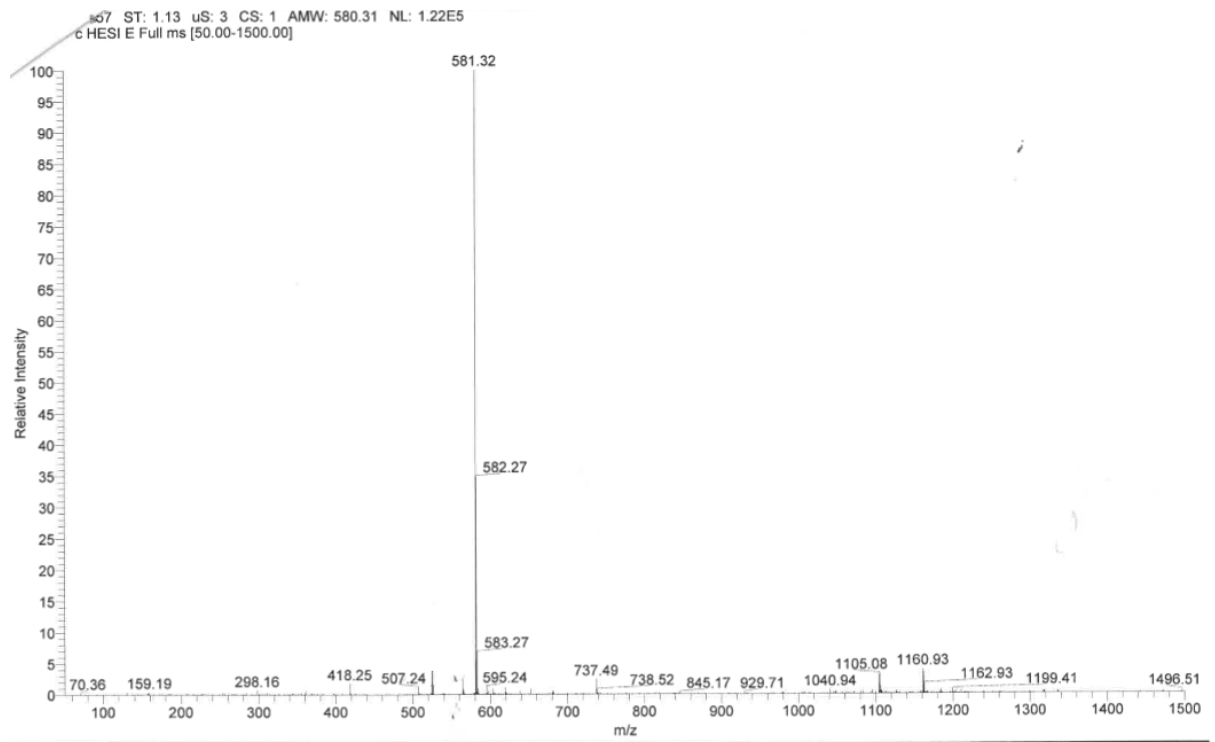
HM-42; calculated MW: 672.81, found: MS (ESI) $m/z = 673.63$ ($[M+H]^+$); HPLC: $t_r = 12.598$ min, 95.4 % at 220 nm.



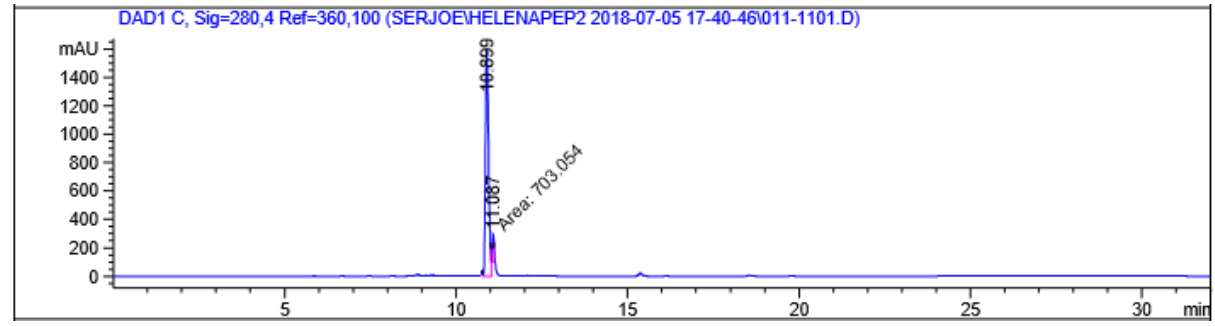
HM-50; calculated MW: 580.63, found: MS (ESI) $m/z = 579.36$ ($[M-H]^-$); HPLC: $t_r = 10.338$ min, 92.7% at 280 nm.



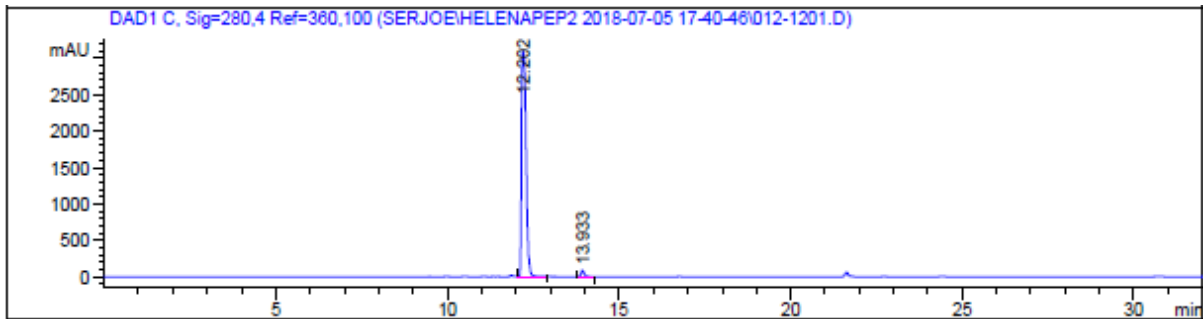
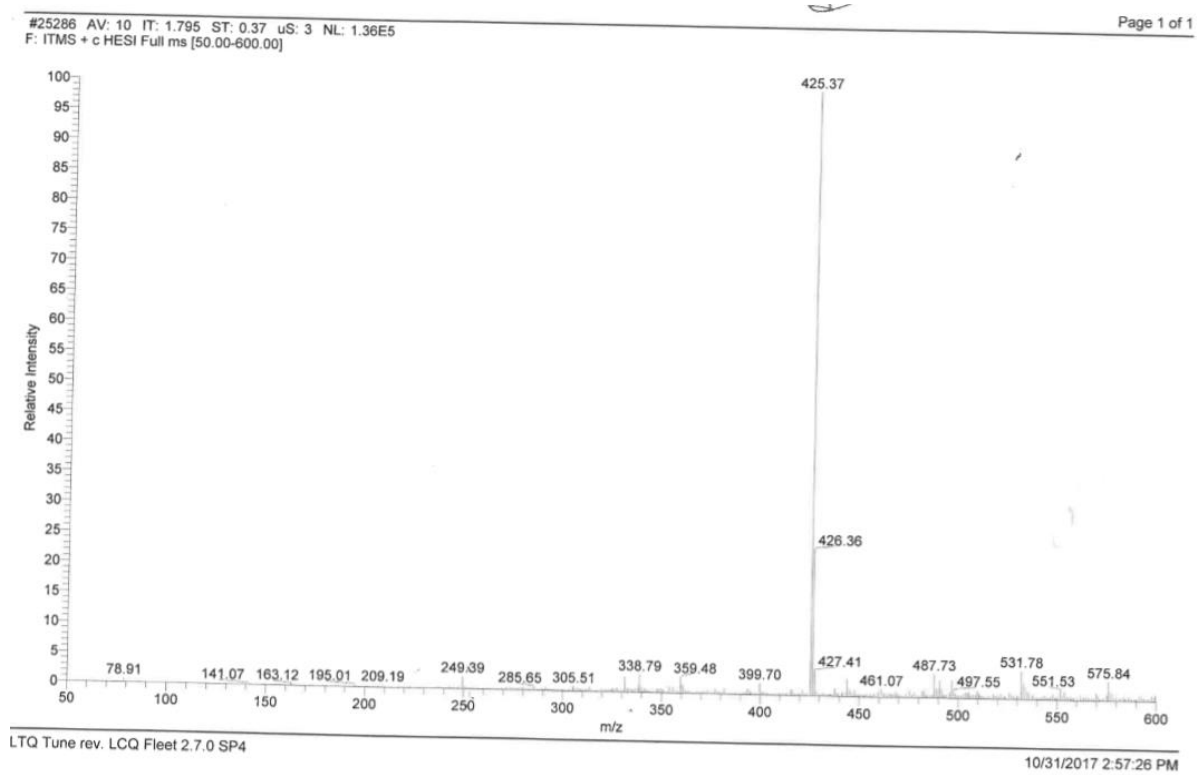
HM-51; calculated MW: 580.63, found: MS (ESI) $m/z = 581.32$ ($[M+H]^+$); HPLC: $t_r = 10.899$ min, 93.5 % at 280 nm.



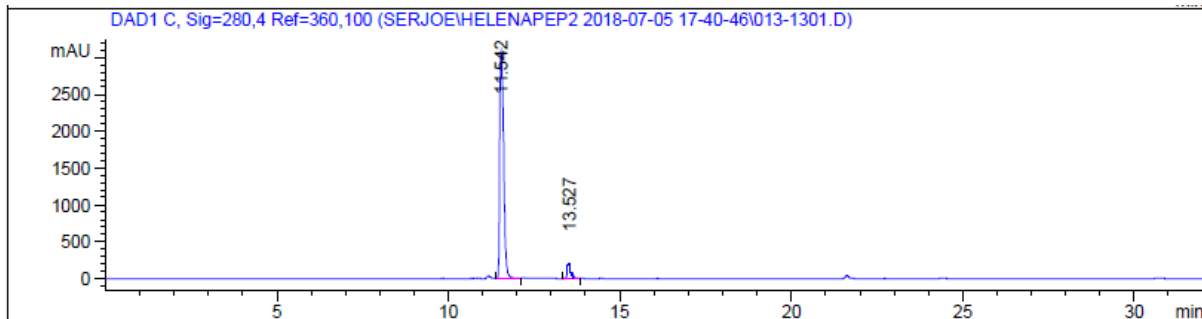
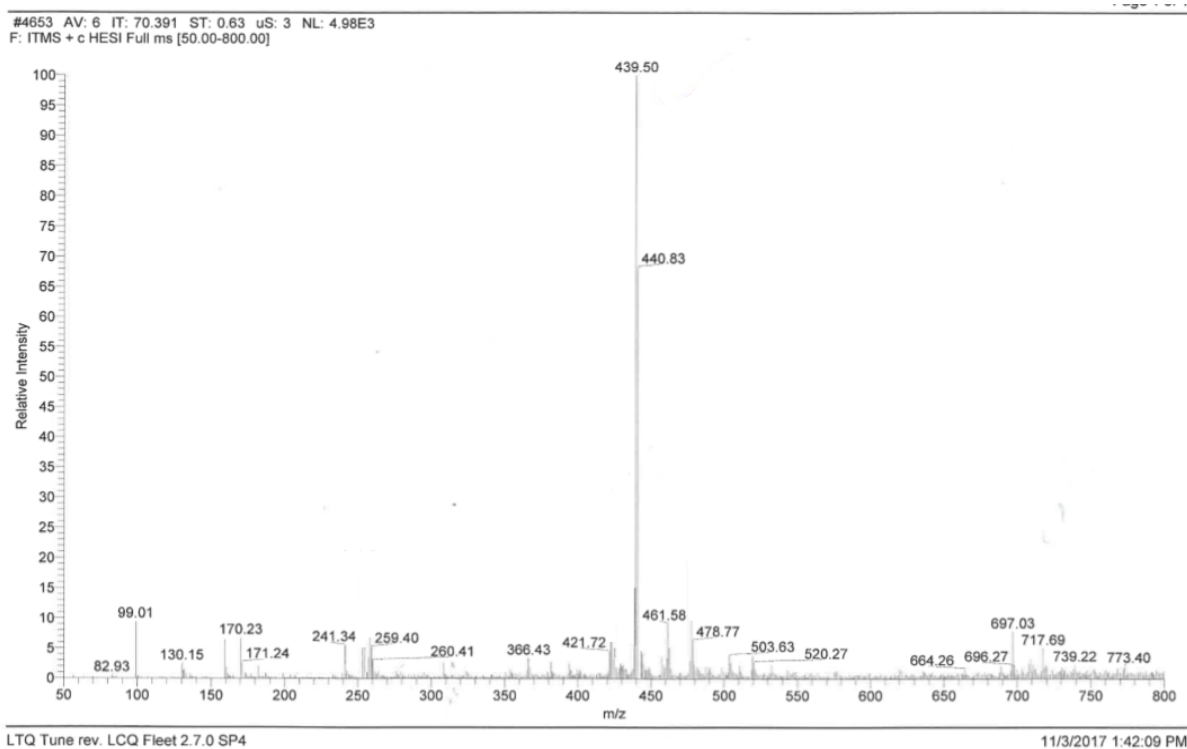
.TQ Tune rev. LCQ Fleet 2.7.0 SP4 10/9/2017 2:10:11 PM



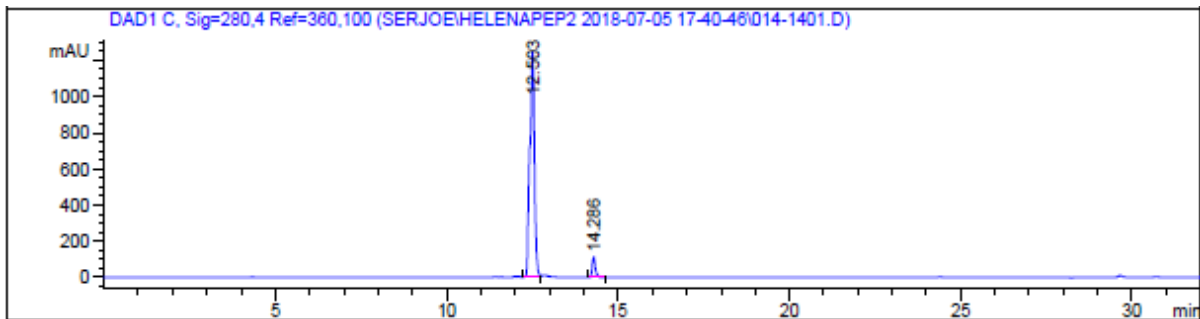
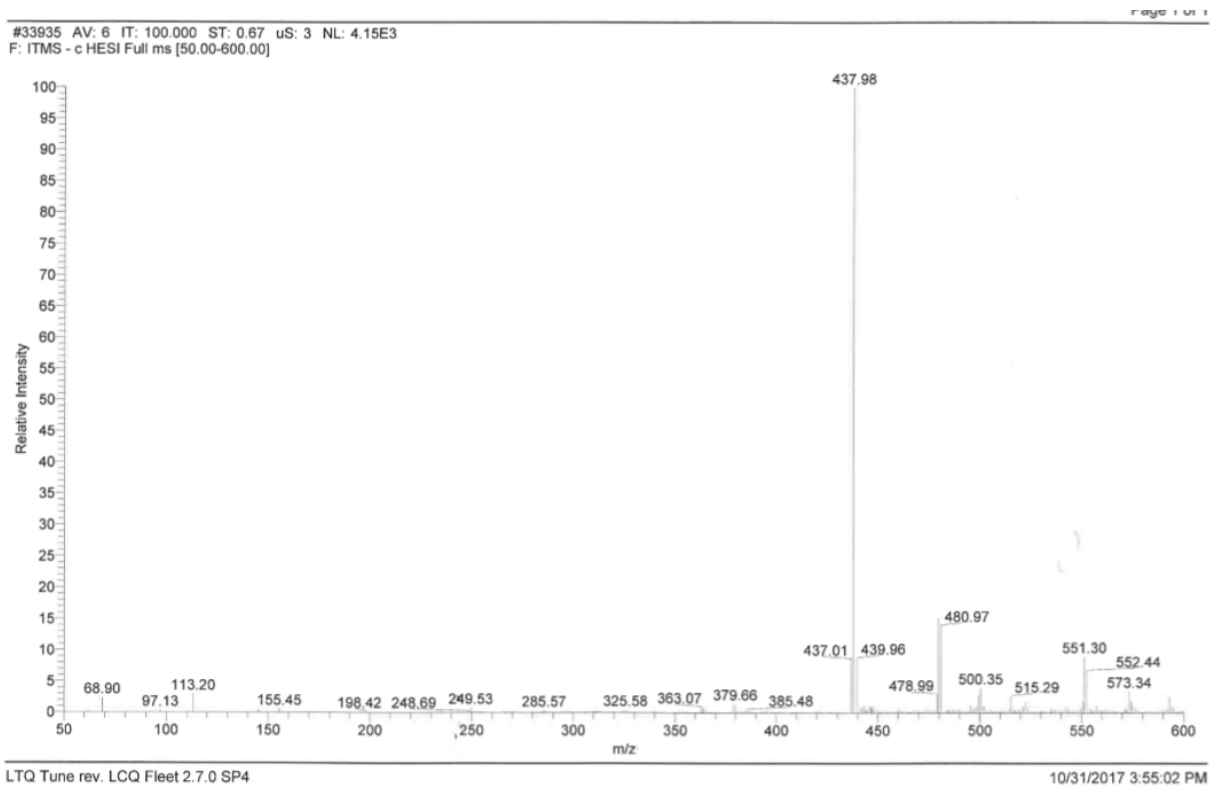
HM-53; calculated MW: 424.45, found: MS (ESI) $m/z = 425.37$ ($[M+H]^+$); HPLC: $t_r = 12.202$ min, 98.2 % at 280 nm.



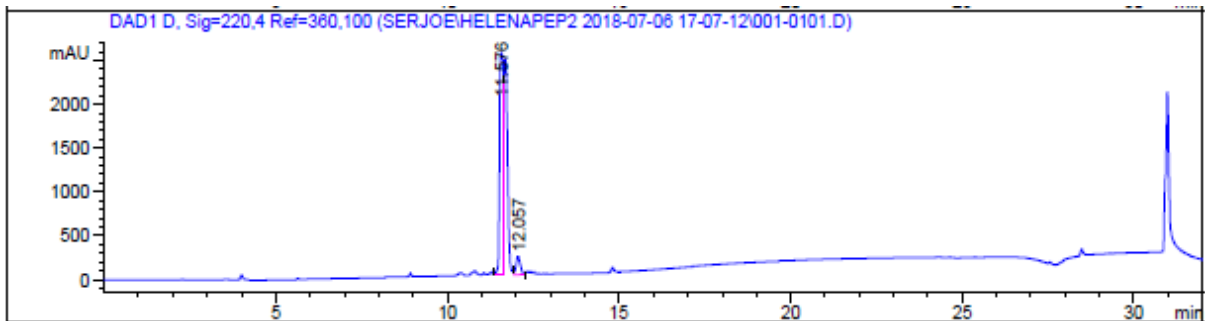
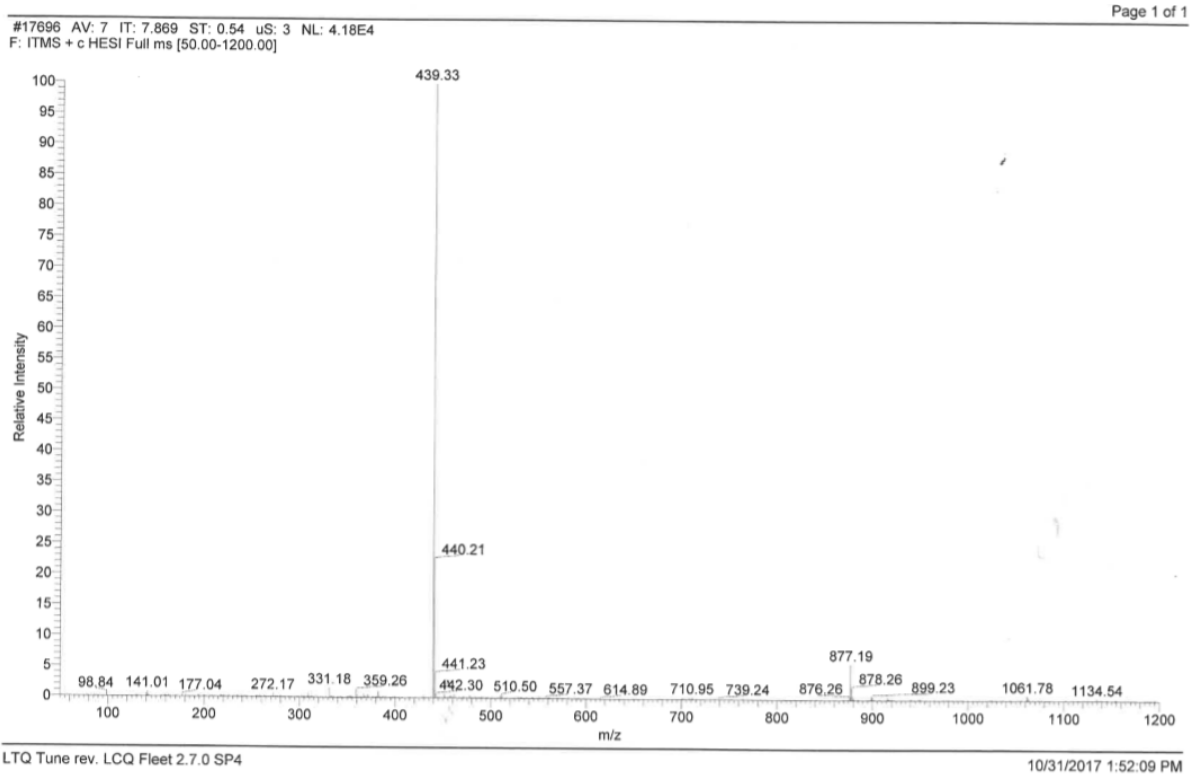
HM-54; calculated MW: 438.48, found: MS (ESI) $m/z = 439.50$ ($[M+H]^+$); HPLC: $t_r = 11.542$ min, 91.8 % at 280 nm.



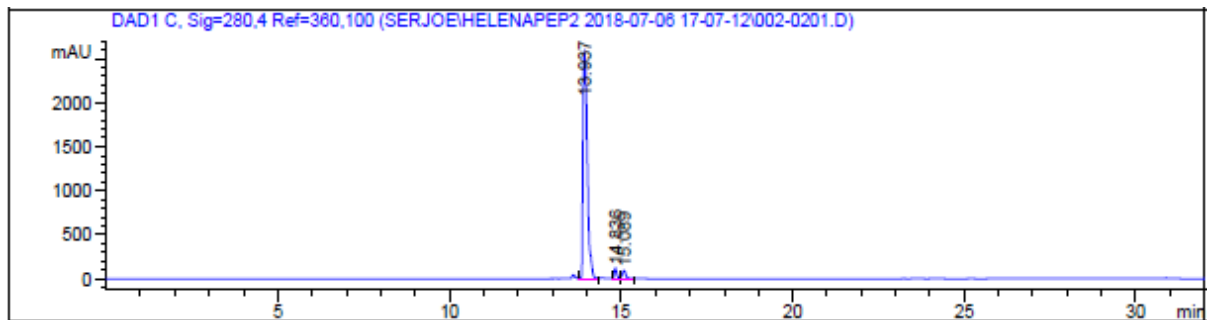
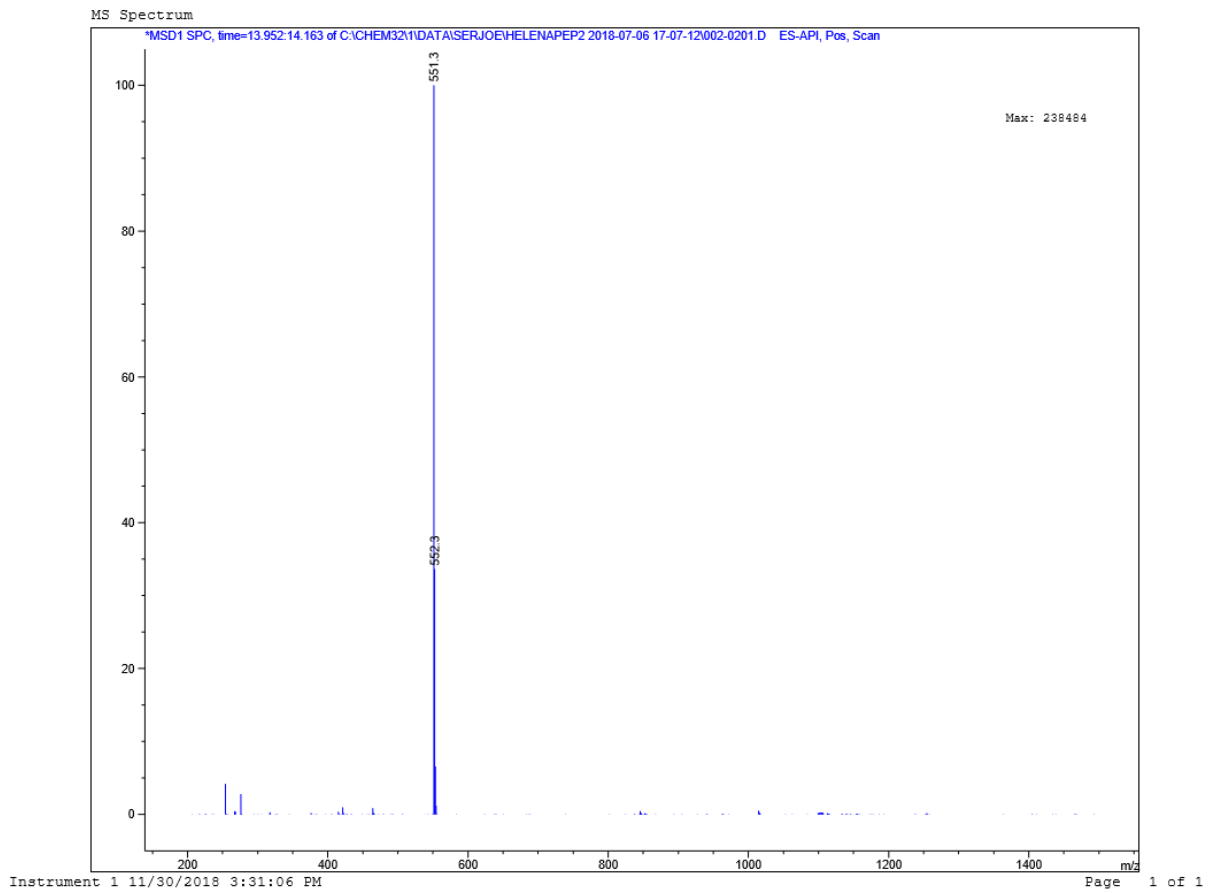
HM-55; calculated MW: 438.48, found: MS (ESI) $m/z = 437.98$ ($[M-H]^-$); HPLC: $t_r = 12.503$ min, 94.2 % at 280 nm.



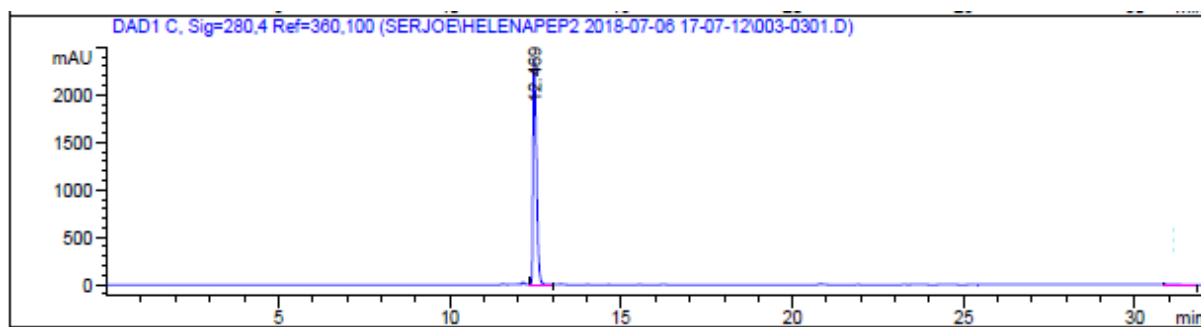
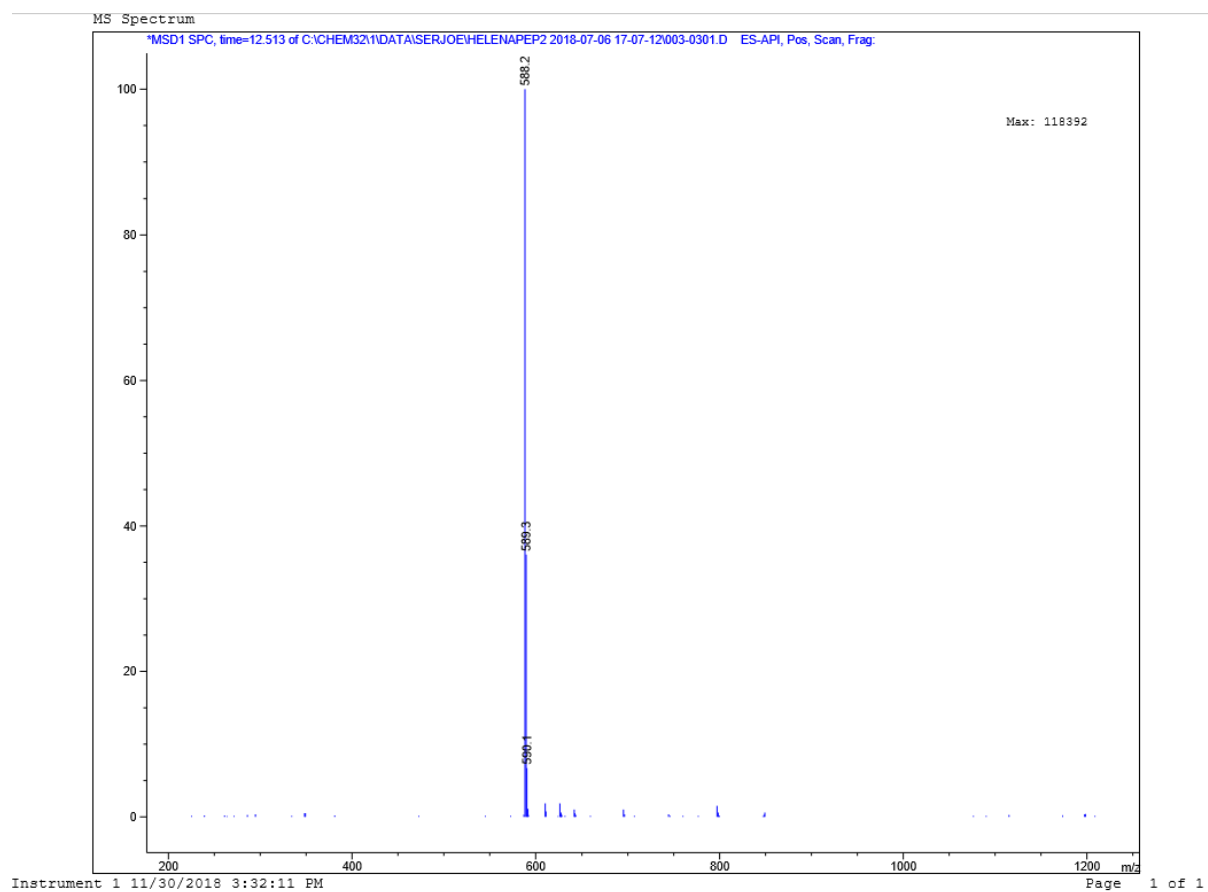
HM-56; calculated MW: 438.48, found: MS (ESI) $m/z = 439.33$ ($[M+H]^+$); HPLC: $t_r = 11.576$ min, 95.1 % at 220 nm.



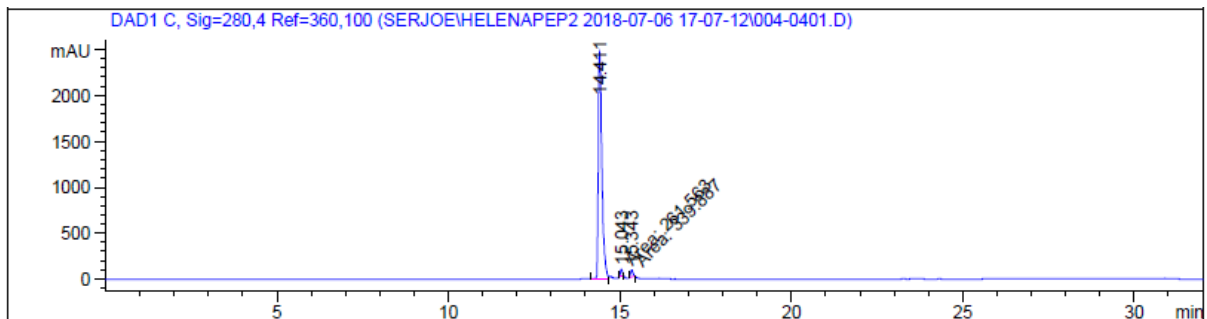
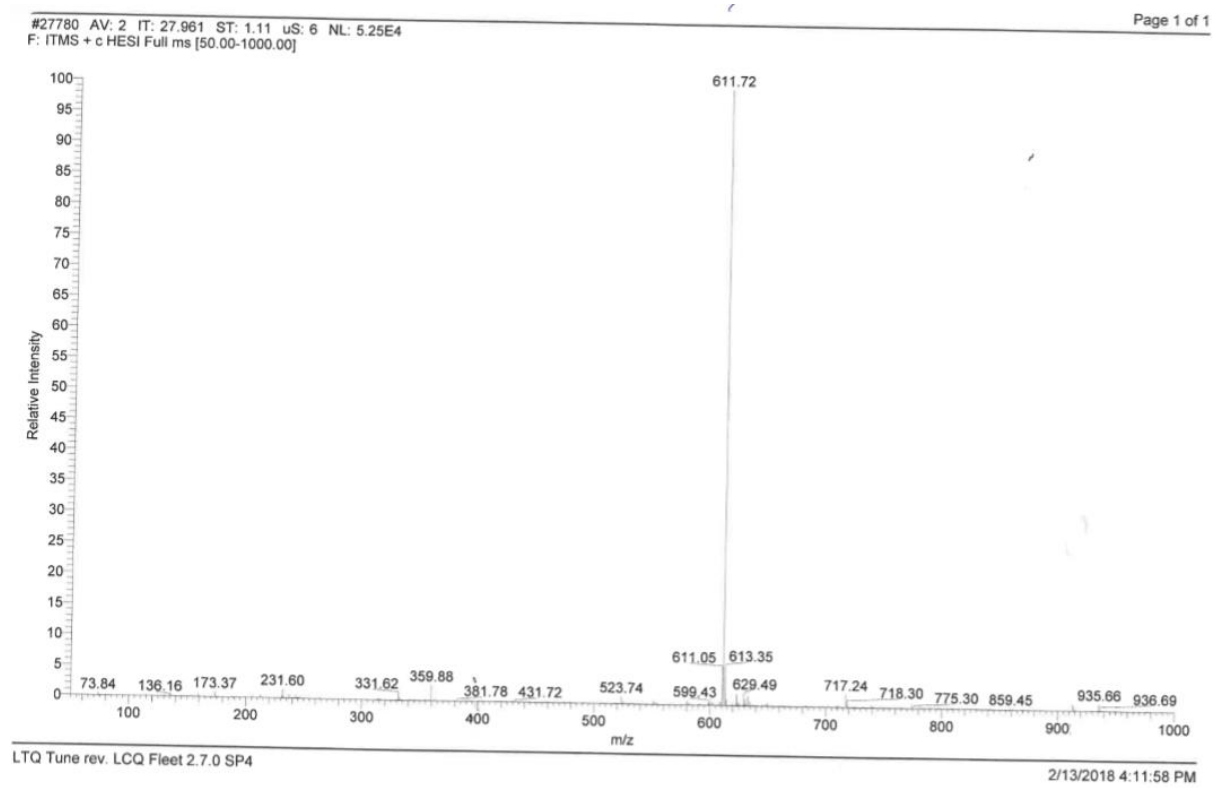
HM-63; calculated MW: 550.63, found: MS (ESI) $m/z = 439.33$ ($[M+H]^+$); HPLC: $t_r = 13.937$ min, 94.5 % at 280 nm.



HM-64; calculated MW: 587.62, found: MS (ESI) $m/z = 588.2$ ($[M+H]^+$); $t_r = 12.469$ min, 100% at 280 nm.



HM-65; calculated MW: 610.66, found: MS (ESI) $m/z = 611.72$ ($[M+H]^+$); HPLC: $t_r = 14.411$ min, 96.8 % at 280 nm.



XI. REFERENCES

1. Hopkins, P.N., *Molecular biology of atherosclerosis*. Physiol Rev, 2013. **93**(3): p. 1317-542.
2. Tavafi, M., *Complexity of diabetic nephropathy pathogenesis and design of investigations*. J Renal Inj Prev, 2013. **2**(2): p. 59-62.
3. Kume, N., M.I. Cybulsky, and M.A. Gimbrone, Jr., *Lysophosphatidylcholine, a component of atherogenic lipoproteins, induces mononuclear leukocyte adhesion molecules in cultured human and rabbit arterial endothelial cells*. Journal of Clinical Investigation, 1992. **90**(3): p. 1138-44.
4. Steinbrecher, U.P., et al., *Modification of low density lipoprotein by endothelial cells involves lipid peroxidation and degradation of low density lipoprotein phospholipids*. Proc Natl Acad Sci U S A, 1984. **81**(12): p. 3883-7.
5. Rafieian-Kopaei, M., et al., *Atherosclerosis: process, indicators, risk factors and new hopes*. Int J Prev Med, 2014. **5**(8): p. 927-46.
6. Weber, C. and H. Noels, *Atherosclerosis: current pathogenesis and therapeutic options*. Nat Med, 2011. **17**(11): p. 1410-22.
7. Ross, R., *Mechanisms of atherosclerosis--a review*. Adv Nephrol Necker Hosp, 1990. **19**: p. 79-86.
8. Davignon, J. and P. Ganz, *Role of endothelial dysfunction in atherosclerosis*. Circulation, 2004. **109**(23 Suppl 1): p. III27-32.
9. Carmeliet, P. and R.K. Jain, *Molecular mechanisms and clinical applications of angiogenesis*. Nature, 2011. **473**(7347): p. 298-307.
10. Schoors, S., et al., *Partial and transient reduction of glycolysis by PFKFB3 blockade reduces pathological angiogenesis*. Cell Metab, 2014. **19**(1): p. 37-48.
11. De Bock, K., et al., *Role of PFKFB3-driven glycolysis in vessel sprouting*. Cell, 2013. **154**(3): p. 651-63.
12. Xu, Y., et al., *Endothelial PFKFB3 plays a critical role in angiogenesis*. Arterioscler Thromb Vasc Biol, 2014. **34**(6): p. 1231-9.
13. Van Schaftingen, E., et al., *A kinetic study of pyrophosphate: fructose-6-phosphate phosphotransferase from potato tubers. Application to a microassay of fructose 2,6-bisphosphate*. Eur J Biochem, 1982. **129**(1): p. 191-5.
14. Cavalier, M.C., et al., *Molecular basis of the fructose-2,6-bisphosphatase reaction of PFKFB3: transition state and the C-terminal function*. Proteins, 2012. **80**(4): p. 1143-53.
15. Claus, T.H., et al., *The role of fructose 2,6-bisphosphate in the regulation of carbohydrate metabolism*. Curr Top Cell Regul, 1984. **23**: p. 57-86.
16. Kountz, P.D., et al., *The stereochemical course of phospho group transfer catalyzed by rat liver 6-phosphofructo-2-kinase*. J Biol Chem, 1988. **263**(31): p. 16069-72.
17. Algaier, J. and K. Uyeda, *Molecular cloning, sequence analysis, and expression of a human liver cDNA coding for fructose-6-P,2-kinase:fructose-2,6-bisphosphatase*. Biochem Biophys Res Commun, 1988. **153**(1): p. 328-33.
18. Sakai, A., et al., *Cloning of cDNA encoding for a novel isozyme of fructose 6-phosphate, 2-kinase/fructose 2,6-bisphosphatase from human placenta*. J Biochem, 1996. **119**(3): p. 506-11.
19. Heine-Suner, D., et al., *Sequence and structure of the human 6-phosphofructo-2-kinase/fructose-2,6-bisphosphatase heart isoform gene (PFKFB2)*. Eur J Biochem, 1998. **254**(1): p. 103-10.

20. Manzano, A., et al., *Molecular cloning, expression, and chromosomal localization of a ubiquitously expressed human 6-phosphofructo-2-kinase/fructose-2, 6-bisphosphatase gene (PFKFB3)*. Cytogenet Cell Genet, 1998. **83**(3-4): p. 214-7.
21. Kim, S.G., et al., *Crystal structure of the hypoxia-inducible form of 6-phosphofructo-2-kinase/fructose-2,6-bisphosphatase (PFKFB3): a possible new target for cancer therapy*. J Biol Chem, 2006. **281**(5): p. 2939-44.
22. Hasemann, C.A., et al., *The crystal structure of the bifunctional enzyme 6-phosphofructo-2-kinase/fructose-2,6-bisphosphatase reveals distinct domain homologies*. Structure, 1996. **4**(9): p. 1017-29.
23. Lee, Y.H., et al., *Tissue-specific structure/function differentiation of the liver isoform of 6-phosphofructo-2-kinase/fructose-2,6-bisphosphatase*. J Biol Chem, 2003. **278**(1): p. 523-30.
24. Minchenko, A., et al., *Hypoxia-inducible factor-1-mediated expression of the 6-phosphofructo-2-kinase/fructose-2,6-bisphosphatase-3 (PFKFB3) gene. Its possible role in the Warburg effect*. J Biol Chem, 2002. **277**(8): p. 6183-7.
25. Warburg, O., *On the origin of cancer cells*. Science, 1956. **123**(3191): p. 309-14.
26. Lunt, S.Y. and M.G. Vander Heiden, *Aerobic glycolysis: meeting the metabolic requirements of cell proliferation*. Annu Rev Cell Dev Biol, 2011. **27**: p. 441-64.
27. Hirata, T., et al., *Inhibition of tumor cell growth by a specific 6-phosphofructo-2-kinase inhibitor, N-bromoacetyethanolamine phosphate, and its analogues*. Biosci Biotechnol Biochem, 2000. **64**(10): p. 2047-52.
28. Carmeliet, P., *Angiogenesis in health and disease*. Nat Med, 2003. **9**(6): p. 653-60.
29. Potente, M., H. Gerhardt, and P. Carmeliet, *Basic and therapeutic aspects of angiogenesis*. Cell, 2011. **146**(6): p. 873-87.
30. Granchi, C. and F. Minutolo, *Anticancer agents that counteract tumor glycolysis*. ChemMedChem, 2012. **7**(8): p. 1318-50.
31. Raez, L.E., et al., *A phase I dose-escalation trial of 2-deoxy-D-glucose alone or combined with docetaxel in patients with advanced solid tumors*. Cancer Chemother Pharmacol, 2013. **71**(2): p. 523-30.
32. Davis, M.I., et al., *Comprehensive analysis of kinase inhibitor selectivity*. Nat Biotechnol, 2011. **29**(11): p. 1046-51.
33. Breen, M.E. and M.B. Soellner, *Small molecule substrate phosphorylation site inhibitors of protein kinases: approaches and challenges*. ACS Chem Biol, 2015. **10**(1): p. 175-89.
34. Knight, Z.A. and K.M. Shokat, *Features of selective kinase inhibitors*. Chem Biol, 2005. **12**(6): p. 621-37.
35. Scapin, G., *Protein kinase inhibition: different approaches to selective inhibitor design*. Curr Drug Targets, 2006. **7**(11): p. 1443-54.
36. Krishnamurty, R. and D.J. Maly, *Biochemical mechanisms of resistance to small-molecule protein kinase inhibitors*. ACS Chem Biol, 2010. **5**(1): p. 121-38.
37. Daub, H., K. Specht, and A. Ullrich, *Strategies to overcome resistance to targeted protein kinase inhibitors*. Nat Rev Drug Discov, 2004. **3**(12): p. 1001-10.
38. Woolley, D.W. and R.B. Merrifield, *Anomalies of the structural specificity of peptides*. Ann N Y Acad Sci, 1963. **104**: p. 161-71.
39. Palomo, J.M., *Solid-phase peptide synthesis: an overview focused on the preparation of biologically relevant peptides*. Rsc Advances, 2014. **4**(62): p. 32658-32672.
40. Paradis-Bas, M., J. Tulla-Puche, and F. Albericio, *The road to the synthesis of "difficult peptides"*. Chemical Society Reviews, 2016. **45**(3): p. 631-654.
41. Albericio, F., P. Lloyd-Williams, and E. Giralt, *Convergent solid-phase peptide synthesis*. Methods Enzymol, 1997. **289**: p. 313-36.

42. *Resins for solid phase peptide synthesis*. [cited 3 4]; 3]. Available from: https://www.sigmaaldrich.com/content/dam/sigmaaldrich/docs/Aldrich/Brochure/al_chemfile_v3_no4.pdf.
43. Bailey, P.D., *An introduction to peptide chemistry*. 1990, New York: Wiley.
44. Knorr, R., et al., *New Coupling Reagents in Peptide Chemistry*. *Tetrahedron Letters*, 1989. **30**(15): p. 1927-1930.
45. Carpino, L.A., et al., *Advantageous Applications of Azabenzotriazole (Triazolopyridine)-Based Coupling Reagents to Solid-Phase Peptide-Synthesis*. *Journal of the Chemical Society-Chemical Communications*, 1994(2): p. 201-203.
46. Rosano, G.L. and E.A. Ceccarelli, *Recombinant protein expression in Escherichia coli: advances and challenges*. *Front Microbiol*, 2014. **5**: p. 172.
47. Sahdev, S., S.K. Khattar, and K.S. Saini, *Production of active eukaryotic proteins through bacterial expression systems: a review of the existing biotechnology strategies*. *Mol Cell Biochem*, 2008. **307**(1-2): p. 249-64.
48. Rosano, G.L., E.M. Bruch, and E.A. Ceccarelli, *Insights into the Clp/HSP100 chaperone system from chloroplasts of Arabidopsis thaliana*. *J Biol Chem*, 2011. **286**(34): p. 29671-80.
49. Sezonov, G., D. Joseleau-Petit, and R. D'Ari, *Escherichia coli physiology in Luria-Bertani broth*. *J Bacteriol*, 2007. **189**(23): p. 8746-9.
50. Sorensen, H.P. and K.K. Mortensen, *Advanced genetic strategies for recombinant protein expression in Escherichia coli*. *J Biotechnol*, 2005. **115**(2): p. 113-28.
51. Graslund, S., et al., *Protein production and purification*. *Nat Methods*, 2008. **5**(2): p. 135-46.
52. Seidel, S.A.I., et al., *Microscale thermophoresis quantifies biomolecular interactions under previously challenging conditions*. *Methods*, 2013. **59**(3): p. 301-315.
53. Seidel, S.A.I., et al., *Label-Free Microscale Thermophoresis Discriminates Sites and Affinity of Protein-Ligand Binding*. *Angewandte Chemie-International Edition*, 2012. **51**(42): p. 10656-10659.
54. Alexander, C.G., et al., *Novel microscale approaches for easy, rapid determination of protein stability in academic and commercial settings*. *Biochimica Et Biophysica Acta-Proteins and Proteomics*, 2014. **1844**(12): p. 2241-2250.
55. Ludwig, C., *Sitzungsber Akad Wiss, Wien Math Naturwiss Kl.*, 1856: p. 539.
56. Duhr, S. and D. Braun, *Why molecules move along a temperature gradient*. *Proc Natl Acad Sci U S A*, 2006. **103**(52): p. 19678-82.
57. Ross, D., M. Gaitan, and L.E. Locascio, *Temperature measurement in microfluidic systems using a temperature-dependent fluorescent dye*. *Analytical Chemistry*, 2001. **73**(17): p. 4117-23.
58. Kurland, I.J., B. Chapman, and M.R. El-Maghrabi, *N- and C-termini modulate the effects of pH and phosphorylation on hepatic 6-phosphofructo-2-kinase/fructose-2,6-bisphosphatase*. *Biochem J*, 2000. **347**(Pt 2): p. 459-67.
59. Whitmore, L. and B.A. Wallace, *Protein secondary structure analyses from circular dichroism spectroscopy: methods and reference databases*. *Biopolymers*, 2008. **89**(5): p. 392-400.
60. Whitmore, L. and B.A. Wallace, *DICHROWEB, an online server for protein secondary structure analyses from circular dichroism spectroscopic data*. *Nucleic Acids Research*, 2004. **32**(Web Server issue): p. W668-73.
61. Boyd, S., et al., *Structure-Based Design of Potent and Selective Inhibitors of the Metabolic Kinase PFKFB3*. *Journal of Medicinal Chemistry*, 2015. **58**(8): p. 3611-25.
62. Goutelle, S., et al., *The Hill equation: a review of its capabilities in pharmacological modelling*. *Fundamental & Clinical Pharmacology*, 2008. **22**(6): p. 633-648.

63. Abeliovich, H., *An empirical extremum principle for the hill coefficient in ligand-protein interactions showing negative cooperativity*. Biophys J, 2005. **89**(1): p. 76-9.
64. Sakakibara, R., et al., *Characterization of a human placental fructose-6-phosphate, 2-kinase/fructose-2,6-bisphosphatase*. J Biochem, 1997. **122**(1): p. 122-8.
65. Hunte C., v.J.G., Schlaeger, H. , *Membrane Protein Purification and Crystallization. A practical guide*. . 2003.
66. Northrop M., K.M., Herriott, R.M., *Crystalline enzymes*. Columbia University Press, 1948.
67. McPherson, A., *Macromolecular crystals*. Sci Am, 1989. **260**(3): p. 62-9.
68. McPherson, A. and J.A. Gavira, *Introduction to protein crystallization*. Acta Crystallographica Section F-Structural Biology Communications, 2014. **70**: p. 2-20.
69. McPherson, A., *Introduction to protein crystallization*. Methods, 2004. **34**(3): p. 254-65.
70. Malkin, A.J., et al., *Mechanisms of growth for protein and virus crystals*. Nat Struct Biol, 1995. **2**(11): p. 956-9.
71. Chayen, N.E., et al., *An Automated-System for Microbatch Protein Crystallization and Screening*. Journal of Applied Crystallography, 1990. **23**: p. 297-302.
72. Hosfield, D., et al., *A fully integrated protein crystallization platform for small-molecule drug discovery*. J Struct Biol, 2003. **142**(1): p. 207-17.
73. McPherson, A., *Preparation and analysis of protein crystals*. 1982, New York: Wiley. vii, 371 p.
74. McPherson, A. and B. Cudney, *Searching for silver bullets: an alternative strategy for crystallizing macromolecules*. J Struct Biol, 2006. **156**(3): p. 387-406.
75. St-Gallay, S.A., et al., *A High-Throughput Screening Triage Workflow to Authenticate a Novel Series of PFKFB3 Inhibitors*. SLAS Discov, 2018. **23**(1): p. 11-22.
76. Maffucci, I. and A. Contini, *Improved Computation of Protein-Protein Relative Binding Energies with the Nwat-MMGBSA Method*. Journal of Chemical Information and Modeling, 2016. **56**(9): p. 1692-704.
77. Malmqvist, M., *BIACORE: an affinity biosensor system for characterization of biomolecular interactions*. Biochem Soc Trans, 1999. **27**(2): p. 335-40.
78. Sciences, G.H.L. *Surface Plasmon Resonance*. Available from: <https://www.gelifesciences.com/en/ar/solutions/protein-research/knowledge-center/surface-plasmon-resonance/surface-plasmon-resonance>.
79. Englebienne, P., van Hoonacker, A., Verhas, M. , *Surface plasmon resonance: principles, methods and applications in biomedical sciences*. Spectroscopy, 2003(17): p. 255-273.
80. Korb, O., T. Stutzle, and T.E. Exner, *Empirical scoring functions for advanced protein-ligand docking with PLANTS*. Journal of Chemical Information and Modeling, 2009. **49**(1): p. 84-96.
81. Ferri, N., et al., *Virtual screening approach for the identification of new Rac1 inhibitors*. Journal of Medicinal Chemistry, 2009. **52**(14): p. 4087-90.
82. *AMBER 14*. 2014, University of California: San Francisco.
83. Maffucci, I. and A. Contini, *Explicit Ligand Hydration Shells Improve the Correlation between MM-PB/GBSA Binding Energies and Experimental Activities*. Journal of Chemical Theory and Computation, 2013. **9**(6): p. 2706-17.
84. *Technical manual for ADP Glo Kinase assay*, Madison, WI 53711-5399 USA: Promega Cooperation.